Antigen Presentation by MHC Class I and CD1 Molecules

Thesis

Antigen Presentation by MHC class I and CD1 Molecules

Stephan D. Gadola, M.D.

A thesis submitted for the degree of Doctor of Philosophy

Submitted: May 2008
Date of award: 19 January 2009

Weatherall Institute of Molecular Medicine
John Radcliffe Hospital, Oxford

Supervised by
Prof. Vincenzo Cerundolo & Prof. Andrew McMichael

ProQuest LLC.
789 East Eisenhower Parkway
P.O. Box 1346
Ann Arbor, MI 48106 – 1346

To my dear wife Sandra

and to my parents Rosmarie and Gion Gadola

Acknowledgements

When I started laboratory research at the IMM in Oxford in November 1998 I had never held a pipette in my hands before. I am immensely grateful to Enzo Cerundolo, who made me feel welcome in Oxford even before I arrived, and who took the risk to give a 31-year old chap from Switzerland with no real research experience in the back a bench in his laboratory. Enzo always believed in my abilities and always supported me in the best possible way. It truly was a fantastic three years!

It is hardly possible to thank all the people who have helped and supported me in the process of becoming a scientist. Uzi Gileadi was my anchor in the lab, and he taught me virtually everything in molecular biology I still know today. Jili Chen gave me a wonderful introduction into inclusion body production and Chinese food, and Michael Palmowski and Rod Dunbar made me "FACS-competent". Michael was also my sparring partner in the "crazy ideas" section and naturally became a great friend. Mao Salio taught me the essentials on dendritic cells, sometimes over a glass of red wine, and Dawn Shepherd gave always a fantastic and immaculate technical support.

People from other labs and also companies were instrumental for various aspects of this thesis. Nikolai Lissin, probably one of the last Russians alive who could repair MIR station in orbit with a piece of shoestring, never got tired to answer all my questions about proteins and BiaCores, and naturally became a friend. Bent Jakobsen was first my first partner in racquet sports in Oxford, then became a very

good friend, and finally a great supporter of my research. Similarly, Tim Elliott helped me stay fit on the Squash court, became a friend, and is now a great support for my current research.

Very special thanks go to Karl Harlos, Yvonne Jones and Nathan Zaccai. I love remembering the exciting times in the "crystal room" and in Grenoble. Likewise with my friend Tassos Karadimitris I share many unforgettable memories of long nights in front of the FPLC, musing on flat curves and Greek philosophy.

The TAP-deficiency story started before my arrival in Oxford, and I'm very thankful to the clinical staff of the vasculitis ward at the "Medizinische Krankenhausabteilung" of the Rheumatology Clinic in Bad Bramstedt, the clinic where I met the first patient, "AK". In particular I'd like to thank Wolfgang Gross for granting me free access to patient files even after I had left his clinic.

It has been a long way since I left Medical School in Basle. My Mum and Dad, Rosmarie and Gion Gadola, have always given everything for their children. Their love and enthusiasm for life has given me the strength to focus on things and get them done.

This thesis would not exist, if I hadn't met Sandra, my dear wife, during my clinical training in Bad Bramstedt. It is impossible for me to measure the amount of support and sacrifice and love that she has continuously given since then to me. This thesis is dedicated to Sandra with all my love.

Funding bodies

My stay in Oxford was generously supported from the following Swiss funding bodies:

Swiss National Science Foundation

Janggen-Poehn Stiftung

Holderbank Stiftung

Novartis Foundation

Hoffmann La Roche Foundation

FAG Stiftung Basel

Abstract

Antigen presentation is the "sine qua non" of the mammalian adaptive immune system. The assembly of MHC class I/peptide complexes in the endoplasmic reticulum (ER) relies on the orchestrated interplay between different chaperonins, which assist MHC class I folding, and the peptide loading complex (PLC). Mutant lymphoblastoid cell lines with defective MHC class I surface expression have greatly helped the functional analysis of the PLC. The TAP transporter associated with antigen processing translocates MHC class I peptide ligands from the cytosol into the ER and is critical for successful MHC class I assembly and maturation. In the first two results chapters of this thesis I will describe the identification, clinical description and molecular and genetic analysis of a new clinical syndrome in a group of patients with dramatically reduced MHC class I surface expression. The disease in these patients could be identified as primary TAP-deficiency.

Mycobacterial infections were conspicuously absent in these TAP-deficient patients whereas TAP-deficient mice are known to be highly susceptible to mycobacteria. The focus of the third and fourth chapter of this thesis lies on lipid antigen presentation via CD1 molecules, which are known to present mycobacterial lipids to T lymphocytes. The first objective of this thesis was to generate recombinant mycobacterial lipid loaded CD1 molecules as tools to measure mycobacterial lipid specific T cell responses in the TAP-deficient patients. Chapters three and four describe novel protocols for the generation of recombinant human CD1b and CD1d molecules with loaded single lipid species.

Preface

Both an insufficient and an inappropriately strong immune response can cause serious diseases in humans. My personal interest in clinical immunology was sparked by my first patient with an inflammatory disease of small vessels back in 1994 in Switzerland. At that time, clinical immunology was still mainly about making the diagnosis and correctly classify immune-mediated diseases, and to develop a long-term treatment strategy for the patients in order to get the best therapeutic effect with the least side effects. While these principles are still valid today, recent advances in targeted immune therapies underline the need for clinicians to understand the basic mechanisms in immunology. However, today, knowledge in immunology is growing exponentially and keeping up to date with all the different areas of immunology is hardly possible.

Primary immune deficiency (PID) syndromes are rare diseases, which offer the clinical immunologist a unique opportunity to get insight into the links between clinical and basic immunology. In my case, an encounter in 1996 with an extraordinary patient, "AK", who was suffering of a then unknown PID with severe mutilation of the face, completely changed my career path and was the "sine qua non" of this thesis. However, after all those years since "AK's" death I do not remember her because of her clinical phenotype or the fascinating research I was allowed to do with her tissues and cells. Like all the other patients with the same disease who I met over the years I remember "AK" for the exceptional bravery with which she endured her illness, and for the feeling of powerlessness her disease evoked in me.

Outline of the thesis

The central theme of this thesis is antigen presentation. The first two results chapters (i.e. chapters 3 and 4) will describe the MHC class I antigen presentation pathway in patients with a very rare PID, TAP-deficiency.

The clinical observation that TAP-deficient humans do not exhibit increased susceptibility to mycobacterial infections, while TAP-deficient mice are highly susceptible to mycobacteria, stimulated my interest in another class of antigen presenting molecules, namely the non-polymorphic lipid presenting CD1 molecules.

The third results chapter describes the development and application of new tools to study human CD1d-restricted lipid-specific T lymphocytes.

Finally, the fourth and last result chapter describes how human CD1b molecules bind and present lipid antigens and offers an explanation of how human CD1b can bind mycobacterial mycolates that have very long alkyl chains.

Publications resulting from this thesis

1) Association of a syndrome resembling Wegener's granulomatosis with low surface expression of HLA class-I molecules. ***Lancet*** 354, 1598-1603 (1999). Moins-Teisserenc HT, Gadola SD (SDG and HTMT joint first authors), Cella M, Dunbar PR, Exley A, Blake N, Baykal C, Lambert J, Bigliardi P, Willemsen M, Jones M, Buechner S, Colonna M, Gross WL, Cerundolo V

2) Valpha24-JalphaQ-independent, CD1d-restricted recognition of alpha-galactosyl-ceramide by human CD4(+) and CD8alphabeta(+) T lymphocytes. ***J Immunol*** 168, 5514-5520 (2002). Gadola SD, Dulphy N, Salio M, Cerundolo V

3) Human CD1d-glycolipid tetramers generated by in vitro oxidative refolding chromatography. ***Proc Natl Acad Sci U S A***, 98:3294-3298 (2001). Karadimitris A, Gadola SD (SDG and AK joint first authors), Altamirano M, Brown D, Woolfson A, Klenerman P, Chen J, Koezuka Y, Roberts IAG, Dusheiko G, Milstein C, Fersht A, Luzzatto L, Cerundolo V

4) Structure of human CD1b with bound ligands at 2.3 A, a maze for alkyl chains. ***Nature immunology*** 3, 721-726 (2002).Gadola SD, Zaccai NR (SDG and NRZ joint first authors), Harlos K, Shepherd D, Castro-Palomino JC, Ritter G, Schmidt RR, Jones EY, Cerundolo V

Index

1	**Background**	**1**
1.1.	**Antigen presentation by MHC class I molecules**	**1**
1.1.1.	The concept of Innate and adaptive immune receptors in higher vertebrates	1
1.1.2.	Immune receptors of adaptive cellular immunity	3
1.2.	**Introduction to MHC class I molecules**	**4**
1.3.	**The role of MHC class I molecules for immune surveillance**	**6**
1.4.	**Molecular interaction of MHC/peptide complexes with NK receptors**	**8**
1.5.	**TCR structure and molecular interaction with MHC/peptide complex**	**10**
1.6.	**MHC class I processing and presentation pathway**	**13**
1.6.1.	Origins of peptide supply to MHC class I molecules	13
1.6.2.	Routes of protein degradation in the cytosol	13
1.6.3.	Cytosolic proteases	15
1.6.4.	Peptide trimming in the ER	18
1.7.	**The MHC class I biosynthetic pathway**	**19**
1.7.1.	Early folding stages of MHC class I molecules in the ER	21
1.7.2.	The peptide loading complex (PLC)	25
1.7.3.	The Transporter associated with Antigen Processing/Presentation: TAP	26
1.7.3.1.	*TAP function*	*27*
1.7.3.2.	*TAP structure and function*	*29*
1.8.	**Tapasin**	**32**
1.9.	**Type 1 Bare Lymphocyte Syndrome**	**34**
1.10.	**Antigen presentation by CD1 molecules**	**35**
1.10.1.	A short history of the discovery of CD1 as a third line of antigen presentation	35
1.10.2.	Group 1 and group 2 CD1 proteins	38
1.10.3.	Classes of CD1 ligands	40
1.10.4.	CD1 protein structures	45
1.10.5.	CD1 ligand loading and intracellular trafficking	50
1.10.6.	CD1 restricted T cells	53
1.10.6.1.	*Group 1 CD1 restricted T cell responses*	*53*
1.10.6.2.	*CD1d restricted T cells*	*54*
1.10.6.2.1.	Definition and phenotype of iNKT cells	54
1.10.6.2.2.	Possible roles for iNKT cells in health and disease	56
1.10.6.2.3.	Molecular interaction of iNKT cells with antigen presenting cells	62

1.11.	**Objectives of the thesis**	**64**
2	**Methods**	**65**
3	**Six patients with defective MHC class I cell surface expression due to C-terminal truncation of TAP1 or TAP2 proteins**	**89**
3.1.	**Introduction**	**89**
3.2.	**Results**	**93**
3.2.1.	Clinical data	93
3.2.2.	Phenotype of peripheral blood mononuclear cell subsets	101
3.2.3.	Analysis of the MHC class I biosynthetic pathway	103
3.2.4.	Additional studies	109
3.2.4.1.	Functional activity of NK and γδ T cells	109
3.2.4.2.	Immunohistochemistry of skin lesions	111
3.3.	**Discussion**	**112**
3.4.	**Conclusions**	**116**
3.5.	**Acknowledgements**	**117**
4	**Type 1 Bare Lymphocyte Syndrome due to a splice donor site mutation in TAP2**	**118**
4.1.	**Introduction**	**118**
4.2.	**Results**	**118**
4.2.1.	Family history	118
4.2.2.	Clinical data	119
4.2.3.	Molecular Analysis of EBV-transformed B-lymphoblasts from patient "BS"	122
4.2.4.	Genetic analysis of TAP2 in "BS" B-cells	129
4.3.	**Discussion**	**137**
4.4.	**Conclusions**	**139**
4.5.	**Acknowledgements**	**140**
5	**Generation and Validation of human recombinant CD1d-tetramers made from inclusion body proteins and their use to study TCR Vα24+ and TCR Vα24- CD1d-restricted T lymphocyte populations in humans**	**141**
5.1.	**Introduction**	**141**
5.2.	**Results**	**143**
5.2.1.	Generation and validation of recombinant human CD1d/α-GalCer-tetramers	143
5.2.1.1.	Refolding of CD1d/lipid complex	144

5.2.1.2.	Specificity of CD1d/α-GalCer tetramers for human Vα24+Vβ11+ iNKT cells	146
5.2.1.3.	Sensitivity of CD1d/α-GalCer tetramers for human Vα24+Vβ11+ iNKT cells	149
5.2.1.4.	Cross-species reactivity of CD1d/α-GalCer tetramers for mouse iNKT cells	152
5.2.2.	Tetramer-aided identification and characterization of CD1d/α-GalCer specific Vα24-Jα18 independent, non-invariant human CD8αβ+ and CD4+ T lymphocytes	154
5.2.2.1.	Expansion of CD1d/α–GalCer specific Vα24-independent T cells *in vitro* from healthy donors' PBMC	155
5.2.2.2.	TCR Vα- and TCR Vβ repertoire of Vα24- CD1d-α–GalCer specific T cells	158
5.2.2.3.	Functional analysis of Vα24- CD1d/α–GalCer specific T lymphocytes	164
5.2.2.4.	CD4/CD8-coreceptor use and CD161-expression by Vα24-CD1d/α–GalCer specific T cells	167
5.2.2.5	Differential binding of CD1d/α-GalCer monomers to CD8αβ+ Vα24- and CD4-CD8- (DN) Va24+ CD1d/α-GalCer specific T cells	170
5.3.	**Discussion**	**172**
5.4.	**Conclusions**	**177**
5.5.	**Acknowledgements**	**178**
6	**Refolding and structure determination of recombinant lipid-loaded human CD1b molecules**	**179**
6.1.	**Introduction**	**179**
6.2.	**Results**	**181**
6.2.1.	CD1b refolding and crystallisation	181
6.2.2.	The structure of human CD1b with bound ligands	185
6.2.2.1.	Structural features of the CD1b binding groove	185
6.2.2.2.	Functional recognition surfaces of CD1b-PI and CD1b-GM2	189
6.2.2.3	Comparison of human CD1b and mouse CD1d structures	190
6.2.2.4.	Implications for other CD1 alleles and glycolipid ligands	193
6.3.	**Discussion**	**196**
6.4.	**Conclusions**	**199**
6.5.	**Accession codes for human CD1b/ligand structures**	**200**
6.6.	**Acknowledgements**	**200**
7	**Conclusions and future perspectives**	**201**
8	**References**	**206**

Figures

Figure	Description	Page
Figure 1	MHC class I molecules are ligands for different types of immune receptors	9
Figure 2	CDR loops of a human αβTCR contacting the MHC/peptide complex	11
Figure 3	The mammalian 20S proteasome structure	17
Figure 4	MHC class I assembly (Overview)	20
Figure 5	TAP structure and function	30
Figure 6	Different classes of CD1 ligands	44
Figure 7	MHC class I and CD1 extracellular domain organisation	45
Figure 8	CD1 lipid binding grooves	47
Figure 9	A TCR's view onto CD1/ligand and MHC/ligand molecular surfaces	49
Figure 10	Definition of the CD1d-restricted invariant Natural Killer T cells (iNKT)	55
Figure 11	Role for iNKT cells in systemic tolerance via immuneprivileged sites	60
Figure 12	CD1d recognition by iNKT TCR	63
Figure 13	Crystals of human CD1d and iNKT TCR/CD1d proteins	88
Figure 14	Clinical manifestations in patient "AK"	94
Figure 15	Clinical manifestations in patient "FT"	96
Figure 16	Mutilation of the midface in Type 1 Bare Lymphocyte Syndrome	97
Figure 17	Bronchiectasis in type 1 BLS (patient "GAB")	98
Figure 18	Mutilating granulomatous skin lesions in patient "GAB"	99
Figure 19	chronic sinusitis in type 1 BLS (patient "SAB")	100
Figure 20	MHC class I expression on B-lymphoblasts in type 1 BLS	103
Figure 21	Pulse chase and isoelectric focusing analysis in patient "AK"	104
Figure 22	Peptide translocation in 4 patients with type 1 BLS	105
Figure 23	TAP and Tapasin expression in 5 patients with type 1 BLS	106
Figure 24	TAP-encoding vaccinia virus restores MHC class I surface expression	108
Figure 25	Activity of NK and γδ T cells in TAP deficiency	110
Figure 26	Immunohistochemistry of TAP-deficient granulomatous lesions	111
Figure 27	MHC class I surface expression in "BS", "NP", "AK", "GAB" and "NV"	123
Figure 28	Molecular analysis of the PLC in patient "BS"	125
Figure 29	Defective peptide translocation in "BS" B-lymphoblasts	127
Figure 30	Complementation of TAP1/TAP2 function in B-cell fusions	129

Figure 31	RT-PCR analysis of "BS" TAP2E	131
Figure 32	Analysis of aberrant alternative splicing of the TAP2E gene in"BS"	133
Figure 33	Predicted TAP2 protein sequence and domain organisation in "BS"	135
Figure 34	Purification of refolded CD1d/β2m/α-GalCer monomers	145
Figure 35	ELISPOT analysis of Vα24+Vβ11+ invariant NKT (iNKT) lines	146
Figure 36	CD1d/α-GalCer tetramers specifically detect Vα24+Vβ11+ T cells in humans	148
Figure 37	Ex vivo detection of iNKT cells with CD1d/αGC-tetramers	150
Figure 38	Detection of human iNKT cells in liver cirrhosis tissue samples	151
Figure 39	Cross-species reactivity of human CD1d/a-GalCer tetramers	153
Figure 40	*In vitro* expansion of Vα24- CD1d/α–GalCer tetramer+ T cells	157
Figure 41	Sorting of Vα24- CD1d/α–GalCer tetramer+ T cell clones and lines	158
Figure 42	Vβ11 usage by Vα24- CD1d/α-GalCer+ T lymphocytes	159
Figure 43	Spectratype analysis of a Vα24-negative, CD1d/α-GalCer-tetramer+ T cell line	160
Figure 44	Specificity of binding of CD1d/α–GalCer tetramers to Vα24- T cells	163
Figure 45	Lysis of α-GalCer pulsed CD1d+ targets by Va24- T lymphocytes	164
Figure 46	Cytokine production by α-GalCer specific Vα24- and Va24+ T cells	166
Figure 47	Co-receptor and CD161 expression on Vα24- and Vα24+ T cells	168
Figure 48	CD8 dependent killing by CD8αβ+ Vα24- CD1d/α-GalCer specific T lymphocyte lines	169
Figure 49	CD1d/α-GalCer Monomer binding to Vα24+ and Vα24- T cells	171
Figure 50	Refolding of human CD1b with and without added lipid ligands	183
Figure 51	Protein crystals of human CD1b/lipid complex	184
Figure 52	Structure of two different human CD1b/β2m/ligand complexes	187
Figure 53	Structural details of the human CD1b/PI structure	188
Figure 54	Headgroups of CD1b-bound GM2 and PI	189
Figure 55	Comparison of human CD1b and mouse CD1d structures	192
Figure 56	Sequence alignment of different CD1 isoforms	194
Figure 57	Models for binding of mycolic acid and triacylglycerol to human CD1b	195

Tables

Table	Description	page
Table 1	Herpes virus proteins targeting TAP	29
Table 2	HLA haplotype in patients with type 1 Bare Lymphocyte Syndrome	92
Table 3	Lymphocyte subsets in type 1 BLS: Patients and healthy relatives	102
Table 4	Spectratype analysis of Vα24- CD1d/α-GalCer tetramer+ T cells	161
Table 5	Statistics for data collection and refinement of CD1b crystal structures	186

Abbreviations

ABC	ATP-binding cassette
ACAID	anterior chamber-associated immune deviation
ANCA	anti-neutrophilic granulocyte cytoplasmic antibodies
AP-2, AP-3	adaptor protein complex-2, -3
APC	allophycocyanin
APC	antigen presenting cell
ATP	adenosine triphosphate
β2m	β2-microglobulin
BAP31	Biotinylation/IgD/IgM/membrane-associated protein 31
BCG	Bacillus Calmette-Guérin
BCR	B cell receptor
β–GalCer	β-Galactosylceramide
BiP	immunoglobulin binding protein
BLS	bare lymphocyte syndrome
C, e.g. C16	carbon atom, e.g. sixteen carbon atoms
CD	cluster of differentiation
CDS	coding sequence
CFTR	cystic fibrosis transmembrane conductance regulator
CMV	cytomegalo virus
Cnx	Calnexin
COPI or COPII	coatomer protein complex I or II
Crt	calreticulin
CT	computed tomography
CTAB	cetyl (or hexadecyl-)triammonium bromide
DC	dendritic cell
Der1in	Der-1 like protein
Didehydroxymycobactin	DDM
DN	double negative (for CD4 and CD8 expression)
DP	double positive (for CD4 and CD8 expression)
DRiPs	defective ribosomal products
DsbA	disulfide isomerase
EAE	experimental autoimmune encephalomyelitis
EBV	Epstein-Barr virus
EDEM	ER degradation enhancing mannosidase-like protein
EEG	electroencephalogram
ER	endoplasmic reticulum
ERAAP or ERAP	ER associated amino peptidase

ERAD	ER-associated degradation
ERGIC	ER/Golgi intermediate compartment
ERp57	ER-resided protein 57
FACS	Fluorescent activated cell sorter
FCS	fetal calf serum
Gal	Galactose
γ-IRE_CS	Interferon-γ response element consensus sequence
Glc	Glucose
GlcNAc	N-acetylglucosamine
GM	monosialoganglioside
GMM	glucomonomycolate
GPI	glycosylphosphatidylinositol
GSL	glycosphingolipid
HLA	histocompatibility leukocyte antigen
HSP	heat shock protein
HSV	herpes simplex virus
htm1	homologous to mannosidase I
ICAM-1	Intercellular adhesion molecule 1
ICP47	infectious virion particle 47
IFN	interferon
Ig	Immunoglobulin
iGb3	isoglobotrihexosylceramide
IL	interleukin
ILT	Immunoglobulin-like transcript
IPGT	Isopropylthiogalactoside
iNKT	NKT cell with an invariant TCRα chain
kDA	kilodalton
KIR	killer inhibitory receptor
KRN7000	Kirin 7000, a C24/C18 alpha-galactosylceramide
LAM	lipoarabinomannan
LCL	lymphoblastoid cell line
LFA-1	lymphocyte function-associated antigen-1
li	invarant chain
LLT1	lectin-like transcript-1
LMP (LMP2 or 7)	Low molecular weight protein
LPS	lipopolysaccharide
MA	mycolic acid
Man	Mannose
μCi	micro Curie
MDR	multidrug resistance
MHC	major histocompatibility class

MRI	magnetic resonance imaging
mRNA	messenger RNA
MS	multiple sclerosis
MTB	mycobacterium tuberculosis
MTP	microsomal triglyceride transfer protein
NAC	Nascent polypeptide associated complex
NBD	nucleotide binding domain
NF-IL-6	Nuclear factor for expression of Interleukin-6
NK	Natural killer
NOD	Nucleotide Oligomerization Domain
P	position (of a residue in a peptide)
P domain	proline-rich domain
PAMPS	pathogen associated molecular patterns
PBL	peripheral blood lymphocytes
PBMC	peripheral blood mononuclear cells
PBS	phosphate buffered saline
PCR	polymerase chain reaction
PDB	protein data base
PDI	protein disulfide isomerase
PE	phycoerythrin
PE	phosphatidylethanolamine
PHA	phytohemagglutinine
PI	phosphatidylinositol
PIM	phospatidylinositol mannoside
PLC	peptide-loading complex
pMHC	peptide-MHC complex
PPARγ	Peroxisome Proliferator-Activated Receptor-gamma
PPBF	phenyl-pentamethyldihydrobenzofurans
PPD	purified protein derivate
PR3	proteinase 3
PRRs	pattern recognition receptors
PSF	peptide supply factor (first name of TAP)
RA	rheumatoid arthritis
RAC	HSP70-associated ribosome associated complex
RANTES	new name: Chemokine ligand 5
RNA	ribonucleic acid
R-PE	phycoerythrin
RT-PCR	reverse transcribed PCR
SDS	sodium dodecyl sulfate
SDS-PAGE	SDS-polyacrylamide gel electrophoresis
SEC	size exclusion chromatography

SLE	systemic lupus erythematosus
SNP	single nucleotide polymorphism
STAT6	Signal transducer and activator of transcription 6
TAP	transporter associated with antigen processing
TB	tuberculosis
TCR	T cell receptor
Th1	T helper 1
Th2	T helper 2
TLR	toll like receptors
TM	transmembrane domain (in TAP)
TNF	tumor necrosis factor
Tpn	tapasin
TR	thioredoxin
Vα24-Jα18	invariant rearrangement of the iNKT TCR alpha chain
Vβ11	variable beta chain family 11
VCV	varicella virus
VHS	virion host gene shut-off

1. Background

1.1. Antigen presentation by MHC class I molecules

1.1.1. The concept of Innate and adaptive immune receptors in higher vertebrates

The immune system of higher vertebrates comprises two principal mechanisms to differentiate "self" from both "non-self" and "altered self", namely the innate and the adaptive immune systems. As the name indicates, the innate immune system relies on a repertoire of germline encoded, and therefore limited set of receptors, which recognize pathogen associated molecular patterns (PAMPs). Innate receptors are therefore also referred to as pattern recognition receptors (PRRs). PRRs have evolved to ensure highly reliable recognition of pathogen associated structural elements, that can't be easily mutated by the pathogens, such as bacterial carboydrates, peptidoglycan, glycolipids, or bacterial and viral nucleotides. Prototypical PRRs include the toll-like receptors (TLRs) which can bind to PAMPs either at the cell surface or intracellularly, and the cytosolic NOD-like receptors [1]. Activation of the innate immune system by PAMPS via innate receptors is of key importance for effective activation of adaptive host defense responses. Consistently, PRRs are preferentially expressed on such immune cells which arrive very early, within a few hours, at the site of inflammation, e.g. neutrophilic granulocytes, macrophages, and dendritic cells. Inherited mutations in genes encoding TLRs or NODs are associated with both susceptibility to infectious disease [2] and autoinflammatory bowel syndromes [3].

An important limitation of the innate immune system is the limited diversity of the repertoire of canonical receptors, and the limited ability to recognise "altered self".

Importantly, the innate immune system is not sufficient to ensure full protection against pathogens. This is illustrated in children with defined primary immune deficiencies of the innate immune system's counterpart, i.e. the adaptive immune system. These children suffer from very severe bacterial, fungal, parasitic, and viral infections [4].

The appearance of the adaptive (synonym: acquired) immune system coincides with the emergence of jawed vertebrates (Gnáthostomata), which were first to use Recombination Activating Genes (RAG) 1 and 2 to generate random T- and B-cell receptors (TCRs and BCRs) by way of somatic recombination of a limited set of germline encoded variable (V), diversity (D), joining (J), and constant (C) gene segments [5]. The main function of jaws, i.e. chewing food, bears considerable risks since the delicate mucosal barrier of the mouth can be easily wounded by mechanical stress, allowing a wide range of pathogens to enter the blood circulation. The greater diversity of antigens that can be "seen" by an immune system employing random receptors might therefore be an essential requirement to defend the host from the broad range of pathogens entering the blood circulation of jawed vertebrates.

However, there are other valuable hypotheses why random T- and B-cell receptors have been added to the immune system's armory. Invasive tumors, like the adaptive immune system, are also limited to jawed vertebrates [6]. Some invasive tumors in animals, such as the facial tumors that can afflict the Tasmanian devil or the invasive venereal tumors affecting dogs are transmissible [6, 7]. Thus, the adaptive immune system might have evolved to better protect the host from tumors.

1.1.2. Immune receptors of adaptive cellular immunity

In contrast to the innate immune system the adaptive immune system employs a virtually unlimited diversity of antigen receptors, i.e. TCRs and BCRs, which are the hallmarks of T-lymphocytes and B-lymphocytes, respectively. The specific functions of T- and B-lymphocytes are crucially dependent on the ability of their T- and B-cell receptors (TCRs, BCRs) to recognise antigen.

The protein structure of both TCRs and BCRs is dominated by immunoglobulin (Ig-) like domains, i.e. antiparallel beta-sheets arranged in a "greek key" pattern, and both types of receptors share many highly conserved framework residues [8]. However, while BCRs can be secreted by B-lymphocytes and are able to bind free antigens in the blood or tissues, TCRs require the antigen to be presented by specialised endogenous antigen presenting molecules on the surface of other cells [9].

The first and still best known class of antigen presenting molecules are the histocompatibility leukocyte antigen (HLA) class I and class II molecules, which are encoded within the major histocompatibility complex (MHC) on the short arm of chromosome 6. They are therefore also called MHC class I and class II molecules. MHC class I molecules have a quaternary structure with an HLA class I heavy chain (HC) and a beta-2 microglobulin light chain (β2m), whereas MHC class II molecules are heterodimers of one α and one β HLA class II heavy chain [10]. Despite these differences MHC class I and class II molecules share a highly similar three dimensional protein structure, the key feature of which is an antigen binding domain built from two alpha-helices overlaying beta-pleated sheets.

Furthermore, both MHC class I and MHC class II molecules present short peptides to T-lymphocytes [11], albeit of slightly different length. However, MHC class I and class II molecules differ in their ability to interact with CD4, CD8αα and CD8αβ co-receptors of CD4+ and CD8+ T-lymphocytes, respectively [12]. The co-receptor of CD4+ T-lymphocyte binds to the extracellular portion of the α heavy chain (more precisely the α3 domain) of HLA class II molecules, while CD8 co-receptors bind to the extracellular α3 domain of the heavy chain of HLA class I molecules [13, 14]. Although both types of co-receptors do participate in the encounter between T-lymphocytes and an MHC molecule expressing antigen presenting cells, their contribution to the overall binding avidity of this interaction is very low compared to the avidity provided by the binding of the TCRs to the antigen presenting MHC/peptide complexes [15]. In fact, the binding kinetics of a T-lymphocyte's TCR to its cognate MHC/peptide complex(es) determines both the T-lymphocytes selection in the thymus and its functional activation in the periphery.

In the following sections I shall focus on antigen presentation by MHC class I molecules.

1.2. Introduction to MHC class I molecules

The function of MHC class I molecules as antigen presenting molecules is underpinned by the three-dimensional structure of their extracellular domains. These domains are formed by a single heavy chain and consist of a membrane proximal α3 domain, which is non-covalently associated with β2m, and two membrane distal alpha domains (α1 and α2) which form the peptide binding groove. The peptide binding

groove comprises six defined pockets, A', B', C', D', E' and F', designed for specific interaction with certain amino acid side chains [10].

Different isoforms of MHC class I molecules, namely HLA-A, -B, -C, -E, -F, –G, and –H (HLA-H is a pseudogene), are encoded within the HLA locus on human chromosome 6. HLA-A, -B, and –C are highly polymorphic, whereas the other isoforms exhibit limited allelic polymorphism (http://www.anthonynolan.org.uk/HIG/lists/class1list.html). HLA-A, -B-, and –C are commonly referred to as "classical" MHC class I molecules, and HLA-E, -F, and –G are called "non-classical" MHC class I molecules. The very prominent polymorphism of classical MHC-class I molecules is thought to reflect their ongoing exposure to significant evolutionary pressure exerted by frequent mutations, i.e. counter-adaptations, of viruses. Conversely, the limited polymorphism of non-classical MHC class I molecules suggests they are involved in immunoregulatory processes, via interaction with NK receptors, rather than host defence to viruses.

As every person has inherited one set of HLA class I alleles from the mother and one from the father the HLA class I haplotype of an individual comprises 3 to 6 different HLA-A, -B, and –C alleles. The statistical likelihood of having 2 identical sets of parental HLA class I alleles is extremely low, unless the parents are first degree relatives.

Importantly, the polymorphic residues in MHC class I-molecules significantly contribute to the structure of the peptide binding groove and therefore the peptide selection of different MHC class I alleles.

The N- and C-termini of MHC class I bound peptides are anchored within the A' and F' pockets, respectively via specific peptide residues. These "anchor residues" of the peptides are typically located at positions P2-P5 for the N-terminal anchor and the peptide's C-terminal position, e.g. P9 of a nonamer peptide, for the C-terminal anchor [16].

MHC class I molecules typically bind short peptides of 8-11 amino acids, but longer peptides, up to 14 amino acids long, can be presented by some MHC class I molecules to CD8+ T cells. Longer peptides such as the HLA-B*3501 bound 11-mer peptide "EPLPQGQLTAY" are anchored via the same positions and the more central parts of such long peptides bulge out of the groove [17]. Interestingly, the conformation of bulged peptide is flexible and the peptide can be flattened upon T cell receptor binding [18].

The peptide anchor residues vary according to the specific MHC class I molecule. For example, HLA-A2 prefers hydrophobic anchor residues, while others use proline anchors (HLA-B7 and HLA-B35) or basic amino acid anchors (e.g. HLA-A3).

Different MHC class I molecules also exhibit significant differences in their dependency on the proteasome, the peptide loading complex and N-glycosylation, as well as in the speed with which they traffic from the ER to the cell surface.

1.3. The role of MHC class I molecules for immune surveillance

While their role in antigen presentation is widely known recent studies have demonstrated that MHC class I molecules are also involved in non-immunological

areas of vertebral biology, namely mating selection [19] and inter-neuronal signalling [20]. In the following I shall keep the focus on their role in host immunity.

Classical MHC class I molecules can present "normal self" as well as tumour- and pathogen-derived peptides to specific cytotoxic CD8+ T-lymphocytes. Specific HLA class I haplotypes are associated with auto-inflammatory diseases, cancer susceptibility and protection against viruses [21-26], supporting the notion that MHC class I molecules are involved in immune surveillance. Furthermore, an indirect yet very persuasive indication for the importance of MHC class I molecules in host defense is the variety of highly sophisticated mechanisms employed by different viruses to subvert presentation of viral peptides by MHC class I molecules (reviewed in [27]). Similarly, MHC class I/peptide presentation is severely suppressed in many malignant tumor cell lines strongly suggesting a role for MHC class I molecules in tumor immune surveillance [28].

While cell surface expressed MHC class I molecules actively report to T-lymphocytes on the presence of intracellular peptides of viral or tumor cell origin, the absence of MHC class I molecules from the cell surface, i.e. "missing self", can trigger innate immune responses by unleashing Natural Killer (NK) cell activation [29]. NK cells are innate-type lymphocytes which can exert strong cytokine secretion and cytolytic activity. They specifically express different sets of germline encoded receptors that bind to MHC class I molecules, namely Killer Inhibitory Receptors (KIRs) and C-type lectin receptors. Both inhibitory KIRs and inhibitory C-type lectin receptors, such as CD94/NKG2A, contain Immunoreceptor Tyrosine-based Inhibitory Motifs (ITMs) in their cytoplasmic domains [30, 31]. Binding of MHC class I molecules

to these receptors delivers a negative signal that inhibit killing by NK cells and certain T cells, e.g. γδ T lymphoctes. The classical MHC class I molecules HLA-A, -B, and -C, in particular HLA-C alleles, bind to inhibitory KIRs. Conversely, the non-classical MHC class molecule HLA-E is a ligand for the inhibitory C-type lectin NK receptors CD94/NKG2A, CD94/NKGK2B and CD94/NKG2C, but not for KIRs [32], and HLA-G can interact with both KIRs and C-type lectins. A third group of germline encoded inhibitory receptors, widely expressed on leukocytes comprises the Immunoglobulin-like transcript (ILT) receptors ILT-2 and ILT-4, which have been demonstrated to bind to the classical MHC class I molecules HLA-A and –B, as well as to HLA-G, -E, and –F [33]. ILT-2 is the only ILT expressed on NK cells. Similar to KIRs and CD94/NKG2A ILT-2 and ILT-4 deliver negative signals to ILT-2 and ILT-4 expressing NK cells and cytotoxic T cells [34] which prevent them from killing MHC class I expressing cells.

1.4. Molecular interaction of MHC/peptide complexes with NK receptors

The available crystal structures of peptide-loaded MHC molecules in complex with either KIRs or C-type lectins show different modes of binding (Figure 1). The crystal structure of the complex formed by KIR2DL2 and HLA-Cw3 (PDB entry 1efx) shows some similarities with TCR-MHC/peptide structures. KIR2DL2 docks onto the C-terminal part of the MHC/peptide groove in an almost orthogonal orientation across the alpha1 and alpha2 helices of HLA class I molecules [35]. Interestingly, the germline encoded KIR makes contacts with residues at position P7 and P8 of the MHC bound peptides. Earlier functional studies had suggested that the bound peptide can influence

the lysis of target cells by NK cell clones [36]. In contrast to KIR binding, the murine C-type lectin receptor Ly49c binds to the alpha3 domain of the mouse MHC class I molecule $H2K^b$, away from the binding site of either KIRs or TCRs [37]. Atomic structures of ILT:MHC/peptide

Figure 1. MHC class I molecules are ligands for different types of immune receptors

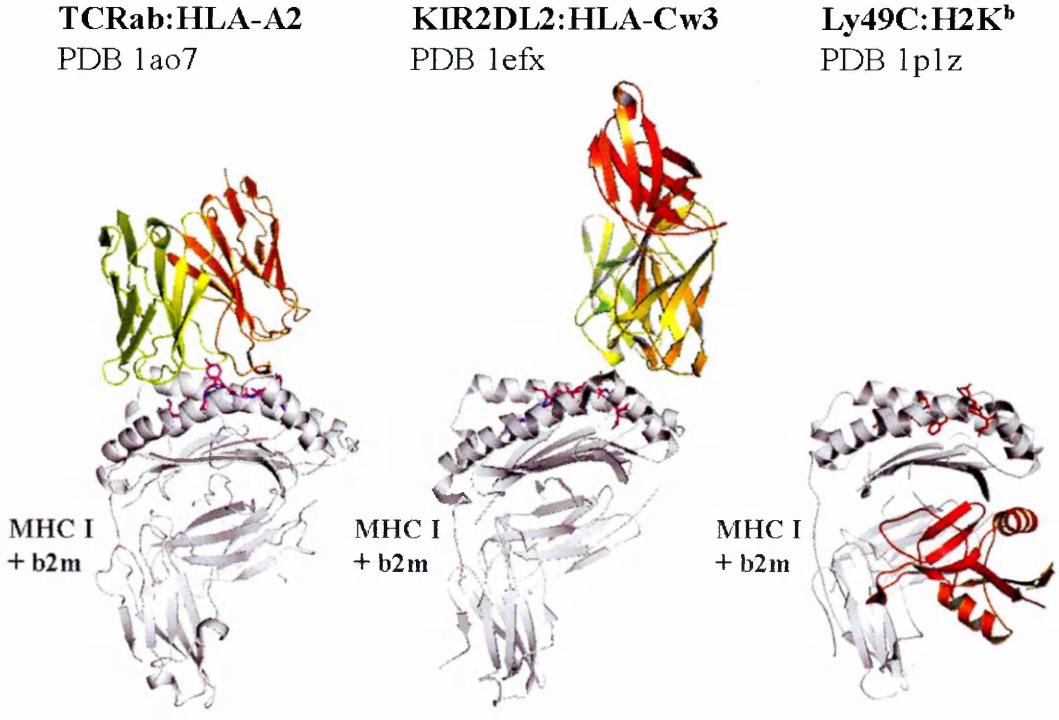

Ribbon diagrams of three atomic structures of MHC class I molecules (in grey colour) and bound immune receptors (in orange and yellow colour). The first solved structure of a human HLA-A2/peptide complex with bound αβTCR[38] (only variable domains are shown) is shown on the left-hand side. Human HLA-Cw3 in complex with a killer inhibitory receptor[35] (KIR2DL2) is shown in the middle, and the mouse MHC class I molecule H2Kb in complex with a C-type lectin receptor[37] is shown on the right-hand side. The figure was created using the indicated PDB files using PyMol software.

complexes have not yet been solved, but functional data have shown that both ILT-2 and ILT-4 effectively compete with CD8 for MHC class I binding, indicating that they both bind to the alpha3-domain and/or β2m [39].

1.5. TCR structure and molecular interaction of TCRs with MHC/peptide complex

TCRs are heterodimers of two heavy chains, each of which is constructed from two immunoglobulin-like domains. The main classes of TCR heterodimers in humans are TCRαβ and TCRγδ. The membrane distal Immunoglobulin-like domains in both classes are encoded by rearranged V-, J-, and D- gene segments. These "variable" domains make direct contact with the antigenic surface and are highly polymorphic (Figure 1 and 2) [38, 40]. In contrast, the membrane proximal "constant" domains, the transmembranous and the cytosolic domains, all of which are encoded by C-gene segments, are nonpolymorphic. The antiparallel beta-strands of the variable TCR domains are connected via highly polymorphic flexible loop structures. These loops determine the shape complementarity between the TCR and the MHC/peptide complex and are hence called complementarity determining region (CDR) loops. Three CDR loops (CDR1, 2, and 3) of each TCR heavy chain are involved in direct antigen contact. The CDR3 loops exhibit by far the highest structural diversity. They are encoded by randomly rearranged V-, J-, and D- gene segments, while the less diverse CDR1 and CDR2 loops are encoded by V-gene segments only. On the other hand, the diversity of the CDR3 loops can be increased by at least ten-fold through random template independent nucleotide insertions and deletions at the V-, J-, and D-gene segment junctions via a terminal deoxynucleotidyl transferase (TdT) [41].

Figure 2. CDR loops of a human αβTCR contacting the MHC/peptide complex

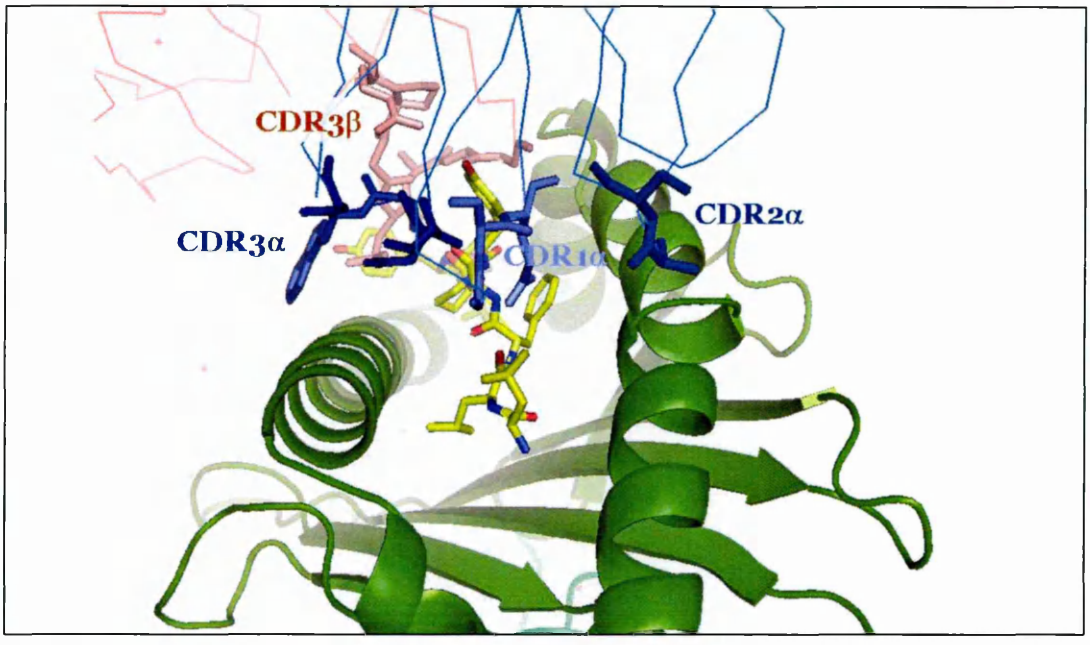

Close-up view of the first solved structure of a complex between human T-cell receptor, a viral peptide and HLA-A2[38] *(PDB accession code 1AO7). The α1/α2 antigen binding domain of HLA-A2 is shown as a ribbon diagram in green colour and the HLA-A2 bound viral peptide is represented as sticks with carbon atoms in yellow, nitrogens in blue and oxygens in red. The T-cell receptor alpha chain is coloured salmon and the beta chain is coloured in blue. The CDR loops are represented as sticks. The figure was generated using PyMol software.*

Crystal structures of mouse and human TCRs and MHC/peptide complexes, both free and in complex with each other have yielded important insights into the molecular basis of antigen recognition by the adaptive immune system[42]. Typically the TCR docks in a diagonal way onto the MHC/peptide complex surface, thereby

allowing contacts between the TCR and both the MHC molecule and the bound peptide antigen. Still unexplained is the fact that the variable alpha chain of the TCR is located more over the N-terminal part of the peptide, while the variable beta chain is situated more over the C-terminal part of the peptide. The hypervariable CDR loops mediate all TCR contacts with the MHC/peptide accessible molecular surface area. In most TCR-MHC/peptide structures to date the CDR3 loops make most contacts with the peptide, while the CDR1 and CDR2 loops make more contacts with the MHC protein surface. Of note, neither the CDR loops nor the MHC/peptide surface are rigid surfaces and both can undergo significant conformational changes upon ligation. Still, the shape complementarity (i.e. geometric fit) of the TCR-MHC/peptide interface, even in "higher affinity" TCR-MHC/peptide complexes, is generally low compared to known molecular interfaces of enzymes and their substrates. This is reflected by the relatively low affinity (KD dissociation constant for most TCRs in the range of 1–100 μM) that characterises the binding between TCRs and their MHC/peptide counterparts. An obvious advantage of a low compared to a high avidity is the higher degree of freedom of movement for the T-lymphocyte while it scans the surface of antigen presenting cells. Importantly, in almost all documented cases the MHC bound peptide has a significant impact on both space complementarity and affinity between the TCR and its cognate MHC/peptide complex, as best illustrated in the differential binding of the "2C" TCR to either H-2K^{bm3} or H-2K^{b} [43].

Interestingly, some human TCRs make hardly any contacts with the MHC bound peptide[44]. However, in any case the peptide serves an essential role by stabilising the MHC class I molecule. In fact, without any bound peptide MHC class I

molecules do not reach the cell surface but are retained in the endoplasmic reticulum (ER).

1.6. MHC class I processing and presentation pathway

1.6.1. Origins of peptide supply to MHC class I molecules

The seminal work by Alan Townsend and colleagues in Oxford has revealed that the antigens recognised by T lymphocytes are not whole proteins bound to MHC molecules but rather small peptide fragments[11, 45].

All proteins have a limited half-life and recycling of amino acids and small peptides via cytosolic proteolysis is a vital housekeeping mechanism for every cell which is adjusted constantly to the cell's metabolic rate. Accordingly, genes encoding for the components of the proteolytic machinery of cells are both ancient and highly conserved between all domains of life.

1.6.2. Routes of protein degradation in the cytosol

Most proteins are very rapidly digested in a sequential way by different proteases. In fact the cytosol digests most proteins completely before they have a chance to reach the ER. At least 10,000 copies of a given protein must be expressed in the cell to create a realistic statistical chance for its peptide fragments to reach the ER and be presented by MHC class I on the cell surface. The speed with which proteins are degraded after their synthesis is of different importance for different challenges, e.g. tumors versus acute viral infections. During acute virus infections viral proteins must be processed and their peptides presented on surface MHC class I molecules before the

virus completes its replication cycle – otherwise the whole exercise is futile. This means, that a proportion of freshly made viral proteins must immediately be directed towards proteolysis. It has been recently proposed that a proportion of all newly made self and foreign proteins are led straightaway into a degradation pathway while ribosomal translation is still running. In fact, ca. 30% of newly synthesized proteins are immediately degraded[46]. Two different routes could be taken by such proteins:

The first route is rather time consuming and involves the covalent attachment of polyubiquitin to the doomed protein. This pathway is thought to be taken by incorrectly folded proteins, and these failed attempts of mRNA translation have been called "defective ribosomal products (DRiPs). One problem of this model is that it predicts a bias towards epitopes from proteins with a higher inherent tendency to misfold, while no such bias has ever been discovered in peptide-elution studies. Another problem of the model is that even misfolded viral proteins "survive" at least several hours before they are digested, since they are cared for by heat-shock proteins (HSP) and chaperonins. Still, ubiquitin-tagged proteins are efficiently captured by the 19S cap of the 26S proteasome, unfolded, and digested into 3-10 amino acid long peptides.

An alternative model to the above first route is simpler and more consistent with the time constraints discussed above. According to the alternative model a certain proportion of proteins is translated by ribosomes that are not occupied by ribosome-associated HSP RAC and NAC (RAC: HSP70-associated ribosome associated complex; NAC: Nascent polypeptide associated complex). The polypeptides released from such ribosomes have a very high chance to misfold. The misfolded polypeptide

could be captured by the HSP-like structural components of the 20S proteasome and immediately digested. This stochastic model does not predict a bias in the peptide repertoire presented by MHC class I. molecules and is compatible with the narrow time window for epitope generation during acute viral infection[47].

1.6.3. Cytosolic proteases

The major protease in the cytosol and the nucleus and the only cytosolic carboxypeptidase is the proteasome (Figure 3). Peptide release by cytosolic proteasomes is essential for surface expression of most MHC class I molecules [48]. A few MHC class I molecules, e.g. HLA-A2 can be stabilised by signal peptides in the ER and their surface expression is therefore not totally dependent on the proteasome.

The proteasome can exist in different forms. The basic catalytic core unit is the 20S proteasome, a cylindrical barrel structure made from two identical α7-β7 units. The alpha units contain members of the ATPase family and form a narrow pore, i.e. the entrance to the inner structure, of 13Å diameter. The beta-1, beta-2, and beta-5 subunits have chymotrypsin-like (cleavage behind hydrophobic and aromatic amino acids), trypsin-like (cleavage behind basic amino acids) and peptidylglutamyl peptide activity (cleavage behind acidic amino acids), respectively [49]. As will be discussed below, both TAP and MHC class I molecules prefer peptides with hydrophobic, basic or aromatic C-termini, but not acidic C-terminal amino acids). The beta-1, beta-2, and beta-5 subunits are exchanged by beta-1i (LMP2), beta-2i and beta-5i (LMP7) upon exposure to IFNγ, and this alternative composition is called the immunoproteasome as opposed to the constitutive proteasome. Interestingly, the immunoproteasome exhibits

enhanced chymotryptic and tryptic activity but decreased peptidylglutamyl activity, which should increase the release of TAP- and MHC class I compatible peptides. Most non-hemato-poetic cells contain copies of the constitutive proteasome, while most hematopoetic cells contain a mixture of immunoproteasome and constitutive proteasome.

The "basic" 20S proteasome structure (Figure 3) can accommodate one or two 19S caps, which are dynamically attached to one or both sides of the 20S proteasome. The combined 20S proteasome and 19S cap form the 26S proteasome, which is specialised in the degradation of polyubiquitinated proteins. Ubiquitin efficiently targets proteins to the 26S proteasome but the proteasome can cleave proteins also independently of ubiquitin [50]. The 19S cap unfolds proteins and directs them through the 13Å pore into the catalytic centre.

Figure 3. The mammalian 20S proteasome structure

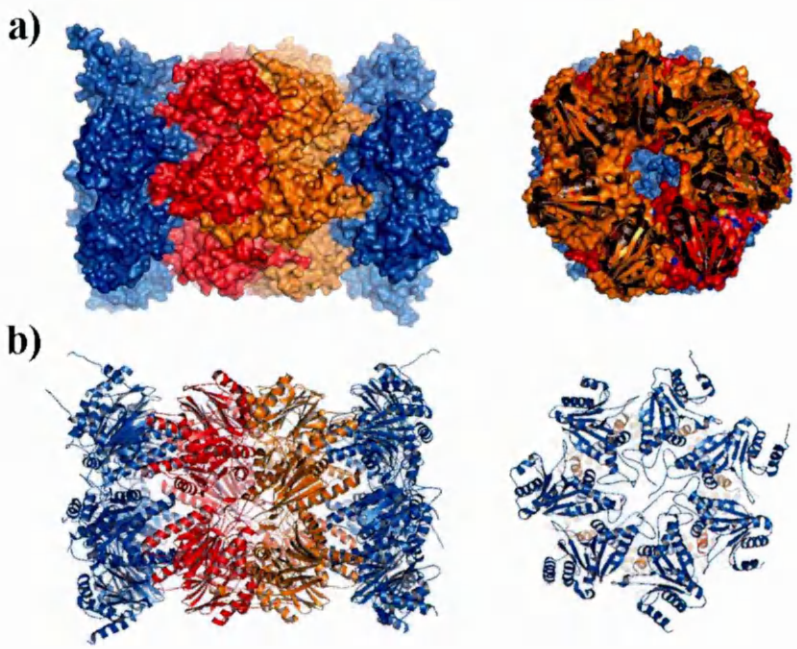

Crystal structure of the bovine 20S proteasome[51] *(PDB ID 1iru) shown as molecular surface (a) and ribbon diagram (b). The outer alpha rings are coloured blue and the inner beta rings in orange and red. (a) The panel on the right shows a crossection through the catalytic center. (b) Each ring is made up of seven subunits (right-hand panel). The figure was created from the original PDB file (1iru) using PyMol software.*

In vitro and in vivo studies of proteasome cleavage have given different results with regard to the length of released peptides. *In vitro* studies found the released peptides to be of 3-20 amino acid length, whereas *in vivo* studies found mainly peptides of more than 15 amino acids length. The latter indicates that peptides released from the proteasome need to be digested further in order to be suitable for MHC class I loading.

Several cytosolic proteases can be involved in this process: Tripeptidyl peptidase II (TPPII) is an aminopeptidase which digests peptides of 6-30, but mainly longer than 15 amino acids length. Although TPPII is the major peptidase involved in the trimming of long antigenic precursors it is not essentially required for all MHC class I antigen presentation. Knockdown of TPPII with gene silencing small hairpin (sh) RNAs leads to a markedly decreased surface expression of many, but not all MHC class I surface[52, 53].

Other cytosolic aminopeptidases include leucine aminopeptidase (LAP), Thymet oligopeptidase (TOP), and neurolysin. All of these are able to generate 9-mer peptides, but could also destroy potential MHC class I ligands. In fact, TOP inhibition with small inhibitory (si)RNA gene silencing markedly increases surface MHC class I expression [54].

1.6.4. Peptide trimming in the ER

Although all cytosolic proteins undergo extensive proteolytic cleavage in the cytosol, many of the resulting peptides reaching the ER are still slightly too long for MHC class I molecules or have suboptimal N-termini. These peptides can be cut to perfect size by the ER resident amino peptidase ERAAP (in humans: ERAP1)[55]. ERAP1 has a broad specificity but prefers 9-16 amino acid long peptide substrates with hydrophobic C-termini[56]. Interestingly, similar to TAP and the immunoproteasome components LMP2 and LMP7, ERAP1 is upregulated by IFNγ. Recent studies have indicated that ERAP1 has an inbuilt "molecular ruler" to suit MHC class I as peptides shorter than 10 amino acids are very poor substrates[57, 58]. In the absence of ERAAP MHC class I

molecules are loaded with unique long peptides of suboptimal affinity. ERAAP might therefore fulfil an important role in editing of the MHC class I bound peptide repertoire. Consistent with this notion, in the absence of ERAAP MHC class I molecules present many highly immunogenic but unstable peptides[59].

Intriguingly, a recent genotype scan of more than 10,000 single nucleotide polymorphisms (SNP) in four different human autoimmune patient groups has found a statistically significant association of two markers residing in the gene encoding ERAAP/ERAP1 (ARTS1) with ankylosing spondylitis, a disease well known for its association with HLA-B27[60].

1.7. **The MHC class I biosynthetic pathway** (Figure 4)

MHC class I molecules are co-translationally integrated into the bilayer of the endoplasmic reticulum (ER). The folding of the MHC class I proteins, including their assembly with β2-microglobulin and acquisition of peptide ligands are assisted by a chaperonin-based refolding and quality control system. Correctly folded MHC class I/β2m/peptide complexes (pMHC) molecules bind to cargo receptors, such as BAP31, and accumulate at ER exit sites [61]. They leave the ER in coatomer protein complex II (COPII-) coated membrane vesicles and traffic via the ER/Golgi intermediate compartment (ERGIC) and the Golgi apparatus to the plasma membrane[62].

Figure 4. MHC class I assembly (Overview)

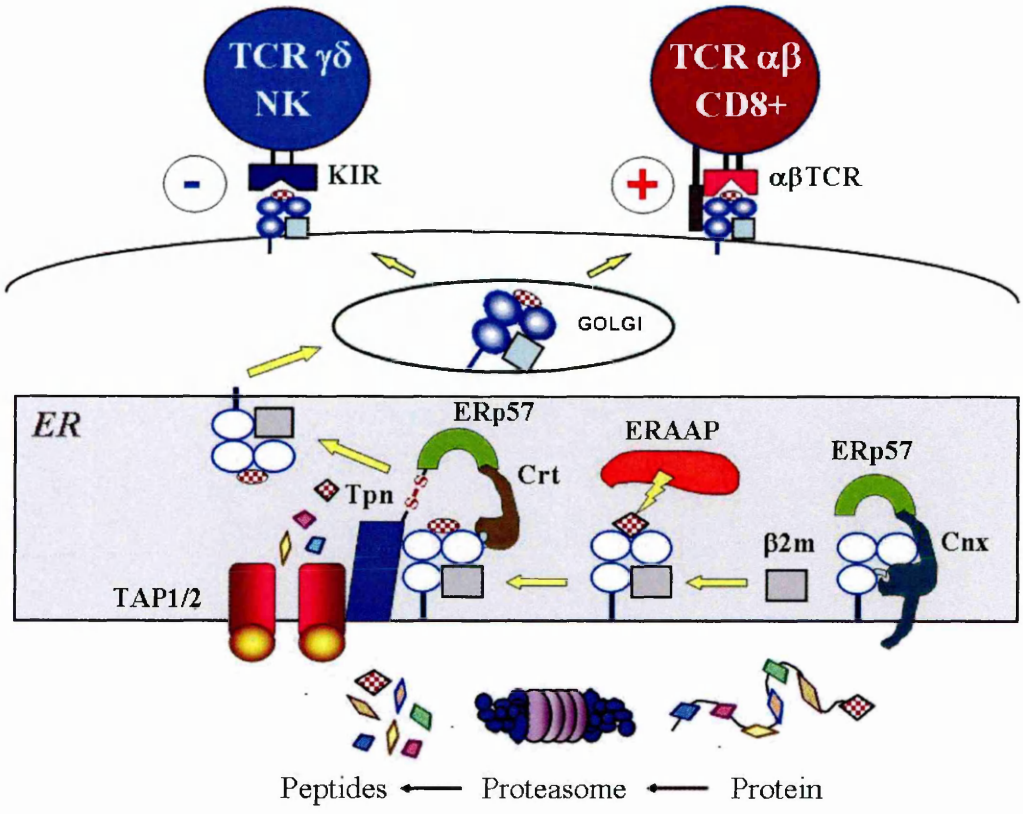

MHC class I assembly in the endoplasmic reticulum (ER). Abbreviations: Cnx, calnexin; ERp57, ER-resided protein 57; Tpn, tapasin; -S-S- symbolizes the disulfide bond between tapasin and ERp57; ERAAP, ER-associated aminopeptidase; Crt, calreticulin; TAP, transporter associated with antigen processing. Negative (-) and positive (+) symbols indicate the inhibitory and activating effects of MHC class I on cell functions on NK cells and CD8+ T cells, respectively.

Improperly folded MHC class I molecules are retained within the ER or are retro-translocated out of the ER to the cytosol via interaction with EDEM/Htm1/Mnl1 and/or Derlin-1[63]. In the cytosol they are degraded by proteasomes. This type of fate of misfolded MHC class I molecules is known as ER-associated degradation (ERAD).

In contrast, proteins that are either incorrectly folded but have escaped the ER, or proteins with incorrect subunit assembly can still be transported back from the ERGIC or Golgi apparatus to the ER by coatomer protein complex I (COPI-) coated vesicles. COPI – coated vesicles are recruited by proteins containing C-terminal di-Lysine motifs, such as tapasin[62, 64].

Similar to other proteins, which are co-translationally integrated into the ER bilayer, the correct folding of MHC class I molecules within the ER is assisted at different stages of the folding process by chaperone proteins, including BiP, calnexin, calreticulin, ERp57 and protein disulfide isomerase (PDI). In addition, assembly of the pMHC is supported by transporter associated by antigen processing (TAP) and by tapasin.

1.7.1. Early folding stages of MHC class I molecules in the ER

Nascent MHC class I polypeptides are first chaperoned and retained in the ER by the immunoglobulin binding protein BiP via BiP's "K-D-E-L" ER retention motif. They undergo post-translational modification by addition of an N-linked glycan to asparagine 89 (N89), which is contained in the consensus sequence "N-X-S/T of the MHC class I heavy chains. The lipid-linked precursor dolichol-PP-$GlcNAc_2Man_9Glc_3$ is used by most eukaryotes as oligosaccharide-donor molecule. After removal of some

glucose and mannose residues by glucosidases I and II the N-linked glycan generally consists of $Glc_1Man_{7-9}GlcNAc_2$ [65]. The protein-linked monoglucosylated oligosaccharide recruits calnexin, a lectin-type, ER-resident membrane bound protein, which replaces BiP as a chaperonin.

Calnexin is known to help the refolding of many different proteins and it can bind to nascent MHC class I molecules before they associate with β2m. However, calnexin plays other roles in physiology, such as Ca2+ storage in the ER. The luminal domain of calnexin consists of a lectin-like N-domain and a stalk-like proline-rich (P-) domain. The C-terminus of calnexin contains an ER-retention signal ("R-K-P-R-R-E") [66], while the P-domain of calnexin is important for binding of another chaperonin to calnexin, i.e. the thiol oxidoreductase ERp57.

Early during the refolding process, before peptides bind to and after β2m associates with the MHC class I heavy chain calnexin is exchanged for calreticulin[67, 68]. Calnexin and calreticulin are homologous proteins and share ca. 40% sequence identity. Like calnexin, calreticulin contains an N- and a P-domain, but it lacks the transmembrane domain and cytoplasmic tail of calnexin. Like BiP the sequence of calreticulin contains a C-terminal "K-D-E-L" ER retention motif [69].

Calreticulin knockout mice show severe failure of cardiac development and all mice die prenatally[70]. However, calreticulin-deficient cell lines are viable and have allowed to assess calreticulin's contribution to peptide loading of MHC class I molecules[71]. The calreticulin deficient mouse fibroblast line K42 exhibits both quantitative and qualitative defects in pMHC surface expression: pMHC clomplexes in K42 are less stable at the cell surface, causing an approximately threefold reduction of

MHC class I surface expression. Interestingly MHC class I molecules in K42 fibroblasts still associate with the transporter associated with antigen processing (TAP) but they are obviously released into the secretory pathway before reaching optimum stability. Calreticulin deficiency cannot be compensated for by calnexin, as overexpression of the latter in K42 is unable to restore a normal phenotype. The different physiological function of the two proteins is also illustrated by the fact that calnexin deficient mice survive up to three month after birth and suffer mainly from the consequences of large myelinated nerve fiber degeneration [72].

The P-domains of calnexin and calreticulin recruit ERp57 to the folding complex (Figure 4)[73, 74]. ERp57 is expressed in many cell compartments, including the ER, the cytosol, the nucleus, and also on the cell surface. On the other hand it serves many cellular functions, e.g. in protein folding, cell metabolism, signaling, and even acts as a cell surface hormone receptor[75-78]. Not surprisingly, ERp57 deficiency (studied in mice) is not compatible with life. An obvious way by which ERp57 could help the folding of pMHC and other proteins is via its capacity to act as both a thiol-dependent reductase and cysteine protease[79, 80]. However, the precise role of ERp57 in the folding of pMHC is still unclear.

ERp57 depletion by RNA interference has only subtle consequences for MHC class I processing and presentation, including slightly delayed heavy chain disulfide bond formation and slowed folding of the heavy chain α3 domain as well as slightly delayed egress of MHC class I molecules from the endoplasmic reticulum to the Golgi [81]. However, the oxidation state of MHC class I molecules is unchanged in ERp57-

deficient cells. It has been suggested that another ER-resident oxidoreductase, ERp72, might support MHC class I folding in the absence of ERp57 [82].

Intriguingly, ERp57 is covalently linked to the ER resident protein tapasin via a stable disulfide bond of its cysteine 57 with tapasin's cysteine 95 [83]. Moreover, IFNγ promotes the association of ERp57 with tapasin [74], suggesting a possible link between immune activation and functional activity of ERp57 in antigen presentation. Of note, ERp57, when bound to other proteins, uses an (oxidoreductase) escape pathway which ensures that the association is short-lived. However, the covalent link of ERp57 with tapasin is stable because of non-covalent links between the two proteins [84].

It has been hypothesized that the firm interaction between ERp57 and tapasin supports the stability of the peptide loading complex (PLC), ensuring longer interaction time between the MHC class I molecule and the PLC, and thereby optimising the loading of peptides onto MHC class I molecules [83]. Consistent with this, one study reported that the assembly of MHC class I into the PLC was strongly reduced in ERp57 deficient primary B cells and immortalized fibroblasts [85]. However, others found that, upon depletion of ERp57 by RNA interference, the peptide loading complex assembled properly, and peptide loading onto MHC class I was apparently normal [81].

Possibly, the unusually stable link between ERp57 and tapasin could serve a rather different purpose: tapasin might actually keep ERp57 in check in order to restrain ERp57 from reducing fully oxidized, peptide-receptive MHC class I/β2m complexes. Full oxidation of the MHC class I heavy chain is a known prerequisite for efficient peptide loading [86]. Conversely, the peptide receptive state of MHC class I

molecules, induced after full oxidation of the heavy chain and association with β2m, is rather unstable. ERp57's thiol-dependent reductase activity might therefore get in the way of efficient peptide loading, unless it is physically separated from peptide-receptive HC by tapasin.

While ERp57, ERp72 and β2m [87] all can independently promote disulfide bond formation in MHC class I, full oxidation of the MHC class I heavy chain, and in particular correct disulfide bond formation in the α2 domain is dependent on protein disulfide isomerase, PDI [88]. Besides a catalytic domain PDI has a functional peptide-binding domain and has been demonstrated to bind peptides and deliver them to MHC class I molecules. In the absence of PDI maturation of MHC class I molecules is clearly delayed and pMHC surface expression is reduced by 40% [88].

1.7.2. The peptide loading complex (PLC)

To exert their role in adaptive immunity MHC class I molecules must assemble with β2m, capture suitable peptide ligands in the ER, achieve a stable quaternary conformation and reach the cell surface. This task is considerably more complex than the refolding of glycoproteins of simple tertiary structure.

The "bottleneck" in the MHC class I antigen presentation pathway is the supply and successful loading of suitable peptides onto MHC class I molecules in the ER. In fact, even an up to 50-fold increase in MHC class I molecule expression has not influence on either the extent of peptide loading or the rate of MHC class I/peptide complex maturation [89]. On the other hand, in the absence of suitable peptide ligands

MHC class I molecules are not able to reach a stable conformation and are retained within the ER.

The peptide loading complex (PLC) is a very large multimolecular complex of proteins [90] which act in concert to ensure peptide supply, peptide selection and peptide loading onto MHC class I molecules. TAP, the transporter with antigen processing, and tapasin (TAP associated protein) are the key elements of the PLC, and defective function of either TAP or tapasin leads to allele-dependent reduction in MHC class I surface presentation.

1.7.3. The Transporter associated with Antigen Processing/Presentation: TAP

The discovery that TAP was critical for MHC class I antigen presentation was greatly helped by previous analyses and selection of gamma-irradiated B-lymphoblasts that had lost MHC class I surface expression [91]. Deletion mapping and chromosome walking techniques of two such B-lymphoblast lines led to the identification of a "peptide supply factor (PSF) gene" in the HLA class II region, now called TAP1, controlling the cell surface expression of MHC class I molecules [92].

Sequence analysis of TAP1 revealed that TAP belongs to the ancient superfamily of ATP-binding cassette (ABC) proteins, specialised in the transport of a wide variety of substrates across extra- and intracellular membranes. Prominent members of the ABC transporter families include the mammalian multidrug resistance (MDR) proteins and the cystic fibrosis transmembrane conductance regulator (CFTR).

1.7.3.1 .TAP function

The importance of a functional TAP transporter for MHC class I antigen presentation is illustrated by the fact that MHC class I surface expression is severely reduced in TAP-deficient cell lines, such as the human B lymphoblastoid cell line (LCL) 721.174 [92].

TAP translocates 8 to 40 amino acid long peptide substrates with free N- and C-termini from the cytosol into the ER [93, 94]. To fulfill this task TAP must first capture suitable peptides in the cytosol and then undergo significant conformational changes that allow the peptides to reach the ER. TAP also generates the energy required for the conformational changes by carrying out ATP hydrolysis. Phosphorylated or glycosylated peptides with side chains of up to 70Å can be transported by TAP. Interestingly, the preferred peptide size for TAP transport is 9-12 amino acids, which corresponds to the typical length of MHC class I bound peptides. Furthermore, human TAP preferentially binds and translocates peptides with hydrophobic, aromatic or basic amino acids at the C-terminus, while it fails to translocate peptides with acidic C-termini and is inefficient to translocate peptides with a proline at P2 or P3 [95]. This bias in the binding motif corresponds well to the known "anchor residues" of most MHC class I alleles, with the exception of some HLA-B alleles (e.g. HLA-B7 and HLA-B35) that have proline anchors at P2. TAP has a very broad peptide binding specificity and TAP polymorphisms in humans or mice have not yet been directly shown to bias cytosol-to-ER translocation of peptide variants [96]. Some studies reported on possible disease associations with TAP polymorphisms, but linkage disequilibrium between TAP alleles and the nearby HLA class II coding regions could not always be

excluded [97]. On the other hand, a TAP2 splice variant widely expressed in lymphocytes, *Tap2iso*, which lacks exon 11 and the original 3'untranslated region, was shown to impact on peptide selectivity [98].

Most MHC class I molecules compete for binding to TAP in the ER [99]. However, some MHC class I molecules do not require to associate with TAP for efficient peptide acquisition. Such MHC classs I molecules include several members of the HLA-B molecule family: HLA-B13, -B*1501, -B*1518, -B*2705, -B35, -B*4405, -B56, -B60, and –B62. Interestingly, HLA-B alleles are also generally less dependent on their association with tapasin and can traffic more quickly to the cell surface.

Other MHC class I alleles, namely HLA-A*0201 and HLA-E can mature in the absence of TAP. These MHC class I molecules have in common the ability to bind signal sequences in the ER. However, the cell surface expression of both HLA-A*0201 and HLA-E is clearly higher in TAP-competent compared to TAP-deficient cell [100].

The significance of TAP for immunity against cancer and pathogens is not clear cut. Evidence for an increased occurrence or enhanced severity of viral infections or tumors in TAP deficient animals is conspicuously sparse [101, 102], but studies in TAP-/- mice have shown a clearly enhanced susceptibility to *Mycobacterium tuberculosis* [103, 104].

TAP's role in immunity against viruses and cancer is underpinned by the fact that many viruses, in particular members of the herpes virus family, have invented ingenious ways to specifically sabotage TAP's function as a peptide transporter. Of

note, *herpesviridae* are large DNA viruses encoding many potential MHC class I epitopes for cytotoxic T lymphocytes. The *herpesiviridae* comprise Herpes simplex (HSV) I and II, Cytomegalovirus (CMV), Epstein-Barr virus (EBV), and Varicella virus (VCV), all of which can establish life-long infection with latent phases and recurrent acute infections. To achieve this commensal-like state these viruses need to be able to escape the immune system without making the host susceptible to other lethal infections. Table 1 shows mechanisms used by herpesviridae to target TAP function.

Table 1. Herpes virus proteins targeting TAP

Virus	Protein	Property	Reference
Human CMV	gpUS6	binds TAP in the ER and freezes TAP's conformation	105, 106
HSV I/II	ICP47	Outcompetes cytosolic peptides for binding to TAP	107, 108
EBV	vIL-10	Downregulates TAP1 and LMP2 expression	109
VCV	UL49.5	TAP conformation arrest and degradation by proteasomes	110
Murine γHSV-68	MK3	Degradation of TAP1 and tapasin	111
Pseudorabies	UL41	Degradation of cellular mRNAs, including TAP mRNA	112

1.7.3.2. TAP structure and function (Figure 5)

TAP is a large heterodimer consisting of one TAP1 (81 kDa) and one TAP2 (76 kDa) ABC halftransporter. Both TAP1 and TAP2 are required for peptide translocation into the ER [113, 114]. Heterodimerisation also greatly enhances the stability of TAP2, which otherwise has a very short half life [115]. The genes encoding for TAP1 and TAP2 are located in the HLA class II region on human chromosome 6. The TAP1 gene lies adjacent to the gene encoding for the low molecular mass polypeptide subunit 2 (LMP2) of the immunoproteasome, while the TAP2 gene lies adjacent to the LMP7

gene. Interestingly, TAP1 and LMP2 share a bidirectional promoter [116], linking epitope generation by the immunoproteasome with peptide supply for MHC class I molecules in the ER.

Figure 5. TAP structure and function

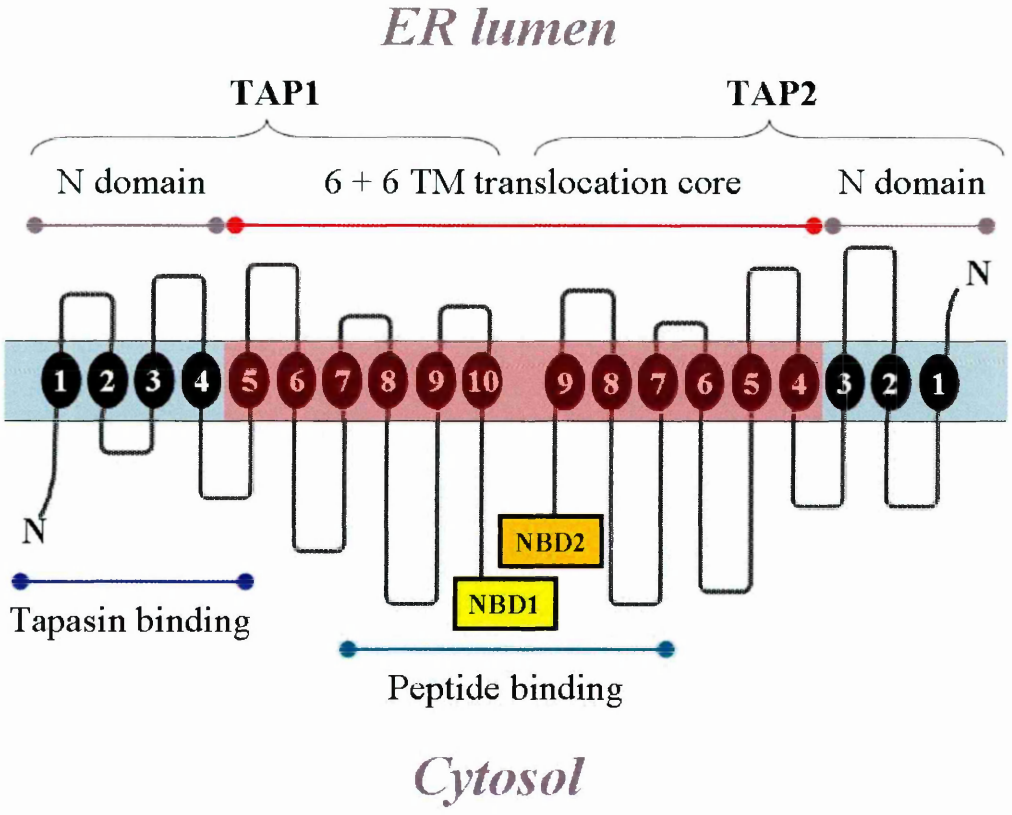

Model of TAP topology based on data obtained with cysteine-mapping[117]. According to the model TAP1 has 10 transmembrane domains (TM) while TAP2 has 9 TM. The C-terminal 6 domains of each TAP subunit form the translocation core domain. The core domain contains the peptide binding loops and the nucleotide binding domains (NBD. Tapasin binding is mediated by the N-terminal domains.

Both TAP1 and TAP2 contain one COOH-terminal cytosolic nucleotide binding domain (NBD) and one transmembrane domain (TMD).

The NBDs of human TAP1 and TAP2 are homolgous to NBDs of other known ABC transporters and contain several highly conserved peptide sequences, such as Walker A and B, and the C- and Q-loop sequences [118]. Functional and structural data indicate that the two NBDs of TAP1 and TAP2 co-operate in the binding and hydrolysis of two ATPs via the Walker A binding motif of one NBD and the C loop of the other NBD [119]. While the function of the Walker B motif is less defined, the glutamine (Q) of the highly conserved Q-loop is thought to sense ATP binding and trigger dimerisation of the TAP1- and TAP2-NBDs [118]. Furthermore, based on structural insights from other ABC transporters, such as the vitamin B12 importer BtuCD the Q-loop is believed to be critical in the cross-talk between the NBDs and the TMD [120].

The membrane topology of the TMD of TAP is still a matter of debate and atomic structures of the TMDs of TAP1 and TAP2 are not available yet. The model which seems to have the most solid foundation from topology algorithms, detailed sequence alignments and experimental studies proposes ten and nine transmembrane spanning helices for TAP1 and TAP2, respectively (Figure 5). The six C-terminal transmembrane spanning segments of TAP1 (residues 167-488) and TAP2 (residues 123-454) form the essential translocation core. These domains govern TAP1/TAP2 heterodimer assembly, peptide binding in the cytosol and the peptide translocation into the ER [117, 121, 122]. On the other hand, the first N-terminal transmembrane helices of TAP1 and TAP2 are important for the recruitment of tapasin and therefore MHC class I molecules and associated chaperonins to the PLC [123]. Within the PLC TAP associates

with 4 tapasin and 4 MHC class I molecules [64], but the association of TAP with tapasin is not required for peptide binding and translocation by TAP.

1.8. Tapasin

Similar to the discovery of TAP, the existence of tapasin was postulated based on studies with a γ-irradiated mutant B-lymphoblast line, .220, unveiling the importance of a physical association of some but not all MHC class I alleles with TAP for efficient cell surface expression [124]. Calreticulin-bound MHC class I/β2m heterodimers are recruited to the PLC by tapasin, which thereby constitutes a bridge between the peptide inflow into the ER and the peptide-receptive MHC class I molecules [125, 126]. As described above, tapasin binds to the N-terminal transmembrane segments of TAP. On the other hand, most MHC class I molecules associate with tapasin and TAP via their F'pockets, through residues 114 and 116, or via residues 122-136 and 222 within their alpha2 and alpha3 domains, respectively [127].

Although TAP-deficient and tapasin-deficient cell lines are both characterized by reduced MHC class I surface expression (with surface expression being more reduced in TAP- compared to tapasin-deficient cell lines) the mechanisms responsible for this phenotype are very different. As described above, in TAP-deficient cell lines MHC class I molecules are not loaded with peptide and retained within the ER. In contrast, in the absence of tapasin MHC class I molecules still acquire peptides and actually traffic to the cell surface faster than in the presence of tapasin. The reason for the reduced cell surface expression of some MHC class I molecules in tapasin-deficient cell lines is the reduced stability of the MHC class I molecules. A likely

cause for the MHC class I molecules' reduced stability is their loading with suboptimal peptide ligands.

Interestingly, some closely related MHC class I molecules are totally different with regard to their tapasin-dependency. This is best exemplified by the highly tapasin-dependent HLA-B*4402 (Aspartate 116) and the tapasin-independent HLA-B*4405 (tyrosine 116) which differ in only one amino acid at position 116 in the F'pocket. Comparative molecular dynamics simulations of these two MHC class I molecules have suggested that, in the absence of peptide, B*4405 more easily adopts a peptide receptive conformation, which would allow for tapasin-independent peptide loading [128]. Hence, tapasin might help stabilization of a peptide-receptive MHC class I conformation. Consistent with this notion it has been recently shown that tapasin skews the peptide repertoire loaded onto MHC class I towards such peptides with slow dissociation kinetics [129].

Tapasin is stably linked to ERp57 and the meaning of this interaction for the function of tapasin is not clear yet. As discussed above tapasin might restrain ERp57 from reducing the disulfide bonds of peptide receptive MHC class I molecules. Two tapasin alleles, which differ by one residue at position 240 (R/T) have been found, with no known implications for tapasin function or association with human diseases. On the other hand, tapasin independent MHC class I molecules might compensate for the loss of function of TAP-dependent MHC class I expression inflicted by viruses or tumors. To date, one case of a 54-year old woman with tapasin deficiency, slightly reduced MHC class I surface expression and glomerulonephritis is

described in the literature. Interestingly, her HLA genotype was found to be homozygous for HLA-B*1501, which is both tapasin- and PLC-independent[130].

1.9. Type 1 Bare Lymphocyte Syndrome

The primary immunodeficiency syndromes characterized by severely reduced or even absent MHC class I cell surface expression are called type 1 bare lymphocyte syndromes (type 1 BLS). Based on clinical and immunological grounds type 1 BLS can be subdivided into at least three groups [131]:

Group 1 type 1 BLS includes patients with severe recurrent bacterial, fungal and parasitic infections starting within the first half year of life. Patients of this group succumb within the first three years of life from infectious complications[132-134]. The immunological defect in these patients consists of both severe reduction of MHC class I and β2m on the cell surface and complete lack of antibody production. The published patients were heterozygous for the HLA haplotype.

Group 2 type 1 BLS patients are completely asymptomatic. Only one family with two affected children has been described so far [135]. Downregulation of MHC class I- and β2m - surface expression was the only observable immunological finding. The two siblings had different heterozygous HLA haplotypes. Northern blot analysis demonstrated a decrease in HLA class I and β2m mRNA, consistent with a transcriptional defect[136].

Before the work of this thesis was published, a third group of type 1 BLS had been characterized in a family from Morocco with 2 affected siblings. The patients' peripheral blood mononuclear cells displayed severely reduced MHC class I surface

expression. In contrast to Group 1, the patients survived into adulthood without major infectious complications but recurrent respiratory infections. The patients shared an identical homozygous HLA haplotype. Further molecular and genetic analysis revealed a frameshift mutation in TAP1 [137].

Chapters 3 and 4 of this thesis will describe the molecular and genetic analysis of a group of patients with type 1 BLS.

The next part of this introduction will describe the biology of CD1, a MHC class I-like family of antigen presenting molecules. In contrast to MHC class I and MHC class II molecules all members of the CD1 protein family have been demonstrated to bind lipids. Some CD1/lipid-specific T-lymphocyte responses have recently been characterised in humans. It is possible that CD1-restricted cellular immune responses could complement MHC class I or MHC class II specific T-lymphocyte functions, or even compensate for the loss of MHC class I antigen presentation in patients with type 1 BLS.

1.10. Antigen presentation by CD1 molecules

1.10.1. A short history of the discovery of CD1 as a third line of antigen presentation

It has been long known that a small but significant proportion of human peripheral blood mononuclear cells were CD4- CD8-, i.e. double negative (DN) memory αβ T cells, which suggested the possibility that these lymphocytes might be restricted by antigen presenting molecules other than MHC class I or MHC class II [138].

In 1975 George Köhler and Cesar Milstein had described a novel technology to produce monoclonal antibodies from hybrid myeloma clones[139] (in 1984 they received

the Nobel prize for their discovery[140]), and in 1979, using a monoclonal antibody generated with this technology, Andrew McMichael and Cesar Milstein defined a human thymocyte antigen, which they named cluster of differentiation (CD) 1[141]. The CD1 locus on chromosome 1 was subsequently shown to contain five genes in humans, CD1A-CD1E[142]. The predicted amino acid sequence of these genes revealed a low but significant homology to human MHC class I molecules[143]. In addition, serological studies had shown that CD1 proteins were associated with β2m on the surface of antigen presenting cells[143]. However, in contrast to the highly polymorphic genes encoding MHC class I and class II, no significant polymorphism could be detected for any of the CD1 genes. A role for CD1 in adaptive T lymphocyte mediated immunity was therefore not suspected at the time.

One decade later, in 1989 Steven Porcelli and colleagues showed for the first time that CD1 molecules could induce MHC class I and II independent, but CD3-mediated activation of human DN T-lymphocyte lines[144]. One DN αβ T-cell line was shown by these authors to be restricted by CD1a, while activation of a DN γδ T-lymphocyte line was dependent on CD1c. In 1992 Steven Porcelli and colleagues described a human DN αβ T-lymphocyte line restricted by CD1b[145]. Using this T cell line they showed for the first time that CD1 could restrict the response of cytotoxic T lymphocytes to microbial antigens. The identification of the first antigen presented by CD1b to a DN αβ T-lymphocyte line followed in 1994[146]. It came as a major breakthrough in cellular immunology and as a shock to many immunologists – the antigen was a lipid! Moreover, the identified lipid antigen was mycolic acid, a

branched, very long-chain fatty acid found in mycobacteria. How could such an antigen be presented by a MHC class I-like molecule to a T cell receptor?

In 1993, studies in mice had revealed a strong bias for the use of TCR Vβ8 among mature DN αβ T-lymphocytes[147]. The selection of these DN T cells in mice was shown to be dependent on hematopoetic cells rather than thymic epithelial cells, which suggested their restriction by non-classical MHC class I or MHC class I-like molecules. Similarly, in 1994 Raulet and colleagues demonstrated the existence of CD4+CD8- αβ T-lymphocytes which were dependent on β2m-expression by hematopoetic cells[148], and, in the same year, Lantz and Bendelac showed that the major fraction of thymic mature DN αβ T-lymphocytes co-expressed the NK marker NK1.1 and an invariant TCR Vα14-Jα281 alpha chain[149]. Importantly, a highly homologous invariant TCR alpha chain, TCR Vα24-JαQ, had also been identified among DN αβ T-lymphocytes in several unrelated human donors in 1993[150]. In 1995 the work of two research groups showed that DN and CD4+ mouse T cells using the invariant TCR Vα14-JαQ rearrangement were restricted by CD1d[151, 152].

The next important breakthrough discovery was published in 1997 by Kawano and colleagues, who showed that the CD1d-restricted iNKT cells could be strongly and specifically activated by KRN7000, an alpha-galactosylceramide glycolipid derived from a marine sponge[153]. Interestingly, KRN7000 had previously been shown by the Pharmaceutical Research Laboratories of Kirin Brewery (Gunma, Japan) to significantly prolong the lifespan of mice in a B16 melanoma metastasis model[154]. Finally, the first atomic structure of mouse CD1d published in 1997 by Zheng and

colleagues basically confirmed that CD1 molecules were designed to present lipid antigens[155].

In the following sections I will give an overview on the biology of CD1.

1.10.2. Group 1 and group 2 CD1 proteins

According to their predicted amino acid sequence the five human CD1 genes on human chromosome 1q22-23 can be categorized into Group 1, containing CD1A, CD1B, CD1C and CD1E, and Group 2, which only comprises CD1D[156]. Phylogenetic analysis has indicated that the human CD1 gene copies were duplicated prior to the evolution of primates and well before the bulk of HLA class I genes[157]. In mammals the CD1 and HLA loci are on different chromosomes, but in chicken they occupy adjacent regions on the same chromosome. Avian CD1 can't be classified as either group 1 or group 2, suggesting that it represents an ancient precursor to "modern" mammalian CD1 genes[158]. Nothing is known yet about the functional role of the chicken CD1.

Interestingly, the two groups of mammalian CD1 molecules segregate with regard to tissue expression and T lymphocyte restriction[159]. Group 1 CD1 molecules are expressed to levels similar to MHC class I on myeloid cells and are highly expressed on immature cortical thymocytes. In addition, CD1c is highly expressed on marginal zone B-lymphocytes, while CD1a is a classic phenotypic marker of Langerhans cells in the skin. In contrast, CD1d surfaceexpression is generally much lower compared to CD1a, but it is more widely expressed in the body. CD1d seems to be constitutively expressed on various epithelial cell types, including keratinocytes,

intestinal epithelial cells and endothelial cells, but it is also expressed on antigen presenting cells. In general, the tissue distribution of CD1d expression resembles that of MHC class I molecules, while group 1 CD1 expression is more similar to MHC class II tissue expression. Group 1 CD1 expression can be induced on epithelial cells under inflammatory conditions, e.g. on neurons in multiple sclerosis lesions[160]. Similarly, CD1d expression can be upregulated by inflammatory cytokines and danger signals, i.e. TNFα and IFNγ, or IFNγ and lipopeptides[161]. Consistent with this, the CD1D gene, which is controlled by dual promoters with multiple transcription initiations sites, contains 9 IFNγ response elements (γ-IRE_CS) as well as 5 putative nuclear factor for IL-6 expression (NF-IL-6) response elements[162]. However, while cell surface expression of CD1a, CD1b and CD1c molecules is upregulated in GM-CSF and IL-4 treated human monocyte, CD1d is downregulated in the same cells[163]. Interestingly, the Peroxisome Proliferator-Activated Receptor-gamma (PPARγ) has been shown to mediate opposite effects on CD1d and group 1 CD1 expression on immature dendritic cells, supporting the notion that group 1 and group 2 CD1 molecules serve different physiological functions[164].

Of the five human CD1 molecules all except CD1e are expressed on the surface. While CD1a-d have all been shown to present lipid antigens to T lymphocytes, CD1e was found to be involved in the processing of complex glycolipids within endocytic compartments[165]. Therefore, CD1e should be viewed as a separate, i.e. third class of CD1 molecules.

CD1d shows other interesting differences to group 1 CD1 molecules. First, CD1d is the CD1 molecule with the highest degree of conservation in mammals. Mice

have two CD1d alleles, CD1D1 and CD1D2, but both rats and mice have deleted the group 1 CD1 encoding genes for unknown reasons[166]. On the other hand, the reason why the CD1D genes have not undergone the same fate is likely to be linked to their specific role in the selection of a highly conserved T lymphocyte subset in mice and men, namely the invariant NKT cells (iNKT). These CD1d-restricted iNKT cells express a semi-invariant T cell receptor which is highly homologous in humans and mice and can recognize human and mouse CD1d in a cross-species specific way[167]. In contrast, group 1 CD1 restricted T cells use highly diverse T cell receptors, similar to MHC/peptide specific T cells[168]. For these reasons it is generally believed that iNKT cells have immunoregulatory functions, while group 1 CD1 specific T lymphocytes might serve roles in host defense.

1.10.3. Classes of CD1 ligands (Figure 6)

The first identified ligand for CD1, which could activate a human CD1b-restricted DN αβ T cell line, was mycolic acid, a class of alpha-branched β-hydroxy fatty acids with very long C70-90 alkyl chains [146]. Mycolic acids (MA) are an essential component of mycobacterial cell walls and actinomyces [169]. They are clearly foreign antigens and no similar lipid structures are synthesized in mammals.

The second identified class of CD1 antigens contains mycobacterial phosphoglycolipids, which include phosphatidylinositol mannosides (PIMs) and lipoarabinomannan (LAM)[170]. Similar to MA, phosphoglycolipids have two alkyl chains. However, LAM has a ca. 17 kDa hydrophilic headgroup, which is too large to be accommodated within any of the CD1 binding grooves and too bulky to allow T

cell receptor binding to both CD1b and LAM. In fact, activation of T cells by LAM-pulsed CD1b-expressing antigen presenting cells requires both internalization via the mannose receptor [171] and endosomal acidification, i.e. processing of the head group [170].

The study of another mycobacterial cell wall lipid and close relative of MA, glucomonomycolate (GMM), provided further important insights into the structural requirements for CD1 mediated glycolipid recognition by the T cell receptor. GMM is a mycolyl glycolipid consisting of a single glucopyranoside residue esterified to mycolic acid. Importantly, the T cell stimulatory activity of GMM is highly dependent on the carbohydrate headgroup, while substantial variations of alkyl chain length have no significant effect [172]. Based on these facts a first general model of lipid antigen binding to CD1 was proposed. According to the model, CD1 ligands were anchored to the protein via two fatty acids that were buried within the CD1 ligand binding groove, while the hydrophilic headgroup of these ligands could be exposed on top of the CD1 protein surface and determine the fine specificity of T cell receptor binding. The first structure of a CD1 molecule, mouse CD1d, was fully consistent with this model, but could not explain how very long fatty acids such as those of MA could be buried within CD1 [155].

The first identified antigen for CD1d was KRN7000, a ceramide structure with a phytosphingosine chain and an alkyl chain, which underpinned the above model[153] and the crystal structure of CD1d with bound KRN7000 provided further insight into CD1 ligand binding[173]: Hydroxyl groups of both the phytosphingosine chain and the galactose headgroup of KRN7000 were found to stabilize binding to the CD1d

molecule. These interactions are not an absolute requirement for binding to CD1d as sphingosine containing glycysylceramides and gangliosides as well as phosphatidylinositol, glycosylphosphatidylinositol (GPI), and diacylated sulfoglycolipids all have been shown to bind to CD1d molecules [174-177]. Moreover, the sulfoglycolipid sulfatide, which is based on a common ceramide backbone, has been shown to bind to all group 1 CD1 molecules[176].

The identification of another mycobacterial cell wall derived CD1 antigen, mannosyl-β1-phosphoisoprenoid (C35), revealed that glycolipids with only one alkyl chain could be presented by CD1c to T cells[178]. Interestingly, phosphoisoprenoids are related to dolichols in mammals, but mammalian dolichols are much larger structures often containing 90 and more carbon atoms. The antigens presented by CD1c to human autoreactive T cell lines are still not defined.

Another class of antigens presented by CD1 comprises lipopeptide antigens. Mycobacterial didehydroxymycobactin (DDM), a relative of mycobactin siderophores, was shown to specifically activate CD1a-restricted T cell clones, which had been previously demonstrated to exert antibacterial effects against mycobacteria-infected macrophages[179]. The structure of DDM shows no obvious similarities with sulfatide, another CD1a ligand, suggesting that the CD1a lipid binding groove can undergo conformational adaptation to the bound ligand.

The most recent addition to CD1 bound ligand classes are synthetic small nonlipidic molecules with multiple aromatic rings, phenyl-pentamethyldihydrobenzofurans (PPBF), which were identified by serendipity as CD1d-restricted T cell antigens[180]. How these small molecules bind to CD1d, inside or

outside of the antigen binding groove, is not known, but their existence indicates that small molecules might become useful tools in the future to regulate lipid-specific T cell functions.

Figure 6. Different classes of CD1 ligands

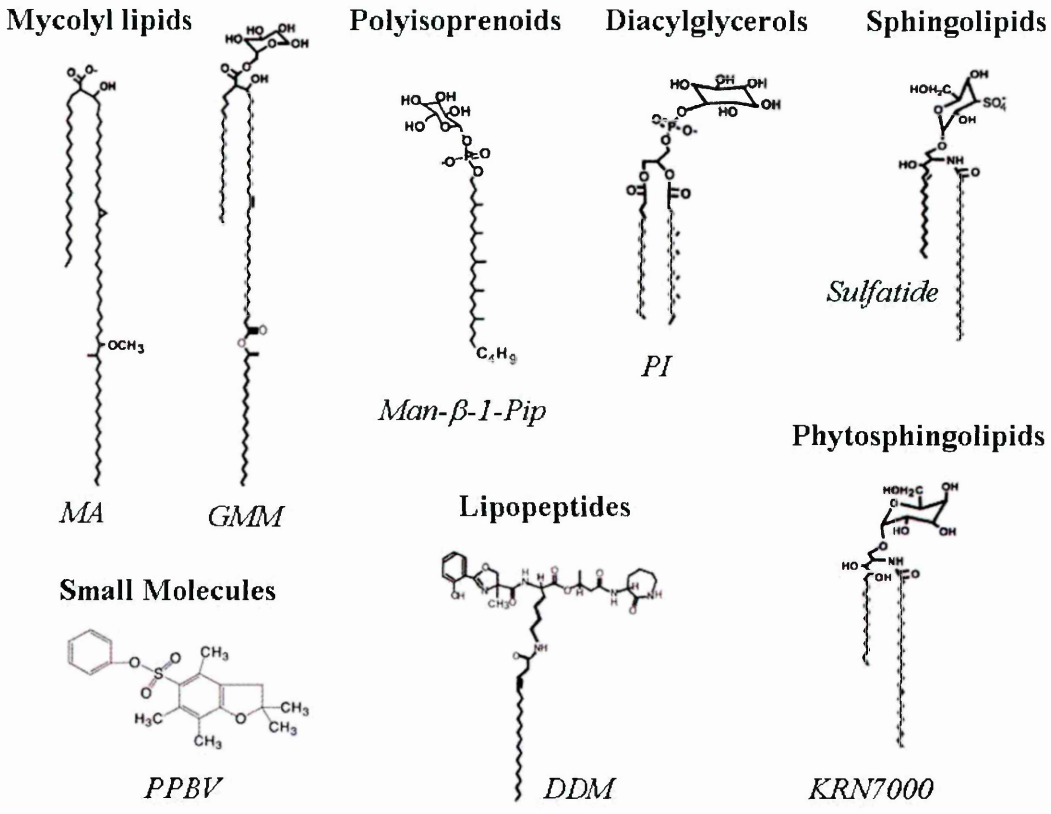

Chemical structures of different classes of ligands for CD1 molecules. The very long MA and GMM can only bind to CD1b, while Man-β-1Pip specifically binds to CD1c and DDM to CD1a. Abbreviations: MA, mycolic acid; GMM, glucomonomycolate; Man-β-1Pip, mannosyl-β-1-phosphoisoprenoid; PI, phosphatidylinositol; PPBV, phenyl-pentamethyldihydrobenzo-furan; DDM, Didehydroxymycobactin; KRN7000, Kirin 7000 (which is representative for the class of α-glycosylceramides).

1.10.4. CD1 protein structures

The crystal structures of mouse CD1d and human CD1a, CD1b and CD1d have been solved[173, 181-185]. These structures revealed that the CD1 and MHC class I molecules shared an identical domain organisation with an immunoglobulin-like, β2m-associated membrane proximal alpha3 domain, and a distal antigen-binding superdomain consisting of two alpha helices overlying beta-pleated sheets (Figure 7).

Figure 7. MHC class I and CD1 extracellular domain organisation.

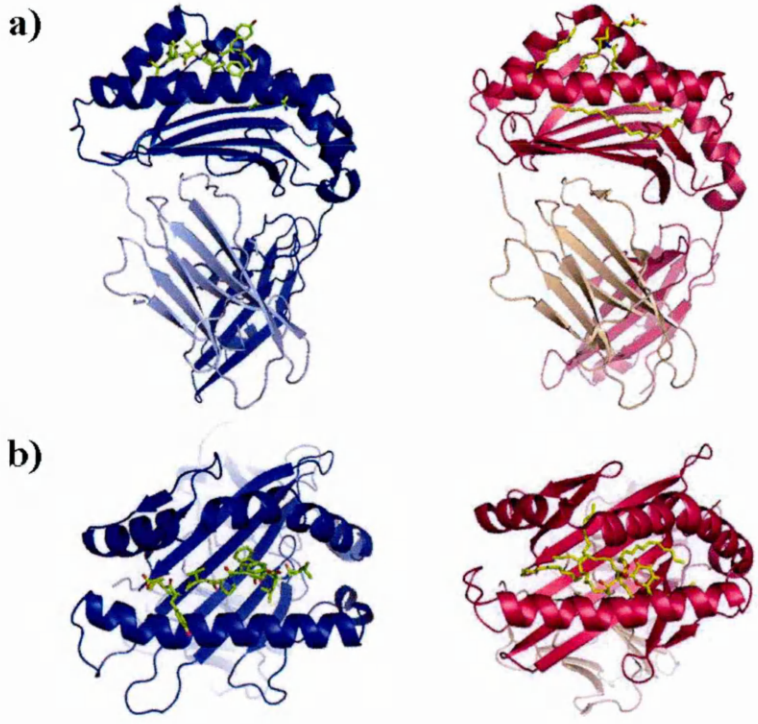

Ribbon diagrams of side (a) and top views (b) of HLA-A2/peptide[38] (left side; α1-α3 domains in dark blue, β2m in lightblue, peptide in yellow; PDB 1AO7) and CD1b/ligand complex[181] (right side; α1- α3 domains in in magenta, β2m in light rose, ligands in yellow; PDB 1GZP). The figure was created with PyMol software.

The major structural differences between the CD1 and MHC class I structures are found in the antigen binding groove of the two classes of proteins. The peptide binding groove of MHC class I molecules comprises 6 distinct hydrophilic pockets A'-F', for accommodation of, and hydrogen bonding with peptide side chains. In contrast, the antigen binding groove of CD1 consists of up to four relatively plump, voluminous hydrophobic channels (Figure 8). In an attempt to adopt the nomenclature used for MHC class I structures these hydrophobic channels in CD1 molecules are designated A', C', and F'. Sequence alignement and direct structural comparison indicates that the A' channel is the most conserved lipid binding region in all CD1 molecules, while the F' channel is the least conserved region[181]. The A' channel runs from the entry of the antigen binding groove at the top of the protein surface down to the bottom of the α1/ α 2 superdomain, where it bends around a conserved hinge region formed by bulky hydrophobic residues (Figure 8).

CD1a and CD1d both bind two alkyl-chain containing ligands, despite significant differences in the architecture of their binding grooves (Figure 8). Structures of CD1c and CD1e are not available yet, but both can accommodate two-alkyl chain ligands.The structure of CD1b, which will be discussed in detail in chapter 6, is special, because the antigen binding groove consists of four interconnected channels, including a unique tunnel T', which runs at the bottom of the α1/ α2 superdomain and connects channels A' and F' with each other[181]. A continous superchannel formed by A', T' and F' can accommodate up to 60 carbon atoms and explains how the very long fatty acids of mycolic acid can be completely buried within CD1b[181, 186]. Tunnel T' is absent in CD1a or CD1d, where bulky amino acid residues

block the connection between A' and F'. Sequence analysis of all CD1 proteins suggests that tunnel T' is a unique feature of CD1b. Also, channel F' is occluded in CD1d and CD1a[181].

Figure 8. CD1 lipid binding grooves

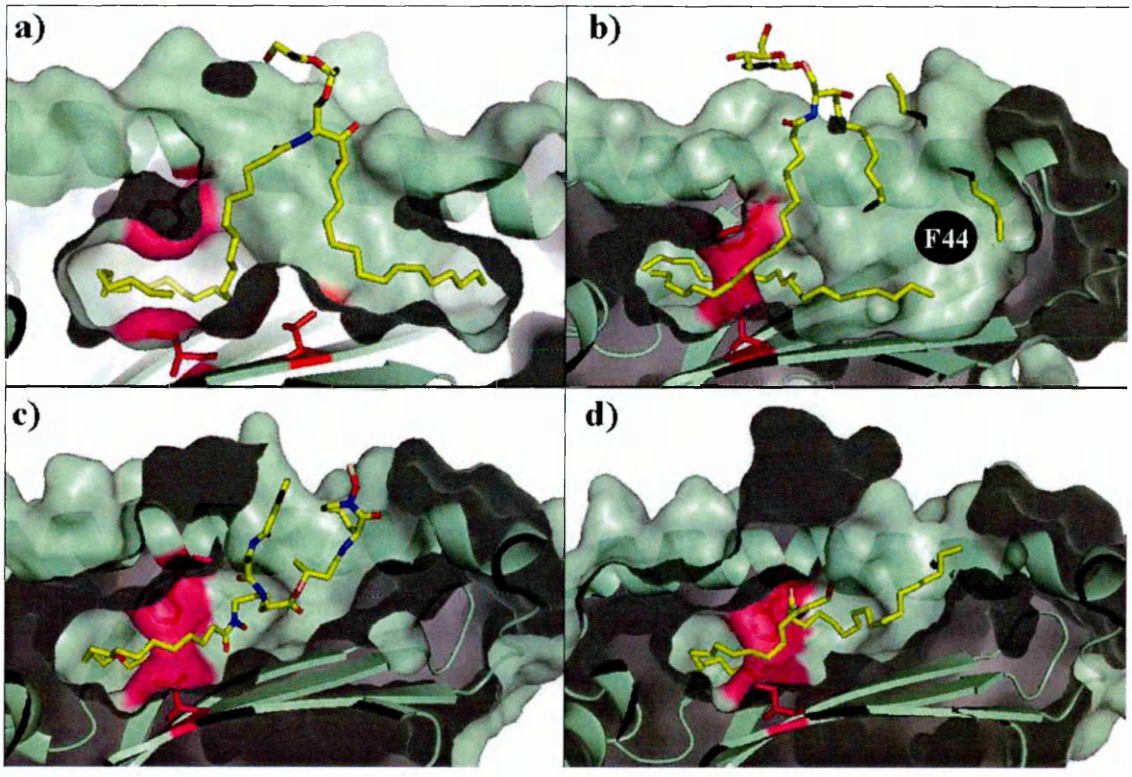

Cross-sections of human CD1d with bound KRN7000[173] (a), human CD1b with bound PI and detergent[181] (b), and human CD1a with bound lipopeptide[184] (c) or sulfatide[185] (d). Ligands are shown as sticks with carbon atoms in yellow, nitrogen atoms in blue and oxygen atoms in red colour. The CD1 protein surface is in pale green except for the "hinge region" (magenta) of channel A' and valine 98 (red) in (a), which closes off channel A'. The position of the second "hinge region" in human CD1b (b), which is formed by phenylalanine 44 (F44) is indicated. The figure was created using PyMol software. PDB files used were: 1 ZT4 (a), 1GZP (b), 1XZO (c) and ONQ (d).

MHC class I and CD1 structures also exhibit significant differences in the region of the CD8 binding loop, which is part of the alpha3 domain. No direct evidence has yet been found that CD8 co-receptors bind to any of the CD1 molecules. However, experimental data generated in mice have strongly suggested that CD8 expression by iNKT cells induces their negative selection in the thymus[166].

Figure 9 shows a view onto the molecular surface of the structures of human CD1d with bound alpha-galactosylceramide[173], human CD1b with bound ganglioside GM2 and detergent[181] and HLA-A2 with bound peptide[38]. The figure illustrates that the galactosyl head group of CD1d bound α-galactosylceramide makes a relatively small contribution to the total molecular surface which is exposed to the TCR, while the ligands bound to both CD1b and MHC complexes occupy a considerably larger area on the molecular surface.

The recently solved crystal structure of a human CD1d/α-galactosylceramide/iNKT receptor – complex has disclosed that most of the TCR-CD1d binding is mediated by protein-protein contacts[187], which might explain the known limited structural diversity of iNKT TCRs compared to CD1b and MHC class I restricted TCRs.

Figure 9. A TCR's view onto CD1/ligand and MHC/ligand molecular surfaces

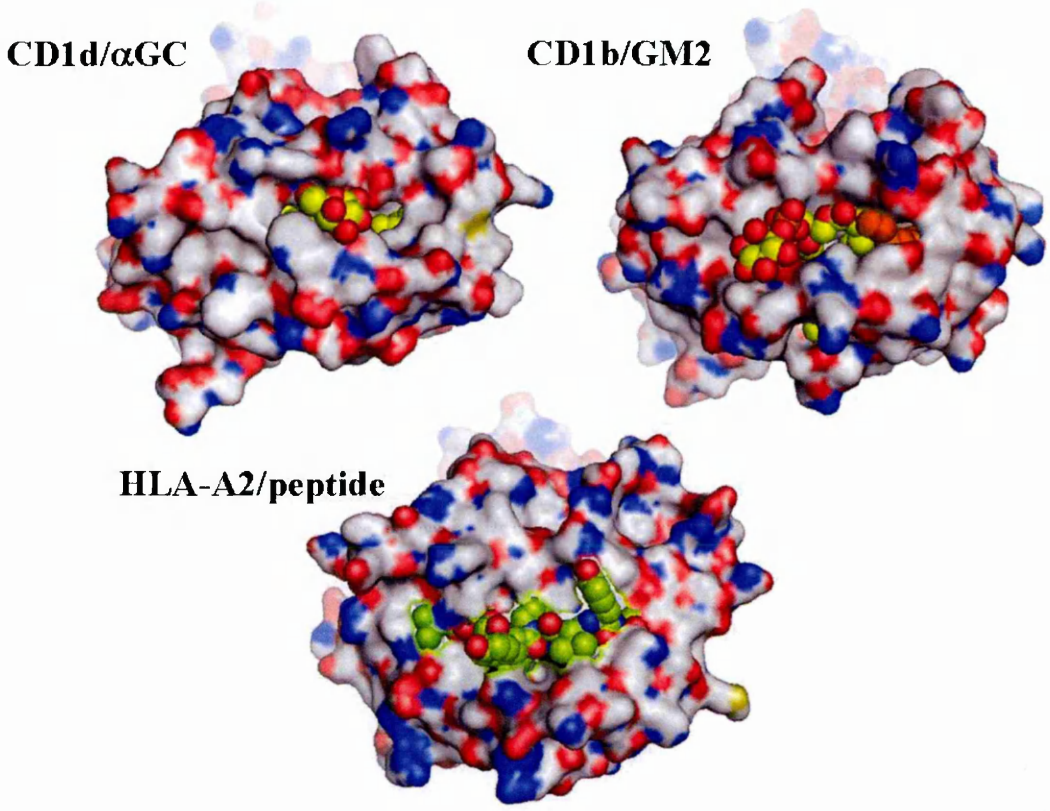

Molecular surfaces of CD1d/KRN7000 (upper left), CD1b/GM2+detergent (upper right) and HLA-A2/peptide complexes are shown. The protein is shown as molecular surface with acidic groups in red, basic groups in blue, thiols in yellow and carbon atoms in grey. The bound ligands are shown as Van der Waals speres with carbon atoms in yellow, nitrogens in blue and oxygens in red. The bound detergent molecule in the CD1b structure is shown in orange. The figure was created with PyMol software. PDB codes used: CD1d/α-GalCer (1ZT4), CD1b/GM2 (1GZP), A2/peptide (1AO7).

1.10.5. CD1 ligand loading and intracellular trafficking

The fact that different CD1 molecules can present the same ligand, e.g. sulfatide, to different T lymphocytes, illustrates their somewhat promiscuous ligand binding properties. However, the different CD1 isoforms are still highly likely to present different lipid antigens to T lymphocytes *in vivo*, because they patrol different cellular compartments where they capture their lipid ligands. Like other glycoproteins in the ER nascent CD1 polypeptides associate with calnexin, calreticulin and ERp57 during early refolding stages [188, 189]. After binding to β2m and perhaps acquisition of chaperone lipid ligands[181, 190, 191], e.g. spacer lipids, phosphatidylcholine, phosphatidylinositol or GPI, CD1 molecules leave the ER and reach the cell surface via the trans-Golgi network. A tyrosine-based cytoplasmic tail motif (YXXZ, where Y is tyrosine, X is any amino acid and Z is a bulky hydrophobic amino acid) present in CD1b, CD1d and CD1c mediates the association of these CD1 isoforms with adaptor protein complex-2 (AP-2) and subsequent re-internalisation via clathrin-coated pits[192]. Human CD1b and mouse (but not human) CD1d can also associate with AP-3 and traffic from early to late endocytic compartments, including lysosomes, while CD1c and human CD1d traffic from the cell surface to early endocytic vesicles[193-195]. Interestingly, lipid ligands of different alkyl chain length target different cellular compartments, and the very long fatty acid containing MA and GMM are recruited specifically to late endosomes and lysosomes, i.e. the same compartments surveyed by CD1b[196].

In contrast to CD1b, CD1c and CD1d, CD1a lacks a tyrosine-based motif and it is currently unknown how CD1a is re-internalised from the cell surfaces. CD1a

shuttles between early endosomes and the cell surface via ADP-ribosylation factor 6 (ARF6)-regulated recycling pathways[197].

A proportion of CD1a, CD1b and CD1d molecules associate with invariant chain (Ii) in the ER. Association with Ii facilitates trafficking of CD1a to the cell surface, while it enables CD1b and CD1d to bypass the secretory pathway and directly reach late endocytic compartments[198, 199]. It is currently not understood why CD1b and CD1d can use two different routes to the same destination and whether they compete with MHC class II molecules for binding to "Ii".

Some accessory mechanisms involved in the loading and the processing of CD1 presented lipid ligands have been unravelled. Interestingly, phosphatidylinositol (PI) and related ligands have been eluted from mouse and human CD1d and human CD1b molecules, and studies with ER-retained human CD1d molecules have indicated that PI is loaded onto CD1 in the ER[200]. An ER-resident microsomal triglyceride transfer protein (MTP) has recently been shown to mediate loading of phosphatidylethanolamine (PE) onto CD1d and to be required for efficient expression of CD1d on the cell surface[201, 202]. However, PI merely serves as a chaperone ligand to stabilise CD1 molecules until exchange of PI for other cargo, e.g. with foreign microbial lipids. This is illustrated by the facts that CD1d/PI-complexes are not stimulatory for either mouse or human iNKT cells, but exogenous lipid antigens can be presented by CD1 molecules to ligand-specific T cell lines. Furthermore, inhibition of endosomal acidification and deletion of the cytoplasmic tail of CD1d can have deleterious effects on both CD1-restricted T cell activation and thymic selection[203]. Also, deletion of the late-endosome-resident protease cathepsin S, which for its

function in degradation of MHC class II-associated "li", negatively affects presentation of exogenous lipid antigens by CD1d to iNKT cells [204].

Based on the above facts it has been proposed that PI-loaded and/or "li"-associated CD1b and CD1d molecules exchange their ligands in endocytic compartments. Further support for this model comes from our own studies in mice with lysosomal glycosphingolipid (GSL) storage diseases. GSL storage interferes with iNKT selection in mice independent of the underlying genetic defects [205].

As indicated above, some CD1-bound glycolipids require processing of their hydrophilic headgroups in order to be recognisable for T cell receptors. Proof of principle for this notion came from a study using a synthetic galactosyl-α-galactosylceramide precursor ligand for iNKT cells. Presentation of this ligand by CD1d to iNKT cells was dependent on the endosomal hydrolase α-galactosidase [206].

The fifth member of the human CD1 protein family, CD1e, is the only CD1 isoform which is not expressed on the surface. CD1e locates to the same late endocytic compartments as CD1d and CD1b do. Interestingly, CD1e seems to exert an important function in the processing of CD1b presented foreign microbial lipids, such as higher molecular weight PIMs. Experimental data suggest that CD1e might present glycolipids with large headgroups to endosomal enzymes, such as α-mannosidases, to enable efficient cleavage of the surplus carbohydrates preventing T cell recognition [165].

Ligand processing can also go "the other way"; microbial lipids can acquire antigenic groups during the process of tissue invasion. One such example is

mycobacterial GMM, which is generated upon tissue invasion of mycobacteria by esterification of MA with glucose residues provided by the host environment [207].

1.10.6. CD1 restricted T cells

1.10.6.1. Group 1 CD1 restricted T cell responses

Most of the current knowledge on the biological role of CD1 restricted T lymphocytes comes from studies on a major subset of CD1d-restricted T cells, i.e. the invariant NKT cells (iNKT). In contrast, little is known about group 1 CD1 restricted T lymphocyte responses. On the one hand, group 1 CD1 molecules are not expressed in rats and mice, and on the other hand, sensitive and specific research tools to study group 1 CD1 specific T cells *ex vivo* in human blood or tissue are not yet available. In addition, only a small number of specific lipid antigens presented by group 1 CD1 molecules to T lymphocytes have been identified to date. However, it is noteworthy that the first CD1 restricted T cell lines were isolated from the DN T lymphocyte fraction in patients with chronic inflammatory rheumatic diseases, namely rheumatoid arthritis and systemic lupus erythematosus (SLE) [144]. Interestingly, DN T lymphocytes are expanded in those diseases, and group 1 CD1 restricted T lymphocyte lines have been shown to stimulate autoantibody production by CD1 group 1 expressing B-lymphocytes[208, 209]. A recent study found that *in vitro* generated CD1 group 1 restricted T lymphocytes are often autoreactive and can promote dendritic cell maturation[207], while another study found evidence for CD1a and CD1c restricted autoreactive T cell responses in autoimmune thyroid inflammation[210].

Interestingly, CD1c was also found to be the major antigen presenting molecule for γδ1 T cells in the gut, but the function of these cells is still unknown [211]. Surprising little evidence has yet been generated for a role of group 1 CD1 restricted T cell responses to mycobacterial infection. One study could demonstrate *in vivo* expansion of α-mannosyl-β-phosphoisoprenoid specific CD1c-restricted T cells in patients with active tuberculosis but not in healthy controls [178], while another study found CD1-restricted IFNγ-producing Bacillus Calmette-Guérin (BCG) specific CD8+ T lymphocytes in the peripheral blood of BCG-vaccinated donors[212].

1.10.6.2. CD1d restricted T cells

To date three different types of CD1d restricted T cells have been described in humans: Invariant Vα24-Jα18+/Vβ11+ NKT cells (iNKT); Vα24-independent CD1d/α-Galactosylceramide (α-GalCer) specific T cells; and diverse CD1d-restricted T cells with mostly unknown ligand specificity. In the following section I will focus on the CD1d/α-GalCer specific iNKT cells.

1.10.6.2.1. Definition and phenotype of iNKT cells

Human and mouse iNKT cells are defined by four characteristics: They are restricted by CD1d; they recognise alpha-glycosylceramides presented by CD1d; they express the pan-NK marker NKR-P1 (NK1.1 in mice, CD161 in humans); and they make use of an invariant TCR alpha-chain rearrangement (Figure 10). Human iNKT cells use TCR Vα24-Jα18 and mouse iNKT cells use the homologous TCR Vα14-Jα18. The CDR3α loop, which is highly variable in peptide-specific T cells, is therefore invariant

in iNKT cells and is highly homologous in human and mouse iNKT TCRs[213]. Interestingly, the same CDR3α loop is also used by a subpopulation of human CD1d/α-GalCer specific Vα24-negative T cells[214].

Figure 10. Definition of the CD1d-restricted invariant Natural Killer T cells (iNKT)

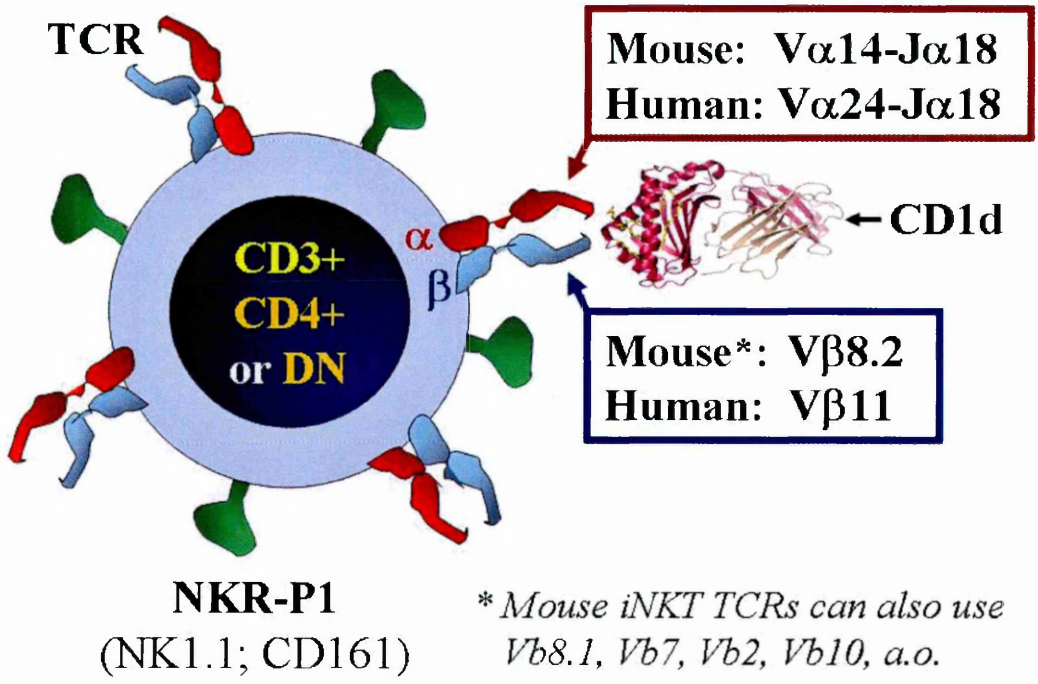

Cartoon showing four criteria defining the human and mouse iNKT cell subsets:

1) Expression of the pan-NK receptor NKR-P1 (mice: NK1.1; humans: CD161);

2) Use of a semi-invariant TCR (invariant TCRα chain, variant TCRβ chain);

3) Restriction by CD1d (ribbon diagram in pink) and

4) Specific recognition of α-GalCer bound to CD1d

Mouse and human iNKT cells exhibit both similarities and differences in their usage of TCR beta chains. The dominant TCR beta chains used by mouse and human iNKT cells are Vβ8.1/Vβ8.2 and Vβ11, respectively. Human Vβ11 is homologous to mouse Vβ8. However, while no other TCR β chains seem to be expressed by human iNKT cells, mouse iNKT cells make use of several additional Vβ families, such as Vβ2, Vβ10 or Vβ7[166].

A characteristic of all iNKT cells is their activated memory phenotype, which is already present before birth or bacterial colonisation of the gut [215, 216]. This "ready to go" phenotype of iNKT cells is complemented by the expression of specific chemokine receptors, such as CXCR2, which are usually not present on T cells but are expressed on granulocytes. Subsets of CXCR2+ iNKT cells migrate within 3 hours to the site of acute inflammation, together with neutrophilic granulocytes and long before any "conventional" peptide-specific T lymphocytes[217]. Their phenotype might therefore enable iNKT cells to bridge innate and adaptive immune responses, a notion clearly underpinned by their functional versatility.

1.10.6.2.2. Possible roles for iNKT cells in health and disease

The discovery of the first α-galactosylceramide ligand, KRN7000, as a potent stimulator of all human and mouse iNKT cells[153] empowered immunologists with an important tool to study the possible role of CD1d in health and disease.

When injected into mice, KRN7000 induces the rapid secretion of copious amounts of a wide range of cytokines. Such studies have revealed that iNKT cells are the main source of the early IL-4 cytokine burst which is observed after i.v. treatment

of mice with anti-CD3 antibodies[166]. Conversely, KRN7000 stimulates strong secretion of IFNγ by iNKT cells with subsequent transactivation of NK cells, dendritic cells and other immune cells[218]. Human iNKT cells induce IL-12 secretion by dendritic cells and they are also able to direct monocytes into a dendritic cell differentiation pathway[219, 220].

Several KRN7000-based studies in mice have found that iNKT cells could induce protection against tumours and against viral and bacterial infections[213]. Similarly, KRN7000 and related synthetic iNKT stimulatory compounds have been shown to exert strong adjuvant effects during peptide vaccination [221, 222]. However, first clinical trials using KRN7000 in cancer patients have been disappointing [223]. Possible reasons for this may include the profound defect in iNKT cells which is often seen in cancer patients[224] and/or possible anergy of iNKT in cancer patients. However, the results of KRN7000-based studies are unlikely to reflect the main physiological functions of iNKT cells *in vivo* as KRN7000 induces complete ablation of iNKT cell development when added to fetal thymic organ cultures[225]. Moreover, alpha-glycosylceramides cannot be synthesised in mammals, and the identification of alpha-anomeric glycosphingolipids in rare bacteria species cannot explain the high degree of iNKT conservation in mammals.

Interestingly, the synthetic alpha-galactosylceramide OCH, which features an identical galactosyl headgroup as KRN7000 but a considerably shorter sphingosine chain (C9 sphingosine) than KRN7000 (C18 sphingosine), elicits a significant, but weaker and qualitatively different *in vivo* response in iNKT cells than KRN7000[226]. In particular, i.v. injection of OCH into mice hardly induces any IFNγ, while it still

induces a strong IL-4 secretion [226]. This TH2-biasing effect of OCH has been used in translational studies where it could be shown that OCH treatment could prevent autoimmune inflammation in TH1-biased models, such as type 1 diabetes, collagen induced arthritis and experimental allergic encephalitis (EAE)[227]. Importantly, protection from autoimmune inflammation can also be achieved by adoptive transfer of iNKT cells from healthy donor mice into autoimmune-prone mice[228]. Interestingly, several autoimmune-prone mouse strains, such as NOD and SJL, which had been used as models for autoimmune inflammation long before anything was known about iNKT function, were later demonstrated to exhibit profound defects in the iNKT repertoire. A few studies have analysed the human iNKT repertoire in autoimmune patients. Interestingly, iNKT cells are deficient in classic human autoimmune diseases such as RA, Sjogren syndrome or scleroderma [229], but the reason for this deficiency is completely unknown. On the other hand, the frequency of iNKT cells in humans shows wide variation and healthy individuals without apparent autoimmune inflammation may have very low iNKT frequencies (own observations). In the absence of a known endogenous iNKT stimulatory ligand, iNKT deficient animals are likely to give the most relevant information about the true physiological function of iNKT cells *in vivo*. Mice with a targeted deletion of the Jα18 gene, which encodes the junctional element forming the invariant CDR3α loop of the iNKT TCR, are completely deficient in iNKT cells, while other immune cells are not affected[230]. Interestingly, these $Ja18^{-/-}$ mice develop a spontaneous late onset autoimmune disease with strong resemblance to SLE [231].

The above facts are all consistent with a role for iNKT cells in maintaining or inducing immunological tolerance. In fact, this notion is supported by evidence from *in vitro* and *in vivo* studies. In the model of anterior chamber-associated immune deviation (ACAID) iNKT cells are essential for the induction of antigen-specific systemic tolerance [232]. Both $CD1^{-/-}$ and $J\alpha281^{-/-}$ NKT cell deficient mice do not develop ACAID unless reconstituted with iNKT cells. A model how iNKT cells might assist in the induction of ACAID can be drawn from the studies of Sonoda and colleagues and Faunce and colleages (Figure 11) [233-235].

Figure 11. Role for iNKT cells in systemic tolerance via immuneprivileged sites

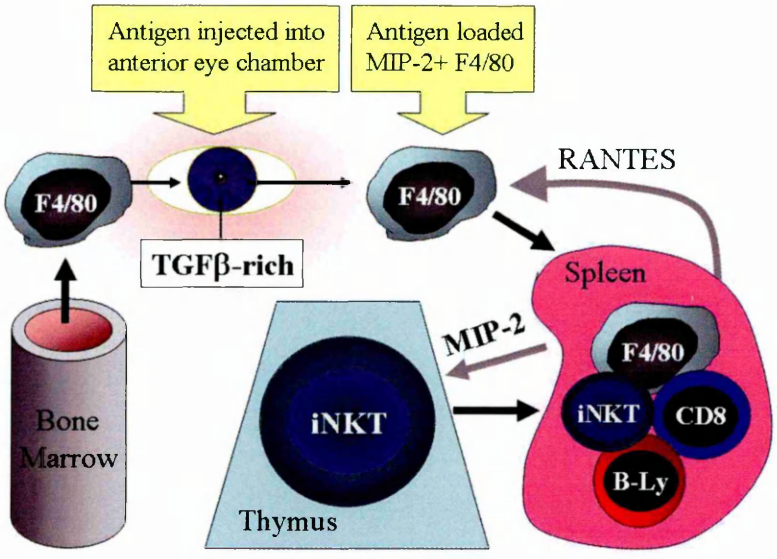

Cartoon of the ACAID model: Bone marrow derived F4/80 suppressor macrophages reside in the anterior chamber (a.c.) of the eye where TGFβ is present at high concentrations. Upon a.c. injection of antigen the antigen is taken up by F4/80 macrophages, which migrate to the spleen and start to express MIP-2 and recruit thymic iNKT cells. iNKT cells in the spleen secrete RANTES, recruiting more F4/80 macrophages. 7 days later, microclusters of F4/80 macrophages, iNKT cells, CD1d-expressing B-cells and CD8 T cells are found in the spleen. RANTES and IL-10 produced by iNKT are essentially required for tolerance induction in ACAID[233, 234].

The model proposes that antigen-specific tolerance is imprinted on naïve T lymphocytes within microclusters of suppressor macrophages, iNKT cells and CD1d-expressing B-lymphocytes. Cell-cell contacts of the naïve T lymphocytes with both F4/80 macrophages and iNKT cells are important in this process, and secretion of

RANTES and IL-10 by iNKT cells is an absolute requirement for induction of ACAID in mice.

Apart from ACAID, iNKT cells have been shown to be essentially required for long term acceptance of cardiac allografts and of rat pancreatic islet xenografts in LFA-1/ICAM-1 and CD28/CD80 monoclonal antibody blocking models[236, 237]. The other side of the coin of the tolerogenic effects of iNKT cells might be a suppressive effect on tumor immunosurveillance. Using a fibrosarcoma tumor model with a growth-regression-recurrence pattern, Terabe and colleagues have elegantly shown that IL-13 secretion by iNKT cells via activation of the IL-4 receptor/STAT6 pathway attenuates the initial anti-tumor cytotoxic T lymphocyte response, thereby interfering with complete elimination of the injected fibrosarcoma cells[238].

In summary, iNKT cells are very versatile T lymphocytes that can bridge innate and adaptive immune response. In the absence of infection iNKT cells seem to be important for both the maintenance and induction of immunological tolerance.

Coreceptors are likely players regulating iNKT functions. The most conspicuous coreceptor for iNKT cells, which is highly expressed on the majority of human iNKT cells, is the lectin-type NK receptor NKR-P1A (CD161). This receptor is also expressed on the majority of NK cells. Ligation of CD161 via its recently described natural ligand, lectin like transcript-1 (LLT1) evokes different responses from NK and NKT cells[239]. While NK cells are inhibited by CD161-LLT1-binding, NKT cells are activated. Previous studies using monoclonal antibodies have demonstrated, that CD161-crosslinking is not stimulatory for iNKT cells on its own, but requires simultaneous TCR crosslinking, e.g. via anti-CD3 antibodies[240]. These

data are consistent with the concept that different signals, coming from TCR- and costimulatory receptor/ligand ligation, are integrated by iNKT cells in order to shape one or another type of response.

1.10.6.2.3. Molecular interaction of iNKT cells with antigen presenting cells

While iNKT cells can rapidly migrate to the site of acute inflammation in a CD1d-independent way, all relevant functional iNKT responses described to date require binding of the iNKT TCR to CD1d. We and others have used recombinant human iNKT TCRs to measure their binding to CD1d/lipid-complexes and study their atomic structure [241, 242]. The binding studies have shown that human iNKT TCR bind with relatively high affinity to CD1d/KRN7000 complexes, with very fast ON- and OFF-rates[241]. We have analysed the structures of three different CD1d/KRN7000-specific human TCRs, two of which were Vα24-negative. Interestingly, sequencing analysis has revealed that these Vα24-negative TCRs, like iNKT TCRs, also use the Jα18 junctional segment to bind to CD1d/KRN7000[241]. In addition, Vβ11 is the dominant TCR β chain used by these Vα24-negative TCRs[214]. The recently solved crystal structure of a ternary CD1d/α-galactosylceramide/iNKT TCR complex has provided further fascinating insights. In particular, the ternary complex structure has disclosed that the iNKT TCR docks virtually parallel to the CD1d-binding cleft and that the position of the iNKT TCR is shifted towards the COOH-terminal end of CD1d (Figure 12b) [187]. In the published structure the polymorphic CDR3β loop makes no contacts with the bound glycolipid ligand and only minimal contacts with the CD1d protein (Figure 12c). Importantly, detailed analysis of this interaction showed that only very

little binding energy is provided by contacts of the iNKT TCR to the glycolipid ligand and that the great majority of contacts are protein-protein contacts between the CDR3α and CDR2β loops of the iNKT TCR with the alpha1 helix of CD1d [243]. Based on these facts it can be argued that the iNKT TCR behaves more like an innate receptor than an adaptive T cell receptor.

Figure 12. CD1d recognition by iNKT TCR

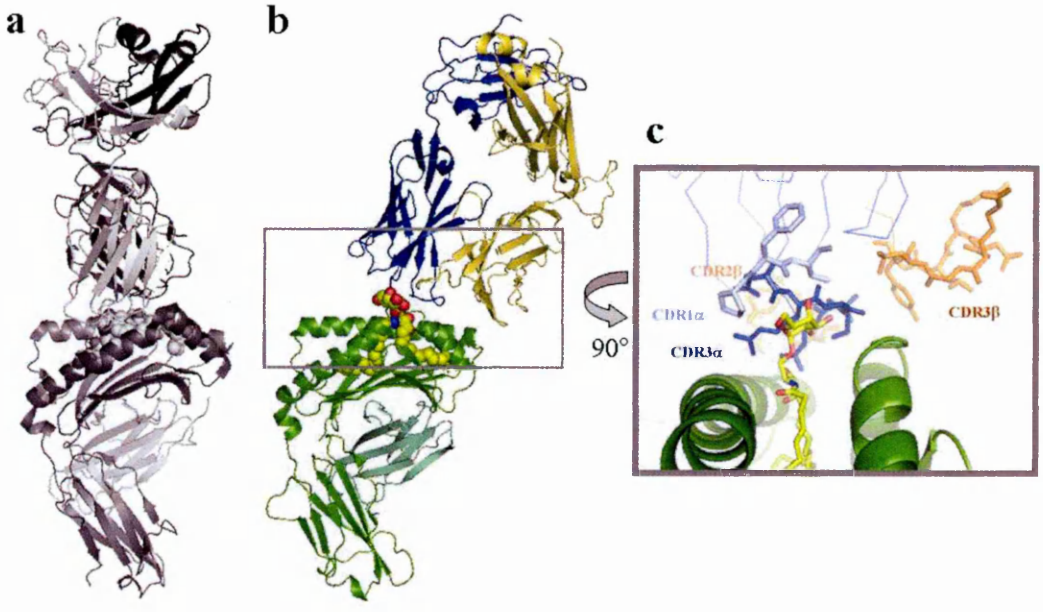

Ribbon diagrams for comparison of the docking of a peptide-specific TCR onto MHC class I/peptide complex[244] *(a) in grey colours (PDB 2VLJ) with docking of a human iNKT TCR onto CD1d/α-GalCer (b, c). NKT TCRα chain in blue, TCRβ chain in gold, CD1d in green, lipid shown as Van der Waals spheres with carbon atoms in yellow, nitrogen in blue, oxygen in red (PDB 2PO6)*[187]*. (c) Detail showing CDR3β loop position..*

1.11. Objectives of the thesis

In 1996 I identified and clinically characterised a primary immunodeficiency syndrome in 6 patients with bronchiectasis, necrotising granulomatous skin lesions, and strongly reduced cell surface expression of MHC class I molecules.

The first objective of my PhD was to unravel the molecular mechanisms and genetic defects causing the reduction of MHC class I cell surfaceexpression in these patients.

Another objective of my studies was to delineate the immunological processes leading to the mutilating granulomatous skin lesions in these patients.

In light of the severe defect in MHC class I antigen presentation I was intrigued by the fact that none of my patients had ever suffered from mycobacterial infections. This led me to ask the question whether peptide-independent antigen presentation via CD1 molecules could protect MHC class I deficient humans from tuberculosis. My PhD therefore also aimed at developing sensitive and specific tools to study CD1-dependent T lymphocytes.

2. Methods

Identification of TAP deficient Patients

The index patient ("AK") was treated for suspected Wegener's granulomatosis (WG), an autoinflammatory disease, at the time when I joined the Rheumaklinik Bad Bramstedt (the German national vasculitis centre) in 1996. Why I doubted the diagnosis of WG and how "AK" was diagnosed with type 1 BLS is described in the introduction of the first results chapter (p. 87). When studying "AK's" clinical files (going back to the early eighties) I came across a handwritten letter from Capa University in Istanbul, describing a first-degree relative of "AK" - "FT"- with similar skin lesions who lived in Turkey, near Istanbul. After having found her dermatologist in Turkey, Dr. Cem Baykal, he kindly asked "FT" to participate in our studies and arranged for the patient's peripheral venous blood to be taken and sent over to Oxford. By searching the Medline database I identified another potential patient with a highly similar clinical syndrome of unknown cause[245]. I contacted the patient's doctor in Brussels, Maria Willemsen, who also kindly arranged for the patient's blood to be tested for MHC class I expression and then be sent to Oxford after informed consent. This was patient "NP". Through Edouard Grosshans, a pathologist at Strassbourg University, who had previously published a few patients with necrotising granulomatous disease of unknown origin in France I made contact with Dr. Julien Lambert, a dermatologist in Brussels who cared for patient "NV". Dr. Julian Lambert also very kindly arranged for "NV's" MHC class I expression to be tested and for her peripheral heparinised blood to be sent to Oxford. After having studied the clinical files of "AK", "FT", "NV" and "NP", all of whom shared a similar clinical syndrome

with recurrent infections of the respiratory tract and mutilating necrotising granulomatous skin lesions, I sent letters to all Swiss Dermatology Clinics, describing the clinical syndrome. Prof. Stanislaw Buechner from the Dermatology Clinic at the University of Basel responded to my letter and he arranged an interview between the family of patient "GAB" and me at the University Hospital in Basel. "GAB"'s sister "SAB" was also present during the interview. Although "SAB" didn't suffer from skin lesions, it became very clear during the interview that she also suffered from recurrent respiratory infections. Both "GAB" and "SAB" gave informed consent to participate in the study and their blood was sent to Oxford for later analysis. "GAB" and "SAB" are still my patients today. A year after I had come to Oxford to study the molecular and genetic basis of this syndrome I received a phone call from my former colleague at the Rheumaklinik Bad Bramstedt, Dr. Peter Lamprecht, who had just made a diagnosis of type 1 BLS in a patient. The patient, "BS", had just been admitted three days before with a suspected diagnosis of Wegener's granulomatosis. The same week I travelled to Bad Bramstedt to interview the patient and view the clinical files. "BS" very kindly donated a venous blood sample for my studies which I brought back to Oxford.

Flow cytometry for analysis of TAP patients

The following antibodies were used at 5µg/ml to detect MHC class I surface expression in different experiments: W6/32 (stains HLA-A,B,and -C molecules), MA2.1 (stains HLA-A2 and -B57), 4D12 (stains HLA-B51), and T116-5-28 (Saxon/UK; stains HLA- A32,and -B44), followed by FITC-goat-anti-mouse F'ab (DAKO). Staining was done on ice in FACS-buffer (phosphate buffered salline/1%

FCS). Cells were washed twice with FACS-buffer in between and after antibody stainings and fixed in FACS-buffer plus 4% formaldehyde before fluorescent activated cell sorter (FACS) analysis (FACScalibur, Becton & Dickinson) or immunofluorescence microscopy (Zeiss, Germany).

The following antibodies were used to phenotype the patients' PBMC : Antibody specific for CD94 (HP3B1; IgG), and immunoglobulin-like transcript 2 (ILT 2; 3F1) were used for both fluorescence-activated-cell-sorter (FACS) analysis and immunostaining of cryostat sections. γδ T cells were stained with the monoclonal antibody B1 (IgG1). The variable δ1-chain (Vδ1)-specific antibody A13, and variable δ2-chain (Vδ2)-specific antibody, 4G6 (IgG1) were kindly provided by Gennaro De Libero (Kantonsspital Basel, Switzerland), and were used to measure the δ1 to δ2 ratio in PBMC and for immunostaining of cryostat sections.

Processing of lesional skin biopsies

Frozen skin biopsy sections were stained by streptavidin-biotin immunoperoxidase technique and counterstained with Mayer haematoxylin.

HLA typing of patients

HLA class I and class II typing was carried out by PCR using sequence-specific primers (PCR-SSP) at the Oxford Transplant Center (Churchill Hospital, Headington, Oxford).

B-Lymphoblast cell lines

Immortalised B-cell lines "AK", "FT", "NP", NV", "SAB", "GAB" and "BS" were generated by transformation of B-cells with Epstein Barr virus according to standard protocols. Lines "AK" and "FT" were generated by Helene Teisserenc before my arrival in Oxford. Briefly, 5-10 x 10^6 PBMC were suspended and incubated in 2 ml of EBV-containing cell-free supernatant from B-958 marmoset cells at 37°C, 5% CO_2. After 2 hours, 8 ml of cell culture medium (RPMI, 20% FCS) supplemented with 1 μg cyclosporin A (final concentration 0.1 μg/ml cyclosporin A) were added. The cells were transferred to a T-25 tissue culture flask and incubated in an upright position. After successful transformation the patients' EBV B-lymphoblast lines were cultured in RPMI and 10% FCS, supplemented with 1% penicillin, 1% streptomycin and 1% glutamine (= R10).

721.174 is a human lymphoblastoid cell line, generated in the laboratory of Rob De Mars[91], which lacks both TAP genes and expresses only the HLA-A2 and HLA-B51 class I molecules. 721.174.TAP is a stable transfectant of 721.174, expressing TAP1 and TAP2. 721.220.B44 is a tapasin-deficient, stable transfectant derived from 721.220, which expresses only the HLA-Cw1- and HLA-B44 class I molecules.

Cell lines 721.174.TAP and 721.220.B44 were cultured in R10 supplemented with 1mg/ml G418 (Gibco). Cell lines .45 and LG2 are TAP and tapasin-competent positive control B-cell lines.

Metabolic labelling of B-lymphoblast lines

B-cells growing in log phase, $2x10^7$ per experiment, were cultured for 1h in Methionine-free medium and labelled at high density ($5x10^7$/ml) with 300μCi ^{35}S-methionine for 20 minutes at 37°C. For some experiments, cells were first labelled with 300μCi ^{35}S- methionine overnight (16h), washed once in methionine-free medium, and labelled again with 300μCi ^{35}S-methionine for 20 minutes or used directly without a second labelling step. Samples were then washed twice with ice-cold PBS before further processing.

Isoelectrofocusing of metabolically labelled MHC class I molecule

^{35}S-methionine labeled EBV B-lymphoblasts from patient AK and from control B-cell lines were lysed with 1% NP-40 either immediately after the ^{35}S-methionine pulse or 3 hours or 15 hours after washing the cells and the addition of the chase medium. MHC class I molecules were immunoprecipitated as described below with the anti-MHC class I antibody W6/32 and protein A sepharose beads and then separated by an isoelectrofocusing gel and exposed to autoradiograph film.

Immunoprecipitation

Metabolically labelled B-cells were washed twice with ice-cold PBS and lysed with 1% NP40 or 1% digitonin for immuno- and co-immuno-precipitation, respectively. Immunoprecipitation with protein A-Sepharose beads (Sigma) and specific antibodies (rabbit-anti-human TAP1 antiserum AK13; mouse anti-human TAP1 monoclonal antibody 147.3) was carried out after an overnight preclearing step at 4°C with

formalin-fixed *Staphylococcus aureus* and normal rabbit serum. The beads were washed four times and proteins were eluted by boiling the beads for 5 minutes in Laemmli sample buffer. The samples were separated by 10% sodium dodecyl sulphate polyacrylamide gel electrophoresis (SDS-PAGE). The gel was dried and exposed to autoradiograph film (Kodak) or analysed with phosphoimager.

Western immunoblotting

Total 1% NP40 cell lysates of patients' EBV B-lymphoblast lines and control lines were centrifuged at 10,000 rpm for 5 minutes at 4°C using a microfuge to remove nuclei, separated by SDS-PAGE (with an equivalent of $3x10^5$ to $1x10^6$ cells per lane) and transferred onto a Hybond-C membrane (Amersham). The membranes were probed with rabbit sera to the C-terminal portion of human TAP1 (AK13) and TAP2 (AK8), or the monoclonal mouse anti-human TAP1 antibody 147.3 (kindly provided by Robert Tampe; Max-Planck Institute, Martinsried, Germany) in blocking buffer (5% Marvel milk/0.1% Tween20). After several washes in PBS/0.1% the membranes were exposed to the secondary antibody (HRP-conjugated goat anti-rabbit or goat anti-mouse), washed, developed with amplifier reagent (ECL; Amersham Pharmacia) and exposed to autoradiograph film (Kodak).

Transient fusion of TAP-deficient and TAP-competent B-cell lines

B-cell lines used for fusion experiments were grown to log phase, and $15x10^6$ cells of each B-cell line, i.e. each fusion partner, were used per experiment. Two fusion partners were thoroughly mixed, washed, and resuspended in 5ml R10 containing

25ug/ml PHA-P (Sigma). After incubation for 1hr at 37°C cells were spun at 400G. To the cell pellet, 400ul of 37°C warm fusion buffer (50% PEG 1300-1600 and 5% DMSO in PBS) was added drop wise over 1 min. After incubation at 37°C for 1 min. 15ml of 37°C warm PBS were added drop wise over 2 min., followed by gentle centrifugation at 250G and careful resuspension of the cells in 10ml 37°C PBS. After incubation for 30min. at 37°C, cells were centrifuged at 400G and resuspended at 10^6/ml in R10. After 24h in culture, cell viability was checked by trypan blue staining and fresh R10 was added to adjust cell density to 0.6 x 10^6/ml. On the next day, fusion products were stained with HLA-specfic antibodies and analysed by immunofluorescence microscopy and FACS.

Restoration of class I expression in TAP-deficient EBV B-lymphoblast lines with a recombinant TAP1/TAP2-encoding vaccinia virus (TAPs-VAC)

2-5 million immortalised EBV B-lymphocytes were infected for 1 hr at 37°C with a recombinant vaccinia virus ("TAPs-VAC"), encoding both human TAP1 and TAP2 proteins [246], or a recombinant control vaccinia virus ("Influenza matrix protein VAC") at 5 plaque forming units/cell and stained with W6/32 and a FITC-labelled anti-mouse antibody, before FACS analysis. Both recombinant vaccinia viruses were kindly provided by Jonathan Yewdell (Bethesda, USA).

Peptide translocation assay

5 x 10^6 B-lymphocytes per experiment were used. Cells were washed once in incubation bufffer (5mM Hepes, pH 7.30, 130mM KCl, 10mM NaCl, 1mM $CaCl_2$,

2mM $MgCl_2$, and 2mM EGTA) and permeabilised with 2 U/ml streptolysin O (Sigma) for 10 minutes at 37°C in 50µl incubation buffer. Then, 10µl of ^{125}iodine-labeled peptide RRYQNSTEL, 10µl of 100mM ATP and 30µl of incubation buffer were added and the samples incubated for another 5 minutes at 37°C, followed by lysis in 1% NP40-buffer on ice. After centrifugation to remove cell nuclei, the glycosylated peptide fraction was isolated using concanavalin A sepharose beads (Sigma) and the radioactive peptide fraction quantified with a gamma-counter.

Radiolabeling of the peptide "RRYQNSTEL"

The peptide RRYQNSTEL is used for TAP translocation assays because it contains both a tyrosine (Y) which can be labelled with iodine and a "NST" glycosylation motif [94]. Stock solutions of radioiodinated peptide RRYQNSTEL were prepared at 10mM concentration in water after removal of free iodine by Sephadex G10 columns. Briefly, 10µl (1mC) of ^{125}iodine (Amersham Pharmacia) were added to 2 washed iodobeads (chloramine-T beads; Pierce) and 90µl PBS in a 1.5ml Eppendorf tube and left at room temperature for 5 minutes to transform ^{125}iodine into the active form ^{125}iodide. 1mg of RRYQNSTEL peptide in 100 µl PBS was added and left at room temperature for 15 minutes. The reaction was stopped by removing the iodobeads. Excess free iodide was removed from the iodinated peptide by separating the reaction mix on a Sephadex G25 column.

TAP2 gene analysis in patient "AK"

The TAP2 coding sequence was determined on both strands by DNA sequencing using an Applied Biosystems automated sequencer. PCR amplification of exons 5 and 6 of the TAP2 gene was performed using the forward primer 5'TGGTGTTTGCTGGCCCTC3' (position 45811) and the reverse primer 5'GAGAGCAGGCT TGGCTTC3' (position 46354). Restriction fragment length polymorphism analysis was carried out using the HpaII restriction enzyme[247] (data not shown).

RT-PCR and sequencing of TAP2 in patient "BS"

Total RNA was prepared from "BS" B-cell line with RNAzol reagent and single-stranded cDNA was synthesized by reverse transcription using Moloney murine leukemia virus reverse transcriptase and an oligo(dT) adaptor in a reaction volume of 50µl. Genomic DNA was purified from BS B-cell line using Purogene DNA isolation kit. Overlapping segments of BS TAP2 cDNA were amplified using the following primers: 5'ACCTCAGCGCTGAAGCAGAAGTCC (FP1), 5'AGCT GGTCACTGTGGG CTGTTCTG (FP2), 5'GAGACTAAGACAGGGGAGCT GAAC (FP3), 5'GAACGCGC CTTGTACCTGCTCGA (FP4), 5'CCTGTGCTCAAGGG GCTG ACGTTT (FP5), 5'GAT GTAGGGGAGAAGGGAAGCCAG (FP6), 3'AGTATCCCTGGGGCCTCAG TCCAT (RP1), 3'AGCCGCCATCACCTTATCATCTTC (RP2), 3'GTAGGAGAAAACCTTCT CTGCAGC (RP3), 3'CTGATGGCGGGTGTTGTACA CCTT (RP4), 3'GTCAAAA TCACCTCCCAGGATGTC (RP5), 3'TAGCTTTAGCAG CCCC CACAGCCC

(RP6). For amplification of genomic TAP2 intron 6 DNA of patient "BS" the following primers were used: 5'GATCTGGGGGCCTGCTGTCTTTGC (FG1), 5'AAAAGTGTATAACAACAAAGCC ATTATC (FG2), 5'TCCAAGAGGCACACA ATGTC TGG (FG3), 3'AGCACAGGATGTATACA TGTGAG (RG1), 3'CTCCTTAAATGCAGGCACTGTGCC (RG2), and RP3 (see above). All PCRs were done in a final volume of 100µl with 200µM of each deoxynucleoside triphosphate, 0.4µM of each primer, 2.5 units of Expand High Fidelity polymerase (Boehringer Mannheim) and 10µl of the corresponding 10x reaction buffer. After an initial denaturation step at 95°C for 2 min., amplification was carried out for 10 cycles of 95°C for 1 min., 55°C for 1min., and 72°C for 4min., followed by 26 cycles of 95°C for 1min., 60°C for 1min., and 72°C for 3min. PCR products were analyzed by agarose gel electrophoresis. Amplified TAP2 segments were gel purified using Qiagen gel purification kit and sequenced using the corresponding primers by automated sequencing. DNA sequences were analysed by EditVIEW, DNAstrider, and Clustal W prgrams.

Generation of TAP-patients' NK and γδ T lymphocyte clones

γδ T cells derived from patients "AK" and "FT" were sorted with the pan-γδ antibody B1 and cloned in 96-well plates at 1–5 cells per well. γδ clones were maintained in Iscove medium, containing 5% human serum supplemented with 200 U of recombinant IL-2. The irradiated B-lymphoblast line LG2 and peripheral-blood mononuclear cells from normal volunteers were used as feeder cells. Natural killer (NK) cell lines were obtained from patient "GAB" after two rounds of negative

selection using antibodies to CD3 and CD14. The lines were restimulated in Iscove medium containing 5% human serum plus 1000 U recombinant interleukin 2. B-cell lines LG2 and "GAB" were irradiated and used as feeder cells for natural killer cells.

Cytotoxic activity of TAP deficient γδ clones and NK polyclonal lines

Chromium release assays with TAP-deficient effector and different target cell lines were carried out according to the standard protocol described below ("Chromium release assays"). In a first series of experiments three γδ T cell clones (γδ clones 1, 7, 12) from patient "FT" were tested against EBV transformed B-lymphoblasts from patient "AK" as well as against the MHC class I-negative and –positive control lines 721.221 and LG2, respectively. "FT" and "AK" B-lymphoblast lines were derived from first degree relatives sharing an identical HLA-haplotype. Target cells, i.e. "AK" B-lymphoblasts were infected overnight either with recombinant TAP-vaccinia ("TAPs VAC") or recombinant "Influenza matrix protein VAC" as a control. In further experiments the γδ clone 6G11 from patient "GAB" was tested against autologous "GAB" lymphoblasts after overnight infection with either "TAPs VAC" or "Influenza matrix protein VAC" and against 721.221 and LG2. In experiments analysing the cytotoxic activity of an NK line obtained from patient "GAB" the following target cells were used: EBV transformed B-lymphoblast lines "GAB" and "AK", NK target lines 721.221 and K562 and the class I positive B cells line LG2.

Generation of human CD1b and CD1d encoding plasmids for expression of the extracellular domains in E.coli.

The extracellular alpha 1-alpha3 domains of human CD1b (Swiss-Prot entry 29016) and human CD1d (Swiss-Prot entry P15813) were amplified by PCR and cloned into the prokaryotic expression vector pET23d (NOVAGEN, USA) using an *NcoI* restriction site (CCATGG) in the sense primer and a *BamHI* restriction site (GGATCC) in the antisense primer. As a template I used cDNA derived from my own monocyte-derived dendritic cells (see protocol for generation of Mo-DC below). The following oligonucleotide primers were used to amplify human CD1d: Sense primer: GACGCCATGGTACCA CAAAGACTTTTCCCA; Antisense primer: GCTGCGGATCCCGGACCCCAGTAG AGGACGATG TCCTGG. Primers used to amplify human CD1b: Sense primer: GACGCCATGGGATCTGAACATGCTTTCCAG GGTCCTACC; Antisense primer: GCTGCGGATCCCGGACCCCAGTATTCGATTTT CTGAGC.

The PCR mix (per one 100µl reaction) typically contained 0.4µM of each primer, 0.2mM dNTPs, 1 µl of the enzyme (Expand High Fidelity polymerase from Roche), 10µl of the 10x Expand High Fidelity reaction buffer (Buffer 2, Roche) and of 1µl of the template. The PCR reactions were run on a Px2 gradient cycler (Thermo Hybaid). All restriction enzymes were from New England Biolabs. *NcoI/BamHI* - double digested pET23d plasmid and PCR products were gel purified before ligation using T4 ligase (New England Biolabs). E.coli strain DH5a was transformed with the ligation product and spread onto (100µg/ml) ampicillin-supplemented Luria Broth agar plates. Bacterial colonies were screened by PCR using the original cloning

primers and 3-5 of the positive colonies were selected for plasmid purification using Miniprep kits from Qiagen. Plasmid sequences were determind by the Oxford Biochemistry Sequencing Facility and results controlled using the software Edit View. The plasmid pET23d-β2m was a gift of Dr. Bent Jacobsen.

Generation of recombinant human inclusion body proteins

All proteins used for *in vitro* refolding were synthesised in *E. coli* strains BL21 and Rosetta according to standard protocols [248]. In brief, competent bacteria were transformed with expression plasmids and single colonies were grown to log phase in ampicillin (100μg/ml) supplemented low salt Luria broth (5g NaCl, 10g BactoTryptone, 5g yeast extract in 1000ml H20). When growth reached an optical density OD_{600} of ca. 0.5 AU protein expression was induced with 0.6mM IPTG (Melford Laboratories). Bacterial pellets were harvested ca. 4 hours later, resuspended in ice-cold PBS and sonicated to break up the cells and liberate the inclusion bodies. The inclusion bodies were washed several times with Triton-X100 containing buffer using a glass homogenizer before they were solubilised at 5-10mg/ml in a buffer containing both reducing and chaotropic agents, i.e. DTT (20mM) and either 8M urea or 6M guanidinium hydrochloride. Soluble inclusion body protein was separated from insoluble material by centrifugation and used immediately or frozen at -80°C.

Generation of CD1d-tetramers

Oxidative refolding chromatography was applied for *in vitro* refolding of CD1d/β2m complexes in the presence of either α-galactosylceramide (α-GalCer) (Kirin Brewery), α-mannosylceramide (α-ManCer) (Kirin Brewery), β-galactosylceramide (β-GalCer) (Fluka) or ganglioside GM1 (G-7641 Sigma-Aldrich) lipid ligands, following the principles of a protocol previously described [249]. Soluble protein fractions were concentrated to a volume of 3ml and directly biotinylated as previously described. Biotinylated monomeric CD1d/β2m/glycolipid complexes were separated from soluble protein aggregates and free biotin by FPLC size exclusion chromatography using a Superdex75pg 26/60 gel filtration column (Amersham-Pharmacia, Uppsala, Sweden), and conjugated to Streptavidin-PE (Sigma-Aldrich).

Liver disease Patient samples

Heparinised peripheral venous blood was obtained from 7 patients (patients 1 to 7) with active hepatitis C virus (HCV) infection during routine follow up visits, and also from 4 healthy donors. Peripheral blood mononuclear cells (PBMC) were separated on a Ficoll-Hypaque gradient. Human liver specimens were obtained from four patients with end stage liver failure due to chronic inflammatory liver disease of various etiologies: patient 8, Hepatitis C (HCV); patient 9, HCV; patient 10, HCV; patient 11, HCV plus Hepatitis B virus (HBV). Informed consent was obtained from all individuals. Intrahepatic mononuclear cells were separated from the liver specimens by cutting the tissue into small pieces using a scalpel, followed by incubation at 37 °C, for 4 hours in complete medium containing 0.5mg/ml type IV collagenase (Sigma-

Aldrich) and 0.02mg/ml DNAse (Boehringer Mannheim). The digested tissue was passed through a 100μm metal mesh filter, washed twice with PBS, layered over Ficoll-Hypaque gradients, and centrifuged at 400xG at room temperature for 20 minutes.

Mice

Wild type C57BL/6 mice, $TAP^{-/-}$ and $\beta 2m^{-/-}$ mice (deficient for murine MHC class I molecules $D^{b-/-}$ and transgenic for a chimeric HLA-A*0201/D^b molecule covalently linked to human β2-microglobulin [250]), were used to study whether the human CD1d/α–GalCer-tetramer could detect murine invariant NKT cells. Splenocytes from these mice were obtained using the following protocol: spleens were cut into small pieces using a scalpel, passed through a 100μm metal mesh filter, washed twice with PBS, layered over Ficoll-Hypaque gradients, and centrifuged at 2000 rpm at room temperature for 20 minutes. Before immunostaining with CD1-tetramers the splenic mononuclear cells were incubated for 10 min. at room temperature with 20μg of unconjugated anti-FcR antibody (BD Biosciences).

Generation of human monocyte-derived dendritic cells (Mo-DC)

PBMC were purified from healthy donors' buffy coat by layering over Lymphoprep (Nycomed, Asker, Norway). Monocytes were then positively selected using magnetic beads coated with anti-CD14 mAbs (MACS, Miltenyi Biotech, Germany). The monocyte-depleted lymphocyte fraction (CD14-negative) was frozen in 50%R10/10%DMSO/40%FCS in liquid nitrogen until needed. Monocytes were

cultured in cell growth medium (RPMI 1640, Sigma, Dorset, UK; 10% FCS, 2mM L-glutamine, GIBCO, Paisley, UK; 1mM non-essential amino acids, 1mM sodium pyruvate, 55μM 2-mercaptoethanol, penicillin G, streptomycin, all Life Technologies, Paisley, UK), containing 50ng/ml GM-CSF (Novartis, Basel, Switzerland) and 1000 U/ml IL-4 [251]. The monocytes were plated in 6 well costar plates at $4x10^5$ cells/ml (3ml per well). After 4 days, maturation was induced in some wells by adding either bacterial lipopolysaccharide (final concentration 1μg/ml LPS of *Salmonella abortus equi*, Sigma), 50ng recombinant TNF-α (R&D Systems, Minneapolis, USA) or $4x10^4$ irradiated (6 Gy) CD40L expressing B-cells [252]. Immature and matured monocyte-derived dendritic cells (Mo-DC) were used for phenotypic analysis and *in vitro* priming after 6 days in culture, i.e. 40 hours after induction of maturation.

T lymphocyte in vitro stimulation

Monocyte-depleted or total PBMC were plated in 24-wells at $1x10^6$ cells/ml in cell growth medium. The following culture conditions were chosen: 1) Freshly isolated or thawed PBMC ($2x10^6$) from a single donor, cultured in the presence of 100nM αGC (KRN7000; Kirin Brewery, Gumna, Japan); 2) Co-culture of $2x10^6$ monocyte-depleted, thawed lymphoctes and $2x10^5$ autologous, αGC pulsed immature or matured Mo-DC, respectively. For pulsing of Mo-DC with αGC, cells were cultured for 2h in 24-wells in a volume of 200μl RPMI1640 containing 1μM αGC, followed by addition of $2x10^6$ lymphocytes in 1.8ml of the above medium (i.e. 100nM final αGC

concentration). After 5 days, IL-2 was added to cultures (25 IU/ml). Thereafter, cultures were fed every 3-4 days with fresh medium containing IL-2 (1000 U/ml).

Flow cytometry studies using CD1d-tetramers

The following antibodies and tetramers were used to stain single cell suspensions of Mo-DC and *in vitro* stimulated T cell cultures : purified anti-CD86 (Pharmingen, San Diego, USA), -CD83 (Immunotech, Marseille, France), -MHC-class II (mAb L243; ATCC), -MHC-class I (mAb W6/32; ATCC), and PE-conjugated goat-anti-mouse pan IgG (SBA, Alabama, USA); APC- and PE- conjugated human CD1d-tetramers loaded with either αGC or α-mannosylceramide (αMC) were generated as previously described [253]; FITC- and PE- anti-hTCR Vα24, FITC anti-hTCR Vβ11 (Serotec, Oxford, UK), FITC-anti-CD3, -CD4, -CD8α, PE-anti-CD4 (all from DAKO, Kobenhavn, Denmark), FITC-anti-CD161, PerCP-anti-CD8α, APC-anti-CD8α, -CD3 (all from BD Pharmingen, San Diego, USA), FITC-anti-TCR Vβ1, -Vβ9, -Vβ12, -Vβ16, -Vβ18, -Vβ23, and PE-anti-CD8β (all from Immunotech, Marseille, France); Initial CD1d-tetramer validation experiments and tetramer staining of intrahepatic lymphocytes cells were carried out in the following way: Cells were first incubated with CD1d tetramers for 20 min. at 37°C. After one wash with warm PBS/1%FCS samples were stained with monoclonal antibodies on ice and propidium idodide was added immediately before FACS analysis to gate out dead cells. For all later studies, cells were generally stained on ice for 30 min., washed twice in ice cold PBS/1% FCS, and directly analysed. In some experiments, cells were first stained with anti-TCR Vβ antibodies, followed by CD1d-tetramers. In monomer competition experiments, cells

were first incubated with CD1d-α–GalCer monomers for 20 minutes at room temperature before addition of CD1d-α–GalCer tetramers on ice for another 30 minutes. Dead cells were stained with propidium iodide and excluded from the analysis. For monomer-binding and chase studies, cells were first incubated on ice with CD1d/α–GalCer monomers for 30 min., washed twice in ice-cold PBS, stained with RPE-Extraavidin (Sigma) on ice for 30 min., and washed twice with ice-cold PBS. Then, cells were centrifuged and immediately fixed using 4% formaldehyde in PBS (Chase time "0 minutes") or else they were incubated at 37°C 5% CO_2 in a volume of 200µl PBS for different chase periods (15, 30, and 60 minutes) before fixation. Samples were analysed on a FACScalibur flow cytometer, and data were processed using CellQuest software (BD, San Jose, USA).

Cell sorting and generation of Va24- CD1d/α–GalCer tetramer+ cell lines

For generation of clones and oligoclonal lines, Vα24- CD1d/α–GalCer-tetramer+ and Vα24+ CD1d/α–GalCer-tetramer+ cells were sorted by a FACSVantage sorter into 96-well plates coated with 500ng OKT3 antibody and restimulated with 1µg/ml Phytohemagglutinin (PHA; Sigma, Dorset, UK) and $1x10^5$ irradiated feeder cells (allogenic PBMC and B-cell line LG2) in medium containing 1000 IU/ml IL-2. Established lines and clones were fed every 3-4 days with fresh medium. In order to generate a polyclonal Vα24- CD1d/α–GalCer-tetramer+ line $3x10^3$ cells were sorted into OKT3-coated 96-wells and cultured in 200µl of IL-2 containing medium in the presence of feeder cells. Purity of all lines was checked after 3 weeks with anti-Vα24 antibodies and CD1d/α–GalCer-tetramers. Clones and oligoclonal lines were

restimulated once with PHA and feeder cells, while the polyclonal line was snap frozen in RNAzol (Biogenesis, Ltd, Poole, UK) until further use for spectratype analysis of TCR usage.

Chromium release assays

TCR Vα24-positive and -negative lines and clones were used as effector cells in a 5h-^{51}Cr release assay 14 days after restimulation. Human CD1d-expressing C1R cells (C1R-CD1d, kindly provided by Cesar Milstein) were used as target cells. C1R-CD1d were labelled for 90 minutes with ^{51}Cr and at the same time pulsed with either 1μM αGC, 1μM αMC, or vehicle, followed by extensive washing in warm RPMI1640. In CD8-blocking experiments, cells were cultured in the presence of the CD8-blocking antibody MF8 [254] or an irrelevant isotype matched control antibody at 1:100, 1:500, and 1:1000 dilution of ascites. Cells were cultured in triplicate in 96-well round bottom microtiter plates. Effector:Target (E:T) ratios were 1:1, 3:1, and 9:1. Maximum release was determined from supernatants of cells that were lysed by addition of 5% Triton-X 100, and spontaneous release was determined from target cells incubated without effector cells. Percent specific lysis was expressed as (cpm of sample - cpm of spontaneous release) / (cpm of maximum release - cpm of spontaneous release).

Intracellular cytokine staining

$2.5x10^5$ T lymphocytes were cultured in 48-well plates in the presence of either glycolipid pulsed C1R-CD1d (see above) or 10^{-7}M phorbol myristate acetate (Sigma, Dorset, UK) and 1μg/ml ionomycin (Sigma). After 90 minutes, 10μg/ml Brefeldin A (Sigma) was added to the cultures to block cytokine secretion. After 6h in culture, cells were washed twice in PBS and fixed in 2% paraformaldehyde. Intracellular cytokine staining was performed after permeabilisation of cells with FACS permeabilisation buffer (BD, San Jose, USA), using the following antibodies from Pharmingen (San Diego, USA): FITC-anti-IFNγ, PE-anti-IL-4, PE-anti-IL-13, and APC-anti-IL-2. Four colour analysis was performed on a FACScalibur flow cytometer (BD, San Jose, USA).

Spectratyping of TCR repertoire

Total RNA was extracted from a pure TCR Vα24- CD1d/α–GalCer tetramer+ polyclonal cell line (see above) using RNAzol reagent according to the manufacturer´s instruction, and single-strand cDNA was synthesized by reverse transcription using Moloney murine leukemia virus reverse transcriptase and an oligo(dT) adaptor in a reaction volume of 50μl. Oligonucleotides used to analyse the 32 different TCR Vα- and 24 different TCR Vβ- families, as well as the Cα- and Cβ-specific primers have been described [255, 256]. Each TCR Vα- and TCR Vβ- PCR product was then used as a template for extension, or run-off, reactions using Cα- and Cβ-specific nested fluorescent primers, respectively. The fluorescent run-off products were subjected to gel electrophoresis in an automated DNA sequencer (Perkin Elmer, Bucks, UK), and

CDR3 size distribution and signal intensities were analysed with GeneScan software (Perkin Elmer). Analysis of Vβ-joining segments (Jβ) was carried out in the same way using previously described fluorescent Jβ-specific oligonucleotide probes [256].

I am indebted to Nicolas Dulphy, who designed the spectratype experiments, carried out the initial experiments, and closely supervised me on all further spectratype experiments.

Generation of recombinant soluble human CD1b/lipid complexes

Initial refolding trials of human CD1b using standard refolding techniques for MHC class I molecules [257] were unsuccessful. Massive protein aggregation was visible almost immediately after addition of the denatured and reduced inclusion body proteins to the standard refolding buffer. Based on the assumption that the lipid presenting CD1b molecule was more prone to hydrophobic aggregation during early refolding stages (in particular during the molten globule state)[258] I designed several detergent assisted refolding protocols based on the principles of published protocols for other proteins[259-272]. From the published detergent-assisted refolding methods it emerged that the optimal detergent and its optimal concentration for refolding would be different for each new protein. For the initial refolding trials I chose 9 different detergents at 3 different concentrations and used these conditions for CD1b, CD1d and HLA-A2. The 81 refolding reactions were carried out in 1ml. To assess whether there were qualitative differences between the different conditions I recorded the UV spectrum (from 200-320nm) of these "minirefoldings". At the time when I did these experiments, back in the spring of 1999 there was no printer attached to the UV

spectrophotometer and I had to draw the curves from the machine's monitor. Based on the shape of the curve in the area of expected light scattering I chose the detergent CTAB (hexadecyl-triammonium bromide) for further optimisation of the refolding protocol. Interestingly, CTAB also led to visible precipitation of HLA-A2 while it seemed to keep CD1 molecules in solution. The following paragraph describes the final protocol:

For refolding of human CD1b and human β2m the fully denatured and reduced inclusion body proteins were diluted into buffer 1 (1M urea, 300mM L-arginine, 50mM Tris pH 7.5, 2mM EDTA, 5mM reduced glutathione, 0.5mM oxidized glutathione) containing 0.5mM hexadecyltrimethyl-ammoniumbromide and either phosphatidylinositol (PI; purified from soy bean; Avantlipids, USA) or synthetic ganglioside GM2 (kindly provided by Richard R. Schmidt). Excess detergent molecules were removed by methyl-β-cyclodextrin (Fluka), and the refolding mix was concentrated using Amicon stir cells (Amicon, USA) and PM10 membranes (Millipore). The soluble protein fractions were separated by size exclusion chromatography using fast liquid pressure chromatography (FPLC; Amersham Pharmacia) and a Superdex75 prep grade column (Pharmacia) equilibrated with buffer 2 (Tris 20mM, pH 6.0, 30mM NaCl). Monomeric hCD1b/hβ2m-ligand complexes were collected at ca. 150ml elution volume and purified again in the same buffer. The pure protein peak containing monomeric hCD1b/hβ2m-ligand complexes was concentrated and used for sitting drop crystallisation.

Protein Crystallisation

Crystallisation trials of CD1b/lipid-complexes, CD1d/α-GalCer complexes and iNKT TCR/CD1d complex were set up manually in microbridges (kindly provided by Karl Harlos) according to the sitting drop method. The proteins were at 5-10mg/ml concentration and for manual crystallisation I used 2µl of the protein solution and 1-2µl of the precipitant. The best crystals for the complexes of both human CD1b/β2m/GM2 and human CD1b/β2m/PI were obtained from 2µl of protein at 5mg/ml with 1µl of PegIon screen precipitant 19 and 21 (Hampton Research). Crystals from both CD1b-complexes diffracted X-rays generated by the in-house beam (of the Wellcome Trust Centre for Human Genetics. These crystals were used for data acquisition at the Synchotron Facility in Grenoble (France). My crystallisation trials with CD1d/α-galactosylceramide complexes yielded only small needle crystals, which were not suitable for X-ray analysis. Later on, using another crystal screen and methods to dehydrate the crystals it was possible to obtain crystals for data acquisition (which resulted in a publication in Nature Immunology [173]). My attempts to crystallise iNKT TCR/CD1d complex (using NaCl screen from Hampton Research) yielded beautiful protein crystals (Figure 13). Unfortunately they did not diffract at all. An atomic structure of an iNKT TCR/CD1d complex was solved by others and recently published in Nature [187].

Figure 13. Protein crystals of human CD1d and CD1d/iNKT TCR complexes

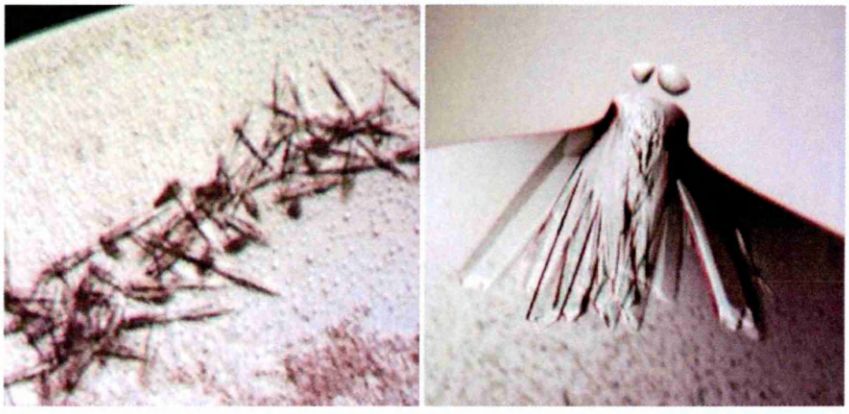

Protein crystals of human CD1d/a-GalCer complex (left) and human CD1d/a-GalCer/iNKT TCR complex (right) are shown. These crystals did not diffract X-rays.

Structure Determination

The atomic structures of human CD1b/GM2 and human CD1b/PI were determined by Nathan Zaccai and Yvonne Evelyne Jones at the Wellcome Trust Center for Human Genetics. The detailed protocols for structure determination have been published [181, 241].

3. Six patients with defective MHC class I cell surface expression due to C-terminal truncation of TAP1 or TAP2 proteins

3.1. Introduction

Patients with complex chronic systemic inflammatory disease present the clinician with a diagnostic challenge, since diagnostic tests to establish the etiology of such syndromes are not available.

In this chapter I will describe the clinical syndrome and the molecular and genetic basis in 6 patients with type 1 Bare Lymphocyte Syndrome (BLS). How I identifed these patients in different European countries is briefly described in chapter 2 ("Methods"). The index patient was "AK", whom I first met in March 1996 on the "vasculitis ward" of the Rheumaklinik Bad Bramstedt. "AK" had been treated since 1990 with various immune suppressive drugs for a suspected diagnosis of "Wegener's granulomatosis" (WG)[273]. However, "AK" had suffered since early childhood from recurrent infections of the respiratory tract, and had suffered several episodes of bacterial lung infection before the start of immune suppressive therapies. Most strikingly, when I first saw "AK" her nose and cheeks were mutilated by granulomatous lesions (Figure 14). Intrigued by this unusual presentation I embarked on a complete clinical work up of this patient's history which revealed the following 5 facts:

1) Whereas 95% of patients with WG respond to the immunesuppressive regimens that had been given to "AK" from 1990 - 1996, i.e. cyclophosphamide [274], the disease course of "AK" seemed to have even accelerated under this treatment. A

photograph of "AK" shortly after the start of cyclophosphamide treatment showed an almost intact outer nose (Figure 14a).

2) Computertomography of "AK"'s lungs revealed the presence of bronchiectasis, i.e. dilatation of lung bronchi caused by severe structural damage, which are not a feature of WG [275].

3) WG is a primary vasculitis syndrome with two different qualities, namely granulomatous tissue inflammation and non-immunecomplex inflammation of small vessels. When both are present, as was assumed to be the case in "AK" (because of the presence of leukocytoclastic skin vasculitis in "AK"), a disease-specific autoantibody directed against proteinase 3 (PR3-ANCA) can be detected in >98% of WG patients [276]. However, PR3-ANCA could never be detected in "AK" despite multiple testing by the German reference laboratory for ANCA-testing.

4) Analysis of the disease history revealed that her upper respiratory problems, which were assumed to be a typical manifestation of WG had started in early childhood. Childhood WG is extremely rare and children with WG suffer also from small vessel vasculitis and have PR3-ANCA.

5) "AK" had a first degree relative in Turkey, "FT", who suffered from very similar necrotising granulomatous skin lesions on her legs (Figure 15). Familial WG is also extremely rare [277].

While some of these facts seemed incompatible with a diagnosis of WG, the combined presence of these features in one and the same patient, "AK", made WG an improbable diagnosis.

Of note, with the exception, ironically, of "AK"'s relative "FT", a diagnosis of WG had been considered also in all other patients (who were treated in other countries) described in this thesis, and all except "FT" had received immune suppressive drugs at some stage during their disease. Of note, both the American College of Rheumatology 1990 criteria [278] and the Chapel Hill 1992 consensus definition [279] could be applied to classify the disease in 4 out of the 6 patients as WG.

The diagnosis of strongly reduced MHC class I expression in "AK", which subsequently lead to the same diagnosis in all other patients, was rather incidental. It was the result of a very broad immunologic testing of "AK"s serum, secretions, and PBMC, once the diagnosis of WG was under doubt.

Once I knew that all patients with the syndrome had reduced MHC class I expression I revisited their family histories and found that all patients were children from consanguineous parents (i.e. first degree cousins). Tissue typing revealed that all the patients were homozygous for the HLA class I and II haplotype which suggested that a primary genetic defect within the HLA region could be the underlying cause for their granulomatous disease (Table 2).

Table 2. HLA haplotype in patients with type 1 Bare Lymphocyte Syndrome

Patient	HLA-A	HLA-B	HLA-C	HLA-DR	HLA-DQ
AK[1]	A*11	B*1502	Cw*0801	DR*15	DQ*0601
	A*11	B*1502	Cw*0801	DR*15	DQ*0601
FT[1]	A*11	B*1502	Cw*0801	DR*15	DQ*0601
	A*11	B*1502	Cw*0801	DR*15	DQ*0601
GAB[2]	A*2601	B*4901	Cw*0701	DR*1301	DQ*0604
	A*2601	B*4901	Cw*0701	DR*1301	DQ*0604
SAB[2]	A*2601	B*4901	Cw*0701	DR*1301	DQ*0604
	A*2601	B*4901	Cw*0701	DR*1301	DQ*0604
NV	A*03	B*1501	Cw*03	DR*1301	DQ*0603
	A*03	B*1501	Cw*03	DR*1301	DQ*0603
NP	A*2301	B*4901	Cw*0701	DR*0301	DQ*0201
	A*2301	B*4901	Cw*0701	DR*0301	DQ*0201
BS	A*32	B*57	Cw*06	DR*12	DQ*07
	A*32	B*57	Cw*06	DR*12	DQ*07

[1/2]: Patients "AK" and "FT" and patients "GAB" and "SAB" were from the same Turkish and Italian families, respectively.

3.2. Results

3.2.1. Clinical data

Patient "AK"

A 36 year old Turkish female suffered since her childhood from recurrent purulent rhinitis with nasal polyps and chronic sinusitis which did not improve after several surgical interventions. In contrast, no severe viral infections were documented and a humoral immune response against Epstein-Barr virus (EBV), Adenovirus, *Toxoplasma*, *Candida* and *Aspergillus* was detected (data not shown). At the age of 10, she developed a chronic spastic bronchitis and from the age of 25, violaceous skin lesions appeared in the face and on the legs (Figure 14). Biopsies of the paranasal sinuses and skin revealed a severe granulomatous inflammation with infiltration of small vessels consistent with a diagnosis of Wegener granulomatosis. This diagnosis was later abandoned because of a clear clinical deterioration under treatment with immunosuppressive drugs. cANCA specific for proteinase 3 (PR3-cANCA) remained negative throughout her life. Multiple tissue culture and acid fast stains failed to demonstrate mycobacterial infection, while skin testing with PPD was positive on several occasions. Clinical features progressively worsened with a complete destruction of her nose, the development of bronchiectasis with recurrent severe bronchopneumonia, retinal vasculitis, chronic encephalitis, and leukocytoclastic skin vasculitis in the skin of arms and legs (Figure 14). Symptoms were not controlled by antibiotic prophylaxis, tuberculostatic drugs and chest physiotherapy. The patient developed antibiotic-resistant pulmonary infections and died of respiratory failure at the age of 36. Autopsy was declined.

Figure 14. Clinical manifestations in patient "AK"

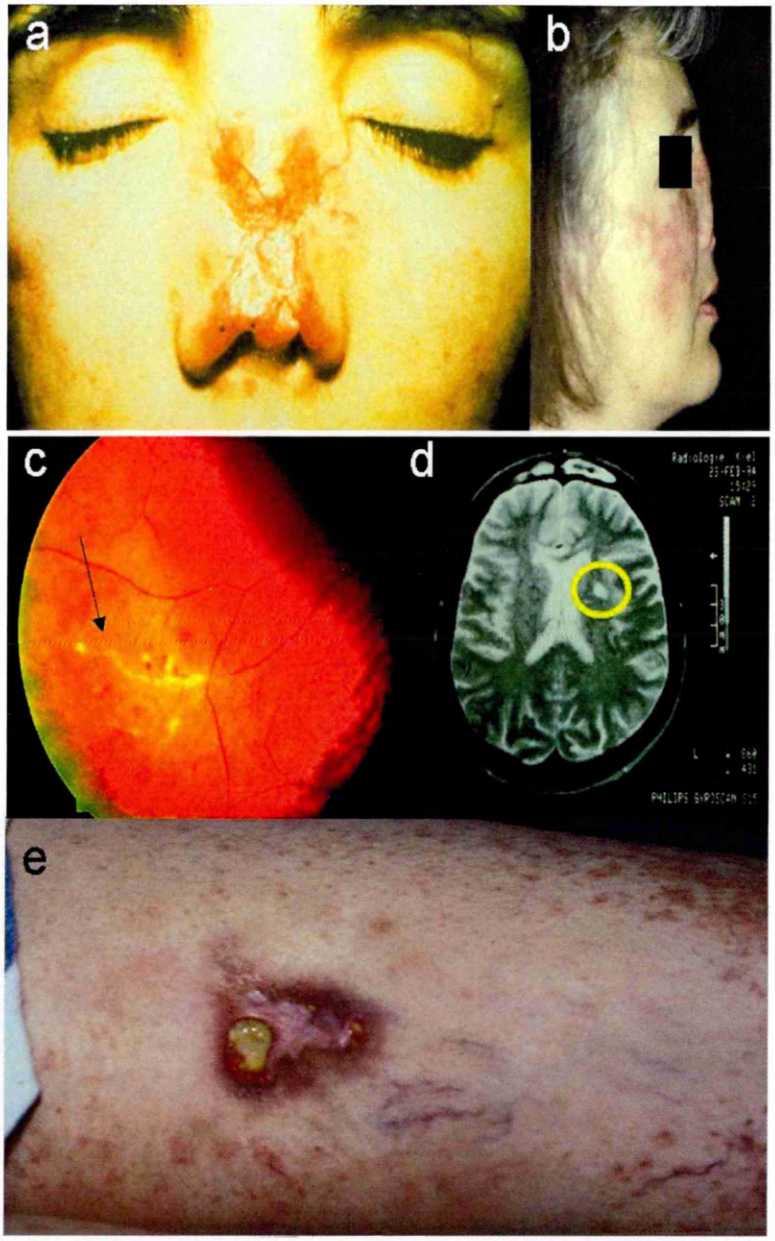

Progressive tissue destruction in « AK » under immunesuppressive therapy from 1990 (a) to 1996 (b). Unusual manifestaions in "AK" included a retina vasculitis (c) and encephalitis (d). Two types of skin lesions in "AK": pyoderma gangrenosum-like (big lesion in panel e) and leukocytoklastic vasculitis (small red dots in panel e).

Patient "FT"

A close relative of AK (FT, born 1947, sister of AK's father), suffered since youth from recurrent upper respiratory tract infections with clinical and radiological signs of chronic sinusitis. During the third decade of her life she developed destructive granulomatous lesions localised around the tip of her nose (Figure 15), with perforation of the nasal septum, and destruction of nasal cartilage. Nodular skin lesions on the legs and arms appeared at the age of 30, with secondary ulcerations (Figure 15). As in AK, multiple biopsies demonstrated a necrotising granulomatous inflammation. Cultures and acid fast staining as well as PCR of the skin lesions failed to demonstrate *M. tuberculosis* and the progression of the granulomatous lesions was not halted by either antibacterial or tuberculostatic drugs. The patient never received immunosuppressive therapy and she is still alive. Tissue typing of AK and FT revealed that they were homozygous for the same extended MHC haplotype (Table 2).

Figure 15. Clinical manifestations in patient "FT"

Mutliating skin lesions at the tip of the nose and on the legs in patient "FT".

Patient "NV"

The patient NV suffered since childhood from recurrent purulent rhinitis, sinusitis and otitis which responded to antibiotic therapy. From age twelve she suffered from chronic spastic bronchitis and at age 18 bilateral bronchiectasis were diagnosed. At age 34 complete destruction of nasal cartilage was observed, and at 35 years of age violaceous papules with secondary ulceration appeared on both legs appeared and in the face, with progressive destruction of the outer nose (Figure 16). Multiple skin biopsies showed severe necrotising granulomatous inflammation in dermis and hypodermis as well as small vessel vasculitis. At the age of 47 years leukocytoclastic skin vasculitis appeared. Multiple staining and cultures of skin biopsies failed to demonstrate mycobacteria, fungi or leishmania and extensive laboratory testing excluded ciliary dyskinesia, common variable immune-deficiency, defects of the phagocyte oxidase system, and SLE. A

diagnosis of Wegener's granulomatosis was considered temporarily but abandoned because anti-neutrophil cytoplasmic antibodies (ANCA) were persistently negative and symptoms clearly progressed during therapy with cyclophosphamid and prednisone. Moreover, therapy with azathioprine and prednisone was complicated by bacterial meningoencephalitis.

Patient "NP"

At the age of 3 years this female patient developed violaceous plaques on the legs which slowly progressed and subsequently ulcerated. By the age of 27 years, mutilating lesions appeared in the face (Figure 16) leading to the destruction of the nasal cartilage. Biopsies showed a necrotising granulomatous inflammation[245]. Neither tuberculostatic nor other antibacterial therapies have influenced the disease course so far. Glucocorticoid monotherapy led to a temporary remission, but did not prevent relapse or progression of the lesions. The patient is now aged 52. Tissue typing of NP revealed that she was homozygous for the MHC haplotype (Table 2).

Figure 16. Mutilation of the nose in Type 1 Bare Lymphocyte Syndrome

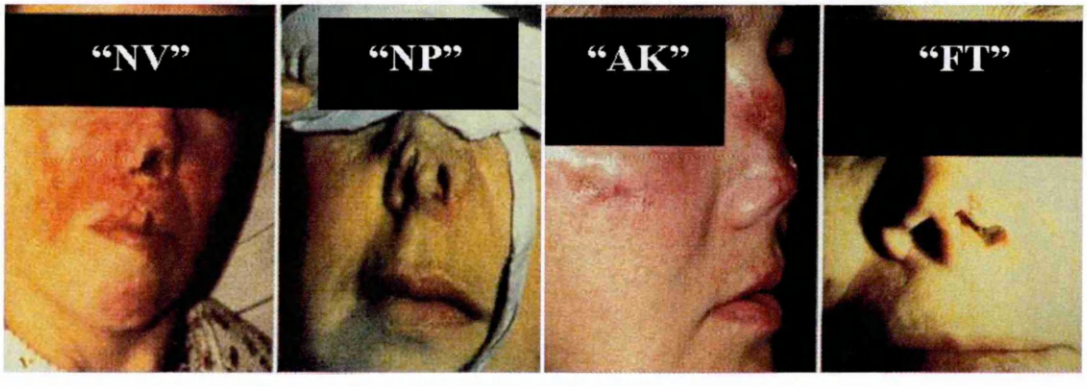

Patients "NV", "NP", "AK", "FT" are shown (From left to right).

Patient "GAB"

From the age of 4, recurrent purulent rhinitis, sinusitis and chronic otitis were documented but no severe viral infections were recorded, and measles and chicken pox ran an uneventful course. From the age of 10, the patient suffered from recurrent bronchopulmonary infections and bronchiectases (Figure 17) were diagnosed at the age of 16. Violaceous papulous skin lesions with secondary ulceration appeared at the age of 19 on the legs (Figure 17) and arms and histology demonstrated necrotising epithelioid granulomata containing multinucleated giant cells. Multiple cultures and stainings did not demonstrate *Mycobacteria*, *Leishmania* or fungi and extensive laboratory testing excluded ciliary dyskinesia, cystic fibrosis, WG, common variable immunodeficiency, chronic granulomatous disease, systemic lupus erythematosus, HIV infection and deficiency of alpha-1-antitrypsin. Skin lesions initially healed during tuberculostatic therapy but recurred despite 12 months of treatment. The patient is still alive at age 41[280].

Figure 17. Bronchiectasis in type 1 BLS (patient "GAB")

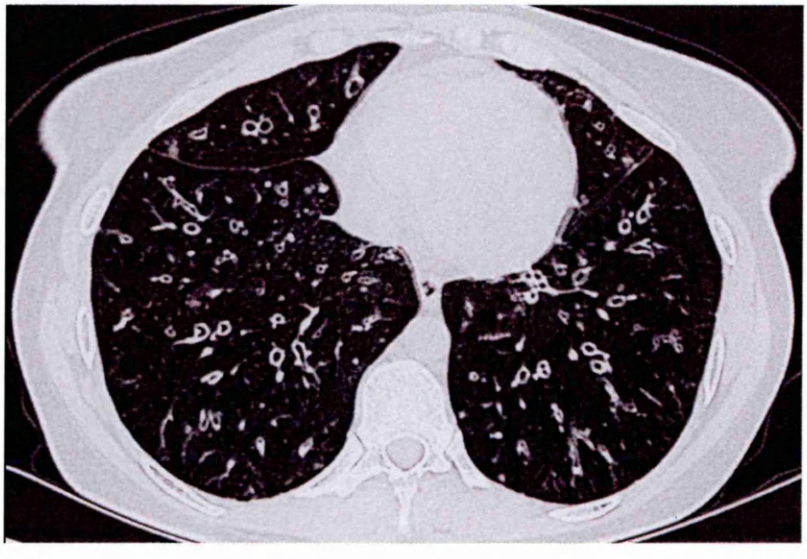

Computertomography of the lungs of "GAB" showing bilateral bronchiectasis

Figure 18. Mutilating granulomatous skin lesions in patient "GAB"

Necrotising granulomatous lesions on the legs of patient "GAB".

Patient "SAB"

At the age of 18 months SAB suffered from a measles infection with high fever. She had received standard vaccines in childhood, including measles (and polio, diphtheria, tetanus, pertussis, mumps, rubella). Since then she suffers from epilepsy, mostly focal but sporadically generalized, which is not totally controlled by antiepileptic drugs. Since the age of 5 she has suffered from recurrent febrile infections in the upper respiratory tract with otitis, rhinitis and chronic sinusitis, and from the age of 19 on she had also suffered from several episodes of pulmonary infections. Antibiotic treatment could control her infectious episodes. When I saw the patient first she had chronic sinusitis (Figure 19) and a chronic productive cough with yellow-green

sputum. In contrast to her sister "GAB" and all other patients she did never develop granulomatous skin lesions.

Figure 19. Chronic sinusitis in type 1 BLS (patient "SAB")

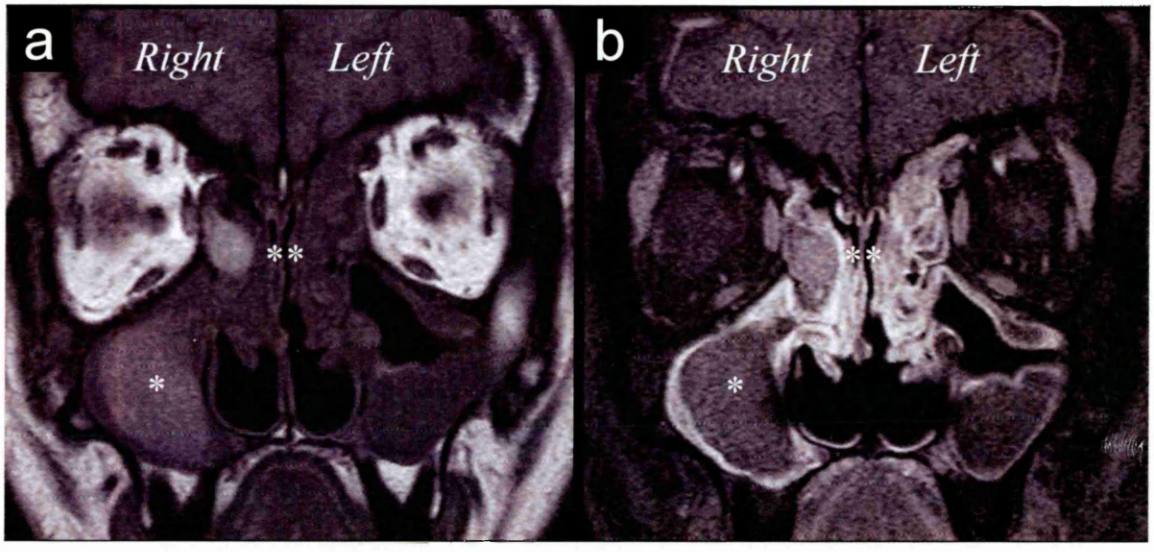

Magnetic resonance imaging (MRI) of the head in "SAB" showing fluid accumulation and mucosal thickening in the paranasal sinuus. Both panels show total occlusion of the right maxillary sinus (*), subtotal occlusion of the left maxillary sinus, and near total occlusion of both ethmoidal sinuus (**). Panel (b) shows increased blood flow (white areas) in the thickened mucosal lining of the sinuus (more pronounced in the right maxillary sinus compared to the left maxillary sinus) which indicates ongoing inflammation.

3.2.2. Phenotype of peripheral blood mononuclear cell subsets

FACS analysis of patients' PBMC demonstrated very low expression of MHC class I molecules compared to positive control samples (Figure 20), while the level of expression of MHC class II molecules was not altered (data not shown). Patients were not lymphopenic, with the exception of patient GAB, due to a reduction of the absolute numbers of CD3+CD8+ cells ($0.250x10^9$/l). Despite the severely reduced MHC class I expression, significant numbers of CD3+CD8+ cells were detected in the PBMC of all patients (Table 1). Analysis of T cell receptor V_β usage demonstrated that CD8+ cells in "FT" were polyclonal (data not shown). A significant expansion of (CD3-CD56+) NK cells and γδT cells was observed in "AK" and, to a lesser extent in "GAB", "NV" and "NP", while CD3+CD56+ cells were expanded in "FT" and NP (Table 3).

Staining of patients' PBMC and γδ bulk cultures with Vδ1 and Vδ2 specific antibodies revealed that the proportion of γδ T cells using the Vδ1 T cell receptor, rather than the Vδ2 T cell receptor, was greater than in other members of the family and control PBMC (data not shown). The inversion of the Vδ1/Vδ2 ratio was particular significant in "GAB" with more than 90% of γδ T cells expressing the Vδ1 T cell receptor.

Table 3. Lymphocyte subsets in type 1 BLS: Patients and healthy relatives

Patient/ Relative	CD3+ CD4+	CD8+	CD56+	CD3- CD16+	CD56+	Pan-γδ	HLA I expression on PBCM
AK	24	19	8	32	32	23	50
FT	39	24	18	16	14.3	12	47
AK-F	47	24	13	7	6	10	1959
AK-M	47	25	8.8	10	11	5	2062
AK-B	47	25	6.7	8.8	8.6	4	1598
AK-S	55	23	4	6	6	7.6	1520
GAB	42	11	4	ND	14	17	10
SAB	54	10.3	5.4	0.3	13.8	13.5	ND
NV	4.8	87.8	0.2	0	1	3.6	10
NP	37.3	24	40	0.5	12	7	57
PBL	54	27	8.5	ND	4.9	4.5	1200

Values shown are percentages of cells within the lymphocyte gate. Healthy family members of patient "AK" were her father (AK-F), mother (AK-M), brother (AK-B) and sister (AK-S). Results are also shown for analysis of peripheral blood lymphocytes (PBL) from a random donor. Figure modified from[247].

3.2.3. Analysis of the MHC class I biosynthetic pathway

The expression of MHC class I molecules on the B-lymphoblast lines from patients of all affected families, assessed by immunostaining with the pan-anti-MHC class I antibody W6/32, was strongly reduced (Figure 20). Pulse chase analysis of MHC class I molecules from the lymphoblast lines "AK" (Figure 21) and "GAB" (data not shown) as well as of control B-cell lines demonstrated that newly synthesised MHC class I molecules associated with β2m, but were retained in the ER.

Figure 20. MHC class I expression on B-lymphoblasts in type 1 BLS

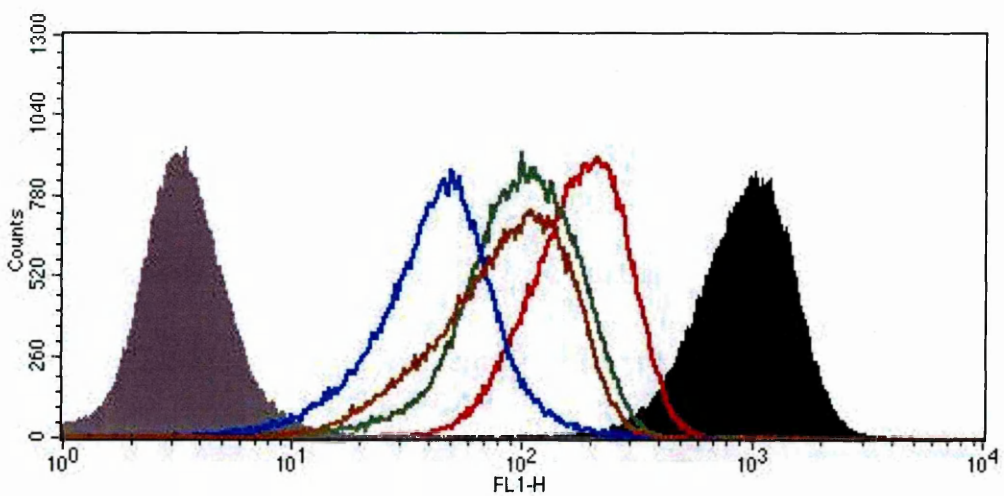

MHC class I expression on EBV-transformed B-lymphoblast lines from patients of affected type 1 BLS families, and control lines. Legend: Filled grey area: "AK", stained with secondary antibody only; all other B-cell lines were stained with both the pan-MHC class I antibody W6/32 (mouse IgG2a) and the secondary PE-conjugated goat-anti-Mouse IgG antibody. Blue line: "SAB"; green line: "NP"; brown line: "NV"; red line: "AK"; filled black area: "LG2" (MHC class I competent).

Figure 21. Pulse chase and isoelectric focusing analysis in patient "AK"

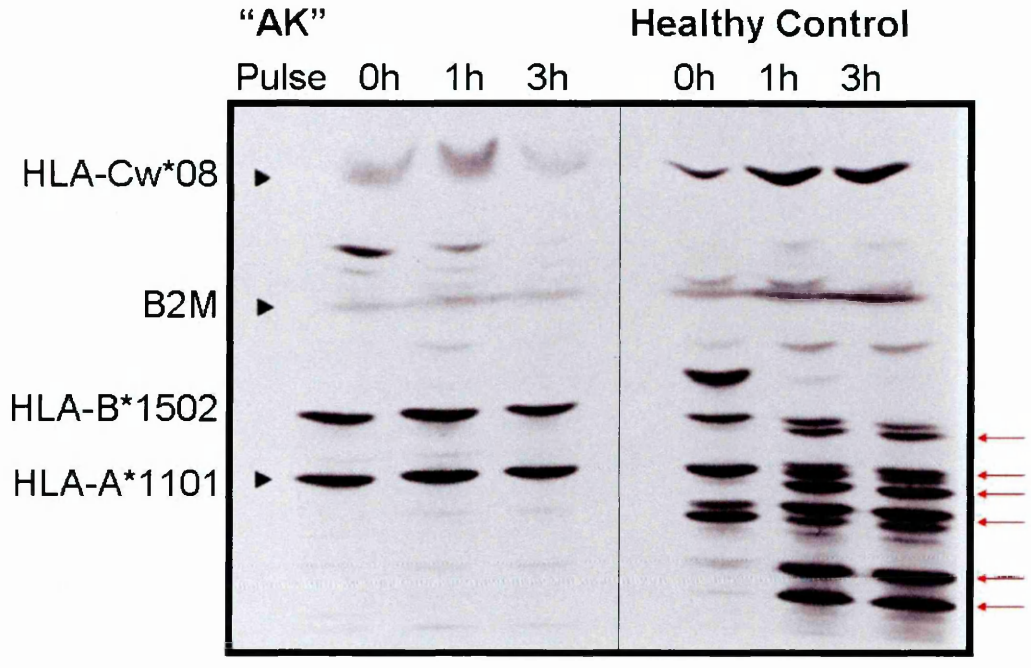

Pulse-chase, immunoprecipitation and isoelectrofocusing of MHC class I molecules of B-lymphoblast lines "AK" and a healthy control line sharing identical HLA-A and HLA-B haplotypes.

MHC class I molecules in the healthy control line undergo maturation, i.e. they undergo glycosylation during the chase period, resulting in the appearance of additional bands for HLA-B*1502 and HLA-A*1101 (red arrows). In contrast, the bands for "AK"'s HLA-B*1502 and HLA-A*1101 show no qualitative changes over the whole chase period, indicating that MHC class I molecules in "AK" did not reach the Golgi apparatus during the 3 hours chase period.

Moreover, transport of a radiolabelled peptide from cytosol to ER was abolished in all tested patient EBV B-lymphoblast lines, implicating a defect of the TAP complex (Figure 22).

Figure 22. Peptide translocation in 4 patients with type 1 BLS

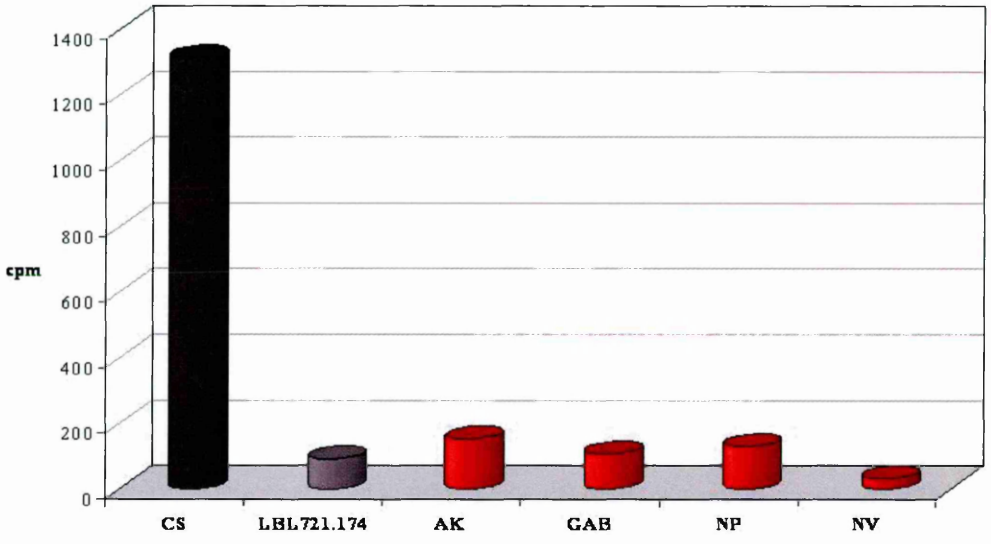

Peptide translocation in EBV-transformed B-lymphoblast lines from patients "AK", "GAB", "NP" and "NV". The healthy donor EBV B-lymphoblast line "CS" and the TAP-deficient lymphoblast line "LBL721.174" served as positive and negative controls, respectively.

Furthermore, infection of AK B cells with a recombinant vaccinia virus encoding the full length EBV LMP2A protein failed to sensitise them for lysis by LMP2A-specific

A11-restricted CTL, while presentation of the same epitope, as a synthetic peptide, was not affected (data not shown).

Western blotting of B-lymphocyte lysates from patients of all affected families demonstrated normal expression of TAP1 in "AK" and "BS" ("BS" will be described in detail in chapter 5) and lack of TAP1 in patients "NV", "NP", and "GAB" (Figure 23). Conversely, using antibodies specific to carboxy terminal residues of the TAP2A and TAP2B alleles TAP2 could not be detected in lysates of patient "AK", but was found in "NV", "NP", and "GAB" (Figure 23).

Figure 23. TAP and Tapasin expression in 5 patients with type 1 BLS

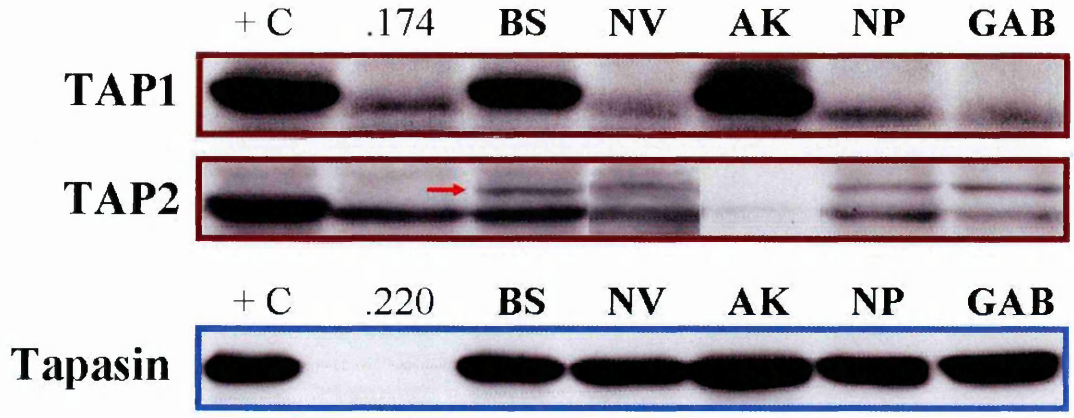

Western blot analysis for TAP1, TAP2 and Tapasin expression, using cell lysates from patient and control lines. The TAP-deficient cell line LBL721.174 (".174") was used as a negative control for both TAPs, while the Tapasin-deficient cell line LBL721.220 (".220") was used as a negative control for the Tapasin western blots. Patient "BS" will be discussed in detail in chapter 5. The red arrow indicates the band for TAP2.

Sequencing of "AK's" full-length TAP2 cDNA showed a deletion of an adenosine (A) in codon 326, which caused a frameshift and a premature stop codon. The adenosine deletion in codon 326 generated a novel HpaII restriction site within exons 5 and 6 which allowed analysis of the distribution of the TAP2 null allele in the patients and their family members. AK and FT were homozygous for the TAP2 null allele, while AK's parents were heterozygous (data not shown).

Finally, MHC class I expression could be restored in all patients' B-lymphoblast lines upon infection with a recombinant vaccinia virus encoding the human TAP1/TAP2 proteins (shown for 4 patients in Figure 24), confirming that the reduction in MHC class I surface expression was caused by a defective TAP complex.

Figure 24. TAP-encoding vaccinia virus restores MHC class I surface expression

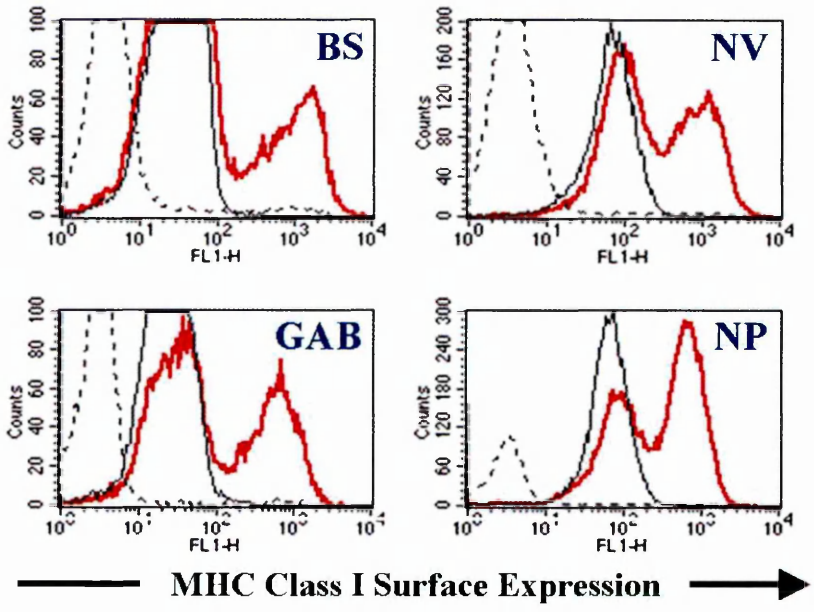

Immunostaining of B-EBV lymphoblastoid lines "BS", "NV", "GAB", and "NP" with the unlabelled pan-MHC class I antibody W6/32(1st antibody) and FITC-labelled anti-mouse antibody (2nd antibody) is shown after infection of the cells with either a recombinant TAP1/TAP2-encoding vaccinia virus ("TAPs-VAC"; bold red line) or a recombinant control vaccinia virus (thin black line). Staining of the "TAPs-VAC" infected cells with only the 2nd antibody is shown as a black dotted line.

3.2.4. Additional studies

The results described in the following two paragraphs were mainly generated by Helen Moins-Teisserenc. They have been included in this part of the thesis in order to give a more rounded picture of the TAP-deficiency story.

3.2.4.1. Functional activity of NK and γδ T cells

We then sought to address whether in patients with a germline down-regulation of MHC class I molecules, the activity of cells expressing MHC class I binding receptors was altered. Several γδ T cell clones were generated from FT, GAB and NV and their phenotype and activity analysed. All γδ T cell clones, rapidly proliferating from the γδ T cell bulk culture, were $V_{\delta}1V_{\gamma}9$ and they all expressed the MHC class I binding receptors ILT2 and CD94/NKG2A (data not shown). Cytotoxic activity of three γδ T cell clones was tested against the MHC class I negative cell line 721.221, the HLA-identical TAP2 negative "AK" B-lymphoblasts and, as control, against MHC class I positive B-lymphoblasts. We demonstrated that 721.221 cells were lysed by the three γδT cell clones, while a higher percentage of cytotoxicity was observed against "AK" B-lymphoblasts. These results were confirmed with autologous B-lymphoblasts. The finding that lysis of target cells was abolished after increasing the level of expression of MHC class I molecules, following infection with TAP vaccinia, suggested that γδ T cell inhibitory receptors were capable of transducing inhibitory signals. Therefore the analysis of NK and γδ T cells was extended to "GAB". It could be confirmed that several Vδ1 positive γδ clones were autoreactive, and that lysis of autologous cells was almost abolished after expressing wild type TAP1 and TAP2 genes, and restoring

normal surface expression of MHC class I molecules. Similar experiments were then carried out using a polyclonal NK line. It could be demonstrated that "GAB's" NK cells were autoreactive, as defined by their ability to lyse autologous B cells.

Figure 25. Activity of NK and γδ T –cells in type 1 BLS (from Reference [247])

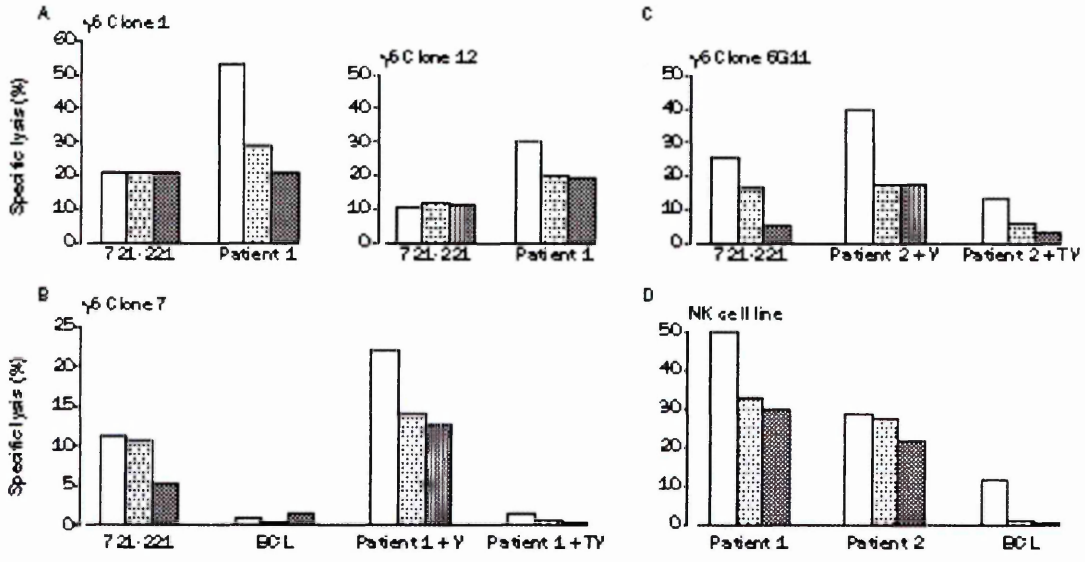

A and B: Three γδ T-cell clones (1, 7, and 12) from patient "FT" were tested against the HLA-identical TAP-2-negative B cells from patient "AK" as target cells. In the experiment done with clone 7, target cells were infected overnight with TAP-vaccinia (TV) or as a control with an irrelevant vaccinia virus (V). C: The γδ clone 6G11 from patient "GAB"

was tested against autologous B cells as target cells. Targets were infected with irrelevant vaccinia (V) or with the TAP-vaccinia (TV).D: An NK cell line from patient 2 was tested against autologous B cells and B cells from patient "AK" as target cells. The class-I-negative B-cell line 721.221 and a class-I-positive B cells line (BCL) were used as controls. Each bar corresponds to a different effector-to-target ratio (white bars 18:1; speckled bars 6:1; dark grey bars 2:1).

3.2.4.2. Immunohistochemistry of skin lesions

Biopsies collected from "AK's" skin lesions revealed the presence of several foci of immune cells infiltrating the dermis. To define the phenotype and origin of the infiltrating cells, the same sections were stained with a large panel of different monoclonal antibodies. The results of this analysis revealed that a large proportion of infiltrating cells were NK (CD3-CD56+), which expressed high levels of the inhibitory receptors CD94 and ILT2. A small but significant proportion of cells were αβ+CD3+ and very few cells were δ1 and δ2 positive. Similar results were observed in skin biopsies from patient "NV". A large proportion of NK cells infiltrating the necrotic lesions were positive for the activation marker HLA-DR+, suggesting a direct role of NK cells in the pathogenesis of the skin lesions.

Figure 26. Immunohistochemistry of TAP-deficient granulomatous lesions (Ref. [247])

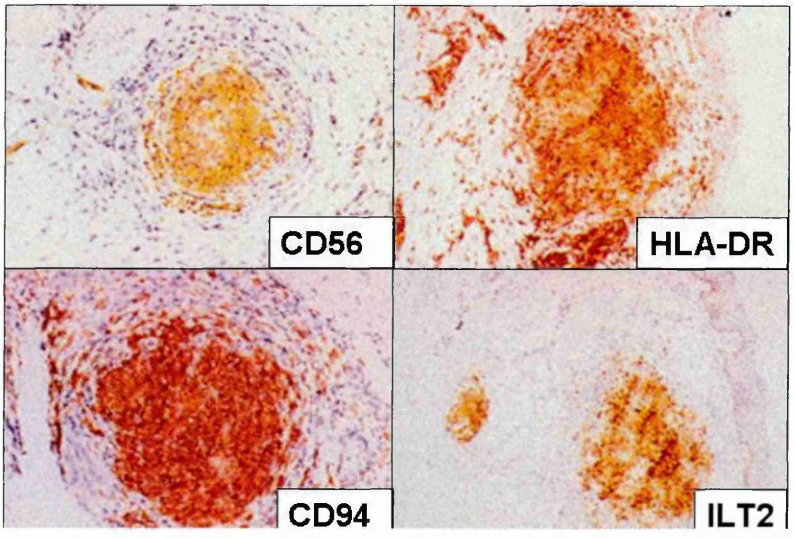

A large proportion of cells infiltrating the dermis were NK cells (CD3-CD56+), which expressed high levels of the inhibitory receptors CD94 and ILT2 and were HLA class-II positive. A small but significant proportion of cells were γδ^{+} CD3 positive (not shown).

3.3. Discussion

The patients described above with type 1 BLS exhibit a remarkable homogeneity of clinical symptoms and disease course, strongly suggesting a link between their unusual features and the low MHC class I expression. All patients except for "NP" suffered since their youth from recurrent bacterial infections in the upper respiratory tract associated with chronic bronchitis and recurrent bronchopneumonia leading to the progressive destruction of lung tissue and development of bronchiectases. All patients except "SAB" suffered from destructive granulomatous skin lesions affecting the extremities of the patients. A peculiar characteristic of this disease is the involvement of the face, which led to total destruction of the outer nose in "AK", "NP" and "NV", and to partial destruction in "FT". Despite intense diagnostic efforts no clear evidence of an infectious etiology could be found. In "NP", the granulomatous lesions appeared much earlier than in the other patients, i.e. during childhood.

A diagnosis of WG was suspected in all patients except "FT" at some stage during the disease course and "AK", "NV", "GAB", "SAB" and "NP" were transiently treated with immunosuppressive therapy. In "AK", immunosuppressive therapy led to chronic clinical deterioration with appearance of recurrent pneumonia, in "NV" it was associated with an episode of bacterial encephalitis, and in "GAB" and "SAB" it was clearly associated with worsening lung function tests and bronchiectasis. In contrast, low dose glucocorticoid treatment might have had some beneficial effect on the granulomatous lesions in "NP".

Type 1 bare lymphocyte syndrome due to frameshift mutation in TAP2 had been previously described in one Moroccan family with two affected children sharing an identical homozygous HLA haplotype [137]. These patients exhibited a similar clinical phenotype as my TAP1-defective patient "SAB" in that they did not suffer from chronic granulomatous inflammation either in the upper respiratory tract or the skin. It is possible that chronic inflammatory lesions in MHC class I negative patients might require exposure to pathogens or to other triggering events. Two other previously published single case reports had described sinobronchial disease and skin lesions on the legs of patients with low MHC class I expression; the skin lesions were described as ulcers or as plaques resembling necrobiosis lipoidica [281, 282].

The pathogenesis of such chronic inflammatory lesions remains unclear. The presence of some multinucleated giant cells in the granulomatous lesions raises the possibility that tissue damage might have been caused by mycobacterial infections. However, tuberculostatic treatments did not provide any prolonged clinical benefit in any patients, and mycobacteria were not identified in the lesions by tissue staining, culture techniques or PCR analysis.

An alternative hypothesis is that the chronic inflammation was caused by autoreactive lymphoid cells, such as the expanded populations of NK and/or γδ T cells found in these patients. This hypothesis is based on the fact that effector functions of NK and γδ T cells are negatively regulated by MHC class I-binding receptors, such as killer inhibitory receptors and ILTs [283, 284]. Furthermore it has been shown that clonal distribution of inhibitory receptors expressed by NK clones from healthy volunteers is capable of inhibiting self-reactivity. In patients with a germline loss of MHC class I

molecule, the threshold of inhibition provided by these receptors may not be reached, leading to autoimmune lesions. A similar hypothesis had been previously suggested by Zimmer and colleagues based on the finding that NK cells from TAP2-deficient children were capable of lysing autologous B cells [285, 286]. It is possible that the degree of self reactivity of NK cells may be different for distinct clones and may be influenced by the level of expression of MHC class I molecules and the HLA haplotype of different patients. Indeed, four clones from "FT" were not autoreactive, although they were capable of killing K562 cells (data not shown). The granulomatous lesions progressed in patient "AK" under treatment with interferon alpha (IFNα). It is possible that IFNα triggered activation and cytotoxicity of "AK's" NK cells, thereby promoting tissue damage.

The lack of severe viral infections in TAP-negative patients is intriguing and clearly indicates that the immune system has the capacity to react effectively to viruses in the absence of a functional TAP complex. The presence in sera from "AK" and "FT" of IgG with specificity for a variety of common pathogens (not shown) demonstrates an efficient antibody response. It is possible that TAP-independent viral peptides were capable of stimulating a protective CTL response, and selection of CD8+ T lymphocytes could have been driven by surface-expressed class I molecules loaded with TAP-independent peptides, as previously described [287]. Alternatively, either neutralising antibodies or other cellular mechanisms, such as those mediated by NK and γδ cells, could have been protective against viral infections.

In summary I have here described a novel syndrome in patients with low levels of expression of MHC class I molecules. The underlying molecular defect in all patients could be localized to the TAP1/TAP2 heterodimer. Both defects of TAP1 and TAP2 were associated with a similar clinical phenotype of otherwise unexplained destructive granulomatous lesions and frequent infections of the respiratory tract. A characteristic of TAP-deficiency which distinguishes it from other forms of type 1 BLS is the relatively benign disease course with all patients surviving into adulthood. The destructive granulomatous skin lesions are infiltrated by activated NK cells and γδ T cells. Together with the findings that some of the patients' NK and γδ T cell clones exhibit clear autoreactivity it seems possible that inappropriately controlled activation of these innate immune cells, e.g. during viral or bacterial infections of the respiratory tract, is responsible for the severe tissue distraction in TAP-deficient patients. Why tissue destruction is mainly localized to the skin and not other organs remains unclear.

Expression of different MHC class I haplotypes by different patients is likely to have an influence on the spectrum of their clinical symptoms and infections. It is interesting that none of the so far described patients with TAP-deficiency is homozygous for HLA-A2, which is known to present TAP-independent peptides. It might be that HLA-A2+ patients with TAP-deficiency do not exhibit a primary immunodeficiency syndrome and that levels of MHC class I surface expression in such patients would be sufficient to inhibit NK activation.

3.4. Conclusions

TAP-deficiency syndrome is an autosomal recessive genetic disorder involving either of the TAP-subunits TAP1 or TAP2. Early diagnosis and state of the art antibiotic treatment are essential in order to prevent development of irreversible lung damage. Immunosuppressive treatment for suspected skin vasculitis is contraindicated and can cause rapid clinical deterioration and severe infectious complications of the lungs, central nervous system and eyes. Reduced MHC class I surface expression is the key laboratory finding. Lessons learned from the clinical and molecular analysis of TAP-deficient patients complement studies performed on murine cell lines or using artificial deletion constructs of TAP, and contribute to a better understanding of the peptide transporter.

3.5. Acknowledgements

I am indebted to the patients and their families for allowing me to use clinical information and for donating peripheral venous blood. I am also indebted to Dr. Andrew Exley (Cambridge) who assisted with the clinical diagnosis of "AK", and to the doctors of the patients who shared clinical information: Stanislaw Buechner (Basle, Switzerland), Jo Lambert (Gent, Belgium), Cem Baykal (Istanbul, Turkey), Maria Willemsen (Brussels,Belgium), Edouard Grosshans (Strassbourg, France) and Wolfgang L. Gross (Bad Bramstedt, Germany). K. Welsh (Oxford Transplant Centre) carried out tissue typing of the patients, Marina Cella and Marco Colonna (Basel Institute for Immunology) analysed the TCR repertoire in "FT" and grew γδ T cell clones (not shown). As stated above, studies with patients' NK and γδ cell were carried out by Helen Moins-Teisserenc. Helen did also generate the EBV-transformed B-lymphoblast lines of "AK", "FT" and "GAB" before my arrival in Oxford.

4. Type 1 bare lymphocyte syndrome due to a splice donor site mutation in TAP2

4.1. Introduction

In this chapter I shall describe the clinical and molecular analysis of type 1 BLS in a family from Eastern Europe with two affected siblings. The clinical manifestations in the two patients described here extend the clinical spectrum of TAP-deficiency and illustrate the harmful consequences of immunosuppressive drug therapy in TAP-deficient patients. The molecular and genetic analysis of one of the two siblings, "BS" is described.

4.2. Results

4.2.1. Family history

Patient "BS" was diagnosed with type 1 BLS in the Rheumaklinik Bad Bramstedt (Germany) in March 2000. She had been admitted with a suspected diagnosis of WG. Family history revealed that "BS" had had an older sister, "RJ", with a nearly identical clinical syndrome, who had died of her disease several years before. The parents of the two patients and three more siblings (one brother, two sisters) were healthy. The parents were first degree relatives. All molecular studies were done on PBMC and EBV-transformed B-lymphoblastoid lines from "BS", the younger of the two affected sisters.

4.2.2. Clinical data

Patient "RJ" (9.6.1960 – 8.12.1991)

From early childhood on, the girl suffered from recurrent upper respiratory tract infections and herpetic fever blisters. Following smallpox vaccination she developed left sided acute hearing loss and transient generalised exanthema. From the age of 13, plaquelike and nodular skin lesions with secondary ulceration, followed by scar formation and hyperpigmentation developed on the left lower leg. Clinically, the lesions were classified as erythema induratum Bazin. Skin swab cultures grew *Staphylococcus aureus* and *Pseudomonas aeruginosa*, and histologic analysis revealed a lymphocyte rich granulomatous inflammatory infiltrate and necrosis. Multiple cultures and acid fast stains failed to demonstrate the presence of mycobacteria and the lesions did not heal under antituberculous quadruple therapy, but extended to the left thigh and right lower leg.

At the age of twenty-eight, immunosuppressive therapy with 100mg azathioprin per day was installed for suspected panarteriitis nodosa. A clinical examination of the eyes before the start of the immunosuppressive therapy revealed postinflammatory atrophy of the right iris. Within the next year the skin lesions progressed further, and the patient started to suffer from frequent bronchopulmonary infections and a progressive atactic syndrome involving the trunk and limbs. One year after the start of immunosuppression cranial computed tomography scan disclosed diffuse cortical and subcortical atrophy of both the cerebrum and cerebellum, and a left frontal lesion consistent with an old lacunar cerebral infarction. Repeated eye examinations now also showed postinflammatory atrophy of the left iris as well as

bilateral subcapsular cataracts. Cyclosporin A was added to the immunosuppressive regimen for suspected progression of the vasculitic process.

Two years later, at the age of 31, the patient died after a series of recurrent strokes complicated by severe bilateral bronchopneumonia.

Patient "BS" (11.8.1962 – 8/99)

From the age of five onwards the girl suffered from recurrent purulent rhinitis and sinusitis, and from frequent bouts of herpetic fever blisters on lips and nostrils. Between the ages of five and ten she developed measles, mumps, rubella, chickenpox and pertussis, all of which ran an uneventful disease course with spontaneous remission. Vaccinations for polio, tuberculosis (bacille Calmette-Guérin), diphteria and tetanus were well tolerated. From the age of ten, she underwent multiple surgeries of the paranasal sinus with no improvement of her chronic sinusitis. At the age of eleven she developed recurrent spastic mucopurulent bronchitis, which responded to antibiotic treatment. Extensive diagnostic investigations excluded cystic fibrosis, alpha-1-antitrypsin deficiency, tuberculosis, common variable immunodeficiency, IgA-deficiency or aspergillosis as the cause of her disease.

At the age of twenty-three, a few months after she had given birth to a healthy boy, nodular and plaque like skin lesions with purple discoloration appeared on the left lower leg and were clinically classified as erythema induratum Bazin. Histologic analysis showed a dense inflammatory infiltrate in the dermis consisting of lymphocytes, histiocytes, and few polymorphnuclear granulocytes, with perivascular

accentuation and necrosis. Treatment with antituberculous quadruple drug therapy had no effect on the lesions.

At the age of thirty, immunosuppressive treatment with 20mg prednisone per day was instigated for treatment of the skin lesions, which were now classified as nodular vasculitis. Extensive diagnostic tests, including an electroencephalography (EEG) and magnetic resonance tomography (MRI) of the cranium were normal except for the finding of chronic bilateral pansinusitis. Under immunosuppressive therapy, the skin lesions did not improve. She now also suffered from recurrent bouts of pneumonia and recurrent herpetic keratitis. Cultures from sputum and bronchioalveolar lavage grew *Staphylococcus aureus* and *Haemophilus parainfluenzae*. Six month after start of prednisone therapy a diagnosis of bilateral bronchiectasis and colonisation of the lungs with multiresistant *Stenotrophomonas maltophiles* was made. Lung function gradually decreased and she became dependent on continuous oxygen supply.

At the age of 36 she suffered from two transient episodes of right sided brachiofacial hemiparesis, the first of which appeared in close time association with a bout of herpetic keratitis and herpetic skin lesions on both eye lids and the right auricle, confirmed by virus culture and PCR. An EEG recorded four weeks later revealed a left temporal focus of steep alpha waves with high amplitudes, while MRI showed multiple bilateral hyperintense lesions in the frontal and occipital lobes, which were considered to be consistent with vasculitic lesions. Duplex sonography of the extracranial arteries and echocardiography showed no abnormalities. One year later, during recovery from an acute severe stroke with right sided hemiparesis she

developed severe bilateral pneumonia refractory to antibiotic treatment. She died aged thirty-seven, of respiratory failure. Four months before her death, analysis of peripheral blood mononuclear cells (PBMC) by fluorescent activated cell sorter (FACS) had revealed a reduced frequency of cytotoxic CD8+/CD57+ T lymphoyctes, increased frequency of γδ T lymphocytes and a strongly reduced cell surface expression of MHC class I molecules.

The clinical syndrome in "RJ" and "BS", together with the low MHC class I cell surface of PBMC in "BS" were consistent with a diagnosis of type 1 bare lymphocyte syndrome due to TAP-deficiency.

4.2.3. Molecular Analysis of EBV-transformed B-lymphoblasts from patient "BS"

In order to study the MHC class I processing and presentation pathway I generated an EBV-transformed B-cell line ("BS") from PBMC of patient "BS".

Tissue typing of "BS" B-lymphoblasts by PCR revealed that she carried a homozygous [HLA-A32, HLA-B57, HLA-Cw6] haplotype.

FACS analysis of "BS" B-lymphoblasts stained with MHC class I-specific antibodies recognising HLA-A,B,C (W6/32), HLA-A32 (T116-5-28) and HLA-B57 (MA2.1) demonstrated a more than 100-fold reduction of cell surface expression for all MHC-class I molecules compared to normal control B-cell lines. Moreover, compared to B-lymphoblast lines derived from other TAP-deficient patients "BS" lymphoblasts expressed the lowest levels of MHC class I molecules (Figure 27).

Figure 27. MHC class I surface expression in "BS", "NP", "AK", "GAB" and "NV"

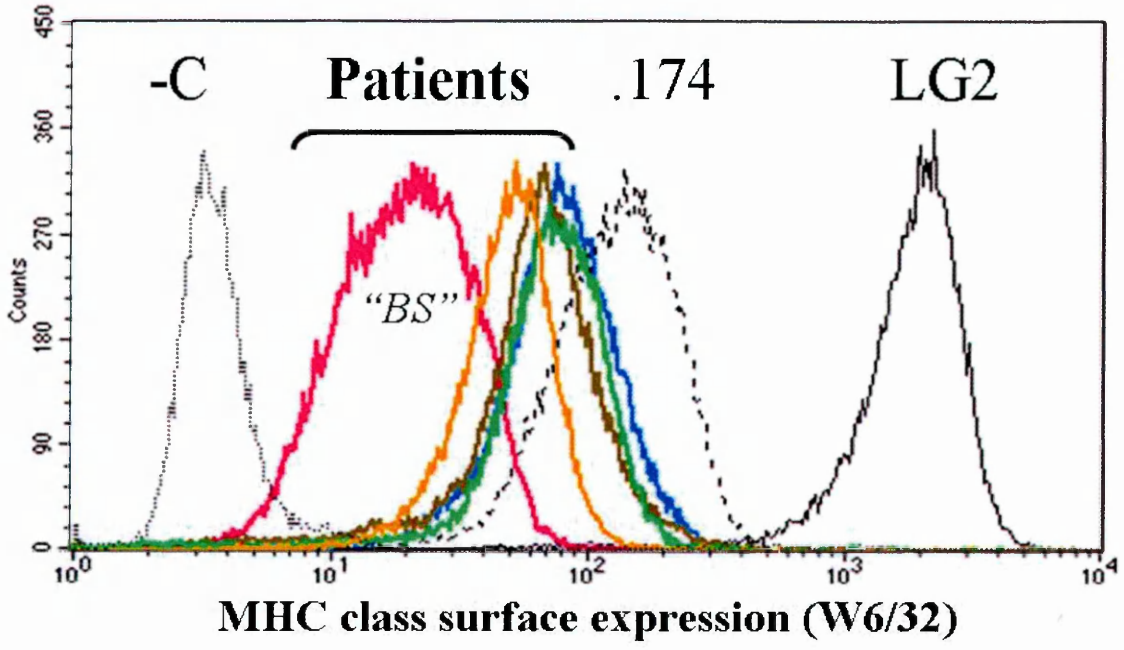

MHC class I surface staining of patients' and control B-lymphoblast lines with the pan-MHC class I antibody W6/32. The negative control (-C) is LG2 stained with secondary antibody only (PE-conjugated goat-anti-mouse IgG, i.e. no first antibody (i.e. no W6/32). Pink line: "BS"; orange line: "NP"; brown line: "AK"; green line: "GAB"; blue line: "NV"; black dotted line: LBL721.174 (TAP-deficient control); black line: LG2 (MHC class I expressing control line).

Comparison of β2m surface expression on "BS" B-lymphoblasts and Daudi cells ($\beta 2m^{-/-}$) ruled out a primary β2m-deficiency in "BS" B-cells (data not shown).

To further analyse the MHC class I pathway I immunoprecipitated the peptide loading complex from "BS" B-cell lysates after prior labelling with ^{35}S-methionine. The cell lysates had been obtained by cell lysis with either the strong ionic detergent NP40 (at 1% concentration) or the weak non-ionic detergent digitonin (at 1%).

Normal TAP has a half-life in the range of 3-4 hours, while MHC class I molecules have half lives of 15-30 minutes. In order to obtain optimal radioactive signal intensities for both TAP and MHC class I molecules in the same experiment I radiolabelled the B-cells during a long pulse of 16 hours, followed by an additional short pulse of only 20 minutes.

Both TAP1 and TAP2 bands could be detected in both digitonin as well as NP40-lysates (Figure 28). TAP2-bands from "BS" B-cells ran slightly higher than TAP2-bands of a control B cell line. Interestingly, the PLC including both TAPs, MHC class I molecules and β2m could be co-precipitated in 1% NP40-lysates of "BS" cells but not normal control cells (Figure 28). These results ruled out a transcripitional defect of MHC class I molecules and suggested an unusually stable conformation of the TAP-loading complex in detergent. They also indicated the presence of functional tapasin, the TAP-MHC class I/β2m-bridging protein. Neither MHC class I molecules nor β2m were co-precipitated in detergent lysates of the tapasin-deficient line 721.220.B44.

When "BS" B-cells were labeled with a single short 20 minutes pulse of ^{35}S-methionine an unusually intense TAP2 band was detected, while the duration of the pulse was not sufficient to efficiently label TAP1. While these results were consistent with the known half live of normal TAP1 they suggested a significantly reduced half-

life of TAP2 in "BS" (Figure 28). Western blot experiments with antisera against the C-terminus of TAP1, TAP2 and tapasin confirmed that they were all expressed in "BS" B-cells (Figure 28). Taken together these results showed cellular expression of both TAP1 and TAP2 in "BS" B-cells, and their association with tapasin, MHC class I and β2m in the peptide loading complex. However, the increased cellular turnover and reduced steady state level of TAP2 in "BS" B-cells suggested that TAP2 in "BS" was defective. Consistent with this hypothesis was the unusually stable conformation of the PLC in "BS" B-cells.

Figure 28. Molecular analysis of type I BLS in patient "BS"

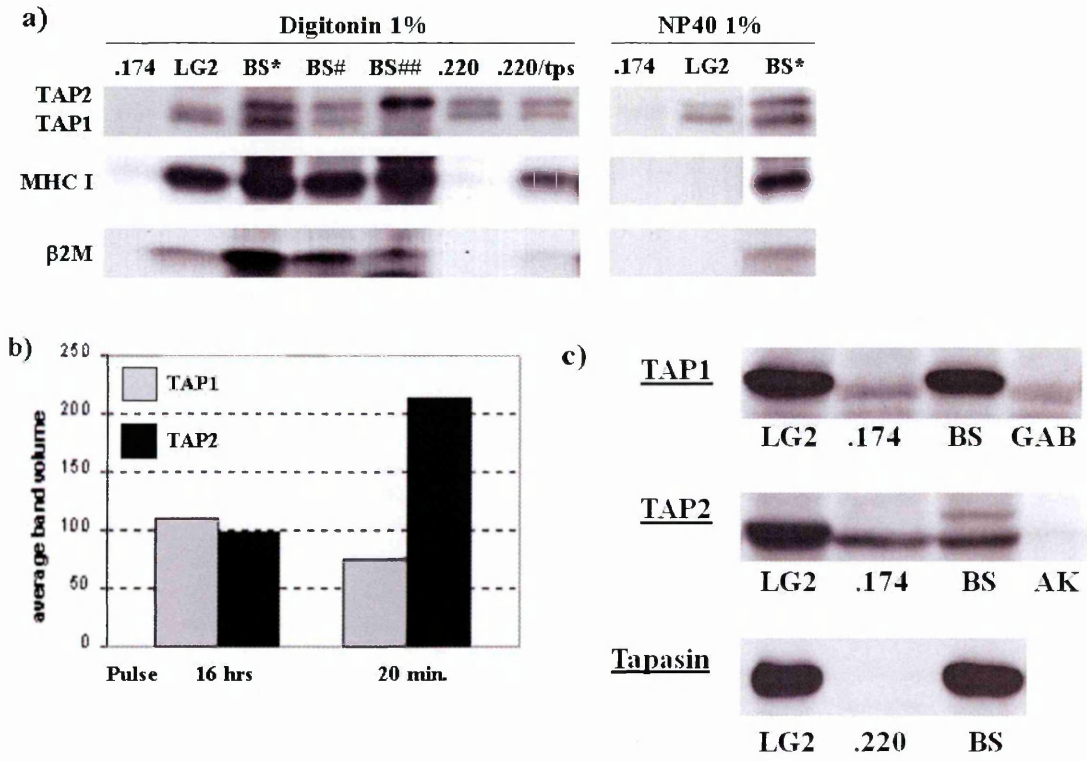

Figure legend on next page.

Legend for Figure 28: *Immunoprecipitation of the peptide loading complex (PLC) in "BS" cell lysates and control lysates (a). Co-precipitation of the PLC in 1% digitonin lysates of cell lines "BS", LG2 (normal control), .220 (tapasin-deficient) and .220/tps (.220 with restored tapasin expression) is shown on the left-hand side. "BS#" and control lines were pulsed for 16 hours with ^{S35}Methionine before detergent lysis. "BS*" were subjected to one 16 hours pulse followed by one 20 minutes pulse and "BS##" were pulsed only once for 20 minutes with ^{S35}Methionine. Immunoprecipitation of the PLC in 1% NP40 lysates (a, right-hand side) revealed that the PLC in "BS" cells was unusually stable. High signal intensity of the TAP2-band was observed with single 20 minutes ^{S35}Methionine labelling and quantified by phosphoimager analysis (b). Western blotting of TAP1, TAP2 and tapasin in "BS" and control lysates is shown in (c).*

In order to directly study the functional integrity of the TAP1/TAP2-complex we compared the efficiency of TAP-dependent peptide translocation from the cytosol into the endoplasmic reticulum of "BS" B-cells and control B-cell lines. The results of these experiments demonstrated a severe impairment of TAP-dependent peptide transport in "BS" B-cells (Figure 29) and thereby strongly supported the suspected diagnosis of TAP-deficiency syndrome in "BS".

Figure 29. Defective peptide translocation in "BS" B-lymphoblasts

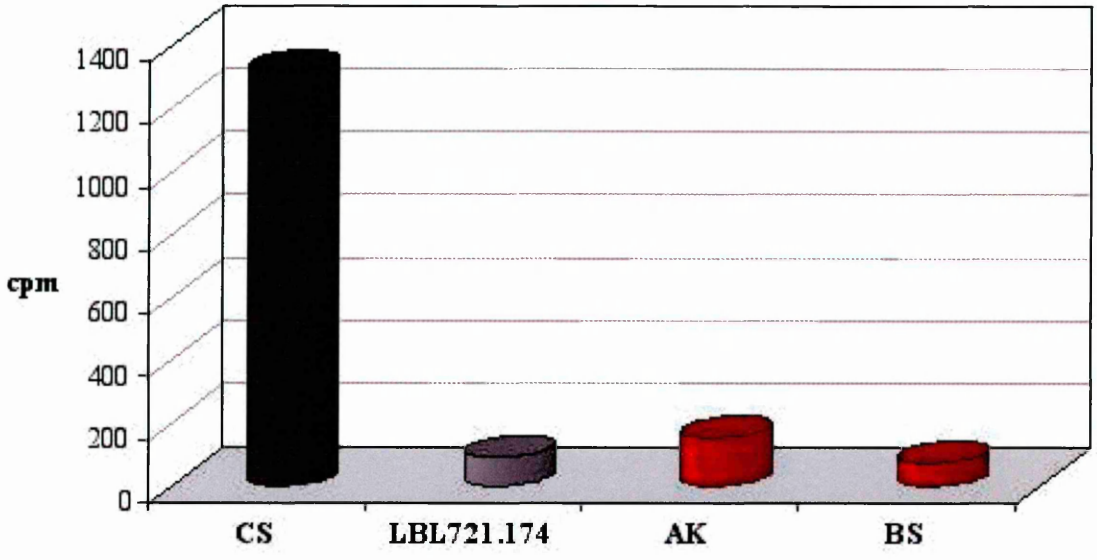

Figure 29. *Peptide translocation in B-lymphoblast lines "CS" (healthy), LBL721.174 (TAP1/2-deficient), "AK" (TAP2-deficient) and "BS". Peptide translocation into the ER corresponds to the radioactivity of the Concanavalin A-retrieved peptide fraction, containing the [125I]-labeled peptide "RRYQNSTEL"*
(Y-axis; cpm, counts per minute).

To determine which TAP subunit, TAP1 or TAP2 was responsible for the functional TAP-defect in "BS" I generated cell fusions of "BS" B-lymphoblasts with TAP1- and TAP2-deficient lymphoblasts from my previously characterized TAP-deficient patients as well as the tapasin-deficient line 721.220.B44. Allele specific and pan-anti-MHC class I antibodies were used to detect restoration of specific HLA-A and HLA-B molecules or total HLA class I molecule expression on the fusion

products (Figure 30). Fusion of "BS" B-cells with the tapasin-deficient, HLA-B44-expressing B-cell line 721.220.B44 restored normal surface expression of HLA-B57 and HLA-B44, demonstrating normal tapasin function in "BS" B-cells (not shown). As expected, surface expression of HLA-A32 was restored in fusions of "BS" with 721.174.TAP, but not with the TAP-deficient mother line 721.174 (not shown). Importantly, fusions of "BS" B-cells with the TAP1-deficient, but TAP2-competent B-cell line "GAB" restored surface expression of HLA-A32 and HLA-B57, while fusion of "BS" B-cells with the TAP2-deficient, but TAP1-competent B-cell line "AK" failed to restore normal MHC class I expression. These results demonstrated that the reduced MHC class I surface expression in patient "BS" was caused by a functional TAP2-deficiency.

Figure 30. Complementation of TAP1/TAP2 function in B-cell fusions

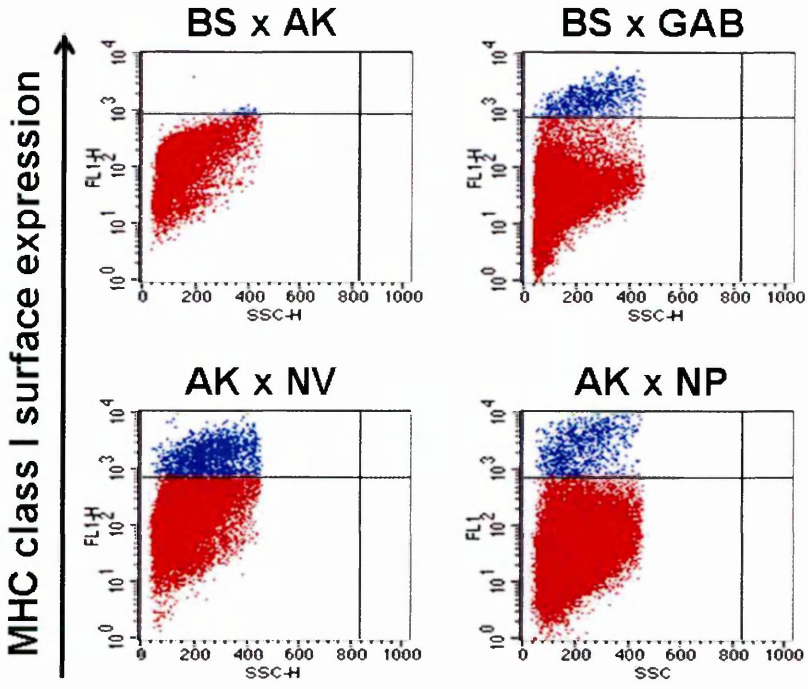

Fusion of B-lymphoblast lines was carried out as described in chapter 2 (Methods). MHC class I expression on fusion products was detected by the pan-MHC class I antibody S6/32 (BSxAK, AKxNV, AKxNP) and the anti-HLA-A32 antibody T116-5-28.

4.2.4. Genetic analysis of TAP2 in "BS" B-cells

Tissue typing of "BS" B-cells revealed that "BS" was homozygous for the TAP1 allele TAP1a (TAP1*0101/0102) and the TAP2 allele TAP2E (TAP2*0102).

To characterise the underlying genetic defect in "BS" TAP2E I amplified and sequenced overlapping segments of TAP2E from "BS" B-cell cDNA by RT-PCR. Six forward primers (FP) and six reverse primers (RP) were designed on the basis of the published TAP2E coding sequence (CDS; Genbank; START–STOP: 77-2137) and used in different combinations. Both sequence analysis and agarose gel electrophoresis

revealed that RT-PCR products amplified with primers spanning the TAP2E CDS region 20 – 1021 (FP1 - RP4), including exons 1 – 4, and the TAP2E CDS region 1526 – 2203 (FP5 – RP1), including exons 7 –11, contained single bands of expected size and nucleotide sequence.

In contrast, none of the RT-PCR products amplified with primer pairs spanning TAP2E CDS region 1021 – 1526 contained bands of the expected size. Instead, amplified DNA products ran either 300 base pairs below ("-300bp") or 1200 base pairs above ("+1200bp") the expected size (Figure 31). Interestingly, 4 different FP/RP combinations yielded two bands, one "-300bp" and one "+1200bp", suggesting alternative splicing of TAP2E in "BS".

This hypothesis was confirmed by sequence analysis, which revealed skipping of exons 5 and 6 in RT-PCR products from "-300bp" bands and inclusion of the first 1184bp of intron 6 in products from "+1200bp" bands. The two splice variants of "BS" TAP2E were named TAP2E S (short) and TAP2E L (long).

Figure 31. RT-PCR analysis of "BS" TAP2E

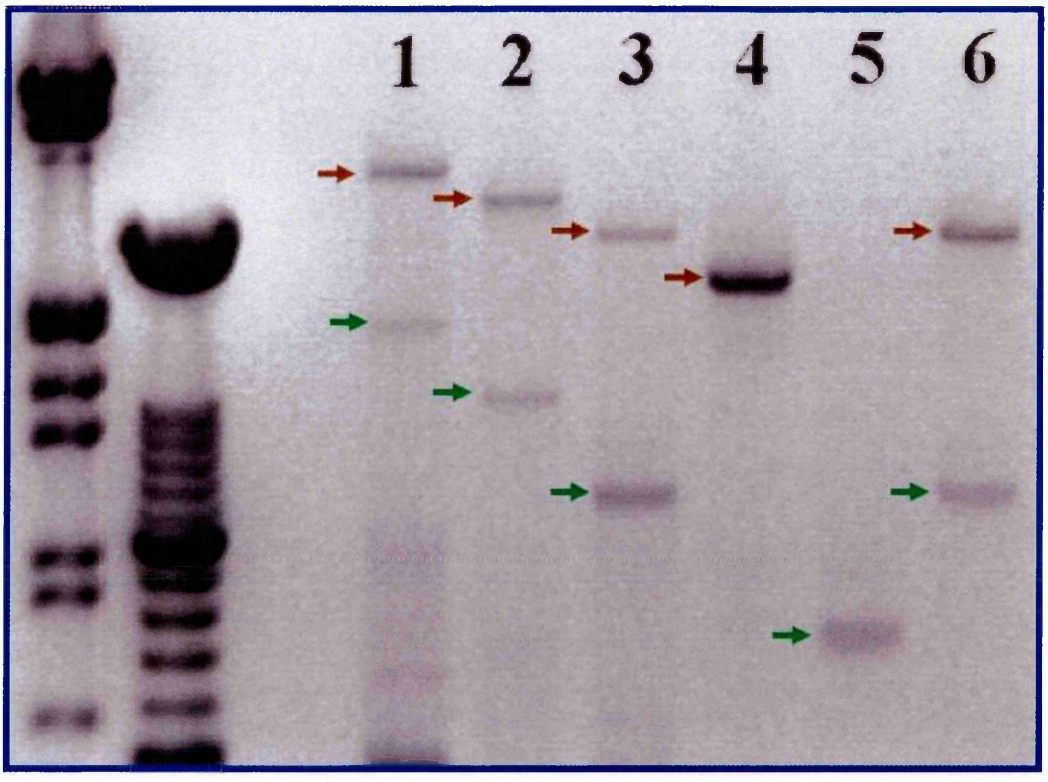

Amplification of "BS" cDNA with primer pairs spanning the region 1021 – 1526 of TAP2E revealed the presence of two splice variants of the TAP2E gene in "BS". The products of the shorter variant "TAP2E S" ran ca. 300bp below the expected fragment size (green arrows) and the products of the longer variant "TAP2E L" ran ca. 1200bp above the expected fragment (red arrows). Sequencing of these bands disclosed a single nucleotide mutation in the splice donor site of intron 6 with resultant exon skipping in "TAP2E S" and partial inclusion of intron 6 in "TAP2E L".

Sequencing of "TAP2E L" showed a single nucleotide mutation (G to C) of the first nucleotide in the splice donor site of intron 6 (GTGAG to CTCAG). The mutation

was confirmed on both strands and by sequencing genomic BS TAP2E DNA (data not shown). On the other hand, the sequence of "TAP2E S" contained a 33 nucleotide sequence interposed between exon 4 and exon 7, which showed 100% homology to a part of the TAP2E wild type sequence in intron 6 and also to the corresponding retained intronic sequence in "TAP2E L". Interestingly, closer analysis of the entire genomic TAP2E intron 6 sequence revealed the presence of a potential cryptic splice acceptor site with a characteristic polypyrimidine enhancer motif immediately upstream of this 33 nucleotide sequence as well as a cryptic splice donor site (GTGAG) immediately downstream of it (Figure 32/a). The proposed scenario for aberrant alternative splicing of genomic "BS" TAP2E based on the sequence analysis is shown in Figure 32/b.

Figure 32. Analysis of aberrant alternative splicing of the TAP2E gene in"BS"

a)

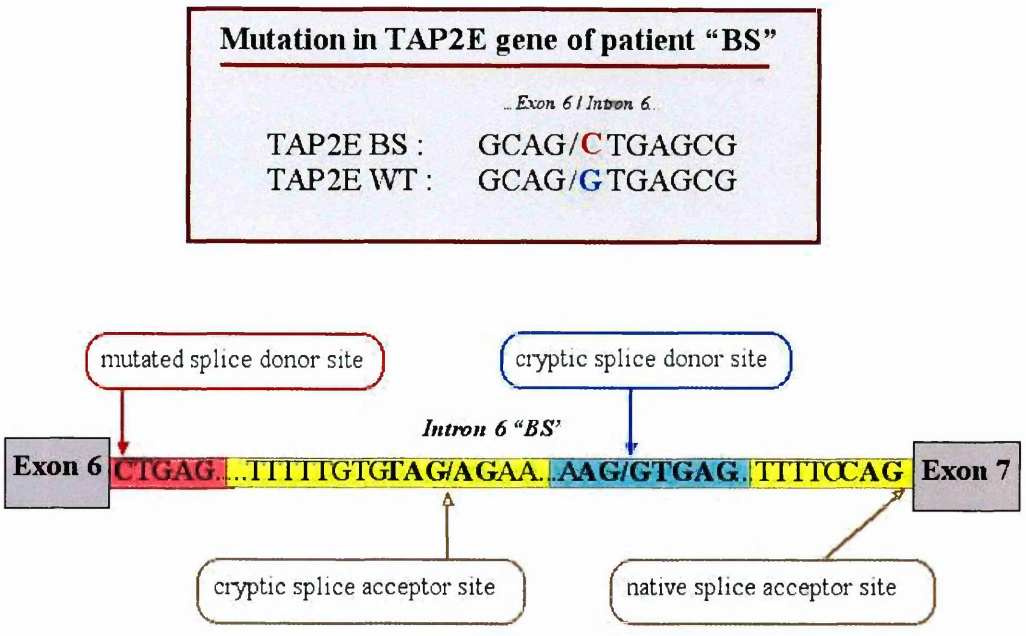

b)

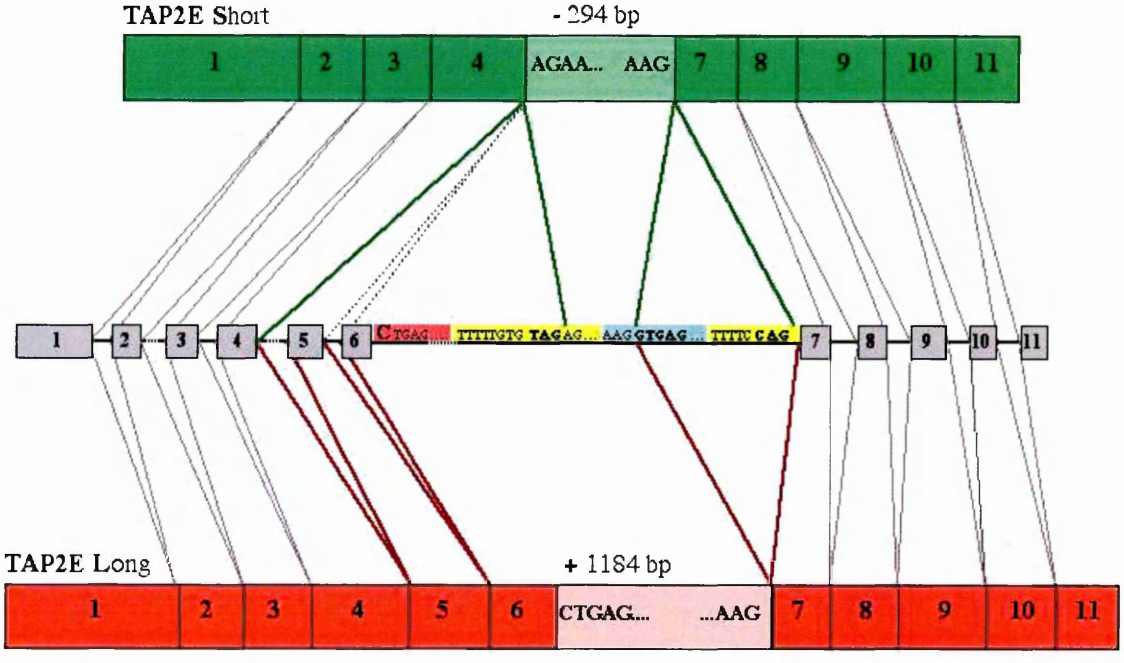

(a) Sequence analysis of intron 6 of genomic TAP2E in "BS" and (b) splicing scenario of genomic "BS" TAP2E DNA resulting in two TAP2E mRNAs.

Interestingly, the 33bp sequence connecting exons 4 and 7 in "TAP2E S" is in frame and contains no Stop codon, while "TAP2E L" contains a Stop codon at nucleotide position 1390, 39 codons downstream from the start of intron 6. The splice variant "TAP2E S" is therefore predicted to encode a protein of slightly lower molecular weight than wild type TAP2E, i.e. 64 kDa compared to 76 kDa (Figure 33). "TAP2E S" is predicted to contain a normal COOH-terminus including the nucleotide binding domain (NBD), which explains why TAP2 could be detected in immunoblotting experiments with antibodies against a COOH-terminal peptide of TAP2. Importantly, the protein encoded by "TAP2E S" lacks the putative peptide binding domain of TAP2, i.e. the cytosolic peptide loop linking TAP2 transmembrane domain (TM) 7 with TM8, and also lacks both the putative TM8 and the major part of TM9 (Figure 33)[117]. In contrast, "TAP2E L" encodes for 51kDa protein with a COOH-terminal truncation, which lacks the nucleotide binding domain and also a part of TM9, but contains the putative TAP2 peptide binding domain (Figure 33). The TAP2 band detected in the western blot experiments could therefore not have originated from TAP2L.

Figure 33. Predicted TAP2 protein sequence and domain organization in "BS"

a) TAP2 encoded by wild type TAP2E

```
MRLPDLRPWTSLLLVDAALLWLLQGPLGTLLPQGLPGLWLEGTLRLGGLW    50
GLLKLRGLLGFVGTLLLPLCLATPLTVSLRALVAGASRAPPARVASAPWS   100
WLLVGYGAAGLSWSLWAVLSPPGAQEKEQDQVNNKVLMWRLLKLSRPDLP   150
LLVAAFFFLVLAVLGETLIPHYSGRVIDILGGDFDPHAFASAIFFMCLFS   200
FGSSLSAGCRGGCFTYTMSRINLRIREQLFSSLLRQDLGFFQETKTGELN   250
SRLSSDTTLMSNWLPLNANVLLRSLVKVVWGLYGFMLSISPRLTLLSLLHM   300
PFTIAAEKVYNTRHQEVLREIQDAVARAGQVVREAVGGLQTVRSFGAEEH   350
EVCRYKEALEQCRQLYWRRDLERALYLLVRRVLHLGVQMLMLSCGLQQMQ   400
DGELTQGSLLSFMIYQESVGSYVQTLVYIYGDMLSNVGAAEKVFSYMDRQ   450
PNLPSPGTLAPTTLQGVVKFQDVSFAYPNRPDRPVLKGLTFTLRPGEVTA   500
LVGPNGSGKSTVAALLQNLYQPTGGQVLLDEKPISQYEHCYLHSQVVSVG   550
QEPVLFSGSVRNNITYGLQSCEDDKVMAAAQAAHADDFIQEMEHGIYTDV   600
GEKGSQLAAGQKQRLAIARALVRDPRVLILDEATSALDVQCEQALQDWNS   650
RGDRTVLVIAHRLQTVQRAHQILVLQEGKLQKLAQL                 686
```

b) TAP2 encoded by "TAP2E S" of patient "BS"

```
MRLPDLRPWTSLLLVDAALLWLLQGPLGTLLPQGLPGLWLEGTLRLGGLW    50
GLLKLRGLLGFVGTLLLPLCLATPLTVSLRALVAGASRAPPARVASAPWS   100
WLLVGYGAAGLSWSLWAVLSPPGAQEKEQDQVNNKVLMWRLLKLSRPDLP   150
LLVAAFFFLVLAVLGETLIPHYSGRVIDILGGDFDPHAFASAIFFMCLFS   200
FGSSLSAGCRGGCFTYTMSRINLRIREQLFSSLLRQDLGFFQETKTGELN   250
SRLSSDTTLMSNWLPLNANVLLRSLVKVVWGLYGFMLSISPRLTLLSLLHM   300
PFTIAAEKVYNTRHQEVLREIQDAVARAGQVVREAVGGLQTVRSFGAEEH   350
EVCRYKEALEQCRQLYWRRDLERALYLLVRRVLHLGVQMLMLSCGLQQMQ   400
DGELTQGSLLSFMIYQESVGSYVQTLVYIYGDMLSNVGAAEKVFSYMDRQ   450
PNLPSPGTLAPTTLQGVVKFQDVSFAYPNRPDRPVLKGLTFTLRPGEVTA   500
LVGPNGSGKSTVAALLQNLYQPTGGQVLLDEKPISQYEHCYLHSQVVSVG   550
QEPVLFSGSVRNNITYGLQSCEDDKVMAAAQAAHADDFIQEMEHGIYTDV   600
GEKGSQLAAGQKQRLAIARALVRDPRVLILDEATSALDVQCEQALQDWNS   650
RGDRTVLVIAHRLQTVQRAHQILVLQEGKLQKLAQL                 686
```

RTALGTLTATK

c) TAP2 encoded by "TAP2E L" of patient "BS"

The sequence and organization of the known TAP2 protein sequence (wild type) is shown in (a). Transmembrane regions TM1-TM9 are in red and alternate TMs are highlighted on yellow and light green background. The putative peptide binding domain is bold dark green writing and the Walker A domain, which belongs to the nucleotide binding domain (NBD) of TAP2 is in bold black writing and highlighted on pink background. The predicted protein sequences and organization of TAP2 encoded by "TAP2E S" and "TAP2E L" are shown in (b) and (c), respectively. Missing pieces of TAP sequences are shown in grey writing on a light-grey background, and missing TMs are highlighted on a dark grey background. New pieces of sequence in these TAP2-variants are highlighted on a cyan background (for" TAP2E S") and orange (for "TAP2E S"). Compare also with Figure 5 ("TAP structure and function", p.30).

4.3. Discussion

The two sisters presented in this chapter, "RJ" and "BS", both suffered from characteristic clinical symptoms of TAP-deficiency syndrome; both patients suffered since early childhood from recurrent bacterial upper respiratory tract infections, and a chronic necrotising nodular skin disease appeared in both patients during adulthood. Also, the disease course in both patients worsened under immunosuppressive therapy and both sisters died of bilateral bacterial lung infection. However, the spectrum of clinical symptoms in "RJ" and "BS" extends the formerly known disease manifestations of TAP-deficiency. In particular, both patients suffered from complicated herpetic fever blisters, herpetic eye involvement and recurrent cerebrovascular strokes with progressive neurologic deterioration. The association of cerebrovascular strokes and herpetic keratitis in both "RJ" and her sister "BS" are of particular clinical interest. The young age of both sisters at the onset of the cerebrovascular complications and the lack of known atherogenic risk factors points towards a vasculitic process as the cause for the recurrent strokes. Consistent with this hypothesis echocardiographic and duplex sonographic examinations in both patients were normal. In light of the defective MHC class I antigen presentation pathway in both patients, progression of both the ophthalmic and cerebral manifestations under immunosuppressive therapy are very well compatible with a viral etiology. Moreover, *Herpesviridae* infections are known causes for both encephalitis and cerebral vasculitis in immunosuppressed patients [288].

The above studies have shown that TAP2-deficiency in "BS" was directly responsible for the dramatic reduction of MHC class I surface expression on B-

lymphoblasts. The functional defect in the MHC class I antigen presentation pathway in "BS" B-cells was therefore equivalent to the TAP2- and TAP1-deficiencies in patients "AK" and "FT", and patients "GAB", "SAB", "NP" and "NV", respectively, whom I have described in the previous chapter. Similar to these patients functional deficiency of TAP2 in "BS" completely abrogated peptide translocation into the ER, and MHC class I molecules were stably bound to the PLC and retained in the ER. However, in contrast to all other TAP-deficient patients so far identified the single nucleotide defect in the TAP2 gene of "BS" did still allow for expression of a TAP2 protein that could be detected with antibodies against the COOH-terminus of TAP2. A previous report in a family with a TAP1-deficient patient found a splice acceptor site point mutation in intron 1 causing a frameshift and resulting in a premature Stop codon at position 228. The truncated TAP1 protein or any TAP1 protein variants resulting from alternative splicing were not detected in this patient's B-cells using a panel of antibodies against a TAP1 COOH-terminal peptide [289]. On the other hand, alternative RNA splicing of TAP2, generating the splice variant TAP2*iso*, is a common event in humans [98]. TAP2*iso* lacks exon 11 and the original 3' untranslated region, but contains a new exon 12 and new 3' untranslated region. Interestingly, TAP2 and TAP2iso encode for TAP2 proteins with different peptide selectivities [98].

The splice donor site point mutation in TAP2E intron 6 of "BS" is unique as it leads to the generation of two alternatively spliced RNAs in "BS" B-cells, i.e. "TAP2E S" and "TAP2E L". The predicted TAP2 protein encoded by "TAP2E L" contains both the pore forming complex and the peptide binding loop, but lacks the NBD. Conversely, the protein encoded by "TAP2E S" contains the complete NBD but lacks

the peptide binding site. The results shown here for TAP2 in "BS" show that two abnormal but complementary TAP2 isoforms can not substitute for one normal TAP2 protein. The results also show that the peptide binding and nucleotide binding domains of both TAP1 and TAP2 need to be intact for proper TAP function. On the other hand, successful restoration of MHC class I expression in fusion products of "BS" and "GAB" B-lymphoblasts ruled out a significant dominant inhibitory effect of the mutant TAP2 proteins. Previous studies with GFP-TAP1 fusion proteins have suggested that the TAP complex contains hundreds of proteins [90]. Normal TAP1/TAP2 heterodimers in the TAP complex of "GAB"x"BS" fusions were obviously sufficiently effective to supply peptides to MHC class I, even in the presence of the abnormal TAP1/"TAP2E S" or TAP1/"TAP2E L" heterodimers. This is entirely consistent with the fact that TAP-deficiency is an autosomal recessive disease, and that no abnormal clinical phenotype has yet been described in heterozygotes [131].

4.4. Conclusions

Detection of both TAP1 and TAP2 proteins in the same patient cell line by immuno-blotting should not be used to rule out a diagnosis of TAP-deficiency, as alternatively spliced mutant TAP RNA can give rise to TAP proteins with a "normal" COOH-terminus. Functional studies of the mutant TAP-complex in patient "BS" underpin the current TAP topology model and support the notion that functional NBDs from both TAP subunits are needed for peptide transport [290].

4.5. Acknowledgements

Dr. Peter Lamprecht, who knew the clinical history and final diagnosis of patient "AK" made the initial diagnosis of type 1 BLS in patient "BS". Prof. Wolfgang L. Gross allowed me to interview "BS" when she was in his clinic. Tissue typing of HLA-A, -B, and –C, and of TAP1 and TAP2 was carried out by staff of the Oxford Transplant Centre. I am indebted to "BS" for a memorable interview and for having allowed me to use clinical information and for donating venous blood.

5. Generation and Validation of human recombinant CD1d-tetramers made from inclusion body proteins and their use to study TCR Vα24+ and TCR Vα24- CD1d-restricted T lymphocyte populations in humans

5.1. Introduction

Because of both their enigmatic granulomatous skin lesions and respiratory problems all TAP-deficient patients described in the previous two chapters were, at several time points, examined for suspected tuberculosis (TB). However, multiple diagnostic investigations, including acid fast staining, culture and PCR of tissue samples failed to demonstrate direct evidence for the presence of mycobacteria. On the other hand, purified protein derivative (PPD) based skin testing was positive in all patients, indicating that they had been previously exposed to mycobacteria. Furthermore, five TAP-deficient patients ("AK", "FT", "GAB", "SAB", "BS") had lived for several years in countries with high TB prevalence rates. The apparent immune competence of these TAP-deficient patients against mycobacteria is still not understood to date. Notably, TAP-deficient mice are highly susceptible to infection with Mycobacteria [103, 104].

In the mid-nineties a major breakthrough in cellular immunology was the discovery of T lymphocyte subsets specifically recognizing lipid antigens presented by the nonpolymorphic MHC class I-like CD1 molecules [146]. One of the CD1 isoforms, CD1d, was found to be highly conserved in mammals. In contrast, CD1a, CD1b, CD1c and CD1e isoforms were found to be present in humans but not in mice. Intriguingly,

the first lipid antigens shown to be presented by CD1 to human T lymphocytes were mycobacterial cell wall lipids [146]. Hence the question arose whether TAP-deficient humans, but not TAP-deficient mice, could use CD1a, CD1b or CD1c specific T cell responses in their defense against mycobacteria.

Recombinant fluorescent-conjugated MHC class I/peptide tetramers had already been successfully used since 1996 to sensitively detect and isolate *ex vivo* peptide-specific CD8+ T lymphocytes [257, 291]. At the beginning of 1999 I embarked on a project to generate CD1-tetramers, as no tools to sensitively and specifically detect and isolate CD1 restricted lipid-specific T lymphocytes *ex vivo* were available at that time.

In this chapter I will describe the generation, validation and use of human CD1d-tetramers. All experimental results obtained with CD1d-tetramers shown in this chapter were obtained with tetramers made from completely denatured and reduced inclusion body proteins using the ternary refolding matrix consisting of the GroEL minichaperone, the bacterial disulfide isomerase DsbA, and bacterial proline isomerase, all immobilized on a sepharose matrix. The same tetramers could also be produced by a second novel refolding protocol, which is discussed in the last results chapter of this thesis.

First, the potential of CD1d-tetramers for detection of invariant NKT cells in peripheral blood and tissue of both human and mice will be shown. In addition, CD1d-tetramer aided detection and isolation of a formerly unknown population of human CD1d/lipid-specific T lymphocytes, TCR Vα24-independent CD1d/α-GalCer specific T lymphocytes, will be demonstrated.

5.2. Results

5.2.1. Generation and validation of recombinant human CD1d/α-GalCer-tetramers

Based on primary structure disparities between human CD1b and CD1d with regard to hydrophobicity and number of cysteine residues I assumed that CD1b and CD1d molecules might have different requirements for successful refolding *in vitro*. In particular, mouse and human CD1d have an odd cysteine residue at position 12[156, 292]. In the first crystal structure of mouse CD1d in 1997 this Cys12 residue was shown to be located at the bottom of the antigen binding groove [155]. Mutation of the odd cysteine to a serine, as had been previously shown to improve refolding of HLA-B27[293], was therefore not considered. However, multiple different refolding protocols failed to yield detectable amounts of correctly folded CD1d/lipid-monomers.

The technical breakthrough, which finally allowed for the generation of correctly refolded CD1d/lipid monomers, came with the availability of the CD1d ligand α-galactosylceramide (α-GalCer or KRN7000, provided by Yasuhiko Koezuka, Kirin Brewery, Japan) and a ternary refolding matrix developed by Myriam Altamirano and Alan Fersht at the MRC Laboratory of Molecular Biology (LMB) in Cambridge [249]. In addition, a novel detergent-based protocol, which I had developed for the refolding of human CD1b could also be used for generating small amounts of functional CD1d monomers (results obtained with this protocol will be shown in chapter 6).

5.2.1.1. Refolding of CD1d/lipid complex

When conventional-type dilution methods were used to refold CD1d, all protein precipitated immediately. In contrast, only discrete protein precipitation was seen when CD1d and β2m inclusion bodies and α-GalCer were refolded with the ternary refolding matrix. Importantly, the UV light absorption profile of the refolding supernatant at 280nm showed a clearly discernible peak at 160ml elution volume, which corresponded to the expected size of 45 kDa for monomeric CD1d/β2m/α-GalCer -complexes and was highly similar to the elution profiles known for MHC class I/β2m/peptide complexes (Figure 34). The same protocol could also be successfully used for CD1d refolding with other lipid ligands, i.e. β-GalCer, α-ManCer, and ganglioside GM1 (data not shown). SDS-PAGE analysis of the eluted 155-170ml fraction, containing the putative monomeric CD1d/β2m/α-GalCer complex, confirmed the presence of both CD1d and β2m in these soluble fractions. The purified CD1d/β2m/α-GalCer complexes were biotinylated, repurified and finally conjugated to fluorescent streptavidin to give R-Phycoerythrin (PE)- or allophycocyanine (APC) - conjugated CD1d//β2m/α-GalCer tetramers.

Figure 34. Purification of refolded CD1d/β2m/α-GalCer monomers

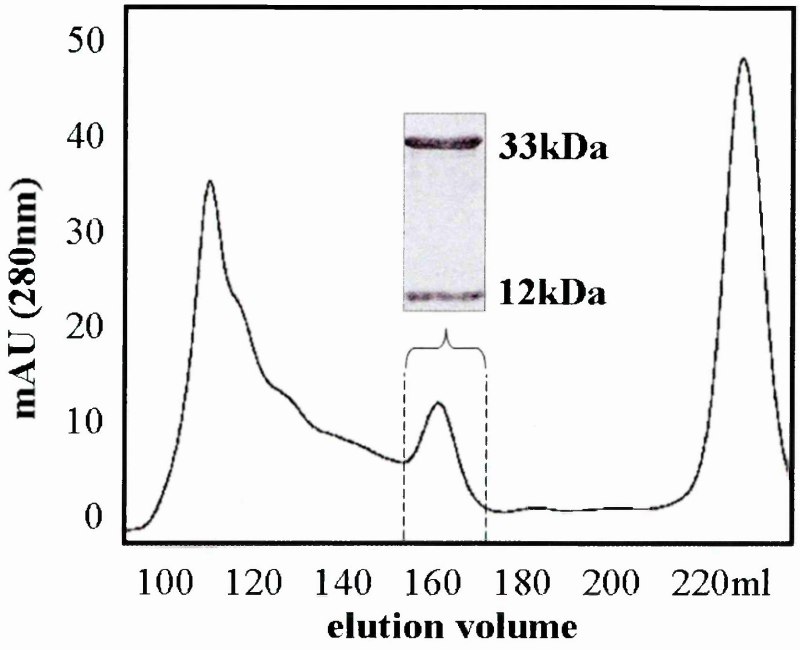

Size exclusion chromatography (SEC) and SDS-PAGE of refolded CD1d/β2m/α-GalCer. The UV light absorption profile at 280nm wave length showed a clearly discernible peak with UV280nm absorption maximum at ca. 160ml elution volume. SDS-PAGE Analysis of the purified fraction containing this peak confirmed the presence of both unglycosylated CD1d (at 33 kDa) and β2m (12 kDa). SEC was carried out using a Superdex SD75pg 26/60 column (Amersham Biosciences).

Next, the CD1d-tetramers generated by this method were validated for their ability to bind sensitively and specifically to invariant Vα24+/Vβ11+ human NKT cells.

5.2.1.2. Specificity of CD1d/α-GalCer tetramers for human Vα24+Vβ11+ iNKT cells

In order to test the specificity of the CD1d/α-GalCer tetramers, we generated human T cell lines enriched in TCR Vα24+Vβ11+ double positive invariant NKT (iNKT) cells by stimulation of healthy donors' PBMC with α-GalCer. The specificity of these iNKT cell lines for α-GalCer was confirmed by ELISPOT assay demonstrating their secretion of both IFN-γ and IL-4 upon addition of α-GalCer, but not upon stimulation with either the vehicle or α-ManCer (Figure 35).

Figure 35. ELISPOT analysis of Vα24+Vβ11+ invariant NKT (iNKT) lines

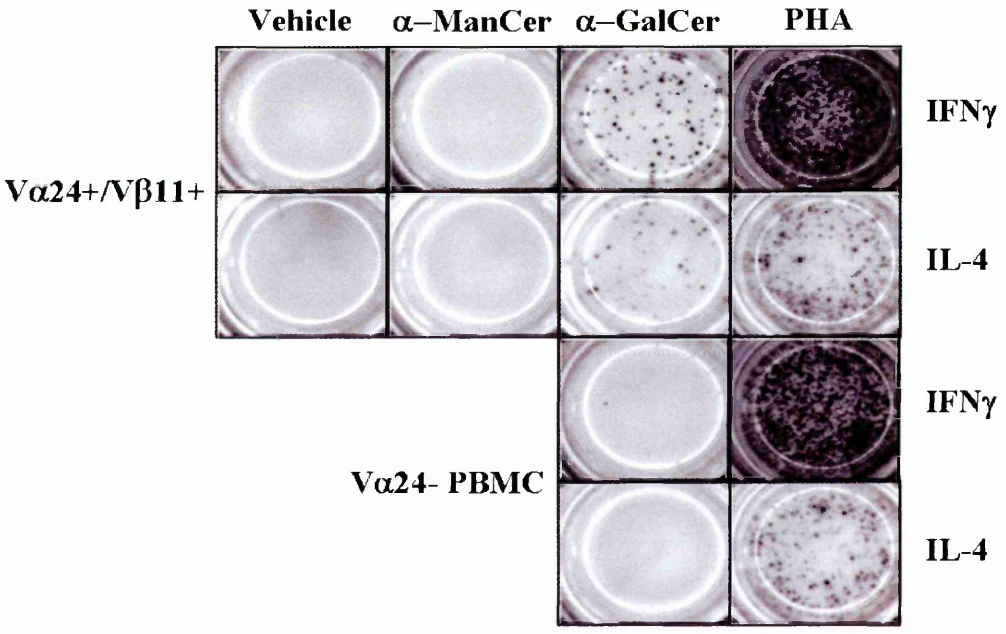

Vα24+Vβ11+ human iNKT lines and Vα24-depleted PBMC were tested for their IFNγ and IL-4 production upon stimulation with eithe the vehicle (0.5% polysorbate 20 in 150mM NaCl), α-ManCer or α-GalCer. Stimulation with phytohaemagglutinin (PHA) was used as a positive control.

Figure 36 shows CD1d/α-GalCer tetramer staining of iNKT cells from a 14 days old α-GalCer stimulated PBMC culture with 44% Vα24+Vβ11+ iNKT cells (Figure 36a). Importantly, CD1d/α-GalCer tetramer staining identified all Vα24+ T cells in this culture, demonstrating the ability of CD1d/α-GalCer tetramers to sensitively detect human Vα24+/Vβ11+ T cells (Figure 36b). In contrast, CD1d-tetramers loaded with β-GalCer failed to stain any iNKT cells in this culture (Figure 36c). Furthermore, preincubation of the iNKT line with unlabelled anti-Vα24 and anti-Vβ11 antibodies completely blocked CD1d/α-GalCer tetramer staining of these lines, confirming the specificity of the CD1d-tetramers (Figure 36d). Finally, CD1d/α-GalCer tetramer+ cells expressing the co-receptor CD4 were sorted, expanded *in vitro*, and analysed for expression of both TCR Vα24 and TCR Vβ11 chains. These experiments showed that iNKT cells were enriched to 96% in these *in vitro* expanded cell cultures, confirming the specificity of the CD1d-tetramers by a second method (Figure 36e).

Taken together, these results showed that human CD1d/α-GalCer tetramers generated from CD1d and β2m inclusion bodies by *in vitro* refolding using a ternary refolding matrix specifically detect human CD1d/α-GalCer specific T cells.

Figure 36. CD1d/α-GalCer tetramers specifically detect Vα24+Vβ11+ T cells

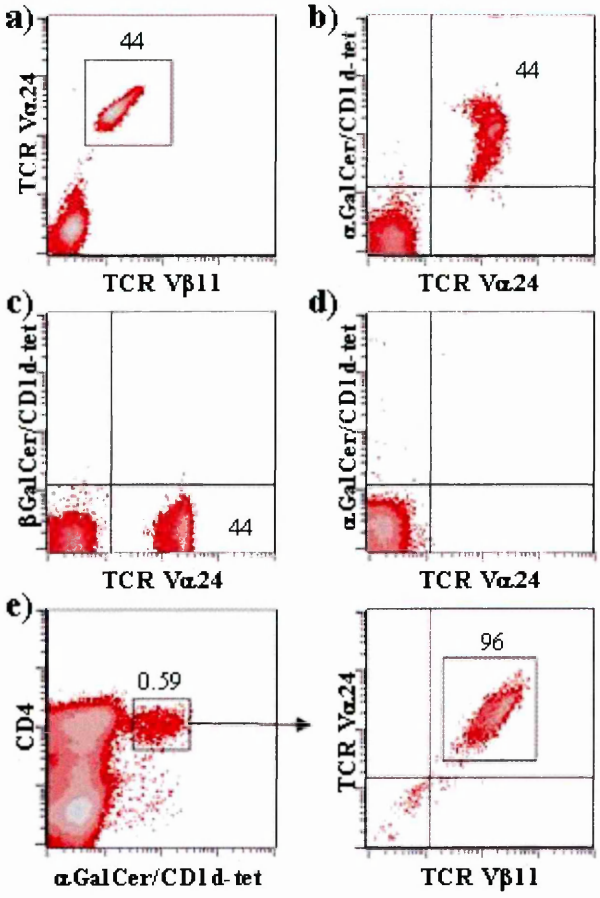

An in vitro generated human iNKT cell line containing 44% Vα24+Vβ11+ T cells (a) was used to validate the specificity of CD1d/α-GalCer tetramers. Double staining of these lines with either CD1d/α-GalCer tetramer and anti-TCR Vα24 antibody (b) or CD1d/β-GalCer tetramer and anti-TCR Vα24 antibody (c) demonstrated the ligand-specificity of these lines. Double staining with CD1d/α-GalCer tetramer and FITC-conjugated anti-TCR Vα24 antibody after incubation with unconjugated anti-TCR Vα24- and anti-TCR Vβ11 antibodies was negative. All density plots were gated on the $CD3^+$ Propidium $iodide^-$ cells; (e) $CD4^+$ CD1d/α-GalCer $tetramer^+$ cells were expanded and then analysed for enrichment of Vα24+Vβ11+ iNKT cells.

5.2.1.3. Sensitivity of CD1d/α-GalCer tetramers for human Vα24+Vβ11+ iNKT cells

To assess the sensitivity of the CD1d/α-GalCer tetramers for detection of human iNKT cells in peripheral blood and tissue we obtained PBMC and tissue samples from patients with liver disease. The rationale to use samples from patients with liver disease was based on the fact that mouse iNKT cells, which use TCR α and β chains that are homologous to those used by human iNKT cells, are highly enriched in mouse liver [166], and on a previous study reporting high frequencies of liver infiltrating Vα24+ T lymphocytes in human viral hepatitis[294].

Ex-vivo staining of iNKT cells in PBMC samples from hepatitis patients with three different staining methods, including double stainings with CD1d/α-GalCer-tetramers and anti-TCR Vα24 or anti-CD3 antibody, and double staining with anti-TCR Vα24 and anti-TCR Vβ11 antibodies, gave very similar results, with iNKT frequencies ranging from 0.06% to 2.5% (Figure 37). These results demonstrated that CD1d/α-GalCer tetramers could be used to sensitively detect iNKT cells in human PBMC samples. They also indicated that the great majority of circulating $V\alpha24^{+}/V\beta11^{+}$ cells in humans was CD1d-restricted.

Figure 37. ***Ex vivo*** **detection of iNKT cells with CD1d/α–GalCer-tetramers**

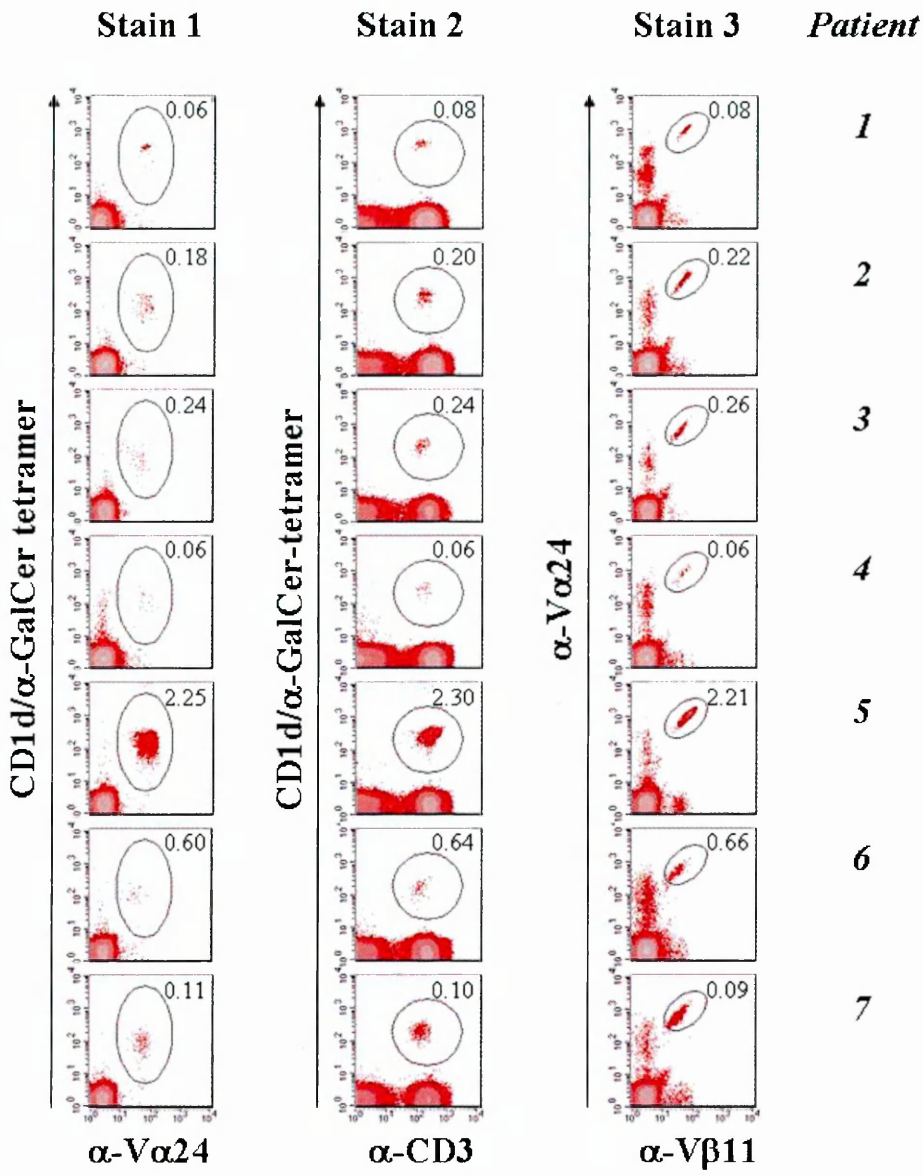

Frequencies of iNKT cells in human PBMC from patients with hepatitis were determined by three different staining methods: Double staining with CD1d/α-GalCer-tetramers and anti-TCR Vα24 antibody (Staining 1), double staining with CD1d/α-GalCer-tetramers and anti-CD3 antibody (Staining 2) and double staining with anti-TCR Vα24 and anti-TCR Vβ11 antibody (Staining 3).

Next, the CD1d/α-GalCer tetramers were assessed for their ability to detect Vα24/Vβ11 iNKT cells in liver samples from patients with endstage liver cirrhosis. While a previous report had found up to 7% $V\alpha24^+$ T cells in viral hepatitis samples our analysis showed only very low frequencies, ranging from 0.03 % up to 0.34%, of intrahepatic Vα24+Vβ11+ iNKT lymphocytes in the virus-induced cirrhosis samples (Figure 38). Importantly, analysis of the same intrahepatic T lymphocyte samples with CD1d/α-GalCer tetramers and anti-CD3 antibodies showed highly similar iNKT cell frequencies.

Figure 38. Detection of human iNKT cells in liver cirrhosis tissue samples

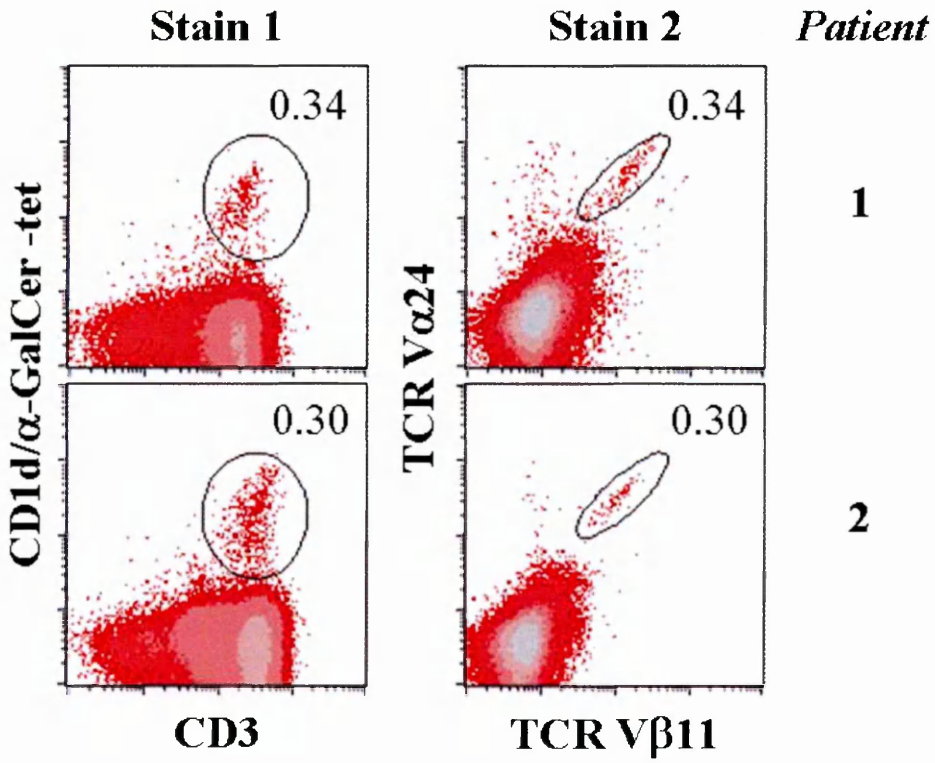

Immunostaining of intrahepatic T lymphocytes. The two patients with the highest frequency of Vα24+Vβ11+ iNKT cells are shown.

Further specificity analysis of the intrahepatic T lymphocytes from two patients with higher iNKT frequencies showed that they could not be stained with either CD1d-tetramers loaded with the ganglioside GM1 or with HLA-A23/peptide tetramers (data not shown).

5.2.1.4. Cross-species reactivity of CD1d/α-GalCer tetramers for mouse iNKT cells

Previous studies have demonstated an unusually high degree of cross-species reactivity of human and mouse iNKT cells for mouse and human CD1d/α-GalCer complex [295-297].

Moreover, insect cell-derived human CD1d/α-GalCer dimers, which had been developed by another group, were shown to stain mouse α-GalCer specific NKT cells [298].

In fact, our human CD1d/α-GalCer tetramers stained mouse iNKT cells in the spleen thymus and liver of wild type and TAP-deficient C57BL/6 mice, but failed to stain any T lymphocytes in β2m-deficient mice (Figure 39).

Taken together these results validated the human CD1d/α-GalCer tetramers generated from inclusion body proteins for use in human peripheral blood and tissue samples and suggested that they might also be of value for studies in mice.

Figure 39. Cross-species reactivity of human CD1d/α-GalCer tetramers

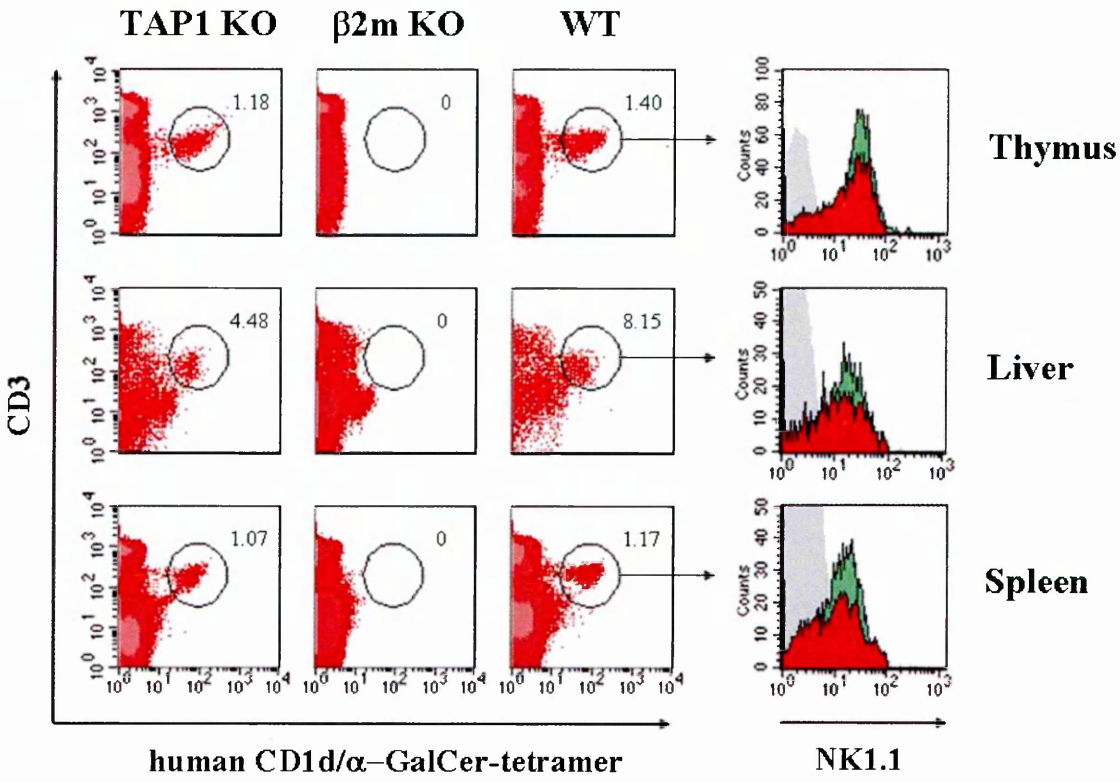

Thymic, intrahepatic and splenic mononuclear cells from C57BL/6 mice, TAP-deficient mice and β2m-deficient mice were stained with antibodies against mouse CD3, the mouse pan-NK marker NK1.1 and the human CD1d/α-GalCer tetramer. Density plots were gated on propidium iodide negative lymphocytes and histogram plots were gated on CD3+CD1d/α-GalCer tetramer+ propidium negative lymphocytes.

5.2.2 Tetramer-aided identification and characterization of CD1d/α-GalCer specific Vα24-Jα18 independent, non-invariant human CD8αβ+ and CD4+ T lymphocytes

In the year 2000, the only known subset of human CD1d/α–GalCer specific T lymphocytes were the CD4+, CD8αα+ or CD4-CD8- double negative (DN) iNKT cells. Previous experiments in mice had indicated that CD8αβ+ iNKT cells undergo negative selection in the thymus due to their high binding avidity to CD1d expressing cortical thymocytes [166].

The hallmark of human iNKT cells is their usage of an invariant TCR alpha chain, which results from the invariant rearrangement of the TCR Variable Alpha 24 family domain (TCR Vα24 according to the Arden Nomenclature; AV10 according to the IMGT nomenclature) with the TCR Junctional Alpha 18 family domain (Arden, TCR Jα18; IMGT, AJ18). In addition, human iNKT T cell receptors (iNKT TCR) always make use of the TCR Variable Beta 11 family (Arden, TCR Vβ11; IMGT, BV25-1)[299].

Several lines of evidence have indicated that iNKT cells originate from common mainstream precursor thymocytes rather than a specific separate precursor cell committed to the iNKT lineage before variable gene rearrangement. For example, pairing of the invariant Vα chain of iNKT TCRs with a particular Vβ chain is not forced by molecular constraint [300]. Also, the unused TCR α and γ loci of iNKT cells are indistinguishable from those of mainstream T cells [149, 301]. Therefore, antigen specificity is more likely to be the driving force for the selection of iNKT cells than is genetic programming. This mainstream precursor or "TCR instructive" model of

iNKT selection has been underpinned by the observation that mouse iNKT cells go through a CD4+CD8+ double positive stage during thymocyte development [302].

I reasoned that, if the selection and peripheral expansion of iNKT cells was driven by antigen, i.e. CD1d/α–GalCer, then the repertoire of iNKT TCRs should contain random rearrangements of different TCR Variable Alpha and Beta segments with different Junctional segments, even if one of these rearrangements, i.e. Vα24-Jα18, was clearly dominant over all other rearrangements.

To test this hypothesis I used the recombinant human CD1d/α-GalCer tetramers to identify potential Vα24-Jα18 independent CD1d/α–GalCer specific T lymphocytes in α-GalCer stimulated *in vitro* cultures of human peripheral blood mononuclear cells.

5.2.2.1. Expansion of CD1d/α–GalCer specific Vα24-independent T cells *in vitro* from healthy donors' PBMC

The frequency of Vα24+Vβ11+ double positive iNKT cells in PBMC from healthy donors ranges from 0.01% to 1.0%. The CD1d/α–GalCer tetramers bound to a very small proportion of Vα24-negative/$CD3^+$ cells in fresh PBMC samples from healthy donors, and the signals obtained by the tetramer staining could actually not be distinguished from background staining with confidence (data not shown). In contrast, clearly distinct Vα24-negative, CD1d/α–GalCer tetramer+ T cell populations were identified by the CD1d/α–GalCer tetramers in all of a series of 14 days old, α–GalCer stimulated *in vitro* cultures from seven healthy donors. Frequencies of these Vα24-CD1d/α–GalCer tetramer+ T cells ranged from 1.0% to 5.5% of total lymphocytes

(Figure 40) and varied with different stimulation protocols. Interestingly, efficient expansion of Vα24- CD1d/α–GalCer tetramer+ T cells required stimulation with α–GalCer pulsed mature autologous Mo-DC in some donors, whereas addition of α–GalCer to PBMC without Mo-DC was sufficient to visibly expand Vα24-CD1d/α–GalCer-tetramer+ T cells in others (Figure 40). In all donors, a greater expansion of Vα24- CD1d/α–GalCer-tetramer+ T cells was observed when mature, rather than immature α–GalCer pulsed Mo-DC were used for stimulation (Figure 40). CD1d-tetramers loaded with α-mannosylceramide (α–ManCer) failed to stain both Vα24+Vβ11+ iNKT cells and Vα24- CD1d/α–GalCer tetramer+ T cells, confirming the specificity of CD1d/α-GalCer tetramer binding (data not shown). The lack of TCR Vα24 expression by these Vα24- CD1d/a-GalCer tetramer+ cells was confirmed on FACS-sorted and *in vitro* expanded Va24- CD1d/α-GalCer tetramer+ lines and clones (Figure 41).

These results showed that recognition of CD1d/α–GalCer in humans is not limited to the invariant Vα24+Vβ11+ TCR. To assess the diversity of human T cell receptors capable of specifically recognizing CD1d/α-GalCer complex we analysed both the TCR usage and antigen specificity of Vα24-CD1d/α–GalCer tetramer+ T lymphocytes.

Figure 40. ***In vitro*** **expansion of Vα24- CD1d/α–GalCer tetramer+ T cells**

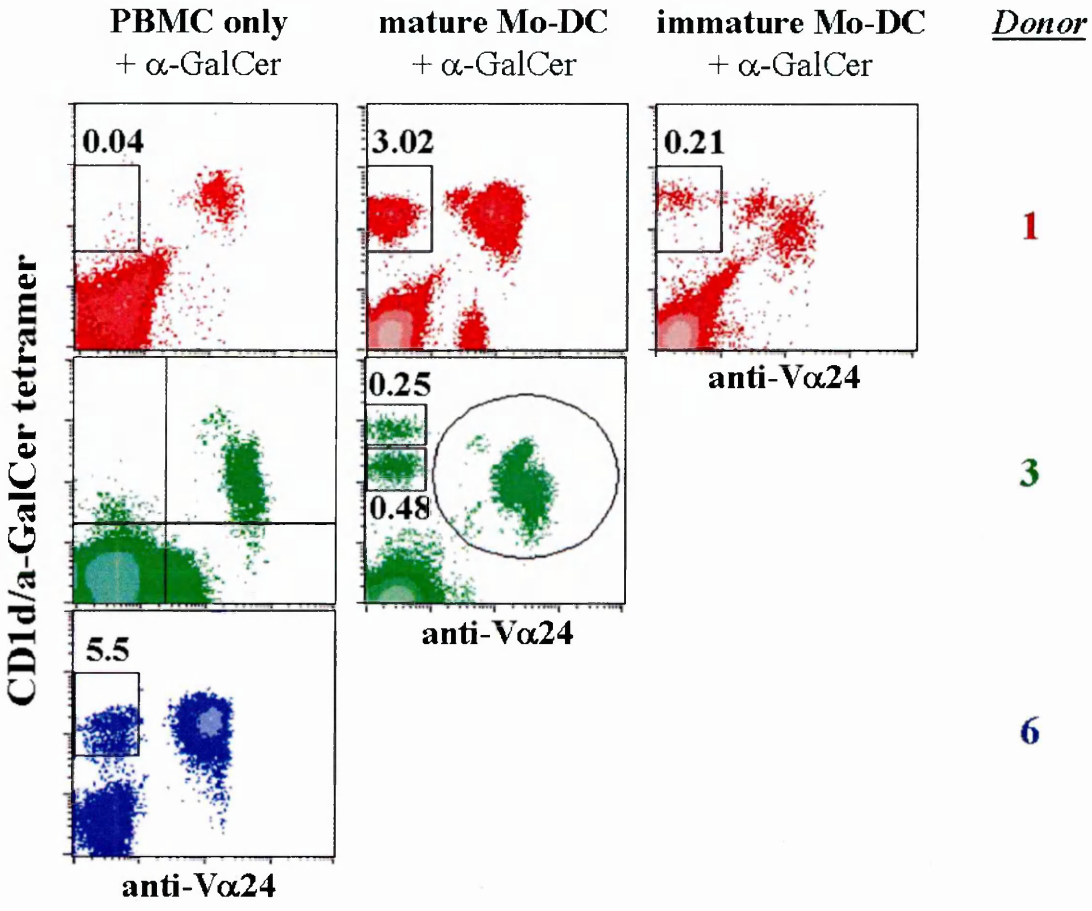

PBMC from different donors (shown are results for Donors 1, 3 and 6) were co-cultured with 100nM α-GalCer alone (density plots on the left-hand side), α-GalCer pulsed immature Mo-DC (density plots in the middle), or CD40L matured, α-GalCer pulsed Mo-DC (density plots on the right-hand side). Percentages of Vα24- CD1d/α-GalCer tetramer+ cells among propidium iodide negative, CD3+ small lymphocytes are shown.

Figure 41. Sorting of Vα24- CD1d/α–GalCer tetramer+ T cell clones and lines

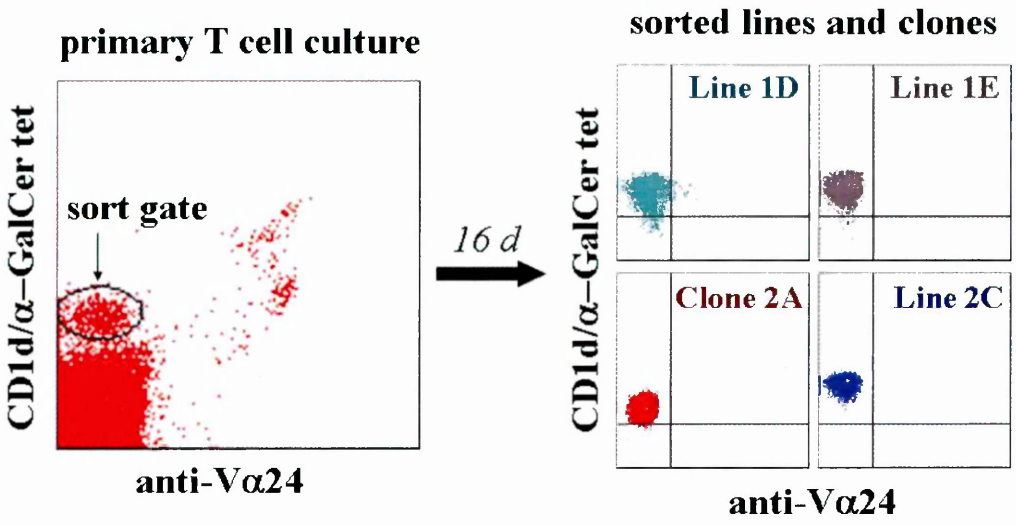

Va24-CD3+CD1d/α-GalCer tetramer+ were sorted by FACSVantage (dot plot on the left hand side) and expanded in vitro for 16 days. The resulting clones and lines were tested again for expression of TCR Vα24 chain and CD1d/α-GalCer tetramer binding. Results for 3 different lines and one clone are shown on the right-hand side.

5.2.2.2. TCR Vα- and TCR Vβ repertoire of Vα24- CD1d-α–GalCer specific T cells

Human Vα24+Vβ11+ iNKT lymphocytes use TCR Vβ11 domains with polymorphic CDR3β regions [303]. On the other hand, the murine equivalent to human Vα24+Vβ11+ iNKT lymphocytes, Vα14-Jα281+ iNKT lymphocytes, use several different TCR Vβ families with polyclonal CDR3β regions [304]. For these reasons it has been proposed, that the Vβ chain does not contribute to the specific recognition of CD1d/α–GalCer[305]. Interestingly, a substantial proportion of Vα24- CD1d/α–GalCer specific T cells expressed Vβ11 (Figure 42).

Figure 42. Vβ11 usage by Vα24- CD1d/α-GalCer+ T lymphocytes

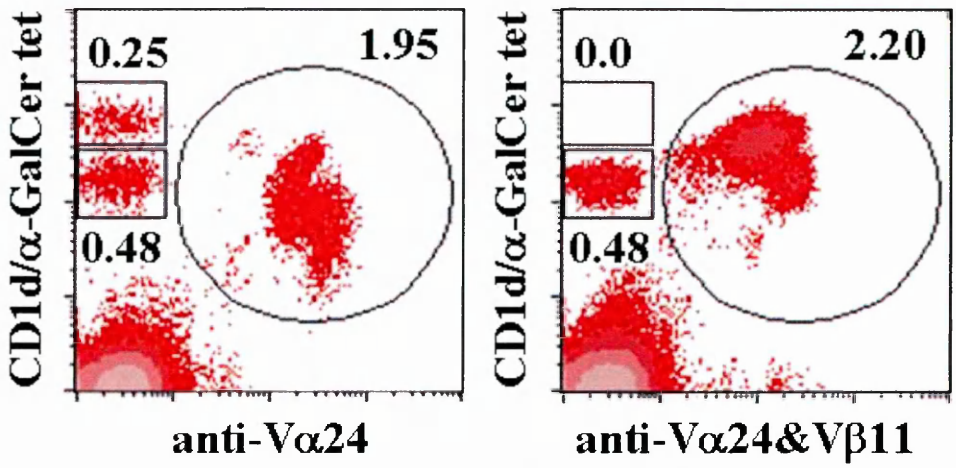

PBMC (shown here for Donor 1) were co-cultured with LPS-matured, α-GalCer pulsed Mo-DC. Immunostaining and FACS analysis were carried out with CD1d/α–GalCer tetramers and either anti-Vα24-specific antibodies (density plot on the left-hand side), or a mixture of anti-Vα24 and anti-Vβ11 specific antibodies (density plot on the right-hand side). Percentages of propidium iodide negative, CD3+ lymphocytes are shown.

In order to determine the usage of TCR Vα- and Vβ-chains of Vα24-CD1d/α–GalCer specific T cells we subjected a polyclonal Vα24-CD1d/α–GalCer tetramer+ line to spectratype analysis. The spectratype analysis demonstrated that this Vα24- CD1d/α–GalCer specific line contained clones using several different TCR Vα families, TCR Vβ families, and Jβ segments (Figure 43 and Table 4). Prominent expansions for seven different TCR Vα families (Vα2, 6, 8, 15, 20, 23, 26) and seven different TCR Vβ families (Vβ1, 3, 9, 11, 12, 18, 23) with different CDR3 lengths, also within the same family (e.g. Vβ3), were shown to be present in this line.

Figure 43. Spectratype analysis of a Vα24- CD1d/α-GalCer-tetramer+ T cell line

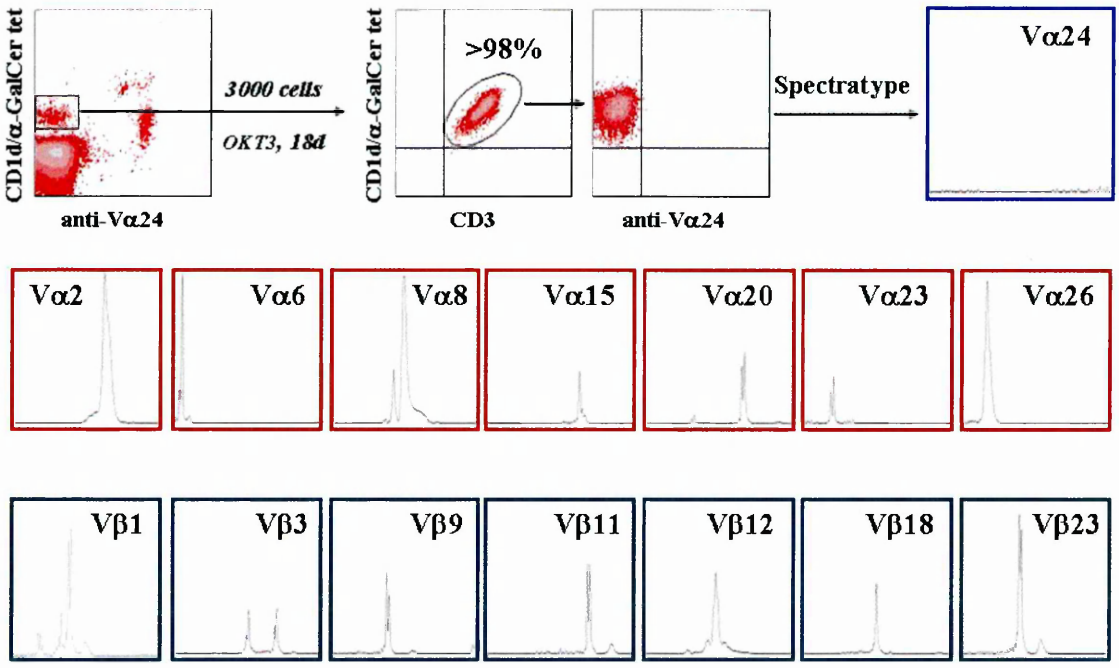

Spectratype analysis was carried out on mRNA from a pure polyclonal Vα24- CD1d-α–GalCer tetramer^{+} line, which had been obtained by FACS-sorting of 3000 Vα24-CD1d-α–GalCer tetramer+ T lymphocytes. Contamination of the samples with cDNA from Vα24+ cells was ruled out (top row, panel on right-hand side).

Table 4. Spectratype analysis of Vα24- CD1d-α–GalCer tetramer+ T cells

Vα family	CDR3α length	Vβ family	CDR3β length	Jβ family
Va2	12	BV1	8	2.7
AV6	1	BV3	10 / 14	2.7 / 2.3
AV8	10	BV9	8	2.7
AV15	15	BV11	14	2.3
AV20	20	BV12	10	2.7
AV23	3	BV18	10	1.4
AV26	3	BV23	8	2.7

Guided by the results of the spectratype analysis, I tested five Vα24- CD1d/α–GalCer tetramer+ oligoclonal lines and one Vα24- CD1d/α–GalCer tetramer+ clone obtained from the same donor for binding to different anti-TCR Vβ antibodies. Consistent with the results from the spectratype analysis, three lines expressed TCR Vβ1, and two lines and the clone were TCR Vβ11+ (data not shown).

Pre-incubation of a pure Vβ1+ Vα24- CD1d/α–GalCer tetramer+ line with an anti-Vβ1-specific monoclonal antibody significantly reduced staining by CD1d/α–GalCer tetramers, while pre-incubation of the same line with anti-TCR Vβ11 antibodies had no effect on tetramer staining (Figure 44a). Similarly, pre-incubation of an oligoclonal Vα24- CD1d/α–GalCer tetramer+ line containing both Vβ1+ and Vβ11+ expressing cells with anti-Vβ11 antibody selectively reduced tetramer staining of Vβ11+ cells (data not shown). These results formally demonstrated that staining of these Vα24- T cell lines by CD1d/α–GalCer tetramers was caused by specific binding of the tetramer to the TCR, but not to other receptors or non-specific binding to the T

lymphocyte membrane. Consistently, CD1d/α-GalCer tetramer staining of Vα24-CD1d/α-GalCer tetramer+ T cell lines could be partially blocked by pre-incubation of the cells with an excess of CD1d/α–GalCer monomers (Figure 44b).

Taken together, these results demonstrated that α–GalCer not only stimulates Vα24+Vβ11+ iNKT lymphocytes, but can also efficiently induce a CD1d/α–GalCer specific polyclonal, Vα24-independent T cell response. TCR Vβ11 is over represented among Vα24- CD1d-α–GalCer specific T cells, suggesting either an inherent affinity of Vβ11 to CD1d molecules or its direct involvement in specific recognition of α–GalCer.

Figure 44. Specificity of binding of CD1d/α–GalCer tetramers to Vα24- T cells

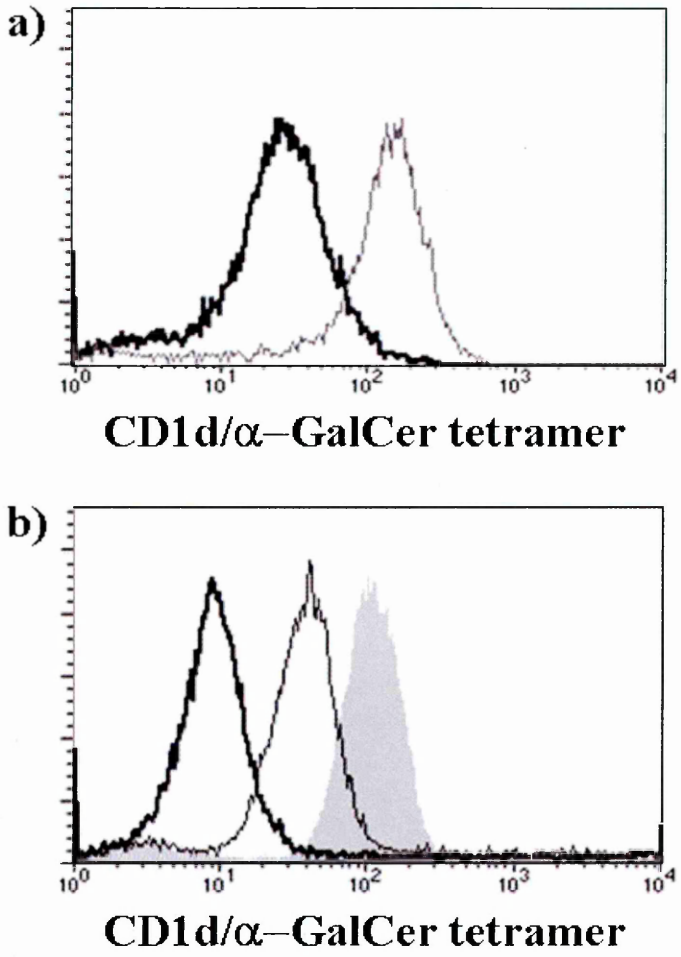

***(a)** Pre-incubation of a Vα24- Vβ1+ T cell line with anti-TCR Vβ1 antibody (bold line), but not with anti-TCR Vβ11 antibody (thin line) reduced the binding of CD1d/α–GalCer tetramers. **(b)** Pre-incubation of a Vα24- Vβ11+ line with 50x excess (bold line) or 25x excess (thin line) of CD1d/α–GalCer monomers partially blocked CD1d/α-GalCer tetramer staining compared to pre-incubation of the cells with PBS (grey area).*

5.2.2.3. Functional analysis of Vα24- CD1d/α–GalCer specific T lymphocytes

To assess antigen specific functions of the Vα24- CD1d/α–GalCer tetramer+ T lymphocytes, I first studied their capacity to specifically kill CD1d-transfected C1R-cells (C1R-CD1d) pulsed with different antigens, i.e. α–GalCer, α–ManCer or the vehicle. $CD4^+$ and CD8αβ Vα24- CD1d/α–GalCer tetramer+ T cells very efficiently lysed α–GalCer pulsed C1R-CD1d, but not C1R-CD1d pulsed with either α–ManCer or vehicle (Figure 45). Vα24- CD1d/α–GalCer tetramer+ T cells and Vα24+Vβ11+ iNKT were equally efficient at killing α–GalCer pulsed targets.

Figure 45. Lysis of α-GalCer pulsed CD1d+ targets by Va24- T lymphocytes

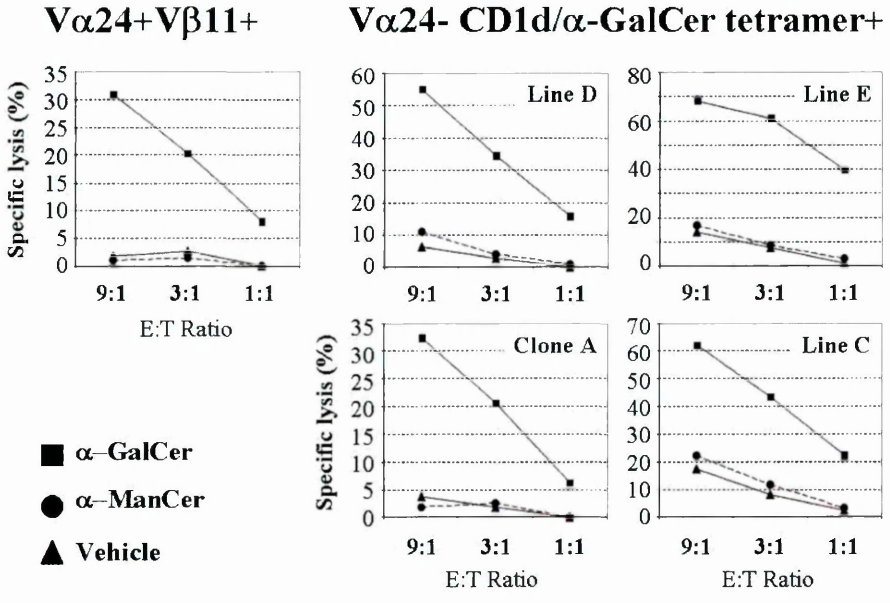

One Vα24+Vβ11+ iNKT line and 4 different Vα24- CD1d/α-GalCer tetramer+ T cell lines and clones were tested for their antigen specific lysis of CD1d-expressing C1R B-lmphoblasts. Specific lysis (%) is indicated on the y-axis and the effector to target (E:T) ratio is shown on the x-axis. Antigens used were α-GalCer, α-ManCer and the vehicle.

Next I assessed antigen- and mitogen-induced cytokine secretion of two Vα24-CD1d/α–GalCer specific T cell lines compared to a Vα24+Vβ11+ iNKT line by intracellular cytokine staining. Either C1R-CD1d lymphoblasts pulsed with glycolipids or a combination of phorbolmyristate acetate plus ionomycin (PMA/IM) were used for T cell stimulation. All tested Va24- and Va24+ lines secreted various cytokines, including IL-2, IFNγ, IL-13 and IL-4 in response to both α-GalCer and PMA/IM, but not in response to α-ManCer (Figure 46). Some lines, such as the CD4+ Vα24- T cell "line 2C" secreted IL-2 (data not shown), IFNγ, IL-13 and IL-4, whereas other Vα24- CD1d/α–GalCer specific lines secreted IL-2, IFN-γ and IL-13, but not IL-4. Interestingly, the Vα24- CD1d/α–GalCer specific "clone 2A", which specifically lysed α–GalCer pulsed C1R-CD1d (compare Figure 45), did not secrete IFNγ. As expected, the tested Vα24+Vβ11+ iNKT lines produced IL-13, IFNγ, IL-4 and IL-2 (data for IL-4 and IL-2 not shown). A similar cytokine secretion pattern for human iNKT cells has been previously reported by others [299].

Taken together these results suggested that Vα24- CD1d/α–GalCer specific T lymphocytes are similarly potent to produce cytokines as Vα24+ iNKT cells.

Figure 46. Cytokine production by α-GalCer specific Vα24- and Vα24+ T cells

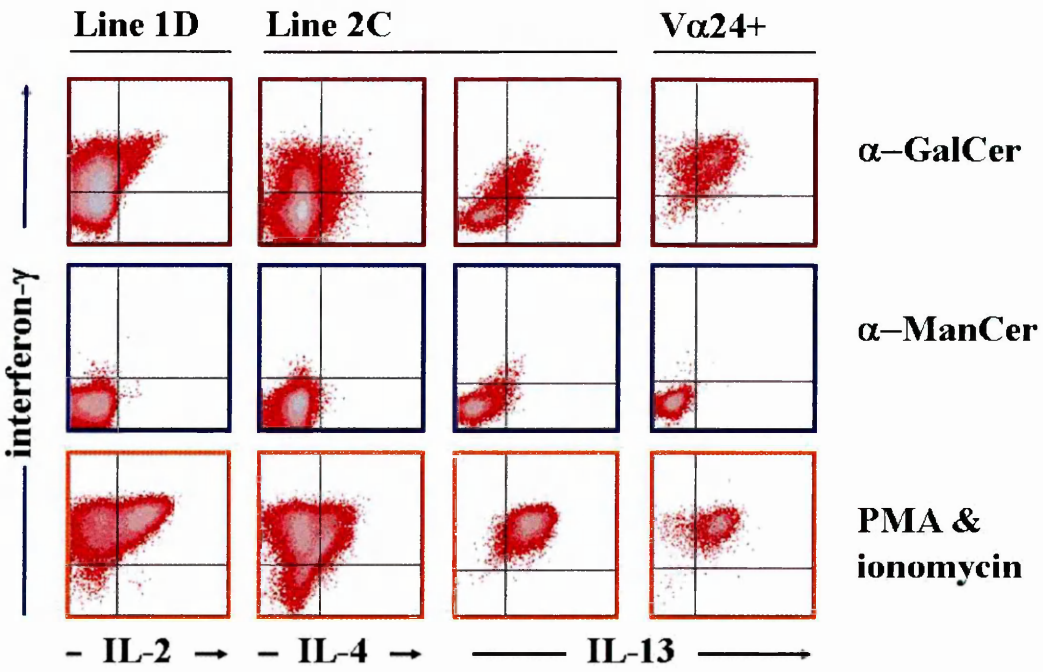

Intracellular cytokine staining of Vα24- and Vα24+ CD1d/α–GalCer tetramer+ T lymphocytes after their stimulation with either α–GalCer pulsed (top row) or α–ManCer pulsed (middle row) C1R-CD1d lymphoblast or after nonspecific activation with PMA and ionomycin (bottom row). The Va24- lines 2C and 1D were >99% pure for Vα24-Vβ1+ and Vα24-Vβ11+ CD1d/α–GalCer-tetramer+ T cells. Results shown are representative of two experiments.

5.2.2.4. CD4/CD8-coreceptor use and CD161-expression by Vα24- CD1d/α–GalCer specific T cells

Mouse and human iNKT cells are either CD4+CD8- or CD4-CD8- (i.e. DN) [166, 299]. Interestingly, a significant proportion of Vα24- CD1d/α–GalCer specific CD4- T cells in several donors expressed the CD8αβ heterodimer (Figure 47), while all other Vα24- CD1d/α–GalCer specific T cells were CD4+CD8- (data not shown). In contrast, CD4-CD8- DN Vα24- CD1d/α–GalCer specific T cells were not found in any of the seven donors included in this study (data not shown).

The great majority of α–GalCer specific mouse and human iNKT cells express the pan-NK marker CD161 (NKR-P1), an NK-locus encoded C-type lectin. The majority of Vα24+Vβ11+ iNKT cells expressed CD161 (Figure 47). In contrast, CD161 was detected only on a small proportion of CD4+ CD8αβ- Vα24- CD1d/α–GalCer tetramer+ cells (data not shown) and was hardly expressed by CD8αβ+ Vα24- CD1d/α–GalCer tetramer+ cells (Figure 47).

In order to investigate the possible functional role of CD8αβ co-receptor expression in Vα24- CD1d/α–GalCer specific T cell lines, I examined specific lysis of α-GalCer pulsed C1R-CD1d cells by CD8αβ+ Vα24- cells in the presence of a blocking anti-CD8 antibody [254]. These experiments showed that incubation with the anti-CD8 blocking antibody, but not with an irrelevant isotype matched control antibody, significantly reduced specific lysis of α-GalCer-pulsed C1R-CD1d cells (Figure 48).

Figure 47. Co-receptor and CD161 expression on Vα24- and Vα24+ T cells

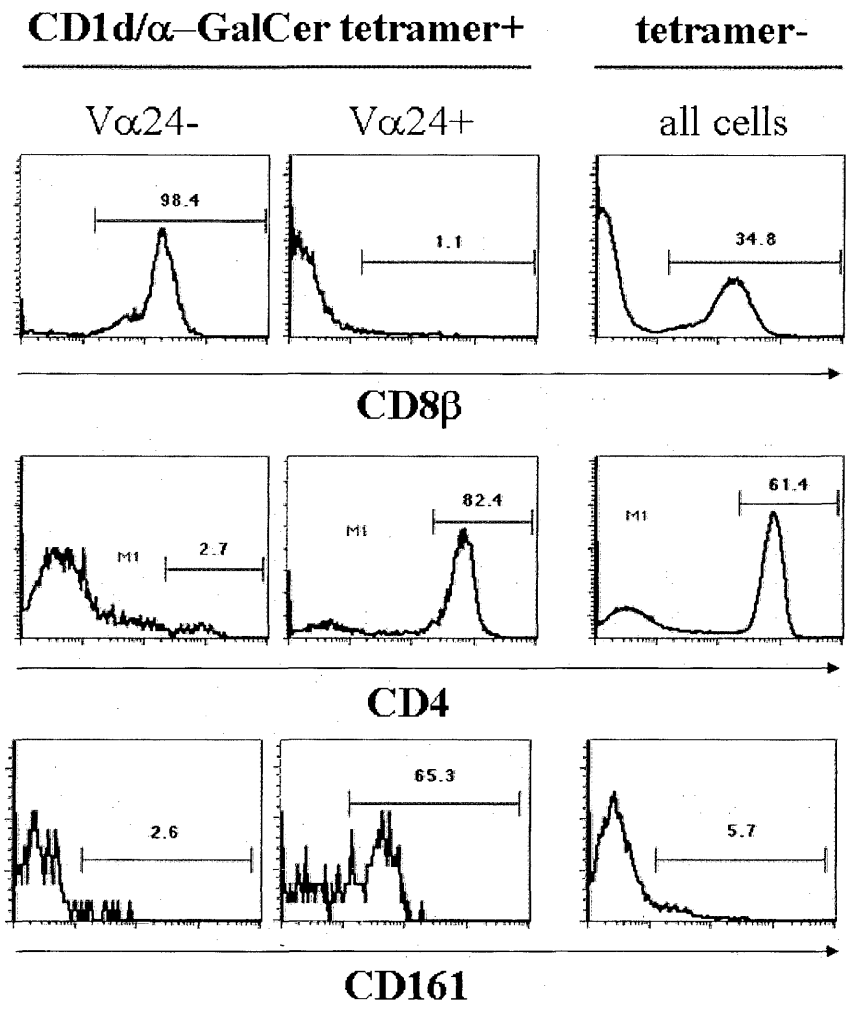

Cells from one healthy donor were stained with CD1d/α–GalCer-tetramer, anti-Vα24, and either anti-CD8β (top row), anti-CD4, (middle row) or anti-CD161 (bottom row) antibodies, two weeks after in vitro stimulation with 100ng/ml α–GalCer. Histogram plots were gated on CD1d/α–GalCer tetramer+ Vα24+ and Vα24- T lymphocytes (left and middle) and on CD1d/α–GalCer tetramer- lymphocytes (right). Percentages of $CD8\beta^+$, $CD4^+$, and $CD161^+$ cells in the gated population are shown. Propidium iodide staining was used to exclude dead cells from the analysis.

Figure 48. CD8 Co-receptor dependent killing by CD8αβ+ Vα24- CD1d/α-GalCer specific T lymphocyte lines

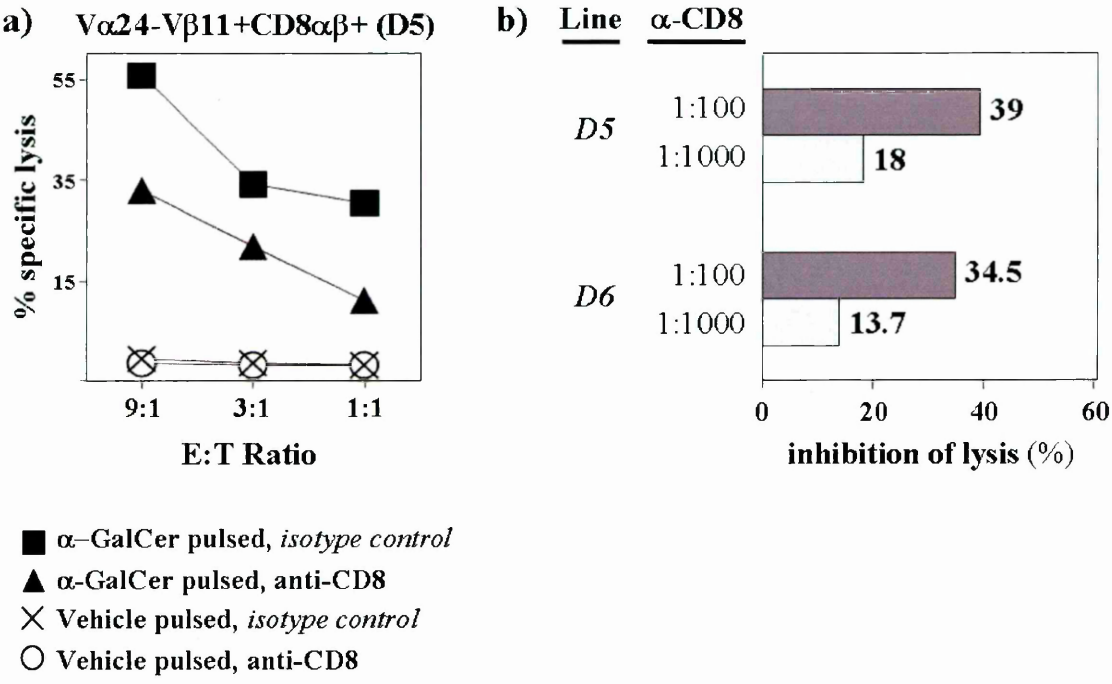

C1R-CD1d lymphoblastoid cells pulsed with α–GalCer or the vehicle were used as targets for two CD8αβ⁺ Vα24- CD1d/α-GalCer tetramer+ T cell lines (D5 and D6) in a standard ^{51}Cr-release assay in the presence of either the anti-CD8 blocking antibody MF8 or an irrelevant isotype matched control antibody. Specific killing by the line D5 in the presence of either antibody is shown in (a), and MF8 antibody mediated inhibition of target cell lysis by lines D5 and D6 at a 9:1 effector:target (E:T) ratio is shown in (b).

5.2.2.5. Differential binding of CD1d/α-GalCer monomers to CD8αβ+ Vα24- and CD4-CD8- (DN) Vα24+ CD1d/α-GalCer specific T cells

Mouse Vα14+ iNKT cells have previously been shown to bind CD1d/α–GalCer monomers [305]. Similarly, I found that CD1d/α–GalCer monomers bound to a DN Vα24+ Vβ11+ line. However, CD1d/α–GalCer monomers failed to stain any of our CD8αβ+ Vα24- CD1d/α–GalCer specific T cell clones or lines (Figure 49/a). Both CD8αβ+ Vα24- and DN Va24+ CD1d/α–GalCer specific cells showed identical levels of both CD3 expression and CD1d/α–GalCer tetramer staining (Figure 49/b, and data not shown).

Interestingly, CD1d/α–GalCer monomer staining of the DN Vα24+ Vβ11+ line disclosed two distinct populations suggesting the presence of clones with different binding affinities to CD1d among these DN Vα24+ Vβ11+ cells. By combining the monomer-staining with a chase-experiment I estimated the half-life of monomer binding to DN Vα24+ Vβ11+ to be in the range of approximately 50 minutes (Figure 49, and data not shown).

These results were consistent with the hypothesis that the CD8αβ+ Vα24- CD1d/α–GalCer specific T cells expressed TCRs with lower affinity for CD1d/α–GalCer compared to DN Vα24+ Vβ11+ iNKT cells.

Figure 49. CD1d/α-GalCer Monomer binding to Vα24+ and Vα24- T cells

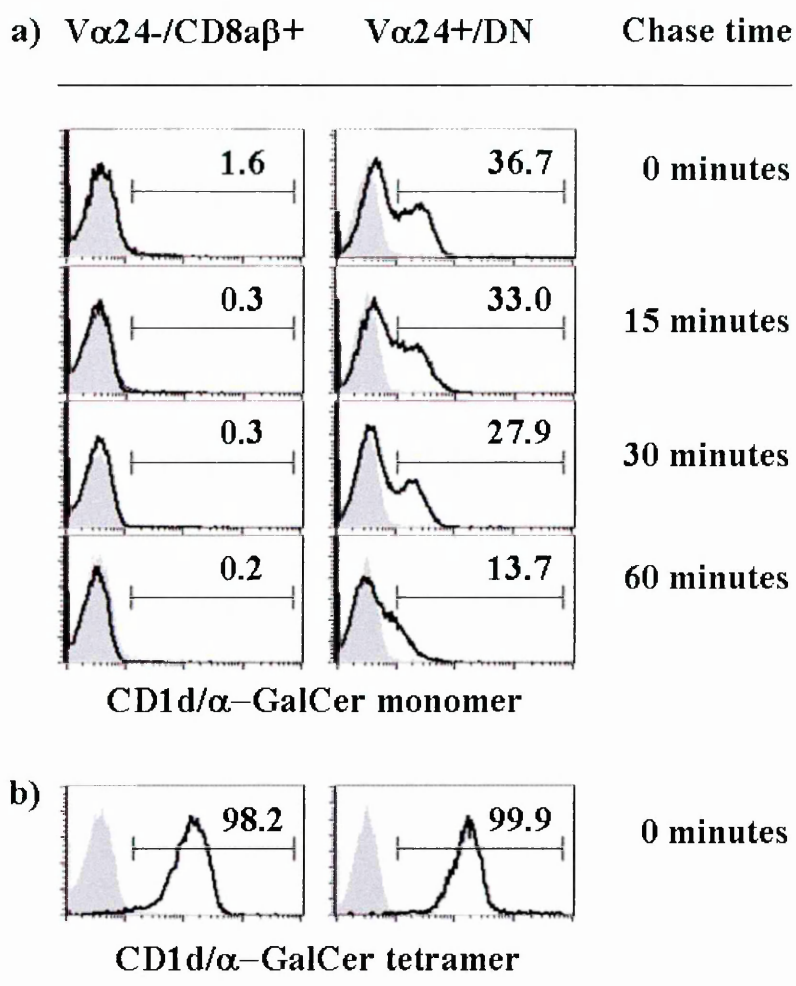

Cells were sequentially stained with CD1d/α̃GalCer monomers and PE-Extraavidin (bold lines in (a)) or with CD1d/α̃GalCer tetramers (bold lines in (b)) or PE-Extraavidin only (grey area in (a,b)). In chase experiments (a) cells were incubated at 37°C for 0, 15, 30, or 60 minutes after PE-Extraavidin staining and two washes with PBS. Percentages of monomer- and tetramer stained cells are shown for each histogram plot.

5.3. Discussion

In this chapter I have described the generation and validation of human CD1d/lipid-tetramers for detection of CD1d-restricted T lymphocytes in peripheral blood and tissue.

Murine CD1d-tetramers using CD1d/β2m monomeric complexes secreted by insect cells have been generated by other research groups [298, 305]. However, loading of these complexes with endogenous lipids[155] might affect their sensitivity and specificity. In contrast, the methods shown here, i.e. *in vitro* refolding of completely denatured and reduced recombinant bacterial inclusion body proteins in the presence of a specific single lipid ligand, should effectively avoid such problems.

My first refolding trials of CD1b and CD1d, using several protocols that were based on the classic dilution method used for refolding MHC class I/β2m/Peptide-complexes[257, 291], completely failed. Similarly, simple detergent-assisted dilution additive methods were unsuccessful. On the other hand an artificial chaperone approach, which I had developed in parallel for the efficient refolding of CD1b/β2m/lipid complexes, yielded only very small amounts of CD1d/α-GalCer monomeric complexes.

The marked hydrophobicity of all CD1 molecules was an obvious likely cause of hydrophobic aggregation of CD1 proteins during early refolding stages. In addition, the presence of an unpaired Cys^{12} in CD1d was also likely to further potentiate protein misfolding and aggregation. These problems could eventually be overcome and the yield of properly refolded CD1d/β2m/lipid monomers significantly increased by using a ternary refolding matrix, which had previously been shown to efficiently assist the

refolding of scorpion toxin, a highly hydrophobic protein with multiple cysteines[306]. The refolding matrix consists of three components, which are immobilized on a sepharose matrix: The GroEL minichaperone can prevent hydrophobic interactions of early folding intermediates, while disulfide isomerase (DsbA) and prolyl isomerase catalyse the formation of native disulfide bonds and correct proline isomerization, respectively [249, 306]. Applying this refolding matrix for human CD1d proteins allowed me to generate milligram amounts of monomeric CD1d/β2m/α-GalCer complexes, which could be purified by size exclusion chromatography.

Fluorescent-conjugated tetramers generated from these CD1d/β2m/α-GalCer complexes sensitively and specifically stained human Vα24+Vβ11+ iNKT cells in peripheral blood and tissue. In addition, *in vitro* generated T lymphocyte lines, which had been expanded from CD1d/α-GalCer tetramer+ CD3+ double positive FACS sorted cells, were enriched to > 95% for Vα24+/Vβ11+ iNKT cells, confirming the specificity of the tetramers.

Using the CD1d/α-GalCer tetramer we measured frequencies of intrahepatic iNKT cells in patients with end-stage liver cirrhosis. Consistent with previous reports in mice, almost all CD1d-tetramer+ CD3+ intrahepatic cells were either CD4 or DN T cells[166]. However, our analysis indicated that iNKT cells are not significantly enriched in cirrhotic human liver, which might indicate differences in tissue distribution between humans and mice.

Interestingly, in three patients with viral hepatitis the CD1d-tetramer+ CD3+ tetramers stained a distinct TCR Vα24-negative T cell population within the DN subset, representing 0.28% - 0.69% of all intrahepatic DN T cells. This suggested the

possibility that, in addition to the known iNKT cell subset, other CD1d-restricted and α-GalCer specific T lymphocytes might exist in humans.

I therefore made use of the CD1d/α–GalCer tetramers to further investigate the hypothesis that recognition of CD1d/α–GalCer complexes was not absolutely restricted to iNKT cells bearing the invariantly rearranged TCR Vα24-Jα18 chain, but could also be mediated by other randomly generated TCRs. In support of this notion, evidence from mouse studies had previously indicated that iNKT cells branch off the mainstream developmental pathway because of their TCR specificity [149, 300-302].

The results of these studies demonstrated the existence of distinct Vα24-negative, CD1d/α–GalCer specific T lymphocyte populations in human peripheral blood. These novel CD1d-restricted T cells could only be reliably detected upon *in vitro* stimulation of PBMC with α–GalCer. α-GalCer pulsed mature Mo-DCs provided the strongest stimulus for *in vitro* expansion of these Vα24-negative T cells. However, simple addition of α-GalCer to PBMC cultures was sufficient to expand Vα24- CD1d/α–GalCer tetramer+ cells to 5.5% in one donor, suggesting that these cells were already expanded *in vivo*, albeit at a frequency below the threshold for tetramer staining.

The restriction to CD1d and specificity for CD1d/α–GalCer of these novel T cell subsets was demonstrated in several ways: Vα24- CD1d/α–GalCer tetramer+ lines and clones specifically killed α–GalCer pulsed, but not α–ManCer pulsed CD1d expressing target cells, demonstrating their specificity for the CD1d bound glycolipid ligand. Furthermore, pre-incubation of Vα24- CD1d/α–GalCer tetramer+ cells with

specific anti-Vβ chain antibodies or an excess of CD1d/α–GalCer monomers clearly reduced CD1d/α-GalCer tetramer staining.

Our spectratype analysis revealed that a wide variety of TCR Vα and Vβ segments can be used by Vα24- CD1d/α–GalCer tetramer+ cells, which supports a mainstream model of iNKT cell thymic selection. However, a marked bias for the use of Vβ11 by Vα24- CD1d/α–GalCer tetramer+ was observed in several *in vitro* cultures from different donors. Previous tetramer based studies of iNKT cells in mice have suggested, that the CDR3β regions are permissive, but do not specifically contribute to the recognition of CD1d/α–GalCer complexes [305]. The findings of my study did not exclude this possibility but they suggested the possibility that certain Vβ11 regions might have an inherent affinity for CD1d, similar to the known inherent affinity of certain Vβ regions for MHC II [307]. In fact, the recently solved crystal structures of unbound human iNKT TCRs and of the CD1d/α-GalCer/iNKT TCR complex have underpinned a role for the CDR2β loop of Vβ11 in the molecular interaction with the α1 helix of CD1d [187, 241].

"Conventional" invariant NKT cells in humans and mice exhibit a $CD4^+$ or a DN phenotype [299]. In contrast, all Vα24- CD1d/α–GalCer specific T cells in the seven tested donors were either CD4+ or CD8αβ+, while no DN Vα24- CD1d/α–GalCer tetramer+ could be detected. Interestingly, the cytotoxic activity of Vα24-CD1d/α–GalCer specific CD8αβ+ T cells was clearly reduced by an anti-CD8 blocking antibody, indicating that CD8αβ exerts a role as a co-receptor for these cells. Previous studies in mice have suggested that CD1d interacts with CD8 [149, 166, 300].

Lantz and colleagues have shown that in Vα14-Jα281-transgenic mice the CD8- compartment is selectively depleted of Vβ7 and Vβ8, i.e. the main Vβ chains used by mouse Vα14-Jα281 iNKT cells [300]. Similarly, Vα14-Jα281 iNKT are negatively selected in CD8 transgenic mice [149], which suggests that iNKT cells bear TCRs with a high inherent affinity for CD1d molecules. Consistent with this notion, I have shown that DN iNKT cells can bind monomeric CD1d/α–GalCer complex, whereas Vα24-CD1d/α–GalCer specific CD8αβ+ T cells do not bind. Lineage decisions for CD1d/lipid-specific human iNKT cells might therefore follow similar principles as MHC/peptide-specific T cells; higher affinities of the TCR-peptide/MHC interaction favor the development of a CD4+ phenotype and lower affinities rather result in a CD8+ phenotype [308, 309].

TCR binding kinetics might also determine the expression of CD161 (NKR-P1) by iNKT cells [310-312]. Intriguingly, CD161 was rarely expressed on CD4+ Vα24-CD1d/α–GalCer specific T cells and not detected at all on CD8αβ+ Vα24-CD1d/α–GalCer cells.

Based on the results presented in this chapter I hypothesize that in humans, a wide variety of CD1d/α–GalCer specific TCRs are generated by random TCR rearrangement, and that the binding affinity of the TCR to CD1d/α–GalCer complex determines both CD161 expression and CD4/CD8αβ/DN lineage commitment. The reason why one type of TCR rearrangement, i.e. the iNKT TCR, is so clearly favoured over other possible TCR rearrangements is unclear. The successful *in vitro* expansion of Vα24- CD1d/α–GalCer specific T cells upon stimulation of PBMC with α-GalCer could be due to lower affinity of their TCRs for CD1d/α–GalCer or by their lack of

CD161 expression. My own recent studies indicate that the former possibility may be less likely[241].

The existence of human Vα24- CD1d/α–GalCer specific T cells has potential clinical implications in that injection of α–GalCer *in vivo* for therapeutic reasons might induce expansion of these T cells. Since the *in vivo* function of these cells is completely unknown, tetramer-based monitoring of Vα24- CD1d/α–GalCer specific T cells as well as iNKT cells should be carried out in α-GalCer receiving patients. In fact, a recent paper has found Vα24- CD1d/α–GalCer tetramer+ T lymphocytes *ex vivo* in the peripheral blood of patients that had been treated with α-GalCer [313].

5.4. Conclusions

Human CD1d-tetramers loaded with single lipid ligands can be generated from completely denatured and reduced inclusion body proteins by *in vitro* refolding. These tetramers are highly sensitive and specific and allow for detailed phenotypic analysis and direct *in vitro* and *ex vivo* isolation of CD1d-restricted, lipid-specific T cells from peripheral blood or tissue. The CD1d-tetramer aided identification and characterization of a novel lipid-specific human T lymphocyte population illustrates the potential of these reagents as powerful tools for the study of CD1 restricted immune responses.

Specific recognition of CD1d/α–GalCer complex can be mediated by human Vα24-JαQ-independent T cell subsets using diverse TCR Vα and TCR Vβ families. The existence of these novel T cells strongly suggests antigen driven selection of

CD1d/α-GalCer specific T cells and therefore underpins a TCR-instructive model of iNKT cell differentiation.

5.5. Acknowledgements

My dear friend Tassos Karadimitris, who came from the Memorial Sloan Kettering Hospital in New York to Oxford for 4 months to learn CD1 refolding techniques from me actually achieved the first CD1d refold using the ternary matrix generously provided by Myriam Altamirano, Nick Foster and Alan Fersht (Cambridge). I am indebted to Nic Dulphy for teaching and supervising me, and actually doing most of the spectratype analysis of the Va24- CD1d/a-GalCer specific T lymphocytes. I'd also like to thank Xiao-Ning Xu for providing the MF8 and CT antibodies, Mao Salio for teaching me how to generate Mo-DC, Dawn Shepard for immaculate technical assistance, and Michael J. Palmowski and Uzi Gileadi for lively discussions in front of the FPLC and in the coffee room of the IMM. The liver cirrhosis samples were provided by Dave Brown and Geoff Dusheiko from the Royal Free Hospital (London) and hepatitis blood samples were provided by Paul Klenerman (Oxford). Alpha-galactosylceramide (KRN7000) was generously provided by Yazu Koezuka and Mie Nieda from Kirin Brewery (Gunma, Japan) and also by Richard R. Schmidt (Konstanz, Germany).

6. Refolding and structure determination of recombinant lipid-loaded human CD1b molecules

6.1. Introduction

The initial objective to obtain recombinant human CD1/lipid-tetramers was to use them for the study of mycobacterial lipid specific, CD1-restricted T cell responses in TAP-deficient patients (see p.135). Human CD1 group 1 isoforms CD1a, CD1b and CD1c[146, 314, 315], but not CD1d or CD1e, had been previously shown to present mycobacterial lipids to T lymphocyte lines *in vitro*, but efficient tools to study these T lymphocytes *ex vivo* were not available.

On the other hand, it was completely unknown how individual group 1 CD1 molecules could present lipid ligands of greatly different fatty acid composition to T cell receptors. This property of CD1 molecules is most dramatically illustrated by human CD1b, which can present either a C32 (i.e. 32 carbon atom containing) or a C84 glucomonomycolate to the same CD1b-restricted T lymphocyte clone [172, 196]. The crystal structure of mouse CD1d1 at a resolution of 2.7 Å, published in 1997, had shown that the CD1d antigen binding groove contained two voluminous hydrophobic pockets [155]. However, the CD1d structure could not explain how CD1b molecules could accommodate very long fatty acids such as mycobacterial mycolic acids on the one hand, and shorter glycolipids, such as sphingosines on the other hand. In addition, some ill-defined electrodensity was apparent inside the pockets of mouse CD1d and was thought to belong to a then unidentified (later shown to be phosphatidylcholine [182]) endogenous lipid ligand from the insect cell derived mouse CD1d molecules used

for crystallisation. Importantly, such "contamination" of insect cell derived CD1 molecules with endogenous ligands might greatly weaken the potential use of such molecules for the detection of lipid-specific T lymphocytes. Therefore, refolding *in vitro* of completely denatured and reduced recombinant CD1 and β2-microglobulin (β2M) inclusion body proteins, produced in E.coli, was chosen as a general approach. In analogy to established successful protocols for refolding of denatured and reduced MHC class I molecules[291] only the extracellular region of CD1 heavy chain (residues 1−283) was used to make recombinant soluble CD1 molecules.

In 1999, at the time when I planned the first refolding trials for CD1 molecules the only known CD1 presented mycobacterial lipids were lipoarabinomannan (LAM), mycolic acid, phosphoinositomannosides PIM2 and PIM4, and glucomonomycolate. LAM contains a ca. 17 kDa large polar headgroup and can only be recognized by CD1b-specific T cells upon enzymatic processing of the headgroup in late endocytic compartments, i.e. after its transformation into PIMs. However, at the time it was not possible for us to obtain milligram amounts of either PIM2 or PIM4 for the refolding trials. Similarly, glucomonomycolate and mycolic acid were not available in high enough quantities. In addition, mycolic acid is extremely hydrophobic, and I therefore did not consider it as a ligand for initial refolding trials. Early reports on CD1 molecules had suggested that CD1 was both thermostable and stable without bound lipid ligands[316]. On the other hand, CD1b restricted, sphingolipid specific T cell responses had been reported by others[177]. With regard to their potential use in my refolding trials, several of these sphingolipids, in particular the gangliosides had two obvious advantages over mycobacterial lipids: they were commercially available and

known to be soluble in aqueous solutions. Based on these facts I decided to first design a protocol for refolding CD1b without lipid ligands and to add sphingolipids such as gangliosides later, once promising results had been achieved with that protocol.

In this chapter I will report the refolding and crystallisation of two human CD1b/lipid complexes and describe their three-dimensional atomic structures.

6.2. Results

6.2.1. CD1b refolding and crystallisation

All known standard protocols used for refolding of MHC class I/β2m-peptide complexes failed when applied to human CD1b molecules. An obvious qualitative difference between MHC class I and CD1b is the higher content of neutral and hydrophobic amino acids in CD1b, which reflects its function as a lipid-binding molecule. Therefore I tested several detergent-assisted refolding protocols to reduce hydrophobic protein aggregation by protecting exposed hydrophobic surfaces of early refolding intermediates (see methods). A screen of 81 minirefoldings using different ionic, non-ionic and zwitterionic detergents at different concentrations suggested that the ionic detergent CTAB (CetylTriAmmonium Bromide) at 0.5mM concentration was effective at keeping CD1b in solution. However, ionic detergents usually form stable interactions with proteins, which can impede completion of the protein folding process. On the other hand, CTAB had previously been successfully applied to refold two relatively hydrophobic proteins, namely citrate synthetase and carbonic anhydrase [317, 318], by using cyclodextrins to remove the protein bound CTAB. I therefore

incorporated β-cyclodextrin in the refolding protocol. The newly developed protocol was first used to refold CD1b and β2m in the absence of added lipid ligands and the concentrated refolding mixture was analysed by size exclusion chromatography. The AU280nm absorption profile of the refolding mixture showed a large aggregate peak followed by a distinct peak at ca. 150-170ml elution volume, i.e. in the expected region for CD1b/β2m monomers. SDS-PAGE analysis of this peak showed that it contained both CD1b and β2m, but re-purification of the same peak after only 1 day suggested that this protein species was not very stable (Figure 50/a, left panel). In subsequent trials I added potential CD1b lipid ligands, e.g. phosphatidyl-inositol, β-glucosylceramide or gangliosides to the refolding. Interestingly, the addition of any of these lipids greatly enhanced the size of the putative CD1b monomer peak and enhanced the stability of these CD1b/β2m complexes (Figure 50a, right panel, and 50b).

The presence of the lipid ligand in these "monomer peaks" was confirmed for CD1b refoldings with the ganglioside GM1. "Monomer peaks" were analysed for the presence of GM1 by ELISA using the highly GM1-specific cholera toxin β subunit (conjugated to horseradish-peroxidase).

These results showed that it is possible to refold CD1 molecules from completely denatured and reduced inclusion body proteins. Furthermore, short-chain detergents such as CTAB can assist the refolding of the hydrophobic CD1b proteins, but they fail to efficiently stabilise non-glycosylated E.coli derived CD1b molecules in the absence of appropriate two-alkyl chain containing lipid ligands. The comparison of "detergent-

only" and "detergent + ligand" CD1b refolding profiles indicated that the dominant protein peak at 152ml contained functional complex.

Figure 50. Refolding of human CD1b with and without added lipid ligands

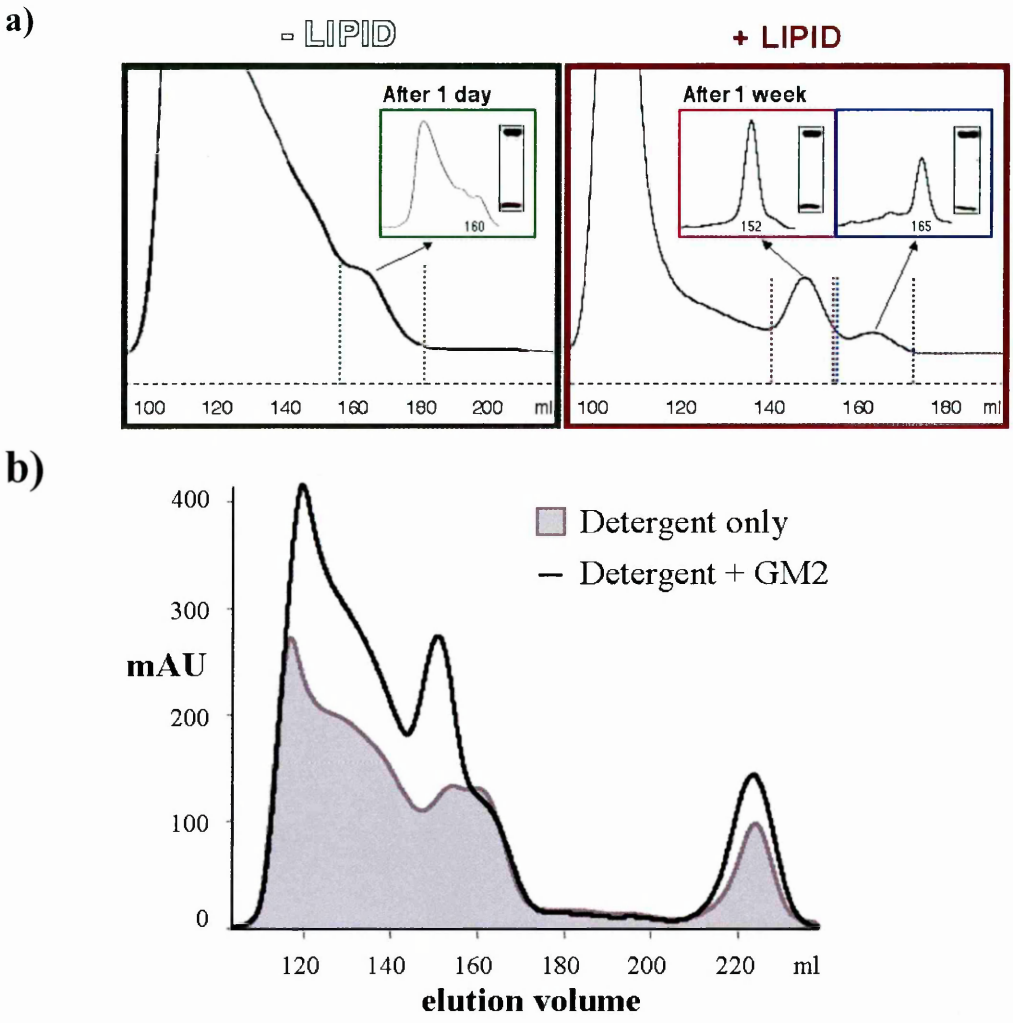

(a, left), Refolding of CD1b in the absence of added lipid ligands. Re-purification of this peak after 1 day showed that it was relatively unstable (inset). (a, right), Refolding in the presence of phosphatidylinositol (PI). The resulting peaks at 152 and 165ml were stable.

(b) Two 250ml refoldings of CD1b with (bold black line) or without (grey area) the CD1b ligand ganglioside GM2, carried out and analysed in parallel.

After further optimization and upscaling of the detergent-assisted refolding protocol I was able to generate milligram amounts of both CD1b/β2m/PI (CD1b-PI) and CD1b/β2m/ganglioside (CD1b-GM2). After screening of 250 different crystallisation conditions I succeeded in obtaining several protein crystals from both complexes (Figure 51). The best diffracting CD1b-PI and CD1b-GM2 crystals yielded data to 2.3 Å and 2.8 Å, respectively, which allowed the atomic structures of both human CD1b/ligand complexes to be determined.

Figure 51. Protein crystals of human CD1b/β2m/lipid complex

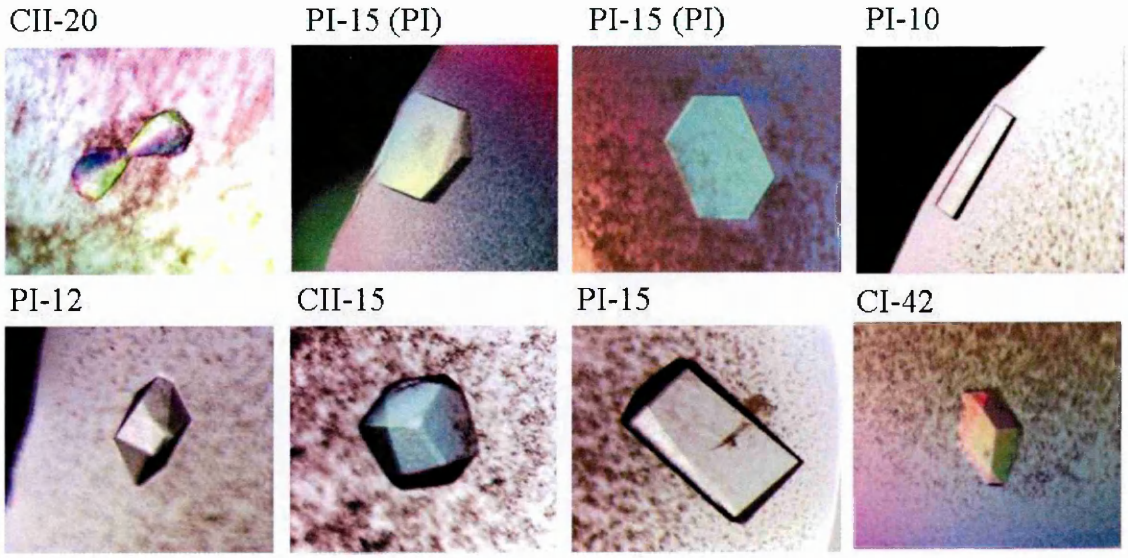

Crystals grown in conditions PI-15 and PI-10 were used for data acquisition.

6.2.2. The structure of human CD1b with bound ligands

Table 5 shows the statistics for data collection and refinement

6.2.2.1. Structural features of the CD1b binding groove

The CD1b heavy chain and β2m structures are identical in CD1b-PI and CD1b-GM2. In the following analysis I will focus on the higher resolution CD1b-PI structure. Both structures reveal a network of hydrophobic channels at the core of the α1α2 domain, which are saturated by four 11–22 hydrocarbon atoms chains (Figure 52). The binding groove architecture of CD1b is radically different from that of classical MHC class I and II molecules. The total volume (2200 $Å^3$) of the network is filled by the hydrocarbon chains. No buried water molecules are present. In an extension of the analogy with MHC class I binding pocket nomenclature introduced for mouse CD1d[155], the three CD1b binding channels that connect directly to the surface are denoted as A', C' and F', with the fourth, a distinct tunnel, designated T' (Figure 52, 53, 54). Details of the key binding groove features are shown in Figure 53. Channels A', C' and F' interconnect *via* a tunnel T' (Figure 53/b). The sequential connection of A', T' and F' could accommodate alkyl chains of up to 60 carbon atoms. Channel C' leads from the T cell receptor (TCR) recognition surface between the α1 and α2 helices to a portal in the side of the molecule beneath the α2 helix (Figure 53/d). The portal is surrounded by CD1b heavy chain residues 126–131 and 145–159 and is stabilized by a disulfide bond (C131-C145), which is unique to CD1b. This channel can shelter 16 carbon atom chains fully from solvent while allowing egress for longer chains. The PI and GM2 ligands occupy channels A' and C', whereas two detergent molecules fill channels F' and T' (Figure 52, 53, 54).

Table 5. Statistics for data collection and refinement of CD1b crystal structures

Data collection	CD1b/GM2	CD1b/PI
Resolution range (Å)	100-2.8	25-2.2
Completeness (%) (outer)	88.8 (71.1)	92.3 (89.8)
Total observations	89500	334867
Unique reflections	13203	27623
Average I/σ(I) (outer)	13.7 (1.8)	39.1 (15.8)
R_{merge} (%) (outer)	10.3 (32.5)	5.1 (20.6)
Model refinement	**CD1b/GM2**	**CD1b/PI**
Maximum resolution	2.80	2.26
Reflections (working set / test set)	12383 / 535	24656 / 751
R_{work} / R_{free} (%)	22.3 / 27.4	20.2 / 23.8
r.m.s.d from standard stereochemistry		
Bonds (Å)	0.012	0.008
Angles (°)	1.62	1.42
Number of atoms		
Protein	3000	3005
Ligand ligands	85	90
Waters	40	232
NO_3	0	12
Ramachandran plot		
Most favoured (%)	88.5	89.4
Additional (%)	11.2	9.3
Generous (%)	0.3	1.2
Disallowed (%)	0	0

Values in parentheses refer to the highest resolution shells (2.91-2.80Å for CD1b/GM2 and 2.28-2.20Å for CD1b/PI).

$R_{merge} = \sum_h \sum_i |I_i(h) - \langle I(h) \rangle| / \sum_h \sum_i I(h)$ where $I_i(h)$ is the ith measurement of reflection h and $\langle I(h) \rangle$ is the weighted mean of all measurements of h.

$R = \sum_h |F_{obs} - F_{calc}| / \sum_h F_{obs}$ where F_{obs} and F_{calc} are the observed and calculated structure factor amplitudes, respectively. R_{work} and R_{cryst} were calculated using the working and test set, respectively.

Figure 52. Structure of two different human CD1b/β2m/ligand complexes

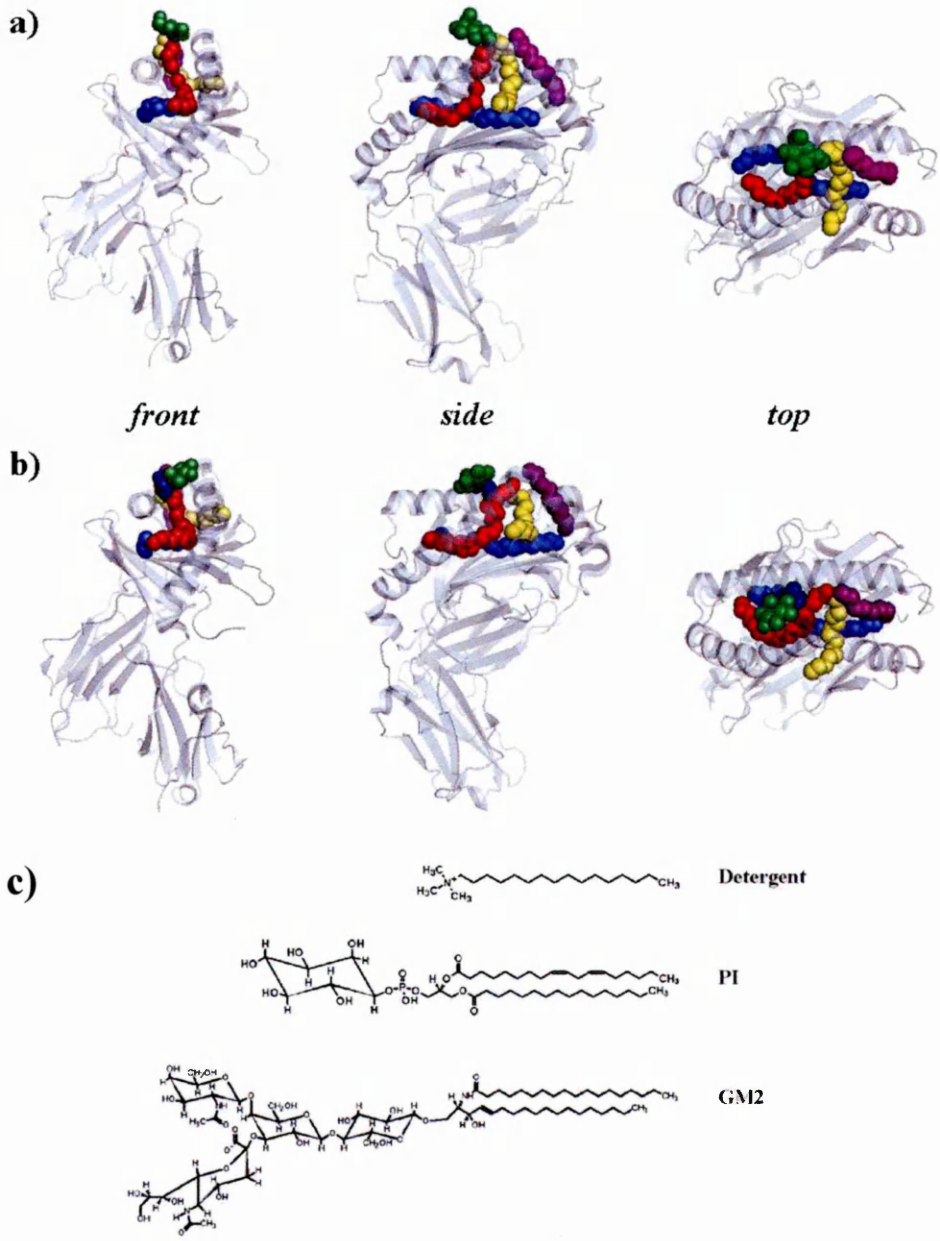

Human CD1b structure (α1- α3 domains and β2m in blue-white) with bound GM2 and CTAB (a) and bound PI and CTAB (b). Ligands are shown as Van Der Waals spheres: alkyl chains are in yellow and red, CTAB deep-purple and blue; GM2 headgroup green; Phosphate blue; inositol blue. (c) Chemical structures of CTAB, PI and GM2.

Figure 53. Structural details of the human CD1b/PI structure

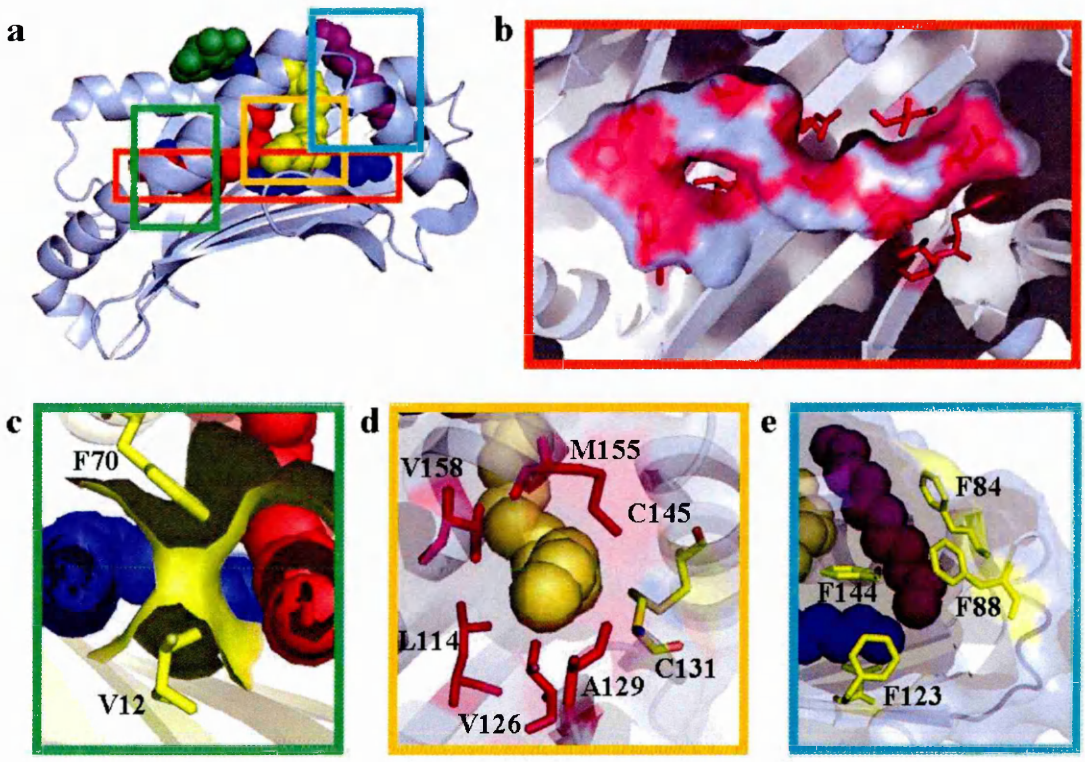

(a) Schematic of the α1α2 superdomain structure of CD1b indicating the positions of panels (b–e) (colour coding). (b) Tunnel T' traverses a path, unobstructed by bulky side chains, between channels A' and F'. (c) The hinge region at bottom of the A' channel is formed by valine12 (V12) and phenylalamine70 (F70), which could guide long lipid ligands from the A' channel into the T' tunnel. (d) A portal in the C' channel, stabilized by a disulfide bond Cys131-Cys145 (yellow), allows egress of the lipid from the interior of the protein. (e) The F' channel with lining phenylalanine residues in yellow.

6.2.2.2. Functional recognition surfaces of CD1b-PI and CD1b-GM2

In the crystal structure determination, there was sufficient electron density to unequivocally position partial head group structures for glycolipids in the CD1b-GM2 and CD1b-PI complexes (Figure 54). The inositol ring of PI is partially ordered in the CD1b-PI complex, whereas only the first of the four sugar rings that branch off the GM2 lipid head is visible in the CD1b-GM2 crystal structure. When compared with a classical MHC class I/peptide complex, the glycolipid head groups presented by CD1b are in a position analogous to the fourth residue (commonly designated P4) of nonamer or decamer peptides presented by MHC class I molecule[319].

Figure 54. Headgroups of CD1b-bound GM2 and PI

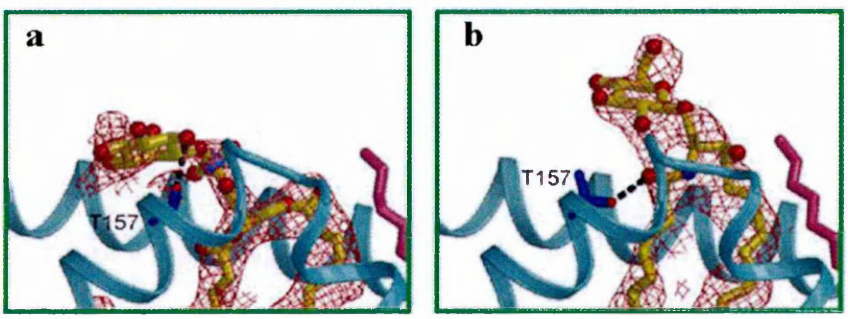

The positioning of the phosphoinositol (a) and the first glucosyl-head group of GM2 (b) are shown. Carbon atoms of the lipid ligand are in yellow, oxygens in red, phosphate in lilac and nitrogen in blue. Hydrogen bonds are shown as black dotted lines. In both panels, the F_o - F_c omit map electron density (red mesh, contoured at 2.5σ) was calculated after simulated annealing with the glycolipid (plus any residues and detergent within a distance of 3.5 Å) omitted. (Figure modified from Ref.[181]).

The main chain topology of CD1b differs markedly from MHC class I in the peak height attained by the kink in the α2 helix (residues 150–154 in CD1b and 149–152 in MHC class I, respectively). Direct substitution of CD1b into the structure of a MHC class I–TCR complex (by superposition of the CD1b structure onto the MHC class I structure) therefore results in marked steric clashes between the TCR and this portion of the CD1b α2 helix. The upward displacement of the TCR, which is necessary to provide a sterically acceptable dock onto the CD1b structure, may also accommodate the glycolipid head group because such head groups are much larger than the amino acid side chains of a peptide antigen. Given this modification, the surface presented by the CD1b-glycolipid complexes appears compatible with standard TCR recognition, a conclusion borne out by mutagenesis studies mapping TCR binding to CD1b[320]. In contrast, key features of the α3 domain required for MHC class I binding to CD8αα[13] are not conserved in CD1b. In particular, the loop comprising residues 223–229 in the α3 domain of MHC class I, which is clamped between the two CD8 subunits in the recognition complex, is truncated in CD1b (residues 226–231). Although there is no steric hindrance for a putative complex between CD1b and CD8, these changes imply a reduced affinity compared to that of CD8 with MHC class I.

6.2.2.3. Comparison of human CD1b and mouse CD1d structures

Comparison of the CD1b complexes with the structure of mouse CD1d, which does not include a specific bound ligand[155], indicates broad equivalences but also marked differences in the architecture of the binding groove (Figure 55). Channel A' runs

deeper in CD1b because Val63 replaces a tryptophan at the equivalent position in mouse CD1d. Channel T' is blocked in mCD1d by the side chains of Leu100 and Val118, equivalent to residues Gly98 and Gly116, respectively, in CD1b. Similarly, the exit portal for channel C' beneath the CD1b α2 helix is closed off in CD1d by Phe128 and Trp133, replacing Val126 and Cys131, respectively, in CD1b (Figure 55). However, in addition to the structural differences resulting from the amino acid changes between CD1b and mouse CD1d, both molecules may share some conformational adaptability at residue 58 of the heavy chain. Whereas channel F' is partially occluded in mouse CD1d by the side chain of Leu84 (Figure 55), the side chain conformation selected by the equivalent residue (Phe84) in the current CD1b structure frees-up sufficient space for F' to accommodate a detergent molecule. However, in the absence of ligand, Phe84 may be expected to adopt an alternate conformation (analogous to that of Leu84 in mCD1d) to pack against Phe144, Phe88 and Met90. This suggests a mechanism whereby the hydrophobic binding capacity of the channels may be tailored to ligand requirements, a phenomenon observed for the binding of non-nucleoside inhibitors to HIV reverse transcriptase[321] and for the groove closure of fatty acid binding protein[322].

Figure 55. Comparison of human CD1b and mouse CD1d structures

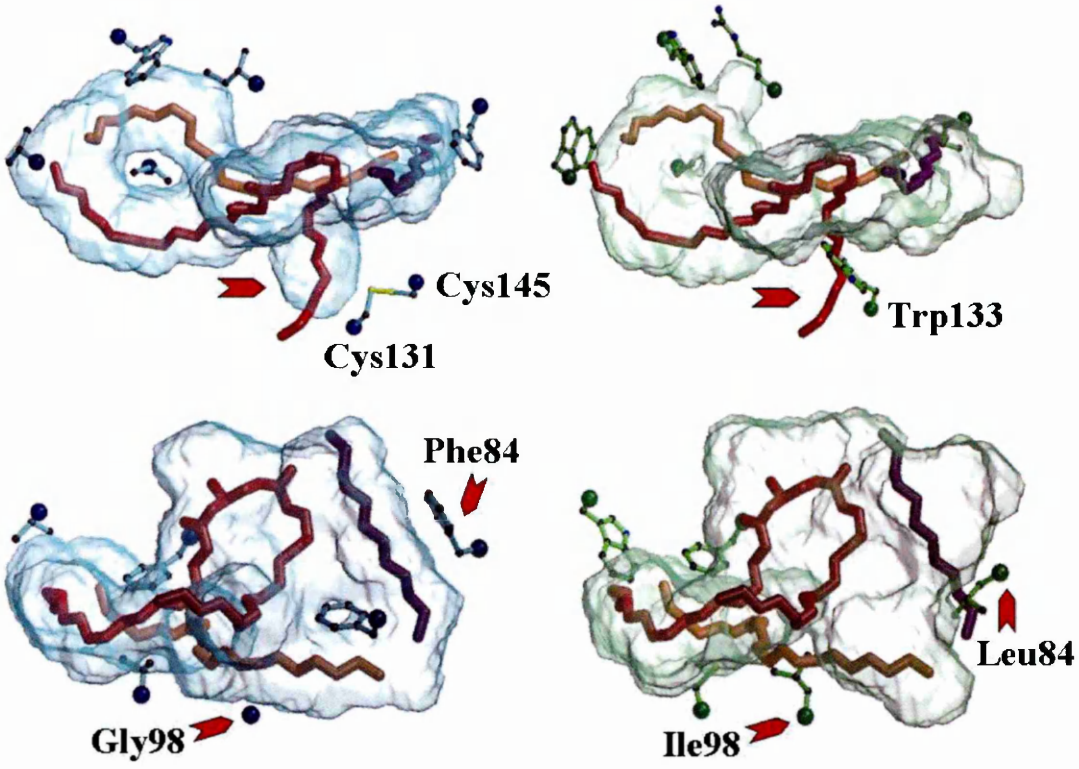

Structure comparison of the hydrophobic antigen-binding cavity for human CD1b (blue, transparent) and mouse CD1d (green, transparent) from top (upper panels) and side (lower panels). Key side chains of CD1b and CD1d are in blue and green. Red filled arrows indicate key structural differences. The ligands present in the CD1b_PI structure have been superimposed onto the CD1d structure for direct comparison (colour coding: PI is red in both A' and C', CTAB is orange in T' and blue in F').

6.2.2.4. Implications for other CD1 alleles and glycolipid ligands

The CD1b structure helps to define the residues that confer the lipid-binding properties of the $\alpha 1\alpha 2$ domain. Sequence alignment of the CD1 family indicates that channel A' and the associated portion of tunnel T' are the most conserved regions of the groove (Figure 56). Conversely, the central portion of tunnel T' is blocked in all other CD1 isoforms by the presence of bulky side chains of residues equivalent to Gly98 and Gly116 in CD1b. Similarly, the C' portal is occluded by tryptophan and phenylalanine residues that substitute for CD1b residues Cys131 and Val126, respectively, in all other CD1 family members. Residues contributing to channel F' are the least conserved. Overall, based on the ligand-binding architecture, CD1b appears to be unique among CD1 molecules.

The arrangement of the combined detergent and lipid ligands in the CD1b-PI and CD1b-GM2 structures provides a general model for describing the interaction of the CD1b binding groove with alkyl chain–containing ligands. A model building exercise was carried out to explore the range of putative glycolipids that could be accommodated within the CD1b ligand architecture (Figure 57). Modeling of mycolic acid into the CD1b structure showed how the long C50-C56 meromycolate chain could be fully contained within a superchannel consisting of the interconnected A', T' and F' channels, with the shorter C22-C26 alkyl chain binding to C'. The superchannel has a maximum length of ca. 70 Å, providing binding capacity for a single fatty acid chain of up to 60 carbons. Similarly modeling of a representative triacylglycerol showed that three acyl chains attached to a single head group could be accommodated within channels A', C' and F' (Figure 57).

Figure 56. Sequence alignement of different CD1 isoforms

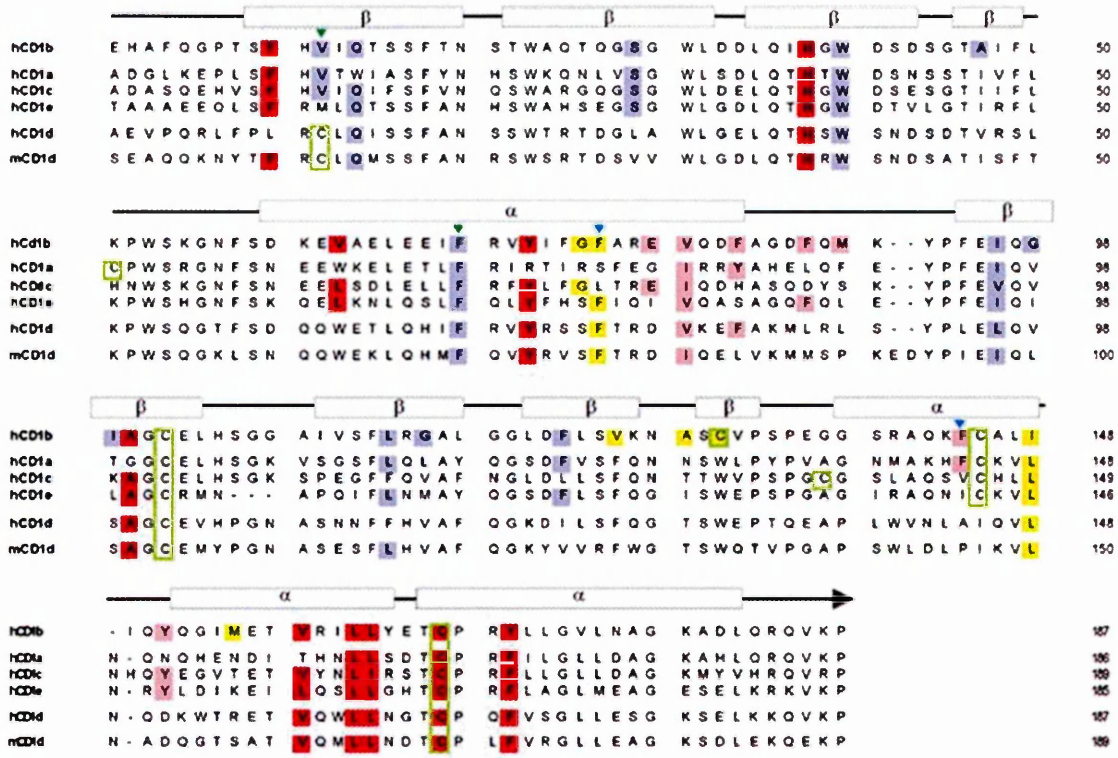

Sequence alignment of the α1α2 domains of human CD1b with human CD1a, CD1c, CD1e and CD1d and with mouse CD1d. Secondary structure elements of CD1b, i.e. alpha helices and beta-pleated sheets, are indicated above the protein sequence. A colored background indicates those residues that confer the lipid-binding properties of CD1b and are conserved at equivalent positions in other CD1 isoforms (amino acids in A' are in red, C' yellow, F' pink, and T' blue). Hydrophobic residues guiding the ligands in CD1b at the bottom of channel A' and between channels C' and F' are marked by green and blue triangles, respectively. Cysteine residues are boxed in green.

Figure 57. Models for binding of mycolic acid and triacylglycerol to human CD1b

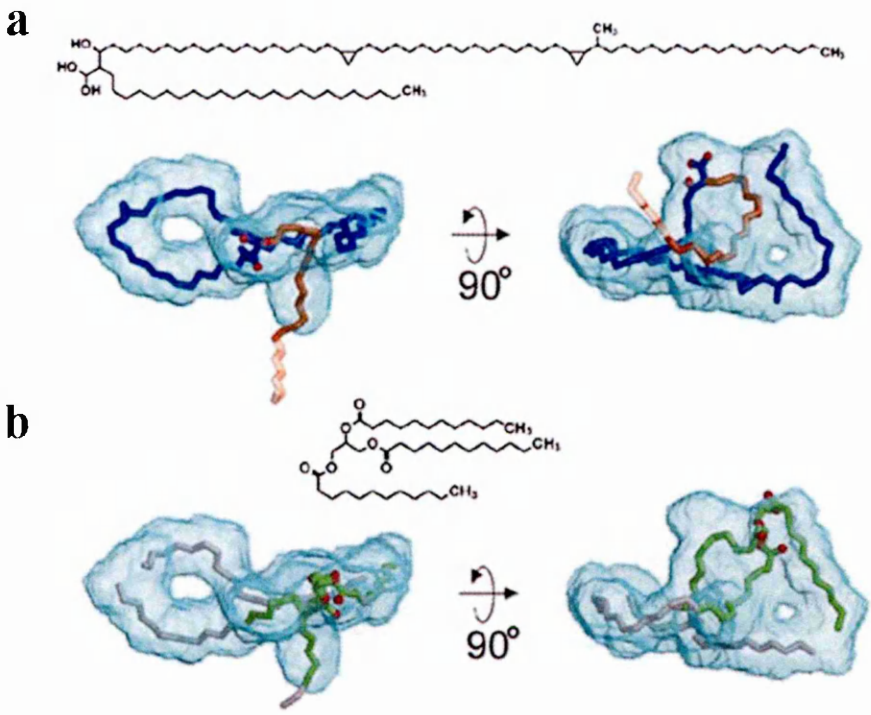

(a) Model for binding of mycolic acid from M. tuberculosis to human CD1b. A pair of orthogonal views with mycolic acid modeled into the CD1b structure is shown. In the model, the C60 long meromycolate chain (blue) is buried within the ca. 70 Å long superchannel formed by continuous alignement of A', T' and F'. The shorter C25 alkyl chain (orange) is bound to C'. The end of the C25 chain in the mycolic acid is indicated by an extended chain shown as a semi-transparent surface. The chemical structure of mycolic acid is shown above the CD1b model structure.

(b) Analogous model for triacylglycerol (trilaurin) binding to CD1b, demonstrating that the three C11 alkyl chains (green) could separately bind to surface-linked channels A', C' and F'. Alkyl chains present in the CD1b-PI and CD1b-GM2 structures but not accounted for by the models are overlaid in light gray.

6.3. Discussion

In this chapter I have shown the development of a novel protocol to generate lipid-loaded human CD1b/β2m complexes from completely denatured and reduced inclusion body proteins. The validity of this refolding method could be directly confirmed by atomic structure analysis of two purified and crystallised monomeric CD1b-lipid complexes.

At first, all known standard protocols used for refolding of MHC class I/β2m-peptide complexes failed when applied by us to human CD1b molecules. In contrast, the novel detergent-assisted protocol described in this thesis enabled the production of soluble lipid-loaded CD1b molecules. The idea to use CTAB was to protect exposed hydrophobic surfaces during early refolding stages, thereby reducing hydrophobic protein aggregation and precipitation. While this might still have happened, crystal structure analysis showed two CTAB molecules bound to the T' tunnel and F' channel of the antigen binding groove, suggesting that CTAB could act as a chaperone ligand during CD1b *in vitro* refolding. Consistent with this hypothesis is the fact that detergent molecules only occupied the T'tunnel and F'channel, despite a 500 fold molar excess of detergent over either GM2 or PI in the refolding buffer.

Similar to CTAB, short C16 chain fatty acids of the endoplasmic reticulum could act as chaperone ligands during refolding of CD1b *in vivo* until binding of higher affinity two-alkyl chain containing ligands. Lipids with only one available alkyl chain have been previously shown to bind to CD1c and CD1d molecules. Binding of such ligands to CD1d is characterised by a fast off rate. On the other hand, previous

BiaCore study had failed to demonstrate binding of a C16 single alkyl chain lipid to insect cell derived human CD1b [316].

However, four years after publication of our human CD1b structures Garcia-Alles and colleagues published a human CD1b structure obtained from insect cell derived CD1b molecules. Their structure showed the presence of both phosphatidylcholine and a long spacer ligand occupying the T'tunnel and F'channel[190]. Although the existence of such a long spacer in humans has not been shown, the Garcia-Alles structure supports the idea that chaperone ligands could play a role during CD1b refolding *in vivo.*

In both the CD1b-GM2 and CD1b-PI structure the alkyl chains were tightly fitted into the A' and F' channels of the CD1b crystal structures with no buried water molecules. This arrangement is consistent with the notion that the interaction of two-alkyl chain containing ligands with CD1b is stable and long-lived.

Site-directed mutagenesis studies have previously analysed the role of CD1b antigen binding groove lining amino acid residues [323], Mutations that lie near the bottom of the binding groove were shown to affect both long and short alkyl chain glycolipid presentation, and were thought to affect the overall architecture of the molecule. Conversely, mutations of residues lining the A' channel and its junction with the T' tunnel specifically affected the presentation of long alkyl chains. The model shown in Figure 57 for mycolic acid binding to human CD1b is consistent with these mutagenesis studies.

The two CD1b-ligand structures offer an obvious explanation how human CD1b can present either very large or the short mycobacterial glucomonomycolate to the same T cell line [172]. Mycobacterial mycolates, which are crucial for mycobacterial growth and survival inside phagolysosomes [169], were the first known ligands for human CD1b[146]. It has long been speculated how such lipids could bind to CD1b without protruding from the groove. Our CD1b-ligand structures show how both fatty acids of mycolic acid can be fully accommodated with human CD1b. The shorter C22-C26 alkyl chain could bind to the C'channel, while the long C50-C56 meromycolate chain could be completely contained within the long, lipid binding super channel which is formed by connecting the A'channel, T'tunnel and F'channel. The super channel, which is unique to CD1b, can accommodate up to 60-65 carbons. In work subsequent to this thesis I was involved in determination of the first crystal structure of human CD1b with bound glucomonomycolate. This structure confirmed the above prediction that long mycolate chains bind to the superchannel[186].

The arrangement of a cluster of phenylalanine residues lining the F'pocket of CD1b, in particular Phe 84, suggests the existence of a shutter mechanism inside the F'channel, which could operate in the absence of long chain fatty acid ligands. By choosing an alternative conformation, Phe 84 could close off the access to the F'channel and therefore protect the molecule from the entry of water. However, as the structure of insect cell derived human CD1b has shown, such a mechanism might not be required if a long spacer ligand was available in human myeloid cells.

The arrangement of the three ligand-filled channels A', F', and C' in the two CD1b structures suggests the exciting possibility that lipids containing three acyl chains, such as endogenous triacylglycerols or mycobacterial triacyl trehalose may bind to human CD1b. Triacylglycerols, which are synthesised on membranes of the endoplasmic reticulum, are known independent risk factors for the development of atherosclerosis [324, 325]. Activated T lymphocytes are found in atherosclerotic plaques[324, 325], and oxidized lipoproteins containing triacylglyerols are immunogenic for T cells [326, 327]. Interestingly, CD1b is highly expressed on foam cell macrophages in atheromatous lesions, but not on normal tissue macrophages[328]. It is therefore intriguing to speculate that CD1b could activate triacylglyerol specific T lymphocytes within atheromatous lesions.

6.4. Conclusions

The highly hydrophobic nature of both the CD1b protein and its lipidic ligands caused initial difficulties in refolding CD1b/lipid complexes in aqueous solutions. These difficulties could eventually be overcome by using detergent-assisted refolding techniques. Crystal structure analysis of CD1b/lipid complexes generated by this method demonstrated correct folding of the molecules. Whether this method will also allow to generate CD1b-tetramers loaded with mycobacterial lipids still needs to be investigated in future studies.

The first crystal structures shown in this thesis were the first ever solved structures of lipid-loaded CD1 molecules. They revealed a general mechanism by which lipids can bind to hydrophobic channels of CD1 molecules and showed the

unexpected presence of four interconnected channels in CD1b - a real maze for alkyl chains.

Finally, the two structures extend the spectrum of known CD1b-ligands and suggest that triacyl chain ligands might be presented by CD1b to T lymphocytes.

6.5. Accession codes for human CD1b ligand structures

Coordinates and structure factors for the human CD1b/β2m/PI and CD1b/β2m/GM2 complexes have been deposited in the Protein Data Bank under accession codes **1gzq** and **r1gzqsf** (for CD1b-PI) and **1gzp** and **r1gzpsf** (for CD1b-GM2).

6.6. Acknowledgments

My friend Nikolai Lissing taught me how to run and repair old FPLC machines. Karl Harlos handled my protein crystals and together with Yvonne Jones acquired the diffraction data in Grenoble. I will never forget our exciting night shift at beamline ID14. My friend Nathan Zaccai, supervised by Yvonne Jones, carried out the molecular replacement and refinement of the structure models. I feel very privileged that I was given the opportunity to discuss the CD1b structures with the late Cesar Milstein on several occasions at the LMB in Cambridge.

7. Conclusions and future perspectives

The results shown in chapters three and four of this PhD thesis describe the clinical phenotype as well as the molecular and genetic defects in a group of patients with "TAP deficiency syndrome". In these patients, defective peptide translocation from the cytosol into the endoplasmic reticulum was caused by mutations in either the TAP1 or TAP2 genes, which encode for the two subunits of the heterodimeric peptide transporter TAP. In fact, MHC class I cell surfaceexpression could be experimentally restored *in vitro* in the patients' EBV-transformed lymphoblastoid cell lines by reinstating TAP function.

However, current understanding of the role of MHC class I molecules for innate and adaptive immunity cannot sufficiently explain some of the most prominent symptoms in these patients, e.g. the necrotising granulomatous skin lesions and the frequent bacterial respiratory infections leading to bronchiectasis. Functional studies of NK and γδ T lymphocytes in three patients showed that these cells, after isolation and cytokine-aided *in vitro* expansion, killed autologous EBV-transformed B-lymphoblastoid cells. These experiments suggested that insufficient MHC class I – mediated inhibition of NK and γδ T cell functions via KIRs or ILTs might have been involved in the pathogenesis of the mutilating autoaggressive skin inflammation. Consistent with this hypothesis, activated NK cells expressing ILT- 2, an MHC class I-binding inhibitory receptor were enriched in granulomatous skin lesions of one patient. However, the reason why tissue destruction by these lymphocyte subsets should be restricted to the skin, and also the underlying cause of NK and γδ T lymphocyte activation *in vivo* remain unknown. Interestingly, chronic inflammation in

other organs, i.e. colitis, retinal vasculitis and encephalitis, was present in some patients during their disease, but these tissues could not be analysed for the presence of NK and γδ T cells. Two affected heterozygous sisters sharing an identical homozygous HLA haplotype, SAB and GAB (described in chapter 3), exhibited significant clinical differences; necrotising granulomatous skin lesions were (and are still) absent in SAB, while they were present in GAB and all other patients. However, this thesis did not address the question whether skin involvement in TAP-deficiency syndrome was generally associated with activation of NK and γδ T cells in the skin or peripheral blood. Also, no systematic analysis of the repertoire of MHC class I-binding inhibitory and activating receptors was carried out. Future studies might address the question of whether mismatched KIR - HLA haplotypes are associated with autoinflammatory tissue damage in TAP-deficient patients.

Another important question that remains largely unanswered is why TAP-deficiency is associated with severe bacterial rather than viral infections. Neutralising autoantibodies against the potent antibacterial protein bactericidal permeability increasing protein (BPI) were present in all my patients [329]. However, although these autoantibodies might have contributed to the susceptibility to bacterial infections they are unlikely to be their primary cause. Anti-BPI antibodies are often found in other human diseases associated with chronic bacterial infections, such as cystic fibrosis and inflammatory bowel diseases[330]. The fact that bacterial infections appear already in early childhood in TAP-deficiency syndrome suggests that a fully functioning MHC class I antigen presentation pathway is required for effective activation of the innate immune system during bacterial infections. It is now well established that phagocytes,

such as neutrophilic granulocytes, have the ability to present exogenous antigens via MHC class I to CD8+ T lymphocytes[331]. This process, which is called "cross-presentation", requires TAP-mediated peptide translocation from the cytosol into the ER and should therefore be compromised in TAP-deficient patients[331, 332]. The occurrence of recurrent bacterial infections in TAP-deficient patients during early childhood might therefore indicate that "cross-presentation" to CD8+ T cells is particularly important in early life.

Of note, HLA-A2, the most frequent HLA class I allele family in Caucasians, was not contained in any of my Caucasian patients' HLA haplotypes. The absence of HLA-A2 in the patients might not have been a coincidence since the spectrum of peptides presented by HLA-A2 contains a significant fraction of TAP independent peptides[333]. Conversely, the symptoms of TAP-deficiency syndrome as described in chapters 3 and 4 might only occur in patients with certain HLA-haplotypes, but not in others, e.g. HLA-A2 homozygous haplotypes. These questions might be answered in the future if additional TAP-deficient patients can be identified and studied.

The presence of necrotising granulomatous skin lesions in my patients not only led to extensive diagnostic testing for suspected *M. tuberculosis* infection, but also, in most patients, instigation of antituberculous drug therapy. The lack of any clinical effect of such treatment combined with the complete failure to demonstrate *M. tuberculosis* either by PCR, multiple acid fast staining or culture firmly ruled out the possibility of *M. tuberculosis* infection in my patients. The lack of susceptibility to mycobacterial infection of TAP-deficient human patients is remarkable, because TAP-deficient mice are highly susceptible to mycobacteria[103, 104, 213]. This difference

between humans and mice pointed to a possible role of CD1 group 1 molecules in the immune defense against mycobacteria, because mice do not possess genes encoding for group1 CD1 molecules[213]. One of the main goals of this thesis, i.e. the development of CD1 group 1-tetramers to study CD1-restricted mycobacterial lipid - specific T lymphocytes in TAP-deficient patients, could not be achieved. On the other hand, the development of recombinant CD1d/lipid-tetramers, described in chapter 5 of this thesis, provided sensitive and specific new tools to study lipid-specific CD1 group 2 specific, i.e. CD1d-restricted invariant NKT cells. Three important factors made the development of the CD1d-tetramers possible: The development of an efficient refolding method for CD1d (chapter 5 of this thesis); availability of the previously identified and characterised CD1d-presented agonistic iNKT ligand KRN7000; and the relatively high affinity of iNKT TCRs for CD1d/KRN7000 [241].

So, why has no research group yet achieved specific staining of mycobacterial lipid-specific T lymphocytes with group 1 CD1-tetramers? In chapter 6 of this thesis I have demonstrated that it is possible to generate correctly folded recombinant human CD1b/lipid-complexes. Moreover, these recombinant CD1b/lipid-complexes could be crystallised, which allowed for the first two atomic structures of human CD1b/lipid-complexes to be solved (chapter 6 of this thesis). These structures revealed a fascinating arrangement of four lipid-binding channels - a real maze for akyl chains – and provided a model of how the very long meromycolate of mycobacterial mycolic acid could be presented by CD1b. Later on, crystal structures of recombinant human CD1b/mycolic acid-complex confirmed this model[186]. CD1b bound mycolic acid has been previously demonstrated to be specifically recognised by human T lymphocyte

lines, using assays of *in vitro* proliferation and cytotoxicity, but not tetramer staining[145, 146]. There is no obvious reason to assume that the lack of success with CD1b-tetramer staining of human T lymphocytes could be caused by an "inherent" low TCR affinity. In fact, the affinity of CD1b-specific TCRs might actually be expected to be rather high, as many CD1b-restricted T cell lines lack expression of CD4 or CD8 co-receptors.

Whatever the reasons for the current lack of success with CD1b-tetramer staining might be, direct detection of human mycobacterial lipid-specific T lymphocytes with CD1b-tetramers *ex vivo* would be an important achievement in the field of cellular immunology, with great potential to open up new avenues for both diagnosis and therapy of human infectious diseases.

8. References

1. Janeway, C.A., Jr. & Medzhitov, R. Innate immune recognition. *Annual review of immunology* **20**, 197-216 (2002).
2. Zhang, S.Y. *et al.* Human Toll-like receptor-dependent induction of interferons in protective immunity to viruses. *Immunological reviews* **220**, 225-236 (2007).
3. Henckaerts, L. & Vermeire, S. NOD2/CARD15 disease associations other than Crohn's disease. *Inflammatory bowel diseases* **13**, 235-241 (2007).
4. Gadola, S., Salzer, U., Schultz, H. & Grimbacher, B. [Adult-onset primary immunodeficiencies]. *Der Internist* **45**, 912-922 (2004).
5. Litman, G.W., Cannon, J.P. & Dishaw, L.J. Reconstructing immune phylogeny: new perspectives. *Nature reviews* **5**, 866-879 (2005).
6. Pearse, A.M. & Swift, K. Allograft theory: transmission of devil facial-tumour disease. *Nature* **439**, 549 (2006).
7. Murgia, C., Pritchard, J.K., Kim, S.Y., Fassati, A. & Weiss, R.A. Clonal origin and evolution of a transmissible cancer. *Cell* **126**, 477-487 (2006).
8. Chothia, C., Boswell, D.R. & Lesk, A.M. The outline structure of the T-cell alpha beta receptor. *The EMBO journal* **7**, 3745-3755 (1988).
9. Zinkernagel, R.M. & Doherty, P.C. Immunological surveillance against altered self components by sensitised T lymphocytes in lymphocytic choriomeningitis. *Nature* **251**, 547-548 (1974).
10. Jones, E.Y. MHC class I and class II structures. *Current opinion in immunology* **9**, 75-79 (1997).
11. Townsend, A.R., Gotch, F.M. & Davey, J. Cytotoxic T cells recognize fragments of the influenza nucleoprotein. *Cell* **42**, 457-467 (1985).
12. Germain, R.N. T-cell development and the CD4-CD8 lineage decision. *Nature reviews* **2**, 309-322 (2002).
13. Gao, G.F. *et al.* Crystal structure of the complex between human CD8alpha(alpha) and HLA-A2. *Nature* **387**, 630-634 (1997).
14. Vignali, D.A., Doyle, C., Kinch, M.S., Shin, J. & Strominger, J.L. Interactions of CD4 with MHC class II molecules, T cell receptors and p56lck. *Philosophical transactions of the Royal Society of London* **342**, 13-24 (1993).
15. Davis, S.J. & van der Merwe, P.A. The kinetic-segregation model: TCR triggering and beyond. *Nature immunology* **7**, 803-809 (2006).
16. Rammensee, H., Bachmann, J., Emmerich, N.P., Bachor, O.A. & Stevanovic, S. SYFPEITHI: database for MHC ligands and peptide motifs. *Immunogenetics* **50**, 213-219 (1999).
17. Tynan, F.E. *et al.* The immunogenicity of a viral cytotoxic T cell epitope is controlled by its MHC-bound conformation. *The Journal of experimental medicine* **202**, 1249-1260 (2005).
18. Tynan, F.E. *et al.* A T cell receptor flattens a bulged antigenic peptide presented by a major histocompatibility complex class I molecule. *Nature immunology* **8**, 268-276 (2007).

19. Slev, P.R., Nelson, A.C. & Potts, W.K. Sensory neurons with MHC-like peptide binding properties: disease consequences. *Current opinion in immunology* **18**, 608-616 (2006).
20. Corriveau, R.A., Huh, G.S. & Shatz, C.J. Regulation of class I MHC gene expression in the developing and mature CNS by neural activity. *Neuron* **21**, 505-520 (1998).
21. Bateman, A.C. & Howell, W.M. Human leukocyte antigens and cancer: is it in our genes? *J Pathol* **188**, 231-236 (1999).
22. Carrington, M. *et al.* HLA and HIV-1: heterozygote advantage and B*35-Cw*04 disadvantage. *Science (New York, N.Y* **283**, 1748-1752 (1999).
23. Gamzatova, Z. *et al.* Analysis of HLA class I-II haplotype frequency and segregation in a cohort of patients with advanced stage ovarian cancer. *Tissue antigens* **70**, 205-213 (2007).
24. Kaslow, R.A. *et al.* Influence of combinations of human major histocompatibility complex genes on the course of HIV-1 infection. *Nat Med* **2**, 405-411 (1996).
25. Lavado, R. *et al.* The HLA-B7 allele confers susceptibility to breast cancer in Spanish women. *Immunol Lett* **101**, 223-225 (2005).
26. Thorsby, E. Invited anniversary review: HLA associated diseases. *Human immunology* **53**, 1-11 (1997).
27. Fruh, K., Gruhler, A., Krishna, R.M. & Schoenhals, G.J. A comparison of viral immune escape strategies targeting the MHC class I assembly pathway. *Immunological reviews* **168**, 157-166 (1999).
28. Aptsiauri, N. *et al.* Role of altered expression of HLA class I molecules in cancer progression. *Advances in experimental medicine and biology* **601**, 123-131 (2007).
29. Ljunggren, H.G. & Karre, K. In search of the 'missing self': MHC molecules and NK cell recognition. *Immunology today* **11**, 237-244 (1990).
30. Brooks, A.G., Posch, P.E., Scorzelli, C.J., Borrego, F. & Coligan, J.E. NKG2A complexed with CD94 defines a novel inhibitory natural killer cell receptor. *The Journal of experimental medicine* **185**, 795-800 (1997).
31. Lanier, L.L. NK cell receptors. *Annu Rev Immunol* **16**, 359-393 (1998).
32. Braud, V.M. *et al.* HLA-E binds to natural killer cell receptors CD94/NKG2A, B and C. *Nature* **391**, 795-799 (1998).
33. Wagtmann, N., Rojo, S., Eichler, E., Mohrenweiser, H. & Long, E.O. A new human gene complex encoding the killer cell inhibitory receptors and related monocyte/macrophage receptors. *Curr Biol* **7**, 615-618 (1997).
34. Colonna, M. *et al.* A common inhibitory receptor for major histocompatibility complex class I molecules on human lymphoid and myelomonocytic cells. *The Journal of experimental medicine* **186**, 1809-1818 (1997).
35. Boyington, J.C., Motyka, S.A., Schuck, P., Brooks, A.G. & Sun, P.D. Crystal structure of an NK cell immunoglobulin-like receptor in complex with its class I MHC ligand. *Nature* **405**, 537-543 (2000).
36. Zappacosta, F., Borrego, F., Brooks, A.G., Parker, K.C. & Coligan, J.E. Peptides isolated from HLA-Cw*0304 confer different degrees of protection

from natural killer cell-mediated lysis. *Proceedings of the National Academy of Sciences of the United States of America* **94**, 6313-6318 (1997).
37. Dam, J. *et al.* Variable MHC class I engagement by Ly49 natural killer cell receptors demonstrated by the crystal structure of Ly49C bound to H-2K(b). *Nature immunology* **4**, 1213-1222 (2003).
38. Garboczi, D.N. *et al.* Structure of the complex between human T-cell receptor, viral peptide and HLA-A2. *Nature* **384**, 134-141 (1996).
39. Shiroishi, M. *et al.* Human inhibitory receptors Ig-like transcript 2 (ILT2) and ILT4 compete with CD8 for MHC class I binding and bind preferentially to HLA-G. *Proceedings of the National Academy of Sciences of the United States of America* **100**, 8856-8861 (2003).
40. Allison, T.J., Winter, C.C., Fournie, J.J., Bonneville, M. & Garboczi, D.N. Structure of a human gammadelta T-cell antigen receptor. *Nature* **411**, 820-824 (2001).
41. Komori, T., Okada, A., Stewart, V. & Alt, F.W. Lack of N regions in antigen receptor variable region genes of TdT-deficient lymphocytes. *Science (New York, N.Y* **261**, 1171-1175 (1993).
42. Rudolph, M.G., Stanfield, R.L. & Wilson, I.A. How TCRs bind MHCs, peptides, and coreceptors. *Annual review of immunology* **24**, 419-466 (2006).
43. Garcia, K.C. *et al.* Structural basis of plasticity in T cell receptor recognition of a self peptide-MHC antigen. *Science (New York, N.Y* **279**, 1166-1172 (1998).
44. Stewart-Jones, G.B., McMichael, A.J., Bell, J.I., Stuart, D.I. & Jones, E.Y. A structural basis for immunodominant human T cell receptor recognition. *Nature immunology* **4**, 657-663 (2003).
45. Townsend, A.R. *et al.* The epitopes of influenza nucleoprotein recognized by cytotoxic T lymphocytes can be defined with short synthetic peptides. *Cell* **44**, 959-968 (1986).
46. Schubert, U. *et al.* Rapid degradation of a large fraction of newly synthesized proteins by proteasomes. *Nature* **404**, 770-774 (2000).
47. Eisenlohr, L.C., Huang, L. & Golovina, T.N. Rethinking peptide supply to MHC class I molecules. *Nature reviews* **7**, 403-410 (2007).
48. Rock, K.L. *et al.* Inhibitors of the proteasome block the degradation of most cell proteins and the generation of peptides presented on MHC class I molecules. *Cell* **78**, 761-771 (1994).
49. Dalton, W.S. The proteasome. *Seminars in oncology* **31**, 3-9; discussion 33 (2004).
50. Orlowski, M. & Wilk, S. Ubiquitin-independent proteolytic functions of the proteasome. *Arch Biochem Biophys* **415**, 1-5 (2003).
51. Unno, M. *et al.* The structure of the mammalian 20S proteasome at 2.75 A resolution. *Structure* **10**, 609-618 (2002).
52. Endert, P. Role of tripeptidyl peptidase II in MHC class I antigen processing - the end of controversies? *European journal of immunology* **38**, 609-613 (2008).
53. York, I.A., Bhutani, N., Zendzian, S., Goldberg, A.L. & Rock, K.L. Tripeptidyl peptidase II is the major peptidase needed to trim long antigenic

precursors, but is not required for most MHC class I antigen presentation. *J Immunol* **177**, 1434-1443 (2006).
54. Goldberg, A.L., Cascio, P., Saric, T. & Rock, K.L. The importance of the proteasome and subsequent proteolytic steps in the generation of antigenic peptides. *Molecular immunology* **39**, 147-164 (2002).
55. Serwold, T., Gonzalez, F., Kim, J., Jacob, R. & Shastri, N. ERAAP customizes peptides for MHC class I molecules in the endoplasmic reticulum. *Nature* **419**, 480-483 (2002).
56. Chang, S.C., Momburg, F., Bhutani, N. & Goldberg, A.L. The ER aminopeptidase, ERAP1, trims precursors to lengths of MHC class I peptides by a "molecular ruler" mechanism. *Proceedings of the National Academy of Sciences of the United States of America* **102**, 17107-17112 (2005).
57. Saric, T. *et al.* An IFN-gamma-induced aminopeptidase in the ER, ERAP1, trims precursors to MHC class I-presented peptides. *Nature immunology* **3**, 1169-1176 (2002).
58. York, I.A. *et al.* The ER aminopeptidase ERAP1 enhances or limits antigen presentation by trimming epitopes to 8-9 residues. *Nature immunology* **3**, 1177-1184 (2002).
59. Hammer, G.E., Gonzalez, F., Champsaur, M., Cado, D. & Shastri, N. The aminopeptidase ERAAP shapes the peptide repertoire displayed by major histocompatibility complex class I molecules. *Nature immunology* **7**, 103-112 (2006).
60. Burton, P.R. *et al.* Association scan of 14,500 nonsynonymous SNPs in four diseases identifies autoimmunity variants. *Nature genetics* **39**, 1329-1337 (2007).
61. Spiliotis, E.T., Manley, H., Osorio, M., Zuniga, M.C. & Edidin, M. Selective export of MHC class I molecules from the ER after their dissociation from TAP. *Immunity* **13**, 841-851 (2000).
62. Paulsson, K.M. & Wang, P. Quality control of MHC class I maturation. *Faseb J* **18**, 31-38 (2004).
63. Lilley, B.N. & Ploegh, H.L. A membrane protein required for dislocation of misfolded proteins from the ER. *Nature* **429**, 834-840 (2004).
64. Ortmann, B. *et al.* A critical role for tapasin in the assembly and function of multimeric MHC class I-TAP complexes. *Science (New York, N.Y* **277**, 1306-1309 (1997).
65. Parodi, A.J. Protein glucosylation and its role in protein folding. *Annual review of biochemistry* **69**, 69-93 (2000).
66. Rajagopalan, S. & Brenner, M.B. Calnexin retains unassembled major histocompatibility complex class I free heavy chains in the endoplasmic reticulum. *The Journal of experimental medicine* **180**, 407-412 (1994).
67. Sugita, M. & Brenner, M.B. An unstable beta 2-microglobulin: major histocompatibility complex class I heavy chain intermediate dissociates from calnexin and then is stabilized by binding peptide. *The Journal of experimental medicine* **180**, 2163-2171 (1994).
68. Townsend, A. *et al.* Assembly of MHC class I molecules analyzed in vitro. *Cell* **62**, 285-295 (1990).

69. Smith, M.J. & Koch, G.L. Multiple zones in the sequence of calreticulin (CRP55, calregulin, HACBP), a major calcium binding ER/SR protein. *The EMBO journal* **8**, 3581-3586 (1989).
70. Mesaeli, N. *et al.* Calreticulin is essential for cardiac development. *J Cell Biol* **144**, 857-868 (1999).
71. Gao, B. *et al.* Assembly and antigen-presenting function of MHC class I molecules in cells lacking the ER chaperone calreticulin. *Immunity* **16**, 99-109 (2002).
72. Denzel, A. *et al.* Early postnatal death and motor disorders in mice congenitally deficient in calnexin expression. *Mol Cell Biol* **22**, 7398-7404 (2002).
73. Frickel, E.M. *et al.* TROSY-NMR reveals interaction between ERp57 and the tip of the calreticulin P-domain. *Proceedings of the National Academy of Sciences of the United States of America* **99**, 1954-1959 (2002).
74. Peaper, D.R., Wearsch, P.A. & Cresswell, P. Tapasin and ERp57 form a stable disulfide-linked dimer within the MHC class I peptide-loading complex. *The EMBO journal* **24**, 3613-3623 (2005).
75. Ellerman, D.A., Myles, D.G. & Primakoff, P. A role for sperm surface protein disulfide isomerase activity in gamete fusion: evidence for the participation of ERp57. *Dev Cell* **10**, 831-837 (2006).
76. Eufemi, M. *et al.* ERp57 is present in STAT3-DNA complexes. *Biochemical and biophysical research communications* **323**, 1306-1312 (2004).
77. Kita, K. *et al.* Evidence for phosphorylation of rat liver glucose-regulated protein 58, GRP58/ERp57/ER-60, induced by fasting and leptin. *FEBS Lett* **580**, 199-205 (2006).
78. Nemere, I. The 1,25D3-MARRS protein: contribution to steroid stimulated calcium uptake in chicks and rats. *Steroids* **70**, 455-457 (2005).
79. Hirano, N. *et al.* Molecular cloning of the human glucose-regulated protein ERp57/GRP58, a thiol-dependent reductase. Identification of its secretory form and inducible expression by the oncogenic transformation. *European journal of biochemistry / FEBS* **234**, 336-342 (1995).
80. Urade, R. *et al.* Functions of characteristic Cys-Gly-His-Cys (CGHC) and Gln-Glu-Asp-Leu (QEDL) motifs of microsomal ER-60 protease. *J Biochem* **122**, 834-842 (1997).
81. Zhang, Y., Baig, E. & Williams, D.B. Functions of ERp57 in the folding and assembly of major histocompatibility complex class I molecules. *The Journal of biological chemistry* **281**, 14622-14631 (2006).
82. Solda, T., Garbi, N., Hammerling, G.J. & Molinari, M. Consequences of ERp57 deletion on oxidative folding of obligate and facultative clients of the calnexin cycle. *The Journal of biological chemistry* **281**, 6219-6226 (2006).
83. Dick, T.P., Bangia, N., Peaper, D.R. & Cresswell, P. Disulfide bond isomerization and the assembly of MHC class I-peptide complexes. *Immunity* **16**, 87-98 (2002).
84. Garbi, N., Hammerling, G. & Tanaka, S. Interaction of ERp57 and tapasin in the generation of MHC class I-peptide complexes. *Current opinion in immunology* **19**, 99-105 (2007).

85. Garbi, N., Tanaka, S., Momburg, F. & Hammerling, G.J. Impaired assembly of the major histocompatibility complex class I peptide-loading complex in mice deficient in the oxidoreductase ERp57. *Nature immunology* **7**, 93-102 (2006).
86. Dick, T.P. Assembly of MHC class I peptide complexes from the perspective of disulfide bond formation. *Cell Mol Life Sci* **61**, 547-556 (2004).
87. Tector, M., Zhang, Q. & Salter, R.D. Beta 2-microglobulin and calnexin can independently promote folding and disulfide bond formation in class I histocompatibility proteins. *Mol Immunol* **34**, 401-408 (1997).
88. Park, B. *et al.* Redox regulation facilitates optimal peptide selection by MHC class I during antigen processing. *Cell* **127**, 369-382 (2006).
89. Joyce, S. Traffic control of completely assembled MHC class I molecules beyond the endoplasmic reticulum. *J Mol Biol* **266**, 993-1001 (1997).
90. Marguet, D. *et al.* Lateral diffusion of GFP-tagged H2Ld molecules and of GFP-TAP1 reports on the assembly and retention of these molecules in the endoplasmic reticulum. *Immunity* **11**, 231-240 (1999).
91. Kavathas, P., Bach, F.H. & DeMars, R. Gamma ray-induced loss of expression of HLA and glyoxalase I alleles in lymphoblastoid cells. *Proceedings of the National Academy of Sciences of the United States of America* **77**, 4251-4255 (1980).
92. Spies, T. *et al.* A gene in the human major histocompatibility complex class II region controlling the class I antigen presentation pathway. *Nature* **348**, 744-747 (1990).
93. Koopmann, J.O., Post, M., Neefjes, J.J., Hammerling, G.J. & Momburg, F. Translocation of long peptides by transporters associated with antigen processing (TAP). *European journal of immunology* **26**, 1720-1728 (1996).
94. Neefjes, J.J., Momburg, F. & Hammerling, G.J. Selective and ATP-dependent translocation of peptides by the MHC-encoded transporter. *Science (New York, N.Y* **261**, 769-771 (1993).
95. Neisig, A. *et al.* Major differences in transporter associated with antigen presentation (TAP)-dependent translocation of MHC class I-presentable peptides and the effect of flanking sequences. *J Immunol* **154**, 1273-1279 (1995).
96. Obst, R., Armandola, E.A., Nijenhuis, M., Momburg, F. & Hammerling, G.J. TAP polymorphism does not influence transport of peptide variants in mice and humans. *European journal of immunology* **25**, 2170-2176 (1995).
97. Rau, H. *et al.* Polymorphisms of TAP1 and TAP2 genes in Graves' disease. *Tissue antigens* **49**, 16-22 (1997).
98. Yan, G., Shi, L. & Faustman, D. Novel splicing of the human MHC-encoded peptide transporter confers unique properties. *J Immunol* **162**, 852-859 (1999).
99. Knittler, M.R., Gulow, K., Seelig, A. & Howard, J.C. MHC class I molecules compete in the endoplasmic reticulum for access to transporter associated with antigen processing. *J Immunol* **161**, 5967-5977 (1998).
100. Braud, V.M., Allan, D.S., Wilson, D. & McMichael, A.J. TAP- and tapasin-dependent HLA-E surface expression correlates with the binding of an MHC class I leader peptide. *Curr Biol* **8**, 1-10 (1998).

101. Johnsen, A.K. *et al.* Systemic deficits in transporter for antigen presentation (TAP)-1 or proteasome subunit LMP2 have little or no effect on tumor incidence. *International journal of cancer* **91**, 366-372 (2001).
102. Raulet, D.H. MHC class I-deficient mice. *Advances in immunology* **55**, 381-421 (1994).
103. Behar, S.M., Dascher, C.C., Grusby, M.J., Wang, C.R. & Brenner, M.B. Susceptibility of mice deficient in CD1D or TAP1 to infection with Mycobacterium tuberculosis. *The Journal of experimental medicine* **189**, 1973-1980 (1999).
104. Sousa, A.O. *et al.* Relative contributions of distinct MHC class I-dependent cell populations in protection to tuberculosis infection in mice. *Proceedings of the National Academy of Sciences of the United States of America* **97**, 4204-4208 (2000).
105. Ahn, K. *et al.* The ER-luminal domain of the HCMV glycoprotein US6 inhibits peptide translocation by TAP. *Immunity* **6**, 613-621 (1997).
106. Hengel, H. *et al.* A viral ER-resident glycoprotein inactivates the MHC-encoded peptide transporter. *Immunity* **6**, 623-632 (1997).
107. Fruh, K. *et al.* A viral inhibitor of peptide transporters for antigen presentation. *Nature* **375**, 415-418 (1995).
108. Tomazin, R. *et al.* Stable binding of the herpes simplex virus ICP47 protein to the peptide binding site of TAP. *The EMBO journal* **15**, 3256-3266 (1996).
109. Zeidler, R. *et al.* Downregulation of TAP1 in B lymphocytes by cellular and Epstein-Barr virus-encoded interleukin-10. *Blood* **90**, 2390-2397 (1997).
110. Koppers-Lalic, D. *et al.* Varicelloviruses avoid T cell recognition by UL49.5-mediated inactivation of the transporter associated with antigen processing. *Proceedings of the National Academy of Sciences of the United States of America* **102**, 5144-5149 (2005).
111. Boname, J.M., de Lima, B.D., Lehner, P.J. & Stevenson, P.G. Viral degradation of the MHC class I peptide loading complex. *Immunity* **20**, 305-317 (2004).
112. Ambagala, A.P., Gopinath, R.S. & Srikumaran, S. Inhibition of TAP by pseudorabies virus is independent of its vhs activity. *Virus Res* **96**, 37-48 (2003).
113. Powis, S.J. *et al.* Restoration of antigen presentation to the mutant cell line RMA-S by an MHC-linked transporter. *Nature* **354**, 528-531 (1991).
114. Spies, T. & DeMars, R. Restored expression of major histocompatibility class I molecules by gene transfer of a putative peptide transporter. *Nature* **351**, 323-324 (1991).
115. Keusekotten, K., Leonhardt, R.M., Ehses, S. & Knittler, M.R. Biogenesis of functional antigenic peptide transporter TAP requires assembly of pre-existing TAP1 with newly synthesized TAP2. *The Journal of biological chemistry* **281**, 17545-17551 (2006).
116. Wright, K.L. *et al.* Coordinate regulation of the human TAP1 and LMP2 genes from a shared bidirectional promoter. *The Journal of experimental medicine* **181**, 1459-1471 (1995).

117. Schrodt, S., Koch, J. & Tampe, R. Membrane topology of the transporter associated with antigen processing (TAP1) within an assembled functional peptide-loading complex. *The Journal of biological chemistry* **281**, 6455-6462 (2006).
118. Abele, R. & Tampe, R. The ABCs of immunology: structure and function of TAP, the transporter associated with antigen processing. *Physiology (Bethesda)* **19**, 216-224 (2004).
119. Gaudet, R. & Wiley, D.C. Structure of the ABC ATPase domain of human TAP1, the transporter associated with antigen processing. *The EMBO journal* **20**, 4964-4972 (2001).
120. Locher, K.P., Lee, A.T. & Rees, D.C. The E. coli BtuCD structure: a framework for ABC transporter architecture and mechanism. *Science (New York, N.Y* **296**, 1091-1098 (2002).
121. Koch, J., Guntrum, R., Heintke, S., Kyritsis, C. & Tampe, R. Functional dissection of the transmembrane domains of the transporter associated with antigen processing (TAP). *The Journal of biological chemistry* **279**, 10142-10147 (2004).
122. Tampe, R., Urlinger, S., Pawlitschko, K. & Uebel, S. in *Unusual Secretory Pathways: From Bacteria to Man* (ed. K. Kuchler, Rubartelli, A. and Holland, B., editors) 115-136 (Springer, New York, 1997).
123. Koch, J., Guntrum, R. & Tampe, R. The first N-terminal transmembrane helix of each subunit of the antigenic peptide transporter TAP is essential for independent tapasin binding. *FEBS Lett* **580**, 4091-4096 (2006).
124. Greenwood, R., Shimizu, Y., Sekhon, G.S. & DeMars, R. Novel allele-specific, post-translational reduction in HLA class I surface expression in a mutant human B cell line. *J Immunol* **153**, 5525-5536 (1994).
125. Grandea, A.G., 3rd, Androlewicz, M.J., Athwal, R.S., Geraghty, D.E. & Spies, T. Dependence of peptide binding by MHC class I molecules on their interaction with TAP. *Science (New York, N.Y* **270**, 105-108 (1995).
126. Sadasivan, B., Lehner, P.J., Ortmann, B., Spies, T. & Cresswell, P. Roles for calreticulin and a novel glycoprotein, tapasin, in the interaction of MHC class I molecules with TAP. *Immunity* **5**, 103-114 (1996).
127. Paquet, M.E. & Williams, D.B. Mutant MHC class I molecules define interactions between components of the peptide-loading complex. *International immunology* **14**, 347-358 (2002).
128. Sieker, F., Springer, S. & Zacharias, M. Comparative molecular dynamics analysis of tapasin-dependent and -independent MHC class I alleles. *Protein Sci* **16**, 299-308 (2007).
129. Howarth, M., Williams, A., Tolstrup, A.B. & Elliott, T. Tapasin enhances MHC class I peptide presentation according to peptide half-life. *Proceedings of the National Academy of Sciences of the United States of America* **101**, 11737-11742 (2004).
130. Yabe, T. *et al.* A subject with a novel type I bare lymphocyte syndrome has tapasin deficiency due to deletion of 4 exons by Alu-mediated recombination. *Blood* **100**, 1496-1498 (2002).

131. Gadola, S.D., Moins-Teisserenc, H.T., Trowsdale, J., Gross, W.L. & Cerundolo, V. TAP deficiency syndrome. *Clin Exp Immunol* **121**, 173-178 (2000).
132. Schuurman, R.K. *et al.* Failure of lymphocyte-membrane HLA-A and -B expression in two siblings with combined immunodeficiency. *Clin Immunol Immunopathol* **14**, 418-434 (1979).
133. Touraine, J.L. The bare-lymphocyte syndrome: report on the registry. *Lancet* **1**, 319-321 (1981).
134. Touraine, J.L., Betuel, H., Souillet, G. & Jeune, M. Combined immunodeficiency disease associated with absence of cell-surface HLA-A and -B antigens. *J Pediatr* **93**, 47-51 (1978).
135. Payne, R., Brodsky, F.M., Peterlin, B.M. & Young, L.M. "Bare lymphocytes" without immunodeficiency. *Human immunology* **6**, 219-227 (1983).
136. Sullivan, K.E., Stobo, J.D. & Peterlin, B.M. Molecular analysis of the bare lymphocyte syndrome. *The Journal of clinical investigation* **76**, 75-79 (1985).
137. de la Salle, H. *et al.* Homozygous human TAP peptide transporter mutation in HLA class I deficiency. *Science (New York, N.Y* **265**, 237-241 (1994).
138. Quaratino, S., Murison, G., Knyba, R.E., Verhoef, A. & Londei, M. Human CD4- CD8- alpha beta+ T cells express a functional T cell receptor and can be activated by superantigens. *J Immunol* **147**, 3319-3323 (1991).
139. Kohler, G. & Milstein, C. Continuous cultures of fused cells secreting antibody of predefined specificity. *Nature* **256**, 495-497 (1975).
140. Uhr, J.W. The 1984 Nobel Prize in medicine. *Science (New York, N.Y* **226**, 1025-1028 (1984).
141. McMichael, A.J. *et al.* A human thymocyte antigen defined by a hybrid myeloma monoclonal antibody. *European journal of immunology* **9**, 205-210 (1979).
142. Yu, C.Y. & Milstein, C. A physical map linking the five CD1 human thymocyte differentiation antigen genes. *The EMBO journal* **8**, 3727-3732 (1989).
143. Balk, S.P., Bleicher, P.A. & Terhorst, C. Isolation and characterization of a cDNA and gene coding for a fourth CD1 molecule. *Proceedings of the National Academy of Sciences of the United States of America* **86**, 252-256 (1989).
144. Porcelli, S. *et al.* Recognition of cluster of differentiation 1 antigens by human CD4-CD8-cytolytic T lymphocytes. *Nature* **341**, 447-450 (1989).
145. Porcelli, S., Morita, C.T. & Brenner, M.B. CD1b restricts the response of human CD4-8- T lymphocytes to a microbial antigen. *Nature* **360**, 593-597 (1992).
146. Beckman, E.M. *et al.* Recognition of a lipid antigen by CD1-restricted alpha beta+ T cells. *Nature* **372**, 691-694 (1994).
147. Bix, M., Coles, M. & Raulet, D. Positive selection of V beta 8+ CD4-8- thymocytes by class I molecules expressed by hematopoietic cells. *The Journal of experimental medicine* **178**, 901-908 (1993).

148. Coles, M.C. & Raulet, D.H. Class I dependence of the development of CD4+ CD8- NK1.1+ thymocytes. *The Journal of experimental medicine* **180**, 395-399 (1994).
149. Lantz, O. & Bendelac, A. An invariant T cell receptor alpha chain is used by a unique subset of major histocompatibility complex class I-specific CD4+ and CD4-8- T cells in mice and humans. *J Exp Med* **180**, 1097-1106 (1994).
150. Porcelli, S., Yockey, C.E., Brenner, M.B. & Balk, S.P. Analysis of T cell antigen receptor (TCR) expression by human peripheral blood CD4-8- alpha/beta T cells demonstrates preferential use of several V beta genes and an invariant TCR alpha chain. *The Journal of experimental medicine* **178**, 1-16 (1993).
151. Bendelac, A. *et al.* CD1 recognition by mouse NK1+ T lymphocytes. *Science (New York, N.Y* **268**, 863-865 (1995).
152. Cardell, S. *et al.* CD1-restricted CD4+ T cells in major histocompatibility complex class II-deficient mice. *The Journal of experimental medicine* **182**, 993-1004 (1995).
153. Kawano, T. *et al.* CD1d-restricted and TCR-mediated activation of valpha14 NKT cells by glycosylceramides. *Science* **278**, 1626-1629 (1997).
154. Kobayashi, E., Motoki, K., Uchida, T., Fukushima, H. & Koezuka, Y. KRN7000, a novel immunomodulator, and its antitumor activities. *Oncology research* **7**, 529-534 (1995).
155. Zeng, Z. *et al.* Crystal structure of mouse CD1: An MHC-like fold with a large hydrophobic binding groove. *Science (New York, N.Y* **277**, 339-345 (1997).
156. Calabi, F., Jarvis, J.M., Martin, L. & Milstein, C. Two classes of CD1 genes. *European journal of immunology* **19**, 285-292 (1989).
157. Kulski, J.K., Dunn, D.S., Gaudieri, S., Shiina, T. & Inoko, H. Genomic and phylogenetic analysis of the human CD1 and HLA class I multicopy genes. *Journal of molecular evolution* **53**, 642-650 (2001).
158. Miller, M.M. *et al.* Characterization of two avian MHC-like genes reveals an ancient origin of the CD1 family. *Proceedings of the National Academy of Sciences of the United States of America* **102**, 8674-8679 (2005).
159. Brigl, M. & Brenner, M.B. CD1: antigen presentation and T cell function. *Annu Rev Immunol* **22**, 817-890 (2004).
160. Battistini, L., Fischer, F.R., Raine, C.S. & Brosnan, C.F. CD1b is expressed in multiple sclerosis lesions. *Journal of neuroimmunology* **67**, 145-151 (1996).
161. Skold, M., Xiong, X., Illarionov, P.A., Besra, G.S. & Behar, S.M. Interplay of cytokines and microbial signals in regulation of CD1d expression and NKT cell activation. *J Immunol* **175**, 3584-3593 (2005).
162. Chen, Q.Y. & Jackson, N. Human CD1D gene has TATA boxless dual promoters: an SP1-binding element determines the function of the proximal promoter. *J Immunol* **172**, 5512-5521 (2004).
163. Szatmari, I. *et al.* Activation of PPARgamma specifies a dendritic cell subtype capable of enhanced induction of iNKT cell expansion. *Immunity* **21**, 95-106 (2004).

164. Szatmari, I. *et al.* PPARgamma controls CD1d expression by turning on retinoic acid synthesis in developing human dendritic cells. *The Journal of experimental medicine* **203**, 2351-2362 (2006).
165. de la Salle, H. *et al.* Assistance of microbial glycolipid antigen processing by CD1e. *Science (New York, N.Y* **310**, 1321-1324 (2005).
166. Bendelac, A., Rivera, M.N., Park, S.H. & Roark, J.H. Mouse CD1-specific NK1 T cells: development, specificity, and function. *Annu Rev Immunol* **15**, 535-562 (1997).
167. Brossay, L. & Kronenberg, M. Highly conserved antigen-presenting function of CD1d molecules. *Immunogenetics* **50**, 146-151 (1999).
168. Grant, E.P. *et al.* Molecular recognition of lipid antigens by T cell receptors. *The Journal of experimental medicine* **189**, 195-205 (1999).
169. Brennan, P.J. & Nikaido, H. The envelope of mycobacteria. *Annual review of biochemistry* **64**, 29-63 (1995).
170. Sieling, P.A. *et al.* CD1-restricted T cell recognition of microbial lipoglycan antigens. *Science (New York, N.Y* **269**, 227-230 (1995).
171. Prigozy, T.I. *et al.* The mannose receptor delivers lipoglycan antigens to endosomes for presentation to T cells by CD1b molecules. *Immunity* **6**, 187-197 (1997).
172. Moody, D.B. *et al.* Structural requirements for glycolipid antigen recognition by CD1b-restricted T cells. *Science (New York, N.Y* **278**, 283-286 (1997).
173. Koch, M. *et al.* The crystal structure of human CD1d with and without alpha-galactosylceramide. *Nature immunology* **6**, 819-826 (2005).
174. Naidenko, O.V. *et al.* Binding and antigen presentation of ceramide-containing glycolipids by soluble mouse and human CD1d molecules. *The Journal of experimental medicine* **190**, 1069-1080 (1999).
175. Rauch, J. *et al.* Structural features of the acyl chain determine self-phospholipid antigen recognition by a CD1d-restricted invariant NKT (iNKT) cell. *J Biol Chem* **278**, 47508-47515 (2003).
176. Shamshiev, A. *et al.* Presentation of the same glycolipid by different CD1 molecules. *The Journal of experimental medicine* **195**, 1013-1021 (2002).
177. Shamshiev, A. *et al.* Self glycolipids as T-cell autoantigens. *European journal of immunology* **29**, 1667-1675 (1999).
178. Moody, D.B. *et al.* CD1c-mediated T-cell recognition of isoprenoid glycolipids in Mycobacterium tuberculosis infection. *Nature* **404**, 884-888 (2000).
179. Moody, D.B. *et al.* T cell activation by lipopeptide antigens. *Science (New York, N.Y* **303**, 527-531 (2004).
180. Van Rhijn, I. *et al.* CD1d-restricted T cell activation by nonlipidic small molecules. *Proceedings of the National Academy of Sciences of the United States of America* **101**, 13578-13583 (2004).
181. Gadola, S.D. *et al.* Structure of human CD1b with bound ligands at 2.3 A, a maze for alkyl chains. *Nature immunology* **3**, 721-726 (2002).
182. Giabbai, B. *et al.* Crystal structure of mouse CD1d bound to the self ligand phosphatidylcholine: a molecular basis for NKT cell activation. *J Immunol* **175**, 977-984 (2005).

183. Zajonc, D.M. *et al.* Structure and function of a potent agonist for the semi-invariant natural killer T cell receptor. *Nature immunology* **6**, 810-818 (2005).
184. Zajonc, D.M. *et al.* Molecular mechanism of lipopeptide presentation by CD1a. *Immunity* **22**, 209-219 (2005).
185. Zajonc, D.M., Elsliger, M.A., Teyton, L. & Wilson, I.A. Crystal structure of CD1a in complex with a sulfatide self antigen at a resolution of 2.15 A. *Nature immunology* **4**, 808-815 (2003).
186. Batuwangala, T. *et al.* The crystal structure of human CD1b with a bound bacterial glycolipid. *J Immunol* **172**, 2382-2388 (2004).
187. Borg, N.A. *et al.* CD1d-lipid-antigen recognition by the semi-invariant NKT T-cell receptor. *Nature* **448**, 44-49 (2007).
188. Sugita, M., Porcelli, S.A. & Brenner, M.B. Assembly and retention of CD1b heavy chains in the endoplasmic reticulum. *J Immunol* **159**, 2358-2365 (1997).
189. Kang, S.J. & Cresswell, P. Calnexin, calreticulin, and ERp57 cooperate in disulfide bond formation in human CD1d heavy chain. *The Journal of biological chemistry* **277**, 44838-44844 (2002).
190. Garcia-Alles, L.F. *et al.* Endogenous phosphatidylcholine and a long spacer ligand stabilize the lipid-binding groove of CD1b. *The EMBO journal* **25**, 3684-3692 (2006).
191. Joyce, S. *et al.* Natural ligand of mouse CD1d1: cellular glycosylphosphatidylinositol. *Science (New York, N.Y* **279**, 1541-1544 (1998).
192. Sugita, M., Barral, D.C. & Brenner, M.B. Pathways of CD1 and lipid antigen delivery, trafficking, processing, loading, and presentation. *Current topics in microbiology and immunology* **314**, 143-164 (2007).
193. Briken, V., Jackman, R.M., Dasgupta, S., Hoening, S. & Porcelli, S.A. Intracellular trafficking pathway of newly synthesized CD1b molecules. *The EMBO journal* **21**, 825-834 (2002).
194. Cernadas, M. *et al.* Lysosomal localization of murine CD1d mediated by AP-3 is necessary for NK T cell development. *J Immunol* **171**, 4149-4155 (2003).
195. Sugita, M. *et al.* Failure of trafficking and antigen presentation by CD1 in AP-3-deficient cells. *Immunity* **16**, 697-706 (2002).
196. Moody, D.B. *et al.* Lipid length controls antigen entry into endosomal and nonendosomal pathways for CD1b presentation. *Nature immunology* **3**, 435-442 (2002).
197. Sugita, M. *et al.* Separate pathways for antigen presentation by CD1 molecules. *Immunity* **11**, 743-752 (1999).
198. Kang, S.J. & Cresswell, P. Regulation of intracellular trafficking of human CD1d by association with MHC class II molecules. *The EMBO journal* **21**, 1650-1660 (2002).
199. Jayawardena-Wolf, J., Benlagha, K., Chiu, Y.H., Mehr, R. & Bendelac, A. CD1d endosomal trafficking is independently regulated by an intrinsic CD1d-encoded tyrosine motif and by the invariant chain. *Immunity* **15**, 897-908 (2001).
200. Park, J.J. *et al.* Lipid-protein interactions: biosynthetic assembly of CD1 with lipids in the endoplasmic reticulum is evolutionarily conserved. *Proceedings of*

the National Academy of Sciences of the United States of America **101**, 1022-1026 (2004).
201. Dougan, S.K. *et al.* Microsomal triglyceride transfer protein lipidation and control of CD1d on antigen-presenting cells. *The Journal of experimental medicine* **202**, 529-539 (2005).
202. Brozovic, S. *et al.* CD1d function is regulated by microsomal triglyceride transfer protein. *Nat Med* **10**, 535-539 (2004).
203. Chiu, Y.H. *et al.* Multiple defects in antigen presentation and T cell development by mice expressing cytoplasmic tail-truncated CD1d. *Nature immunology* **3**, 55-60 (2002).
204. Riese, R.J. *et al.* Regulation of CD1 function and NK1.1(+) T cell selection and maturation by cathepsin S. *Immunity* **15**, 909-919 (2001).
205. Gadola, S.D. *et al.* Impaired selection of invariant natural killer T cells in diverse mouse models of glycosphingolipid lysosomal storage diseases. *The Journal of experimental medicine* **203**, 2293-2303 (2006).
206. Prigozy, T.I. *et al.* Glycolipid antigen processing for presentation by CD1d molecules. *Science (New York, N.Y* **291**, 664-667 (2001).
207. Moody, D.B. *et al.* CD1b-mediated T cell recognition of a glycolipid antigen generated from mycobacterial lipid and host carbohydrate during infection. *The Journal of experimental medicine* **192**, 965-976 (2000).
208. Sieling, P.A. *et al.* Human double-negative T cells in systemic lupus erythematosus provide help for IgG and are restricted by CD1c. *J Immunol* **165**, 5338-5344 (2000).
209. Vincent, M.S. *et al.* CD1-dependent dendritic cell instruction. *Nature immunology* **3**, 1163-1168 (2002).
210. Roura-Mir, C. *et al.* CD1a and CD1c activate intrathyroidal T cells during Graves' disease and Hashimoto's thyroiditis. *J Immunol* **174**, 3773-3780 (2005).
211. Spada, F.M. *et al.* Self-recognition of CD1 by gamma/delta T cells: implications for innate immunity. *The Journal of experimental medicine* **191**, 937-948 (2000).
212. Kawashima, T. *et al.* Cutting edge: major CD8 T cell response to live bacillus Calmette-Guerin is mediated by CD1 molecules. *J Immunol* **170**, 5345-5348 (2003).
213. Kronenberg, M. Toward an understanding of NKT cell biology: progress and paradoxes. *Annu Rev Immunol* **23**, 877-900 (2005).
214. Gadola, S.D., Dulphy, N., Salio, M. & Cerundolo, V. Valpha24-JalphaQ-independent, CD1d-restricted recognition of alpha-galactosylceramide by human CD4(+) and CD8alphabeta(+) T lymphocytes. *J Immunol* **168**, 5514-5520 (2002).
215. van Der Vliet, H.J. *et al.* Human natural killer T cells acquire a memory-activated phenotype before birth. *Blood* **95**, 2440-2442 (2000).
216. Park, S.H., Benlagha, K., Lee, D., Balish, E. & Bendelac, A. Unaltered phenotype, tissue distribution and function of Valpha14(+) NKT cells in germ-free mice. *European journal of immunology* **30**, 620-625 (2000).

217. Mempel, M. *et al.* Natural killer T cells restricted by the monomorphic MHC class 1b CD1d1 molecules behave like inflammatory cells. *J Immunol* **168**, 365-371 (2002).
218. Carnaud, C. *et al.* Cutting edge: Cross-talk between cells of the innate immune system: NKT cells rapidly activate NK cells. *J Immunol* **163**, 4647-4650 (1999).
219. Kitamura, H. *et al.* The natural killer T (NKT) cell ligand alpha-galactosylceramide demonstrates its immunopotentiating effect by inducing interleukin (IL)-12 production by dendritic cells and IL-12 receptor expression on NKT cells. *The Journal of experimental medicine* **189**, 1121-1128 (1999).
220. Hegde, S. *et al.* NKT cells direct monocytes into a DC differentiation pathway. *Journal of leukocyte biology* **81**, 1224-1235 (2007).
221. Silk, J.D. *et al.* Utilizing the adjuvant properties of CD1d-dependent NK T cells in T cell-mediated immunotherapy. *The Journal of clinical investigation* **114**, 1800-1811 (2004).
222. Hermans, I.F. *et al.* NKT cells enhance CD4+ and CD8+ T cell responses to soluble antigen in vivo through direct interaction with dendritic cells. *J Immunol* **171**, 5140-5147 (2003).
223. Jerud, E.S., Bricard, G. & Porcelli, S. CD1d-Restricted Natural Killer T Cells: Roles in Tumor Immunosurveillance and Tolerance. *Transfus Med Hemother* **33**, 18-36 (2006).
224. Molling, J.W. *et al.* Peripheral blood IFN-gamma-secreting Valpha24+Vbeta11+ NKT cell numbers are decreased in cancer patients independent of tumor type or tumor load. *International journal of cancer* **116**, 87-93 (2005).
225. Pellicci, D.G. *et al.* Intrathymic NKT cell development is blocked by the presence of alpha-galactosylceramide. *European journal of immunology* **33**, 1816-1823 (2003).
226. Miyamoto, K., Miyake, S. & Yamamura, T. A synthetic glycolipid prevents autoimmune encephalomyelitis by inducing TH2 bias of natural killer T cells. *Nature* **413**, 531-534 (2001).
227. Miyake, S. & Yamamura, T. Therapeutic potential of glycolipid ligands for natural killer (NK) T cells in the suppression of autoimmune diseases. *Current drug targets* **5**, 315-322 (2005).
228. Mars, L.T., Novak, J., Liblau, R.S. & Lehuen, A. Therapeutic manipulation of iNKT cells in autoimmunity: modes of action and potential risks. *Trends in immunology* **25**, 471-476 (2004).
229. van der Vliet, H.J. *et al.* Circulating V(alpha24+) Vbeta11+ NKT cell numbers are decreased in a wide variety of diseases that are characterized by autoreactive tissue damage. *Clinical immunology (Orlando, Fla* **100**, 144-148 (2001).
230. Cui, J. *et al.* Requirement for Valpha14 NKT cells in IL-12-mediated rejection of tumors. *Science (New York, N.Y* **278**, 1623-1626 (1997).
231. Sireci, G. *et al.* Immunoregulatory role of Jalpha281 T cells in aged mice developing lupus-like nephritis. *European journal of immunology* **37**, 425-433 (2007).

232. Sonoda, K.H., Exley, M., Snapper, S., Balk, S.P. & Stein-Streilein, J. CD1-reactive natural killer T cells are required for development of systemic tolerance through an immune-privileged site. *The Journal of experimental medicine* **190**, 1215-1226 (1999).
233. Faunce, D.E. & Stein-Streilein, J. NKT cell-derived RANTES recruits APCs and CD8+ T cells to the spleen during the generation of regulatory T cells in tolerance. *J Immunol* **169**, 31-38 (2002).
234. Sonoda, K.H. *et al.* NK T cell-derived IL-10 is essential for the differentiation of antigen-specific T regulatory cells in systemic tolerance. *J Immunol* **166**, 42-50 (2001).
235. Sonoda, K.H. & Stein-Streilein, J. CD1d on antigen-transporting APC and splenic marginal zone B cells promotes NKT cell-dependent tolerance. *European journal of immunology* **32**, 848-857 (2002).
236. Ikehara, Y. *et al.* CD4(+) Valpha14 natural killer T cells are essential for acceptance of rat islet xenografts in mice. *The Journal of clinical investigation* **105**, 1761-1767 (2000).
237. Seino, K.I. *et al.* Requirement for natural killer T (NKT) cells in the induction of allograft tolerance. *Proceedings of the National Academy of Sciences of the United States of America* **98**, 2577-2581 (2001).
238. Terabe, M. *et al.* NKT cell-mediated repression of tumor immunosurveillance by IL-13 and the IL-4R-STAT6 pathway. *Nature immunology* **1**, 515-520 (2000).
239. Aldemir, H. *et al.* Cutting edge: lectin-like transcript 1 is a ligand for the CD161 receptor. *J Immunol* **175**, 7791-7795 (2005).
240. Exley, M., Porcelli, S., Furman, M., Garcia, J. & Balk, S. CD161 (NKR-P1A) costimulation of CD1d-dependent activation of human T cells expressing invariant V alpha 24 J alpha Q T cell receptor alpha chains. *The Journal of experimental medicine* **188**, 867-876 (1998).
241. Gadola, S.D. *et al.* Structure and binding kinetics of three different human CD1d-alpha-galactosylceramide-specific T cell receptors. *The Journal of experimental medicine* **203**, 699-710 (2006).
242. Kjer-Nielsen, L. *et al.* A structural basis for selection and cross-species reactivity of the semi-invariant NKT cell receptor in CD1d/glycolipid recognition. *The Journal of experimental medicine* **203**, 661-673 (2006).
243. Wun, K.S. *et al.* A minimal binding footprint on CD1d-glycolipid is a basis for selection of the unique human NKT TCR. *The Journal of experimental medicine* **205**, 939-949 (2008).
244. Ishizuka, J. *et al.* The structural dynamics and energetics of an immunodominant T cell receptor are programmed by its Vbeta domain. *Immunity* **28**, 171-182 (2008).
245. Willemsen, M., De Coninck, A., Goossens, A., DeCree, J. & Roseeuw, D. Unusual clinical manifestation of a disfiguring necrobiotic granulomatous disease. *Journal of the American Academy of Dermatology* **33**, 887-890 (1995).
246. Russ, G. *et al.* Assembly, intracellular localization, and nucleotide binding properties of the human peptide transporters TAP1 and TAP2 expressed by

recombinant vaccinia viruses. *The Journal of biological chemistry* **270**, 21312-21318 (1995).
247. Moins-Teisserenc, H.T. *et al.* Association of a syndrome resembling Wegener's granulomatosis with low surface expression of HLA class-I molecules. *Lancet* **354**, 1598-1603 (1999).
248. O'Callaghan, C.A. *et al.* Production, crystallization, and preliminary X-ray analysis of the human MHC class Ib molecule HLA-E. *Protein Sci* 7, 1264-1266 (1998).
249. Altamirano, M.M. *et al.* Ligand-independent assembly of recombinant human CD1 by using oxidative refolding chromatography. *Proceedings of the National Academy of Sciences of the United States of America* **98**, 3288-3293 (2001).
250. Pascolo, S. *et al.* HLA-A2.1-restricted education and cytolytic activity of CD8(+) T lymphocytes from beta2 microglobulin (beta2m) HLA-A2.1 monochain transgenic H-2Db beta2m double knockout mice. *The Journal of experimental medicine* **185**, 2043-2051 (1997).
251. Traunecker, A., Oliveri, F. & Karjalainen, K. Myeloma based expression system for production of large mammalian proteins. *Trends Biotechnol* **9**, 109-113 (1991).
252. Lane, P., Burdet, C., McConnell, F., Lanzavecchia, A. & Padovan, E. CD40 ligand-independent B cell activation revealed by CD40 ligand-deficient T cell clones: evidence for distinct activation requirements for antibody formation and B cell proliferation. *Eur J Immunol* **25**, 1788-1793 (1995).
253. Karadimitris, A. *et al.* Human CD1d-glycolipid tetramers generated by in vitro oxidative refolding chromatography. *Proc Natl Acad Sci U S A* **98**, 3294-3298. (2001).
254. Xu, X.N. *et al.* A novel approach to antigen-specific deletion of CTL with minimal cellular activation using alpha3 domain mutants of MHC class I/peptide complex. *Immunity* **14**, 591-602 (2001).
255. Han, M. *et al.* Invariant or highly conserved TCR alpha are expressed on double-negative (CD3+CD4-CD8-) and CD8+ T cells. *J Immunol* **163**, 301-311 (1999).
256. Puisieux, I. *et al.* Oligoclonality of tumor-infiltrating lymphocytes from human melanomas. *J Immunol* **153**, 2807-2818 (1994).
257. Ogg, G.S., Rod Dunbar, P., Romero, P., Chen, J.L. & Cerundolo, V. High frequency of skin-homing melanocyte-specific cytotoxic T lymphocytes in autoimmune vitiligo. *The Journal of experimental medicine* **188**, 1203-1208 (1998).
258. Engelhard, M. & Evans, P.A. Kinetics of interaction of partially folded proteins with a hydrophobic dye: evidence that molten globule character is maximal in early folding intermediates. *Protein Sci* **4**, 1553-1562 (1995).
259. Anfinsen, C.B. Principles that govern the folding of protein chains. *Science (New York, N.Y* **181**, 223-230 (1973).
260. Cleland, J.L. & Wang, D.I. Refolding and aggregation of bovine carbonic anhydrase B: quasi-elastic light scattering analysis. *Biochemistry* **29**, 11072-11078 (1990).

261. Stockel, J., Doring, K., Malotka, J., Jahnig, F. & Dornmair, K. Pathway of detergent-mediated and peptide ligand-mediated refolding of heterodimeric class II major histocompatibility complex (MHC) molecules. *European journal of biochemistry / FEBS* **248**, 684-691 (1997).
262. Tandon, S. & Horowitz, P. The effects of lauryl maltoside on the reactivation of several enzymes after treatment with guanidinium chloride. *Biochimica et biophysica acta* **955**, 19-25 (1988).
263. Tandon, S. & Horowitz, P. Detergent-assisted refolding of guanidinium chloride-denatured rhodanese. The effect of lauryl maltoside. *The Journal of biological chemistry* **261**, 15615-15618 (1986).
264. Tandon, S. & Horowitz, P.M. Detergent-assisted refolding of guanidinium chloride-denatured rhodanese. The effects of the concentration and type of detergent. *The Journal of biological chemistry* **262**, 4486-4491 (1987).
265. Horowitz, P.M. & Simon, D. The enzyme rhodanese can be reactivated after denaturation in guanidinium chloride. *The Journal of biological chemistry* **261**, 13887-13891 (1986).
266. Kelly, S.M. & Price, N.C. Reactivation of denatured citrate synthase. *The International journal of biochemistry* **24**, 627-630 (1992).
267. Gerschitz, J., Rudolph, R. & Jaenicke, R. Refolding and reactivation of liver alcohol dehydrogenase after dissociation and denaturation in 6M guanidine hydrochloride. *European journal of biochemistry / FEBS* **87**, 591-599 (1978).
268. Rudolph, R., Gerschitz, J. & Jaenicke, R. Effect of zinc(II) on the refolding and reactivation of liver alcohol dehydrogenase. *European journal of biochemistry / FEBS* **87**, 601-606 (1978).
269. Gupta, P., Hall, C.K. & Voegler, A.C. Effect of denaturant and protein concentrations upon protein refolding and aggregation: a simple lattice model. *Protein Sci* **7**, 2642-2652 (1998).
270. Xie, Y. & Wetlaufer, D.B. Control of aggregation in protein refolding: the temperature-leap tactic. *Protein Sci* **5**, 517-523 (1996).
271. Karuppiah, N. & Sharma, A. Cyclodextrins as protein folding aids. *Biochemical and biophysical research communications* **211**, 60-66 (1995).
272. McCoy, L.F., Jr., Rowe, E.S. & Wong, K.P. Multiparameter kinetic study on the unfolding and refolding of bovine carbonic anhydrase B. *Biochemistry* **19**, 4738-4743 (1980).
273. Gross, W.L. Wegener granulomatosis, in *Oxford Textbook of Rheumatology*, Vol. 2. (ed. P.J. Madison, Isenberg, D.A., Woo, P., Glass D.N.) 1331-13511998).
274. Fauci, A.S., Wolff, S.M. & Johnson, J.S. Effect of cyclophosphamide upon the immune response in Wegener's granulomatosis. *The New England journal of medicine* **285**, 1493-1496 (1971).
275. Polychronopoulos, V.S., Prakash, U.B., Golbin, J.M., Edell, E.S. & Specks, U. Airway involvement in Wegener's granulomatosis. *Rheumatic diseases clinics of North America* **33**, 755-775, vi (2007).
276. Ludemann, J., Utecht, B. & Gross, W.L. Anti-neutrophil cytoplasm antibodies in Wegener's granulomatosis recognize an elastinolytic enzyme. *The Journal of experimental medicine* **171**, 357-362 (1990).

277. Nowack, R., Lehmann, H., Flores-Suarez, L.F., Nanhou, A. & van der Woude, F.J. Familial occurrence of systemic vasculitis and rapidly progressive glomerulonephritis. *Am J Kidney Dis* **34**, 364-373 (1999).
278. Leavitt, R.Y. *et al.* The American College of Rheumatology 1990 criteria for the classification of Wegener's granulomatosis. *Arthritis and rheumatism* **33**, 1101-1107 (1990).
279. Jennette, J.C. *et al.* Nomenclature of systemic vasculitides. Proposal of an international consensus conference. *Arthritis and rheumatism* **37**, 187-192 (1994).
280. Caversaccio, M., Bonel, H.M., Carter, R., Williams, A.P. & Gadola, S.D. TAP deficiency syndrome: chronic rhinosinusitis and conductive hearing loss. *Eur Arch Otorhinolaryngol* (2008).
281. de la Salle, H. *et al.* HLA class I deficiencies due to mutations in subunit 1 of the peptide transporter TAP1. *The Journal of clinical investigation* **103**, R9-R13 (1999).
282. Plebani, A. *et al.* Defective expression of HLA class I and CD1a molecules in boy with Marfan-like phenotype and deep skin ulcers. *Journal of the American Academy of Dermatology* **35**, 814-818 (1996).
283. Colonna, M. Specificity and function of immunoglobulin superfamily NK cell inhibitory and stimulatory receptors. *Immunological reviews* **155**, 127-133 (1997).
284. Lanier, L.L. & Phillips, J.H. Inhibitory MHC class I receptors on NK cells and T cells. *Immunology today* **17**, 86-91 (1996).
285. Zimmer, J. *et al.* Inefficient protection of human TAP-deficient fibroblasts from autologous NK cell-mediated lysis by cytokines inducing HLA class I expression. *European journal of immunology* **29**, 1286-1291 (1999).
286. Zimmer, J. *et al.* Activity and phenotype of natural killer cells in peptide transporter (TAP)-deficient patients (type I bare lymphocyte syndrome). *The Journal of experimental medicine* **187**, 117-122 (1998).
287. Lee, S.P., Thomas, W.A., Blake, N.W. & Rickinson, A.B. Transporter (TAP)-independent processing of a multiple membrane-spanning protein, the Epstein-Barr virus latent membrane protein 2. *European journal of immunology* **26**, 1875-1883 (1996).
288. Elliott, K.J. Other neurological complications of herpes zoster and their management. *Annals of neurology* **35 Suppl**, S57-61 (1994).
289. Furukawa, H. *et al.* Splice acceptor site mutation of the transporter associated with antigen processing-1 gene in human bare lymphocyte syndrome. *The Journal of clinical investigation* **103**, 755-758 (1999).
290. Karttunen, J.T., Trowsdale, J. & Lehner, P.J. Antigen presentation: TAP dances with ATP. *Curr Biol* **9**, R820-824 (1999).
291. Altman, J.D. *et al.* Phenotypic analysis of antigen-specific T lymphocytes. *Science (New York, N.Y* **274**, 94-96 (1996).
292. Martin, L.H., Calabi, F. & Milstein, C. Isolation of CD1 genes: a family of major histocompatibility complex-related differentiation antigens. *Proceedings of the National Academy of Sciences of the United States of America* **83**, 9154-9158 (1986).

293. Bowness, P., Allen, R.L., Barclay, D.N., Jones, E.Y. & McMichael, A.J. Importance of a conserved TCR J alpha-encoded tyrosine for T cell recognition of an HLA B27/peptide complex. *European journal of immunology* **28**, 2704-2713 (1998).
294. Nuti, S. *et al.* Dynamics of intra-hepatic lymphocytes in chronic hepatitis C: enrichment for Valpha24+ T cells and rapid elimination of effector cells by apoptosis. *European journal of immunology* **28**, 3448-3455 (1998).
295. Ishihara, S. *et al.* Alpha-glycosylceramides enhance the antitumor cytotoxicity of hepatic lymphocytes obtained from cancer patients by activating CD3-CD56+ NK cells in vitro. *J Immunol* **165**, 1659-1664 (2000).
296. Nicol, A. *et al.* Human invariant valpha24+ natural killer T cells activated by alpha-galactosylceramide (KRN7000) have cytotoxic anti-tumour activity through mechanisms distinct from T cells and natural killer cells. *Immunology* **99**, 229-234 (2000).
297. Nieda, M. *et al.* Activation of human Valpha24NKT cells by alpha-glycosylceramide in a CD1d-restricted and Valpha24TCR-mediated manner. *Human immunology* **60**, 10-19 (1999).
298. Matsuda, J.L. *et al.* Tracking the response of natural killer T cells to a glycolipid antigen using CD1d tetramers. *The Journal of experimental medicine* **192**, 741-754 (2000).
299. Porcelli, S.A. & Modlin, R.L. The CD1 system: antigen-presenting molecules for T cell recognition of lipids and glycolipids. *Annu Rev Immunol* **17**, 297-329 (1999).
300. Bendelac, A., Hunziker, R.D. & Lantz, O. Increased interleukin 4 and immunoglobulin E production in transgenic mice overexpressing NK1 T cells. *J Exp Med* **184**, 1285-1293 (1996).
301. Dellabona, P. *et al.* In vivo persistence of expanded clones specific for bacterial antigens within the human T cell receptor alpha/beta CD4-8- subset. *J Exp Med* **177**, 1763-1771 (1993).
302. Gapin, L., Matsuda, J.L., Surh, C.D. & Kronenberg, M. NKT cells derive from double-positive thymocytes that are positively selected by CD1d. *Nat Immunol* **2**, 971-978 (2001).
303. Dellabona, P., Padovan, E., Casorati, G., Brockhaus, M. & Lanzavecchia, A. An invariant V alpha 24-J alpha Q/V beta 11 T cell receptor is expressed in all individuals by clonally expanded CD4-8- T cells. *J Exp Med* **180**, 1171-1176 (1994).
304. wwwwwMatsuda, J.L. *et al.* Natural killer T cells reactive to a single glycolipid exhibit a highly diverse T cell receptor beta repertoire and small clone size. *Proc Natl Acad Sci U S A* **98**, 12636-12641 (2001).
305. Benlagha, K., Weiss, A., Beavis, A., Teyton, L. & Bendelac, A. In vivo identification of glycolipid antigen-specific T cells using fluorescent CD1d tetramers. *J Exp Med* **191**, 1895-1903. (2000).
306. Altamirano, M.M., Garcia, C., Possani, L.D. & Fersht, A.R. Oxidative refolding chromatography: folding of the scorpion toxin Cn5. *Nature biotechnology* **17**, 187-191 (1999).

307. Blackman, M., Kappler, J. & Marrack, P. The role of the T cell receptor in positive and negative selection of developing T cells. *Science* **248**, 1335-1341 (1990).
308. Itano, A. *et al.* The cytoplasmic domain of CD4 promotes the development of CD4 lineage T cells. *J Exp Med* **183**, 731-741 (1996).
309. Matechak, E.O., Killeen, N., Hedrick, S.M. & Fowlkes, B.J. MHC class II-specific T cells can develop in the CD8 lineage when CD4 is absent. *Immunity* **4**, 337-347 (1996).
310. Curnow, S.J., Boyer, C., Buferne, M. & Schmitt-Verhulst, A.M. TCR-associated zeta-Fc epsilon RI gamma heterodimers on CD4-CD8- NK1.1+ T cells selected by specific class I MHC antigen. *Immunity* **3**, 427-438 (1995).
311. Iwabuchi, C. *et al.* Intrathymic selection of NK1.1(+)alpha/beta T cell antigen receptor (TCR)+ cells in transgenic mice bearing TCR specific for chicken ovalbumin and restricted to I-Ad. *Proc Natl Acad Sci U S A* **95**, 8199-8204 (1998).
312. Schulz, R.J., Parkes, A., Mizoguchi, E., Bhan, A.K. & Koyasu, S. Development of CD4-CD8- alpha beta TCR+NK1.1+ T lymphocytes: thymic selection by self antigen. *J Immunol* **157**, 4379-4389 (1996).
313. Chang, D.H. *et al.* Sustained expansion of NKT cells and antigen-specific T cells after injection of alpha-galactosyl-ceramide loaded mature dendritic cells in cancer patients. *The Journal of experimental medicine* **201**, 1503-1517 (2005).
314. Rosat, J.P. *et al.* CD1-restricted microbial lipid antigen-specific recognition found in the CD8+ alpha beta T cell pool. *J Immunol* **162**, 366-371 (1999).
315. Beckman, E.M. *et al.* CD1c restricts responses of mycobacteria-specific T cells. Evidence for antigen presentation by a second member of the human CD1 family. *J Immunol* **157**, 2795-2803 (1996).
316. Ernst, W.A. *et al.* Molecular interaction of CD1b with lipoglycan antigens. *Immunity* **8**, 331-340 (1998).
317. Daugherty, D.L., Rozema, D., Hanson, P.E. & Gellman, S.H. Artificial chaperone-assisted refolding of citrate synthase. *The Journal of biological chemistry* **273**, 33961-33971 (1998).
318. Rozema, D. & Gellman, S.H. Artificial chaperone-assisted refolding of carbonic anhydrase B. *The Journal of biological chemistry* **271**, 3478-3487 (1996).
319. Madden, D.R., Garboczi, D.N. & Wiley, D.C. The antigenic identity of peptide-MHC complexes: a comparison of the conformations of five viral peptides presented by HLA-A2. *Cell* **75**, 693-708 (1993).
320. Melian, A. *et al.* Molecular recognition of human CD1b antigen complexes: evidence for a common pattern of interaction with alpha beta TCRs. *J Immunol* **165**, 4494-4504 (2000).
321. Hopkins, A.L. *et al.* Complexes of HIV-1 reverse transcriptase with inhibitors of the HEPT series reveal conformational changes relevant to the design of potent non-nucleoside inhibitors. *Journal of medicinal chemistry* **39**, 1589-1600 (1996).

322. Sacchettini, J.C., Scapin, G., Gopaul, D. & Gordon, J.I. Refinement of the structure of Escherichia coli-derived rat intestinal fatty acid binding protein with bound oleate to 1.75-A resolution. Correlation with the structures of the apoprotein and the protein with bound palmitate. *The Journal of biological chemistry* **267**, 23534-23545 (1992).
323. Niazi, K. *et al.* The A' and F' pockets of human CD1b are both required for optimal presentation of lipid antigens to T cells. *J Immunol* **166**, 2562-2570 (2001).
324. Assmann, G., Schulte, H. & von Eckardstein, A. Hypertriglyceridemia and elevated lipoprotein(a) are risk factors for major coronary events in middle-aged men. *The American journal of cardiology* **77**, 1179-1184 (1996).
325. Hokanson, J.E. & Austin, M.A. Plasma triglyceride level is a risk factor for cardiovascular disease independent of high-density lipoprotein cholesterol level: a meta-analysis of population-based prospective studies. *Journal of cardiovascular risk* **3**, 213-219 (1996).
326. Stemme, S. *et al.* T lymphocytes from human atherosclerotic plaques recognize oxidized low density lipoprotein. *Proceedings of the National Academy of Sciences of the United States of America* **92**, 3893-3897 (1995).
327. Wu, R., Giscombe, R., Holm, G. & Lefvert, A.K. Induction of human cytotoxic T lymphocytes by oxidized low density lipoproteins. *Scandinavian journal of immunology* **43**, 381-384 (1996).
328. Melian, A., Geng, Y.J., Sukhova, G.K., Libby, P. & Porcelli, S.A. CD1 expression in human atherosclerosis. A potential mechanism for T cell activation by foam cells. *The American journal of pathology* **155**, 775-786 (1999).
329. Schultz, H. *et al.* BPI-ANCA in transporter associated with antigen presentation (TAP) deficiency: possible role in susceptibility to Gram-negative bacterial infections. *Clin Exp Immunol* **133**, 252-259 (2003).
330. Schultz, H., Weiss, J., Carroll, S.F. & Gross, W.L. The endotoxin-binding bactericidal/permeability-increasing protein (BPI): a target antigen of autoantibodies. *Journal of leukocyte biology* **69**, 505-512 (2001).
331. Beauvillain, C. *et al.* Neutrophils efficiently cross-prime naive T cells in vivo. *Blood* **110**, 2965-2973 (2007).
332. Shen, L. & Rock, K.L. Priming of T cells by exogenous antigen cross-presented on MHC class I molecules. *Current opinion in immunology* **18**, 85-91 (2006).
333. Aladin, F., Lautscham, G., Humphries, E., Coulson, J. & Blake, N. Targeting tumour cells with defects in the MHC Class I antigen processing pathway with CD8+ T cells specific for hydrophobic TAP- and Tapasin-independent peptides: the requirement for directed access into the ER. *Cancer Immunol Immunother* **56**, 1143-1152 (2007).